Development of a Physics-based Morphodynamic Model and its Application to Braided Rivers

by

Haiyan Yang

A thesis submitted in candidature for the degree of

Doctor of Philosophy

Cardiff School of Engineering, Cardiff University, UK

September, 2013

DECLARATION

This work has not been submitted in substance for any other degree or award at this or any other university or place of learning, nor is being submitted concurrently in candidature for any degree or other award.

Signed…… (Haiyan Yang) Date ……

STATEMENT 1

This thesis is being submitted in partial fulfillment of the requirements for the degree of PhD

Signed…….. (Haiyan Yang) Date ……

STATEMENT 2

This thesis is the result of my own independent work/investigation, except where otherwise stated.
Other sources are acknowledged by explicit references. The views expressed are my own.

Signed…….. (Haiyan Yang) Date ……

STATEMENT 3

I hereby give consent for my thesis, if accepted, to be available for photocopying and for inter-library loan, and for the title and summary to be made available to outside organisations.

Signed…….. (Haiyan Yang) Date ……

STATEMENT 4: PREVIOUSLY APPROVED BAR ON ACCESS

I hereby give consent for my thesis, if accepted, to be available for photocopying and for inter-library loans after expiry of a bar on access previously approved by the Academic Standards & Quality Committee.

Signed…….. (Haiyan Yang) Date ……

Acknowledgements

Foremost, I would like to express my sincere gratitude to my supervisor Prof. Binliang Lin, for his continuous support to my research, for his patience, motivation, enthusiasm and immense knowledge. His guidance helped me over through the research and thesis writing. His fascination of personality will influence the rest of my life.

Besides, I would like to thank my second supervisor, Prof. Roger Falconer who has been inspirational in my work by his smart ideas, abundant knowledge and enthusiasm on research. Furthermore, I would like to thank my thesis committee, Prof. Simon Tait and Dr. Shunqi Pan, for their encouragement, insightful comments and constructive criticism.

I wish to express my deep appreciation to Dr. Jian Sun for his enormous patience and great efforts in supporting my programing work, and to Dr. Guoxian Huang for his kindly help in the simulation work.

My sincere thanks also go to all my colleagues at the Hydro-environmental Research Centre in Cardiff University for their kindness, company and continuous assistance during my study.

Last but not least, I would like to thank my family: my parents Jingxi Yang and Donglan Wang for supporting me spiritually throughout my life, and my husband Zhenhuan Liu for constant encouragement, useful advices, and great help in my life.

Abstract

An understanding of the interaction between flow, sediment and bed morphology is essential for dealing with engineering problems such as floods, river bank erosion and sedimentation in reservoirs. However, the morphodynamic processes in natural braided rivers are still not well understood due to difficulties in measurements in field. Numerical models provide a considerable assistance to investigate these complicated processes in natural rivers.

In the present study, a physics-based two-dimensional model based on DIVAST with suspended load and bed load transport has been developed to simulate the braiding processes and morphodynamic changes in braided rivers. In this model, the hydrodynamic equations are solved using the ADI scheme and the advective-diffusion equations are solved using a modified ULTIMATE QUICKEST scheme. The TVD scheme has also been included to simulate trans-critical flows.

Regarding sediment transport, a new module based on bed load transport theories has been developed. A module for suspended load transport based on energy theory has been improved. Secondary flow and slope effect are integrated into the model by altering the sediment transport rate. A multiple layer technique with a vertical sorting process has been applied including bank erosion. Graded sediment fractions are adopted to represent the coarsening and fining processes with sheltering effect.

The model has been verified by solving a 2-D dam-break problem which worked well in predicting the water surface changes in trans-critical flow. It has also been tested by a sediment aggradation case and found to predict the flow and bed deformation effectively.

The model has been applied to predict a laboratory river with bed load, with its prototype being the Sunwapta River, Canada. Braiding mechanisms and channel pattern responses to abruptly increased discharge have been investigated and compared with those of laboratory and natural rivers. Growth and relationship of active braiding intensity and total braiding intensity show similar trends to those of

the laboratory river. The predicted river shows anisotropic scaling with periodical braiding morphology presented by sequential maximum scour depths.

The model also simulates a large idealised braided river with suspended load transport. Its braiding mechanisms have been discussed and compared with the river with bed load and natural rivers. Important processes at bars and confluences have been investigated. Statistical characteristics of the river have been analysed with braiding indices, state-space plots and bar parameters. These findings have been compared with those from real rivers to assess the model simulating real braided rivers.

Contents

List of Figures

List of Tables

Notations

C, C_0	Chézy coefficients related to flow
C'	Chézy coefficient related to grains
C_e	eddy viscosity coefficient
C_r	Courant number
C_w	wind resistance coefficient
d_k	representative particle diameter of the kth size fraction
D_{50}, D_{65}, D_{84}, D_{90}	diameters with grain sizes finer than 50%, 65%, 84% and 90%
D_k, D_{k+1}	lower and upper limits of the kth size fraction
D_w	wind-induced dispersion coefficient
D_{xx}, D_{xy}, D_{yx}, D_{yy}	depth-averaged dispersion-diffusion coefficients in the x and y directions, respectively
D_*	dimensionless particle parameter
E	parameter representing ξ, p or q
f	Coriolis parameter due to the Earth's rotation
F	flux term in corresponding equations
Fr	Froude number
F_x, F_y	drag force components induced by hydraulic obstructions per unit area in the x and y directions, respectively
g	gravitational acceleration
h	water depth below datum
h_x	water depth below datum in the x direction at i+1/2, j

h_y	water depth below datum in the y direction at i, j+1/2
H	water depth
H_U, H_M, H_L	thicknesses of the upper, middle and lower bed layers
i, j	grid point locations in the x and y directions, respectively
k	sediment fraction
k_l	longitudinal depth-averaged dispersion constant
k_s	roughness height
k_t	depth-averaged turbulent diffusion constant
$k_{\delta,s}$, $k_{\delta,n}$	coefficients of longitudinal and transverse slopes
L_L	length of the Lth channel
L_s	non-equilibrium adaptation length
L_r	straight reach length
M (X, Y)	mean mass in a box (X*Y)
n	Manning roughness coefficient
n'	roughness coefficient related to grains
n_j (X, Y)	number of black pixels contained in a box (X*Y)
N_b	number of black pixels in a picture
N_i	number of channels in the ith cross-section
N_j	number of active channels in the jth cross-section
N_s	number of cross-sections
N_*	coefficient of the strength of secondary flow
p, q	discharges per unit width in the x and y directions, respectively

p'	porosity of bed material
p_k	percentage of the kth size fraction of suspended load
p_{bk}	percentage of the kth size fraction in the mixing layer of the bed
p_{ak}	areal percentage of the kth size fraction in the mixing layer of the bed
P_{Uk}, P_{Mk}, P_{Lk}	volumetric fractions of the upper, middle and lower bed layers
q_b	bed load transport rate on a horizontal bed
q_{bk}	bed load transport rate
q_{b*k}	equilibrium bed load transport rate
$q_{b,s}$	bed load transport rate on a sloping bed
r_s	radius of curvature of the stream line
R_h	hydraulic radius
R_e	Reynolds number
s	sediment specific density
s_k	suspended load concentration
S	solute concentration
S_a	source term
S_t	total suspended load concentration
T	dimensionless transport stage parameter
$\overline{u}$	depth-averaged flow velocity
u_*	bed shear velocity related to flow
u'_*	bed shear velocity related to grains
u_b, u_{bk}	bed load transport velocities

u_{bx}, u_{by}	bed load transport velocities in the x and y directions, respectively
$u(z)$	vertical velocity profile in the main flow direction
U, V	depth-averaged velocity components in the x and y directions, respectively
v_x, v_y	scaling exponents in the x and y directions respectively
W_x, W_y	wind velocity components in the x and y directions, respectively
X, Y	length and width of a rectangular object
$z\ (X, Y)$	logarithmic mean mass in a box (X*Y)
z	vertical coordinate above datum
z_b	bed elevation above datum
α, α_k	adjustment coefficients for suspended load
α_{bx}, α_{by}	direction cosines of bed load movement
α_s	Bagnold slope factor
β	momentum correction factor
γ, γ_s, γ_m	specific weights of water, sediment, and water mixed with sediment
δ_n	longitudinal slope angle
δ_s	transverse slope angle
Δ	bed form height
Δt	computational time step
Δx, Δy	computational spatial steps in the x and y directions, respectively
ε	depth-averaged turbulent eddy viscosity
θ	sediment repose angle

θ_1, θ_2, θ_1', θ_2'	channel angles at a confluence
θ_c	critical particle mobility parameter
θ_e	geographical angle of latitude
κ	von Karman's constant
λ	bed form length
ν	kinematic viscosity coefficient
ξ	water surface elevation above datum
ϵ	mixing coefficient
ρ, ρ_a, ρ_s	densities of fluid, air and sediment
σ_i	ith positive root of equations relating to the adjustment coefficient α
τ_b	bed shear stress
τ_b'	bed shear stress related to grains
τ_c	critical shear stress
τ_c'	critical shear stress corrected with a linear expression
$\tau_{c,o}$	critical shear stress for median particle
$\tau_{c,s}$	critical shear stress considering slope effects
τ_e	mean shear stress in turbulent flow
φ	deviation angle between flow and bed load transport velocity
ϕ_k	suspended load transport capacity
Φ	total suspended load transport capacity
Φ_{bk}	dimensionless bed load transport rate
χ	fall velocity coefficient of suspended load

ψ	bed form steepness
ω	average fall velocity of suspended load
ω_e	angular rotation speed of the earth
ω_k	fall velocity of suspended load
ω_{mk}	fall velocity of suspended load considering the influence of high sediment concentration
Γ	variable related to Courant number

Abbreviations

ADI	alternating direction implicit
AWW	average wetted width
DIVAST	depth-integrated velocities and solute transport
SWEs	shallow water equations
TVD	total variation diminishing

Chapter 1 Introduction

1.1 Overview

Rivers play a fundamental role in the civilization of human history. They not only provide renewable resources, but also have potential threats to human life through floods and water pollution. The understanding of rivers is essential for dealing with engineering problems such as floods, water supply, river bank erosion, sedimentation in reservoirs, navigated waterways, and the design and construction of artificial channels and bridges. In earth science and engineering, they are important in understanding the activities of water flow, sediment transport, bed deposition and erosion, and how these processes control the form of river channels, floodplains, alluvial fans and deltas. River morphologic changes during flood periods are important for their destruction in human lives and properties.

Flow, sediment transport and bed morphology interact with each other to form rivers with different geometries, generally including straight, meandering and braided rivers. The processes in braided rivers are more complicated than the other two because of their high flow energy and multiple flow channels. Braided rivers are characterised by frequently channel changes, which play important roles in flood

management and engineering structures. When flow increases with high sediment supply, active channels shift laterally by bank erosion or avulsion and drown land and crops. When sediment supply or peak flows are reduced, braided rivers are typically narrow and incise their beds. The degradation can destabilise bridges, dams, erosion control works and other infrastructure. However, the present knowledge on the formation of braided patterns and the related morphologic changes in natural rivers is insufficient due to the difficulties in measuring flow, sediment transport and morphology in this rapidly changing natural environment. Therefore, numerical models have been increasingly developed to predict the morphodynamics in braided rivers.

In the previous studies of braided river modelling, the early models are mainly focused on simulating the braiding networks, such as the random walk model and the linear model. Cellular models have been widely used in braided river modelling work, yet their advances in producing real morphodynamic processes in natural rivers are limited due to their simplified flow and sediment rules. Recently, physics-based models which integrate the basic theories of flow hydrodynamics and sediment transport, have been developed to simulate braided rivers. They are more capable of reproducing the processes and morphodynamics in real rivers. However, their development and application are still in an early stage, with insufficient investigations to braiding mechanisms, morphologic units, sorting effects, bed changes and comparisons with real rivers. Large braided rivers on plains with suspended load have been rarely simulated. Moreover, the hydraulic equations are solved mostly by the

implicit scheme ADI (alternating direction implicit method), whereas sometimes supercritical flow occurs in local areas of natural braided rivers.

It is time for physics-based models to be connected with natural and laboratory rivers quantitatively. The combination of these models with real rivers can promote our understanding in channel pattern changes, braiding mechanisms and processes of braided rivers. It can enhance the prediction of real rivers, such as local channel migrations, bifurcation activities and morphodynamic changes during floods, and will be helpful for engineering works and flood controls.

1.2 Objectives of the Research

The primary goal of the present research is to develop a 2-D physics-based model which can better represent the processes in natural rivers and apply it to model real braided rivers to investigate the braiding mechanisms and morphodynamics. The main objectives can be summarised as follows:

1. To develop a model with bed load and suspended load transport

Sediments in rivers can be transported in forms of bed load and suspended load, with different transport theories applicable. Braided rivers commonly occur in mountain areas in which bed load transport is more important. Yet for some large braided rivers on plains suspended load plays a dominant role in bed deformation. A model which aims to represent processes in real rivers should include both bed load and suspended load, and apply one or both of them according to specific situations. In the present study, a bed load transport model with its equations mainly drawn from the

studies of van Rijn (1984a, 1993), are combined into the original 2-D model. Non-equilibrium sediment governing equations are considered in solving bed load transport rate. Secondary flow, which is important in sediment transport especially in channel bend areas, is integrated into the equation of bed load transport rate.

2. To develop new techniques in sediment transport and bed changes

During the evolution of rivers, local erosion or deposition will change the bed morphology and composition. Alternatively, changes in bed morphology and composition will influence the flow velocity, sediment transport process and river pattern formation. Therefore, it is meaningful to include the interaction of flow and river bed. Moreover, sediment gradation plays an important role in the processes of bed deformation. Each size fraction in a mixture of non-uniform sediments may transport at a different rate to uniform sediments. Bank erosion has been found to be meaningful for the initiation of braiding with a straight channel (Jang, 2005b). In the present model, sediment transport and bed deformation are considered by solving the 2-D non-equilibrium equations, with the effects of slope and bank erosion and multiple bed layers included. Graded sediments are adopted with the consideration of sheltering effect by the projected area of sediment particles.

3. To link the TVD scheme to the model for predicting trans-critical flows

The ADI scheme (alternating direction implicit method) has been widely used in the solution of shallow water equations in previous simulation works of braided rivers. It works well for slow flow when the Froude number is much less than unity.

Nevertheless, it is not suitable for the ADI method to calculate trans-critical flows with the Froude number approaching or exceeding unity. On the contrary, the TVD-MacCormack (total variation diminishing) scheme is a kind of shock-capturing scheme which is efficient in simulating rapidly varying flows. Therefore, in the present study, the TVD scheme is integrated into the model to solve the shallow water equations in predicting a braided river with bed load in which the Froude number approaches unity.

4. To test the model for simulating flow and sediment deposition

Before applying the numerical model to river simulation, it is necessary to validate the model for predicting flow condition and sediment transport. Therefore, the newly developed model has been used to predict a 2-D dam-break problem, and to simulate a bed aggradation case. By doing this, the TVD scheme has been verified to work well in solving trans-critical flow. The bed aggradation case tests the ability of the model in simulating the sediment transport and deposition.

5. To apply the model to investigate the processes in bed load dominated braided rivers

Physical models have been used to investigate the processes and morphodynamics in natural braided rivers. However, it is still difficult to obtain accurate data of the flow field, sediment transport rate and bed deformation from a physical model. The processes observed in natural rivers, including braiding mechanisms and consequential changes in sediment transport, morphology and sediment coarsening in

morphologic units, have been rarely discussed quantitatively. The present study tries to produce a braided pattern with laboratory data, analyse the braiding processes and response to abruptly increased discharge, and assess the model in a quantitative way.

6. **To apply the model to investigate the processes in suspended load dominated braided rivers**

Braided rivers on plains play an important role in human life. It is not easy to study the evolution processes of these rivers in laboratory due to the transport mode of suspended load, whereas the braiding mechanisms, morphodynamics and bed coarsening effect in these rivers can be very different from those with bed load. The present study models an idealised river with suspended load, studies its braiding mechanisms, processes and characteristics and tries to examine the differences between the predicted rivers with bed load and suspended load and natural rivers.

1.3 Structure of the Thesis

This thesis has been divided into seven chapters and the detailed content of each chapter is summarised as follows:

- Chapter 1 gives a brief introduction to this study, followed by its aims and objectives and the structure of the thesis.
- Chapter 2 reviews the previous studies relating to braiding mechanisms and essential processes in real rivers, presents the previous models for braided river simulation, discusses their advantages and shortcomings, and proposes the

necessity of developing more efficient models.

- Chapter 3 introduces the 2-D hydrodynamic governing equations and their solution methods. The continuity and momentum equations for the 2-D frameworks are outlined. A module based on the TVD scheme is integrated into the original model with an ADI scheme. The ADI and TVD schemes are briefly introduced for the solution of hydraulic equations under different conditions as subcritical and trans-critical flows.
- Chapter 4 presents the theories of sediment processes and the solution method with the QUICKEST scheme in the present model. A module for simulating bed load transport in rivers is developed and integrated into the original model. The module for suspended load simulation is introduced with different transport theories.
- Chapter 5 provides the details of the model tests and its first application to simulate a laboratory river with bed load. A 2-D dam-break problem and an aggradation experiment are used to test the model in solving hydraulic and sediment transport problems. A braided river with bed load has been predicted with the same parameters as the experiment and the results are compared with those from natural rivers and experiments. Braiding mechanisms similar to those observed in natural rivers have been found and investigated in detail. The present model is tested with braiding intensity and some statistical methods.
- Chapter 6 presents the results of the model in predicting the processes and braiding mechanisms in a large idealised braided river with suspended load.

Typical braiding activities have been discussed and compared with those of the river with bed load and natural rivers. Processes in important morphologic units have been investigated accompanied by comparison with natural rivers. Braiding characteristics are analysed through braiding indices and some statistical methods.

- Chapter 7 summarises the present study, presents the conclusions, and gives some recommendations for future research.

Chapter 2 Literature Review

2.1 Introduction

In braided rivers the interaction of channel geometry, water flow and sediment transport results in erosion and deposition of the river bed, growth and migration of bars, and formation and migration of channel segments. An understanding of this interaction is important in modern environmental and engineering problems such as channel changes and bank erosion, flood management and so on (Bridge, 1993). However, it is difficult to measure flow rates, sediment fluxes and morphologic changes in the rapidly changing environment in nature, especially the dynamic processes of channel shifting and sediment transport.

Numerical simulation is a useful method to obtain an understanding of the morphodynamic processes in braided rivers. Cellular models have been widely used in braided river modelling and some advances have been achieved (e.g., Murray and Paola, 1994), yet they also showed limitations. Physics-based models have made some progresses in modelling braided rivers but are still in their early stage. In this chapter, the braiding mechanisms and essential processes in the river evolution processes from field and laboratory rivers are reviewed in detail. Three aspects of

river modelling in previous studies, including the hydrodynamics, sediment transport and bed level change are analysed to develop a better model for braided river simulation.

2.2 Braided Rivers in Nature

2.2.1 Occurring Environment and Characteristics

2.2.1.1 Conditions for Braided River Formation

Hydraulic, sedimentary and energy conditions are conclucive for the development of rivers in different channel patterns (Tooth and Nanson, 2004). Braided rivers can be formed due to either an overload of sediments or a steep valley slope (e.g., Parker, 1976; Chang, 1979; Huang et al., 2004). They usually occur with an abundant bed load, erodible banks, a highly variable discharge and steep valley slopes (Knighton, 1998). Braiding tends to be most prevalent with these factors in conjunction. Braided rivers usually develop wide channels with a large width/depth ratio. Studies have shown that the main control on braiding is the width/depth ratio, with a value greater than 50 being required for braiding to occur (Engelund and Skovgaard, 1973; Fredsoe, 1978; Ferguson, 1987; Fukuoka, 1989). One typical braided river is shown in Figure 2.1.

Figure 2.1 The Waimakariri River, a typical braided river in south New Zealand.

In nature a large number of braided rivers occur in the areas with steep valley slopes and coarse sediments. Rivers with gravel bed load have been studied comprehensively. However, there still exist braided rivers on plains with low slopes, such as the Yellow River in China and the Brahmaputra River in Bangladesh. They are characterised by large flow discharges, high sediment concentrations, fine sediment particles and large floods (e.g., Sarma, 2005). Moreover, braided rivers often exist in valleys with a steeper slope than that of meandering rivers. Studies have shown that braiding occurs when the valley slope is above some thresholds (Leopold and Wolman, 1957; Schumm, Khan, 1972; Parker, 1976). The Squamish River experiences a downstream sequence of braided-wandering-meandering in a 20 km reach with slope decreases from 0.0058 to 0.0015 (Brierley and Hickin, 1991), shown

in Figure 2.2.

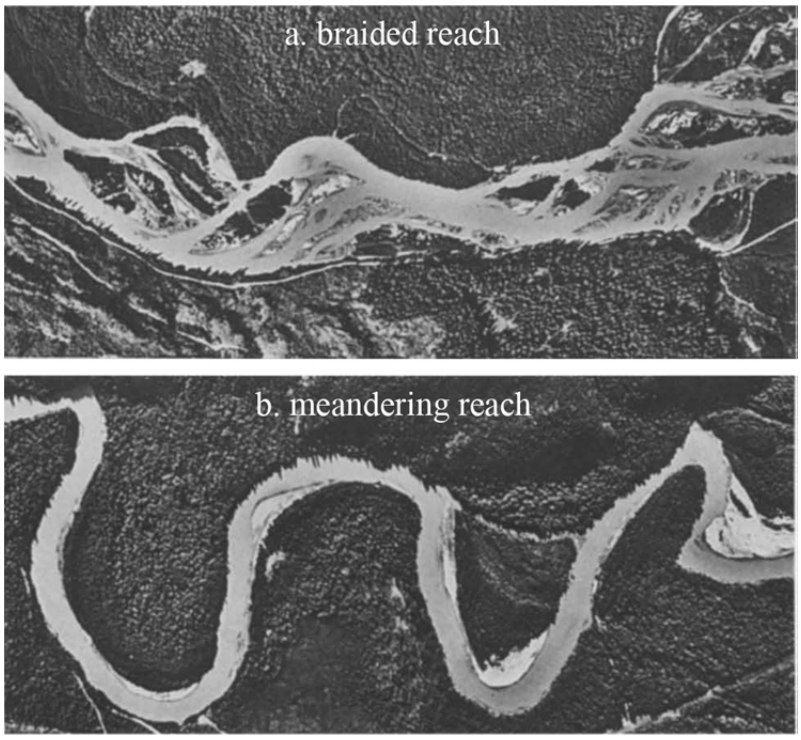

Figure 2.2 Channel planform changes in the Squamish River (Brierley and Hickin, 1991).

The sediment supply is an essential condition for braiding. Braiding may result from either a lack of capacity to transport the amount of bed material supplied, or a lack of competence to remove the large fractions of sediment supplied from upstream reach (Knighton, 1998). The lower William River in Canada adjusted its channel from a relatively narrow and deep single-channel stream to a thoroughly braided pattern after picking up a 40-fold increase of bed load over a 27 km reach (Smith and Smith, 1984). The channel width, width/depth ratio and braiding intensity all increase downstream under a constant discharge.

Large floods are the main cause of river adjustment and play important roles in channel morphologic changes. Characteristics of braided rivers are studied frequently

in connection with floods, since dune and bar formation are the most dramatic and spectacular at high stages (Kiss, 2007). Widened channel sections under large floods can be considered as large-scale riffles and provide prominent locations of braid bar formation (Bridge, 2003). Ham and Church (2000) investigated the lower reach of Chilliwack River in Canada, which is partially braided, and found that large floods with a return period of about five years can be considered significant channel-forming events. Floods erode banks extensively, supplying considerable sediments to the active channel zone. Bertoldi et al. (2010) showed that large floods (with a return period longer than two years) can induce a complete rearrangement of the network configuration, while flood pulses (events on average occurring one or more times per year) mainly cause a few active branches yet still have a crucial role on the morphologic evolution of a gravel bed braided river.

Bank erodibility is also important for braiding evolution. Sediment and vegetation conditions are two important factors affecting bank erodibility. On one hand, sediment size, cementation and other properties strongly influence the erodibility of river banks. Where the banks are not easily erodible the development of the braiding pattern may be inhibited. Huang et al. (2004) studied flow patterns from minimum flow energy and found that meandering rivers may occur even as flow energy has reached the level for braiding, since scouring has been confined by relatively cohesive or vegetated banks. Bartholdy and Billi (2002) suggested that the channel gradient versus discharge plot of the Cecina River is very close to the braiding threshold but it does not braid, just because of the raised bank resistance

caused by cohesive bank deposits. On the other hand, vegetation reduces bank erosion by changing bank strength and resisting flow. Nevins (1969) reported how the Turdnganui River channel in New Zealand quickly converted from a braided to a meandering pattern under the planting of willow shrubs at some bends. Hickin and Nanson (1984) have shown that with the same erosive forces river banks which are bounded well by roots can offer far greater resistance than unvegetated banks.

Generally, though one single factor above can initiate braided rivers, in nature frequently two or more of them occur simultaneously. Moreover, it is very important to study rivers over an extended time span, because their appearance is controlled by the history of changing flow stages, and some geometries arise specially as a result of changing discharge, particularly the dissection and modification of emerging alternate, point and braid bars (Bridge, 1993).

2.2.1.2 Characteristics of Braided Rivers

Braided rivers are characterised by high width/depth ratio (>40), steep slopes, relatively high bed load (>11%) and generally low sinuosity (<1.3) (Miall, 1977). The braided reaches taken as a whole are steeper, wider and shallower than undivided reaches carrying the same flow (Leopold and Wolman, 1957). They normally have energetic flow, high bank erodibility and high or medium sediment supply (Knighton and Nanson, 1993). The deposits of braided streams normally are coarser than those of the other river types, and are dominated by sand or gravel (Miall, 1977).

Channel shifts occur much more frequently in braided streams than other river types. Major floods may be responsible for the onset of braiding as well as triggering

large shifts in channel position. Repeated division and joining of channels is another characteristic feature of braided rivers. The transition between flow convergence and the downstream division may be of fundamental importance to the development of braid bars (Ashmore, 1991b). Aggradation is associated with channel multiplication and bar deposition, while degradation has a correlation with channel pattern simplification and bar emergence (Hoey and Sutherland, 1991).

2.2.2 Non-uniform Sediment Transport

The transport of sediment particles in a river can be in the form of bed load and/or suspended load, depending on the size of sediments and the flow conditions. There is no definite division between them. Usually, the transport of particles by rolling, sliding and saltating is called the bed-load transport (van Rijn, 1984a). Braided rivers in mountain areas, normally with steep valley slopes and relatively in small scales, often transport sediments of large grain size even cobbles, in which bed load transportat dominants. Large braided rivers on plains are often characterised by suspended load transport. Suspended load may also contain some wash load, the portion of suspended load which is governed by the upstream supply rate instead of the bed material.

In the transport of sediment, local and downstream sorting is a typical characteristic for non-uniform rivers. However, Wilcock et al. (1988, 1993a, 1993b) have done some work to analyse the threshold shear stress and transport for non-uniform sediments, andhave found that in sand-gravel bed rivers all sizes of

sediments in a mixture begin to move at nearly the same bed-shear stress.

2.2.2.1 Bed Load

Normally, bed load transports in a thin layer near the bed. Based on the data obtained from flume experiments and natural rivers, van Rijn (1984a) investigated the motion of the bed load particles and established simple expressions for the particle characteristics and transport rate (for particles in the range of 0.2–2 mm). The effects of slope and bed form were also considered by van Rijn (1993). Besides, Englund and Hansen (1967), Marti and Bezzola (2009) and others developed different equations for bed load transport. Wu (2007) proposed a complete theory for non-uniform bed load transportation, with the bed load transport rate equation deducted from field and laboratory data which cover a wide range of sediment sizes from 0.062 to128 mm. Based on the equal mobility concept, Parker (1990) developed a gravel transport function for coarse sediments, with the lower boundary as 2 mm.

Braided rivers with bed load sediment are widely studied in nature and laboratory. These studies are focused on the flow pattern, sediment transport and sorting processes (Ferguson et al., 1992), braiding mechanism (Ashmore, 1991a), channel avulsion processes (Leddy, 1993) and so on. Some of these findings can be used to explain the process in braided rivers with suspended load.

2.2.2.2 Suspended Load

Unlike the bed load transport, the suspended load can be transported in the whole flow depth. Equations have been proposed by Engelund and Fredsoe (1967), van Rijn

(1984b) and Cao (1999) for near bed concentration of single-sized suspended load, and by Einstein (1950), Garcia and Parker (1991), Hu and Wang (1999) for the near bed fractional concentration of non-uniform sediments. Based on Bagnold's (1966) stream power concept, Wu et al. (2000) suggested relating the suspended load transport rate to the flow energy. Zhang and Xie (1993) derived a relationship between the suspended load transport capacity based on data measured from the Yangtze River and the Yellow River.

Compared with the frequent occurrence of braided rivers with bed load in mountain areas, suspended load transport plays a key role in the evolution of large braided rivers on plains which usually have mild bed slopes and large discharges. Typical large braided rivers with suspended load include the Brahmaputra River in Bangladesh and the Yellow River in China, both of which have been studied profoundly due to their important roles in human life (e.g. Cao et al., 2006, 2007; Sarma, 2005).

2.2.2.3 Sediment Sorting Processes

Deposition begins once the flow or shear velocity falls below the settling velocity of a particle, which for a given particle size is less than what is required for entrainment. Settling velocity is closely related to particle size, so that the coarsest fraction in motion should be deposited first, with progressively finer grains settling out as the flow velocity continues to fall (Knighton, 1998). Bed load and suspended load travel at different speeds and in different parts of the flow, leading to sediment sorting of grains with different settling velocities.

Bend sorting. At channel bends, classical bend sorting occurs with coarser sediment in deeper outer bends and finer sediment towards the shallower inner bends. The higher critical bed shear stress in the outer bends increases the transport selectivity. Fine and coarse fractions of the load are differentially routed in the bend, such that fine grains are swept inward over the point bar along the inside of the bend, while coarse grains are routed outward toward the pool, which is controlled by the balance between fluid forces and body forces (Clayton and Pitlick, 2007; Clayton, 2010). Ferguson (1993) pointed out that the periodic coarsening and fining of median bed-material diameter happen along each side of the channel as the talweg swings from side to side across and around alternate bars.

Bar sorting. River bed with bars may sort vertically through sorting in troughs and at the lee-side slopes. Due to preferential deposition of the coarse fractions, accumulation of coarse grains develops in bed troughs (Kleinhans, 2001, 2005) and winnowing of the finer fractions occurs in situations of partial transport (Blom, 2003). Sorting at the lee-side slopes occurs when coarse grains roll further down the lee face than fine ones, because they have greater velocities and experience less friction (Allen, 1982). Topographic sorting results from the tendency of coarser grains to be concentrated preferentially on topographic low surfaces (Frings and Kleinhans, 2008). Ashworth et al. (1992) suggested that the coarse bed load tends to be deposited on the bar head whereas finer sediment is deflected around the bar where it may be deposited on the tail.

Downstream fining. Generally in the upper reach of rivers, mean grain size of

sediment in the bed surface and in transport commonly decreases exponentially in the direction of flow (Bridge, 2003, Cui et al., 1996). This may be related to a reduction in sediment transport capacity (Wright and Parker, 2005).

Armouring. Sometimes an armouring layer develops where there are sufficient large immobile grains on an eroding bed to protect the potentially mobile grains underneath from entrainment. Although armour layers may strongly affect downstream fining in gravel-bed rivers, they are of minor importance for large sand-bed rivers (Frings, 2008a).

2.2.3 Braiding Mechanisms

The investigation of initiation and evolution of braiding has always been an important research area for its important role in understanding the morphodynamics in braided rivers. Central bar deposition, chute cutoff of point bars, multiple dissection of bars and avulsions have been suggested as the main braiding mechanisms (Ashmore, 1991a; Ferguson, 1993). Avulsion is considered as an important mechanism in the evolution of braiding and will be mainly discussed. Besides, bar dissection is also found in laboratory river experiments with bed load.

2.2.3.1 Avulsion

Avulsion is an important braiding mechanism in river processes. Generally, avulsion is defined as the relatively sudden switching of course from one channel to another (Ferguson, 1993). The activities of avulsion have been classified in different ways by some researchers. Based on a laboratory physical model study, Leddy et al.

(1993) and Ferguson (1993) summarised three main mechanisms of avulsion in braided rivers, including constriction avulsion, apex avulsion and chocking avulsion. Slingerland and Smith (2004) proposed three kinds of avulsions including: avulsion by incision (avulsion I), avulsion by progradation (avulsion II), and avulsion by annexation (avulsion III). Kleinhans (2010) suggested four kinds of avulsions including avulsion by incision and formation of a new channel (avulsion I), avulsion by progradation of splays of lacustrine deltas through which a dominant channel may eventually develop (avulsion II), by avulsion annexation of a small active or abandoned channel (avulsion III), and avulsion following the formation of a mouth bar with an unstable bifurcation (avulsion IV).

Some avulsions in different classifications are the same or similar to each other. Generally, they can be related in this way: 1) constriction avulsion: one case of avulsion by incision, avulsion II; 2) apex avulsion: another case of avulsion by incision, avulsion II; 3) choking avulsion: avulsion by progradation, avulsion III. Avulsion IV proposed by Kleinhans (2010) is mainly applicable for specific situations of floodplain and river mouth bar, respectively, which are not common in traditional braided rivers. Therefore, the classifications of Leddy et al. (1993), Ferguson (1993) and Slingerland and Smith (2004) are applied in the present study. Figure 2.3 presents a summary of these categories.

1) *Avulsion by incision.* Incision avulsions involve the erosion of new channels directly into the floodplain (Slingerland and Smith, 2004). As the flow proceeds down the floodplain, it seeks paths connecting areas of the lowest elevations until it

intercepts another channel or a downstream reach of the parent channel. Ferguson (1993) and Leddy et al. (1993) divided them into two categories according to different causes, including constriction avulsion and choking avulsion.

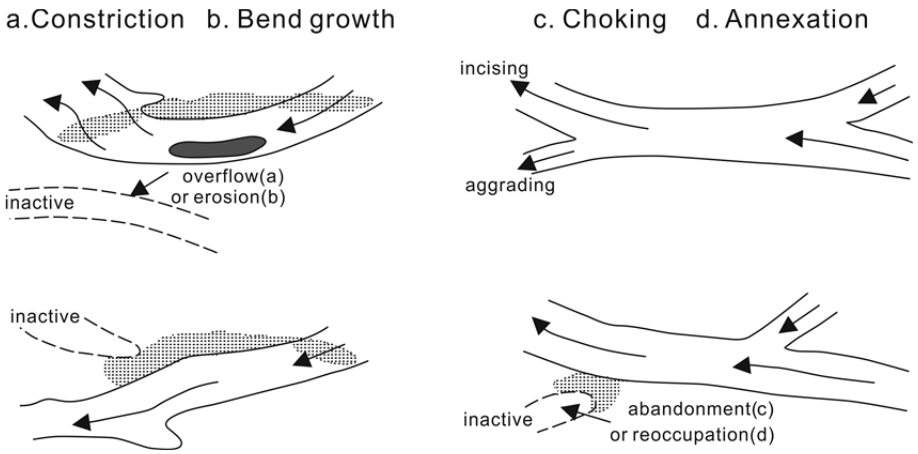

Figure 2.3 Avulsion activities in braided streams: (a) constriction avulsion; (b) apex avulsion; (c) choking avulsion; and (d) avulsion by annexation (adapted from Ferguson, 1993).

Constriction avulsion (*avulsion by incision 1*)*:* Flow ponded behind an aggrading diagonal bar front in upper diagram goes overbank into an adjacent inactive channel, and then incises headwards, causing abandonment of original channels (Ferguson, 1993). This type of avulsion involves constriction of one channel by the inward movement of a lobe from an adjacent channel which forces deflection of flow, rapid bank erosion and channel diversion into a topographically lower area (Leddy et al., 1993). The most favourable sites for constriction avulsion are channel junctions where one of the confluent channels might become dominant either in discharge or sediment supply.

Apex avulsion (*avulsion by incision 2*): It can be defined as an alternative

mechanism which has the same effect as constriction avulsion yet develops the new channel by bank erosion (Ferguson, 1993). It is connected with flow acceleration around a sinuous thalweg, subsequent lateral or point bar accretion on the inside of the bend and erosion and flow diversion on the outside of the bend (Leddy et al., 1993). As to the cause of apex avulsion in natural braided rivers, the occurrence of avulsion may be partly determined by the ratio between the avulsion course slope to the existing channel slope (Jones and Schumm, 1999), of which the value was found to be between 3 and 5 (Törnqvist and Bridge, 2002) or exceeds 5 (Slingerland and Smith, 1998).

2) *Avulsion by progradation* (*Chocking avulsion*). It is a kind of avulsion in which one anabranch of a confluence is choked and abandoned. In the field it often appears to follow a change in the discharge ratio of the channels entering the X unit (Ferguson, 1993). As to the cause of choking avulsion in natural braided rivers, Slingerland and Smith (2004) analysed the stability of bifurcating channels and suggests that thresholds in the relative energy slope and Shields parameter of the bifurcating channel system are key factors for causing avulsions. If sediment transport in two bifurcated channels is not in proportion to their sediment-carrying capacities, deposition or erosion will occur in one or both channels, thereby changing their discharges, slopes and/or cross-sections, and consequently changing their capacities.

3) *Avulsion by annexation.* It is a kind of avulsion related to the annexation of an active, partially active or abandoned channel which lies outside the dominant trunk channel (Slingerland and Smith, 2004). Sometimes avulsion by reoccupation is used

instead of annexation. Such floodplain channels are considered to be efficient ready-made conduits for routing some or all flow away from the diversion sites.

2.2.3.2 Central Bar Deposition

The central bar braiding mechanism is frequently cited in fluvial geomorphology studies. Leopold and Wolman (1957) reported the central bar braiding mechanism in a laboratory stream, which is caused by local decline in flow competence and sediment sorting, followed by channel scour and shift. Ashmore (1991a) described the central bar deposition in laboratory models, which began with the stalling of coarse bed load sheets and formation of the sedimentary nucleus of the mid-channel bar. Then it was enlarged by the lateral and headward accretion of portions of bed-load sheets that passed along the channel. The accretion process was accompanied by progressive downstream fining due to selective sorting of bed load around the bar: coarser sediment was deposited on the upstream bar margin while the finer sediment was transported through the bend to the downstream margin of the bar.

2.2.3.3 Chute Cutoff

Chute cutoff is a local, within channel type of avulsion (Ferguson, 1993). It is an erosion process which involves headwards incision by flow taking a short cut across the bar. In laboratory experiments, bed load sheets can grow into migratory lobate bars and scour pools on alternating sides of the channel (Ashmore, 1991a). Flow in the sinuous thalweg causes headward erosion, captures large volumes of water and enlarges rapidly. And then the new channel cuts across the transverse bar, which

grows into a medial bar. After the chute is cut off the original channel might be blocked as the new channel grows (Bridge, 1985). It is commonly reported in gravel-bed streams and laboratory with low sinuosity channels (e.g. Ashmore, 1991a). Actually it is also a well-known feature of meandering rivers (e.g. Carson, 1986). If the angle between the enlarging and filling channel segment is relatively small, as in low-sinuosity channels and chute cut-offs, flow is maintained in both the segments. With larger angles of divergence, both ends of the abandoned channel are quickly blocked.

2.2.3.4 Bar Dissection

The dissection of transverse unit bars developed downstream of confined channel section of flow confluences has been stated as another approach for braiding (e.g., Krigström, 1962). Bar dissection has been found in gravel-bed braided streams (Rundle, 1985a, 1985b). It was also suggested to be an important braiding mechanism in laboratory experiment by Ashmore (1991a). The evolution of braiding by bar dissection includes the formation of the transverse bar and its dissection, which have been described and analysed by Smith (1970, 1971). Braiding (bar dissection) begins during decreasing discharges when the flow passing through the bar mouth becomes unable to sustain active sediment transport over the entire bar surface. The development processes of bar dissection, chute cutoff and central bar deposition are illustrated in Figure 2.4.

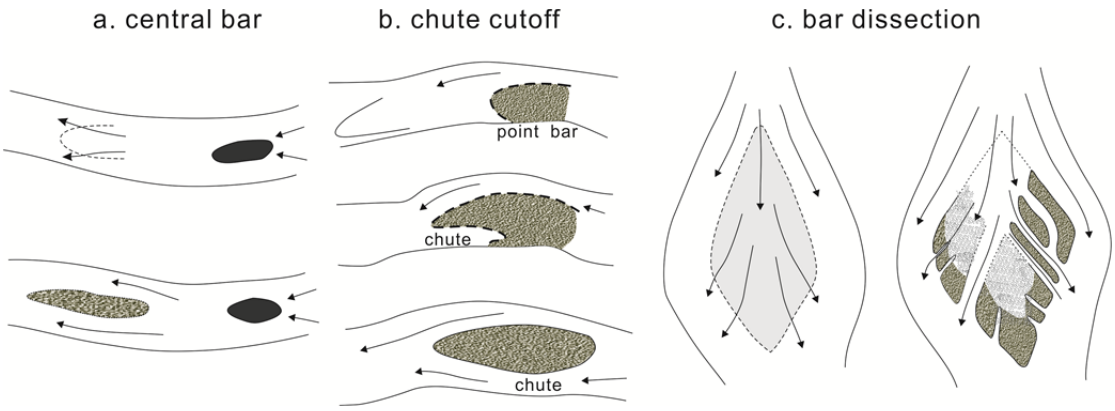

Figure 2.4 Braiding development by: (a) central bar deposition; (b) chute cutoff; and (c) bar dissection (adapted from Ferguson, 1993).

2.2.4 Essential Morphologic Units and Concepts

Confluence, bifurcation and bar between them are key morphodynamic nodes in braided rivers. Their flow field, sediment transport and channel morphology are important for Hydraulic and sedimentological behaviour in braided rivers. The instability of water and sediment distribution at the nodes has been demonstrated to play a crucial role in determining the planimetric configuration of the river network (Bertoldi et al., 2010). One essential recurring element in braided river pattern is the pool and bar unit, which consists of a constriction (the chute) followed by an expansion leading to separate talwegs on either side of a topographic high area (the lobe) (Ferguson et al., 1992).

2.2.4.1 Confluence

Stream confluences are important locations in drainage networks where abrupt changes in flow structure, sediment transport, and channel morphology occur to accommodate convergence of water and sediment from combining tributaries (Rhoads

et al., 2009). They play a key role in controlling the movement of bed material through braided reaches in that they act as funnels for the conveyance of material supplied from upstream. They are themselves a source of sediment as a result of bed scour, and often have bars deposited immediately downstream from which renewed braiding can develop (Ferguson et al., 1992).The principle variables which control the flow structure and channel morphology at confluence include the confluence angle and its planform asymmetry, the flow or momentum and sediment discharge ratios between the two confluent channels, and the degree of bed concordance between two confluent rivers (Szupiany et al., 2009).

Scour depth of confluences has been related to the confluence angle and the relative discharge of the anabranch channels (Mosley, 1976, 1982; Ashmore and Parker, 1983; Best, 1986, 1988). For a given relative discharge, the scour depth increases with the confluence angle and appears to approach an upper limit asymptotically (Bridge, 1993). For a given total discharge in the two channels, the scour depth decreases as the discharge concentrates in one of the anabranches (Mosley, 1976). However, Ashmore and Parker (1983) investigated the scour depth at confluences in gravel braided streams of laboratory experiments and field data and found that, the confluence angle is the major influence on scour depth, whose relationship is influenced slightly by the relative discharge of the two channels when the difference becomes large. Bed material sorting and cohesiveness also have impact on scour depth. Cohesive bed material generates markedly lower depth than noncohesive material, while poorly sorted sand may give slightly lower depths than

well sorted sand of the same mean size.

The geometry and orientation of confluence scour zones are influenced by the confluence angle and relative discharges of the entering channels. The scour zone may change from trough shaped to more basin-like as confluence angle increases (Ashmore and Parker, 1983; Best 1986). If the discharges of the two channels are similar, the long axis of the scour tends to bisect the confluence angle (Best, 1986). If one channel is dominant the axis of scour zones tends to parallel the direction of this channel (Ashmore and Parker, 1983; Best, 1987). The confluence angle may be larger at low flow stages relative to high flow stages, and the position of the confluence may be further upstream (Bridge, 1993).

The position of the confluence scour zone will shift in response to erosion of the outer banks of both entering channels and consequent deposition near the downstream tip of the upstream braid bar (Bridge, 1993). Szupiany et al. (2009) investigated the morphology, flow structure and suspended sediment transport of two large asymmetrical confluences and found that, the position of the scour hole can be predicted better by the momentum ratio between the cores of high velocity fluid than the momentum ratio across the entire channel width.

The confluence morphology of large sand bed braided rivers has been found to be similar with smaller confluences. Best and Ashworth (1997) showed the morphology of confluences in Jamuna River has a striking similar geometry to junctions of smaller natural channels and those in laboratory experiments, except that the bed slope leading into the scours is generally low angle without a significant

avalanche face. Moreover, secondary circulation is found in confluence scour holes, which plays an important role in river confluence morphology (Lane et al., 2000; Parsons et al., 2007). Biron et al. (2002) studied the confluences of two rivers, which could be extended to channel confluences, such as flow structure, morphology characteristic and water surface topography.

2.2.4.2 Bifurcation

Channel bifurcation mechanism represents the main cause of the braided nature of a river and strongly influences the way through which water and sediments are distributed and delivered further downstream (Zolezzi et al., 2006; Bertoldi and Tubino, 2007). The morphology and development of a bifurcation is mainly governed by the dominant sediment transport mechanism (Pittaluga et al., 2003): when suspended load is dominant, the partition of water discharge determines the sediment discharge rates into the downstream channels; when bed load is dominant the local bed slope may play a crucial role in governing sediment partition. The transverse exchange of sediment induced by topographical effects close to the channel division plays a key role on the stability of the bifurcation (Pittaluga et al., 2003). Local bed structure just upstream the bifurcation plays a crucial role in governing the dynamics of the bifurcation, while the alternate bars in the upstream channel do not have significant influence on it (Bertoldi and Tubino, 2007).

The division of the flow field into multiple flow threads and the associated growth of mid-channel bars have long been recognized to be fundamental for braiding evolution (Ashmore, 1991a; Ashworth, 1996). Federici and Paola (2003) observed

that flow divergence invariably leads to the formation of central bars for any Froude number and aspect ratio (width/depth) of the incoming stream. In the model of Ashmore (1991a) and Ashworth (1996), the divergence of flow drove the stalling of bed material around the centerline of the channel and the consequent development of bifurcation. Richardson and Thorne (2001) investigated the Brahmaputra River and found that the division of the velocity field into multiple threads within a single channel is a necessary prerequisite for bifurcation development. Bertoldi et al. (2005) established an objective criterion for the occurrence of the bifurcation using the laboratory data relating to the amplitude of width variations and channel sinuosity.

Bifurcations are almost invariably asymmetrical, particularly at relatively low values of the Shields stress, implying an uneven partition of low and sediment discharge in downstream channels (Bertoldi et al., 2005). Bifurcations in a braided river are typically unstable. The flow partitioning at a bifurcation is reflected by asymmetry in the width of the downstream anabranches and related to local bed aggradation in the main channel (Zolezzi et al., 2006). Besides, bend sorting upstream of a river bifurcation concentrates coarse grains in the outer bend and fine grains in the inner bend, which can cause bed load supply to the branch that originates in the outer bend to be very low (Frings and Kleinhans, 2008).

The above studies about the relationship between bifurcation and flow divergence may indicate that, braiding is a flow-driven phenomenon. The deposition of bed material load at the channel centre is driven by flow instability, and flow division is the only one cause of braiding. Therefore, the main mechanisms of

braiding are all initiated by bifurcation. Conversely, the dynamic behaviour of the bifurcation may be strongly affected by the development and migration of bar (Bertoldi et al., 2005).

2.2.4.3 Bars

Braid bars have a diverse range of planform shapes that are strongly stage dependent and grow by lateral, upstream and downstream accretion (Ashworth et al., 2000). Field studies of bar development are less than laboratory experiments, since it is hard to measure flow hydraulics and speed under the rapidly changing conditions in braided rivers. Figure 2.5 shows the talwegs, averaged flow velocity and erosion and deposition during different flow stages (Bridge, 1993).

Bed topography of bars changes with seasonally changing discharge (Bridge, 1993), shown in Figure 2.5. During rising flow stages erosion tends to occur in bend thalwegs, confluence scours and the upstream ends of bars, whereas these areas receive deposits during falling stages. In contrast, the downstream and topographically highest parts of bars tend to be areas of deposition at high flow stages, with erosion at low flow stages. The study of Ashworth et al. (2000) shows that at waning and low flow, the mid-channel bar widened through the lateral accretion of dunes onto the margins of the initial bar core, while during the next flood, the mid-channel bar extended its bar-tail largely downstream.

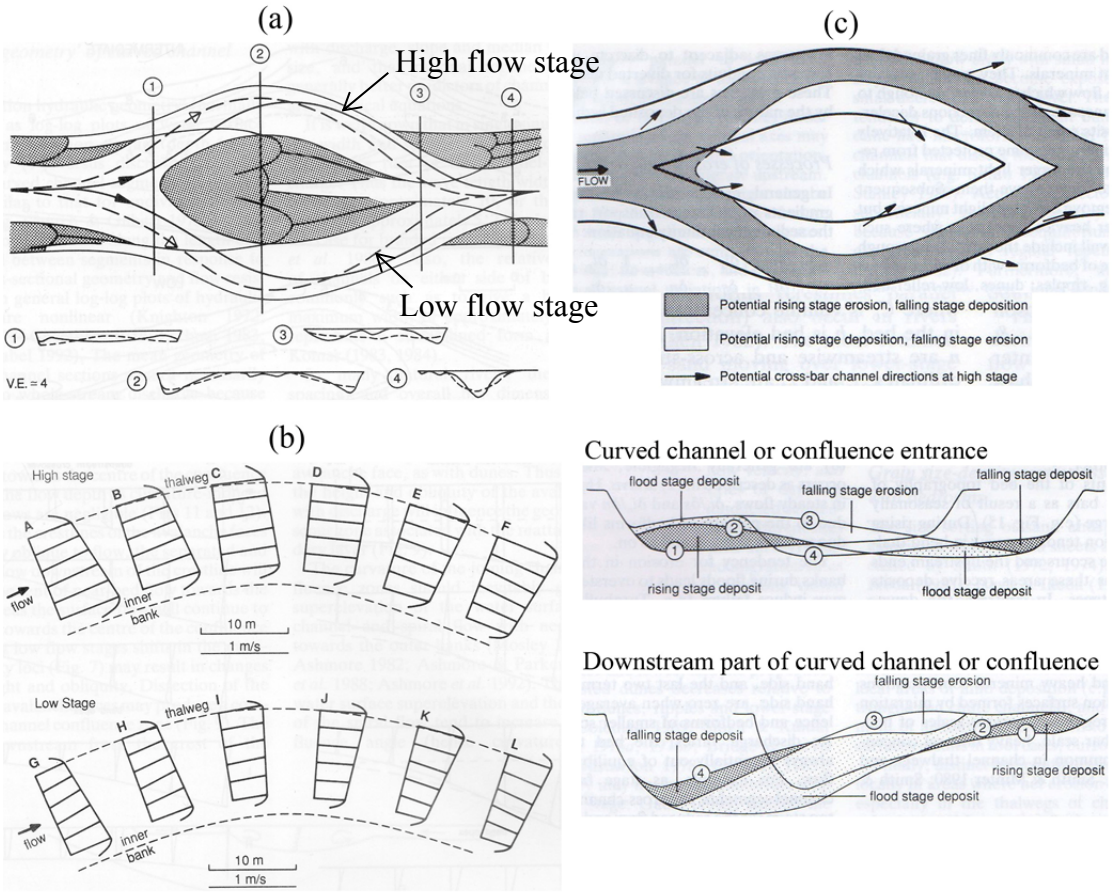

Figure 2.5 Flow velocity distribution and morphologic changes of braid bar (Bridge, 1993): (a) idealised channel geometry for typical braid bar; (b) theoretical vertically averaged flow velocity at high and low flow stage for curved channel segments; and (c) locations of erosion and deposition for changing flow stage.

Bar initiation is closely related to the development of bifurcation. Sediment transport is essential for the occurrence of instability in flow, and under appropriate conditions division of the flow into multiple threads is inevitable (Parker, 1976; Federici and Paola, 2003). Nonlinear analysis of stability phenomena within flow and sediment transport processes using the approach pioneered by Parker (1976) has produced theoretical criteria for braid bar development within single channels (e.g. Tubino, 1991; Crosato and Mosselman, 2009). Moreover, the development of bars in

braided rivers has also been explained from the view of energy consumption. For those over widened sections in braided streams, the river accumulates sediment either in the form of islands or bars (Fujita, 1989). Central bar formation is related to the widening and shallowing of high-gradient channels, which results in a decrease of the bed shear stress and the deposition of the coarser portion of bed load near the centre of the channel (Federici and Paola, 2003). Gradual enlargement of this deposit ultimately results in flow diversion, incision of the divided flow and exposure of a mid-channel bar.

Bars grow mainly by incremental lateral and downstream accretion (Best et al., 2003; Bridge and Lunt, 2006). As channels migrate lateral and downstream, the deposits from different parts of the channel bars get vertically superimposed (e.g., Bar head deposits overlying bar tail deposits, and bar tail deposits overlying confluence scour deposits). If erosion and deposition largely occur around the bankfull stage, the large flow velocity near the outer banks of the downstream half of the bends should result in dominantly downstream bend migration, which would lead to preferential preservation of bar tail scrolls and erosion of bar heads (Bridge, 1993). The principal mechanism of sand braid-bar growth is through the amalgamation of large dunes that form a central bar nucleus. Bar-top aggradation continues through both dune superimposition and development of accretionary dune on the bar-top and margin. It contributes to lateral and downstream bar growth, which ultimately deflects flow encouraging further bank and bed erosion, increasing channel sinuosity as the morphology develops.

As to flow talweg distribution around the bar, at high flow stage the channel segments near the upstream tip of the bar are deepest close to the bar, whereas further downstream they are deepest near the outer cut banks (Bridge, 1992). As discharge falls the thalwegs near the upstream part of the bar tend to move towards the outer banks in association with deposition near the upstream tip of the bar, resulting in a tendency to reverse the cross-sectional asymmetry of the channels here. Falling discharge would cause decreasing height and trimming margins of ancestral multiple-row alternate bars. Conversely, increasing discharge would result in increasing alternate bar height and the tendency to migrate downstream.

High shear stress and flow velocity occurred in the shallow flow over the depositional lobe, leading to consequent erosion and water depth (Ferguson et al., 1992). Whiting and Dietrich (1991) found that, local boundary shear stress decreases out of the upstream bend, increases over the bar top to values approaching the threshold for motion, and then decreases in deeper flow. The curvature of the converging channels in river confluences may give rise to super-elevation of the water surface in mid-channel and spiral flow with near-bed flow components towards the outer banks (Best et al., 2003).

Bridge (1993) summarised the sediment transport, deposition and bed sediment size distribution in bar areas. Studies of bed load transport in the curved channel segments adjacent to braid bars demonstrate that, the loci of maximum bed load transport rate and grain size are similar to those of mean flow velocity and bed shear stress. The largest mean grain sizes should occur in the base of the scour zone,

whereas the finest grains should occur immediately upstream of the scour zone and near the banks adjacent to the downstream end of the scour zone. With progression around a curved channel segment the bed load grains larger than the average tend to move preferentially towards the outer bank, whereas those finer than the average tend to move towards the inner bank. The coarser materials are buried below the advancing bed forms on the lee sides and the finer ones are transported further downstream. From a flume experiment Ashmore (1991b) found that near the river bed some internal sorting of sediment exists, with a tendency for coarse material to accumulate at the downstream margin and finer material to be concentrated near the centre. Ashworth et al. (1992) suggested that the coarse bed load tends to be deposited on the bar head whereas finer sediment is deflected around the bar where it may be deposited on the tail. Ferguson (1993) depicted that periodic coarsening and fining of median bed-material diameter happen along each side of the channel as the talweg swings from side to side across and around alternate bars.

2.2.4.4 Pool-bar Units

Alternating channels and bars form "pool-bar units" and then form braided rivers. Pool-bar units have been found by many field works and flume experiments as common elements in gravel-bed rivers of all channel patterns. But in braided rivers they are characteristic. It is referred to as "chute and lobe" in some previous works (e.g. Ashmore, 1991a; Ferguson et al., 1992). In braided streams, the pool-bar units occur alongside each other in two or more parallel rows. The pools are linked by talwegs which define two or more back-to-back meandering traces, alternately

converging and diverging (Bridge, 1993). Each braid bar is part of three separate pool units and thus presents a compound feature: the bar head is the distal part of one unit, and the left and right sides of the bar tail are lateral parts of two other units alongside each other.

2.2.4.5 Active Channels

Recently, active channels have been proposed by some researchers as an important variable to measure the activities of braided rivers (Ashmore, 1991a, 2001; Bertoldi et al., 2007; Bertoldi et al., 2009). Their observations suggest that at any given time, only a subset of the total channels is actually transporting bed material and actively forming the braided pattern and river morphology. The implication is that the braided channel network observed at a given time forms progressively over time by the shifting of a few active channels rather than by simultaneous development of all channels (Egozi and Ashmore, 2009). Active channels are found to be meaningful to the study of the instantaneous morphologic activity (e.g., the active width and braided index, the percentage of active bifurcations).

2.3 Braided River Modelling

Many numerical models have been developed to predict the morphodynamic process in the river systems. Braided rivers are simulated mainly using reduced-complexity approaches (Murray and Paola, 1994; Coulthard et al., 2007) and physics-based models (Jang and Shimuzu, 2005a, 2005b; Nicholas, 2013). Some other models were also developed, such as the linear model for the investigation of the

number migration of the alternate bars (Crosato and Saleh, 2011; Crosato et al., 2012), and random walk models mainly for braided channel system geometry (Howard et al., 1970; Webb, 1994, 1995).

2.3.1 Cellular Models

In recent years, cellular models, a type of simple and deterministic numerical models, have been widely used in modelling the morphodynamics of braided rivers (e.g. Tal and Paola, 2010; Coulthard and Van De Wiel, 2012). These models are based on the Cellular Automata method. A cellular model was first applied to investigate the conditions necessary for the occurrence of braiding by Murray and Paola (1994) and was quickly developed to model river avulsion activities, alluvial architecture and river catchment evolution for its efficiency in exploring the processes in long reaches and large catchment processes over useful time (e.g. Jerolmack and Paola, 2007; Coulthard et al., 2007; Hajek and Wolinsky, 2012).

A cellular model applies simplified versions of the complex flow and sediment transport equations rather than the discretization of the exact physics (Murray and Paola, 1994, 1997). Importantly, it does not include the calculation of water depth, flow velocity and flow momentum (Coulthard et al., 2007). Instead, it routes discharge downstream by allowing water to lower neighbouring cells referring to local variations in topography. The bed load sediment transport was considered by a nonlinear exponent (>1) to describe its relationship with flow discharge, with erosion and deposition included in the model. However, the model produced realistic braided

patterns, generating the dynamic behaviour of braided channel with the downstream and lateral migration of bars and channels, which is essential action for braiding occurrence. Moreover, it was suggested that the basic conditions for braiding generation include laterally unconstrained flow, mobile bed material and erodible banks. These models were also used to investigate the vegetation effect in influencing the braided channel pattern (Murray and Paola, 2003; Tal and Paola, 2010), and simulate river avulsion activities which was suggested to show some similar behaviours with the observations (Jerolmack and Paola, 2007).

Following the work of Murray and Paola (1994, 1997), a series of subsequent models led to the development of more advanced cellular braided river models. Nicholas et al. (2006) developed a novel nested modelling strategy which combines a high-resolution hydraulic model based on the shallow equations with a reduced complexity overbank sedimentation model and coarse resolution catchment sediment model. The model was used to predict the morphologic changes of braided river system due to upstream sediment supply (Thomas et al., 2007) and provide good predictions of some hydraulic variables in braided rivers (Nicholas and Quine, 2007). A novel scanning algorithm was adopted which can simulate flow movement in four directions, including the calculation of flow depth, a more detailed representation of sediment transport using multiple grain sizes and hill slope processes (Coulthard and Macklin, 2001; Coulthard et al., 2005). The model was applied to simulate the landscape evolution and the environmental impact on catchment and showed some promise in simulating braided streams and landscape evolution (e.g. Coulthard et al.,

2007). Recently, a cellular model was used to predict flow velocity and the predictions were compared with those by a physics-based model (Nicholas et al., 2012) and modelling river avulsion and alluvial architecture (Hajek and Wolinsky, 2012).

However, limitations exist in cellular models. First, the Murray-Paola model cannot develop realistic braided planform and topographic patterns when initialised with fully developed topography of a physical model, and it cannot predict flow velocity and depth precisely (Doeschl and Ashmore, 2005). Some new techniques have demonstrated that some planform and the topographic characteristics of the cellular model are different from that of a real river, such as the transect topographies and the cumulative frequency of lateral slopes (Doeschl et al., 2006). It was suggested that over-simplified representation of the flow and exaggerated sensitivity to local bed slopes are the main causes of these differences between the cellular model and the physical model. Second, in a cellular model, most morphologic changes are concerned nearly in one or two cells (Jerolmack and Paola, 2007). Although channel avulsion and reoccupation were captured in the modelled river, it is hard for them to represent the hydrodynamic and morphodynamic conditions during these processes. Third, some white-noise elevation perturbations may be needed for a cellular model to produce river braiding (Murray and Paola, 1997).

2.3.2 Physics-based Models

Physics-based models provide more valuable tools for the understanding of fluvial processes and morphologic evolution in braided rivers due to their better

representation in hydraulics and morphodynamics. Some physics models have been developed to simulate the sediment transport, bed deformation, evolution of bifurcation and bar, and sediment downstream fining in rivers (Cui et al. 1996; Duc et al., 2004), and have shown considerable potential for simulating braided river morphodynamics (Jang and Shimuzu, 2005a; Nicholas, 2013). Local important nodes in braided rivers including bar (Luchi et al. 2010), bifurcation (Pittaluga et al., 2003) and confluence have been studied separately and advances have been made in these areas. Important research results in braided river morphology and process modelling using physics-based models are introduced in detail. Generally, three aspects including the hydrodynamics, sediment transport and bed morphologic change compose the numerical models in representation of the morphodynamics of braided rivers.

2.3.2.1 Hydrodynamic Models

In the present physics-based models which have been applied to study the morphodynamics in braided rivers, 2-D depth-averaged shallow water equations are most commonly considered for the hydrodynamic model (e.g. Takebayashi and Okabe, 2008; Nicholas, 2013). A moving boundary-fitted coordinate system was applied to simulate the deformation of the side banks (Jang and Shimizu, 2005a; 2005b). The effect of secondary flow was determined by different ways, such as included in the shallow water equations with a function of the spiral flow intensity which is related to the streamline radius of curvature (Nicholas, 2013; Schuurman and Kleinhans, 2011), included in the sediment transport rate equation by curvature (Jang and Shimizu,

2005a; 2005b; Takebayashi and Okabe, 2008), and combined in the calculation of the dispersion stresses as Lien et al. (1999) did.

The 2-D shallow water equations were solved with the implicit scheme ADI (e.g. Williams et al., 2013; Wang et al., 2010a, 2010b) and some explicit schemes such as the CIP scheme without time-splitting technique (Jang and Shimizu, 2005a, 2005b) and TVD-MacCormack scheme (Takebayashi and Okabe, 2009). The ADI has been tested to be very useful in balancing numerical accuracy with computational efficiency, which works well for slow flow, when the Froude number is much less than unity. Nevertheless, the ADI method is not suitable to calculate trans-critical flows with the Froude number approaching or exceeding unity. Therefore, in the present study the laboratory river modelling with shallow water and high flow speed are completed with the TVD-MacCormack scheme.

However, as in braided rivers, supercritical flow may exist in local areas in braided rivers with bed load (Egozi and Ashmore, 2009; Takebayashi and Okabe, 2009), TVD scheme might be more efficient in solving the conservation equations. The TVD scheme was put forward by Harten (1983) and was used in hydrodynamics for free-surface flow in recent decades, especially in simulating the problem of complex dam-break flow (Ming and Chu, 2000; Liang et al., 2006, 2007). It is a kind of shock-capturing scheme which is efficient in simulating rapidly varying flows (Wang et al., 2000). The modelling of braided rivers with bed load which often occur in mountain areas may benefit from the application of TVD scheme in solving the shallow water equations.

2.3.2.2 Sediment Transport Models

Both of suspended load and bed load transport have been considered in the present braided river modelling work. Nicholas (2013) divided sediments into two grain size fractions of sand and tilt, and modelled the sediment transport in an equilibrium way with the transport rate applying Engelund-Hansen equation (Engelund and Hansen, 1967) for both of suspended load and bed load. Bank erosion was considered only in the computation of silt size fraction. The effect of gravity on sediment in motion on a sloping bed was considered by introducing a component of sand transport normal to the flow. Jang and Shimizu (2005a, 2005b) and Takebayashi and Okabe (2009) calculated the sediment transport rate along stream line by the formula of Ashida and Michiue (1972), with the gravity effect on the side bank included. Sediment transport rate in the normal to the stream line used the equation of Hasegawa (2000) including the secondary flow. Wang et al. (2010a, 2010b) adopted a non-equilibrium equation for simulating the sediment transport process. Lotsari et al. (2013) calculated the sediment transport rate by the equations of Meyer-Peter and Müller (1948) and van Rijn (1990). Sediment transport including effects of transverse slope and mass conservation of sediment were considered in the 3-D Delft model (Schuurman and Kleinhans, 2011).

The fractional method has been proposed by many researchers, yet rarely used in sediment transport simulation in the present models for braided river simulation. However, the size distribution of sediments in transport varies with time due to consecutive aggregation and disaggregation processes. Different critical shear stresses

and transport rates exist in non-uniform sediments (Wu, 2007). Consequently, it is necessary to consider sediments in multiple fractions. The different transport modes for suspended load and bed load also make it necessary to adopt different transport equations respectively. The sediment transport modes of different sizes in a mixture have been studied by some researchers such as van Rijn (2007) and Wilcock (1988, 1993a).

2.3.2.3 Bed Evolution Models

During river evolution process, the amount of sediment in transportation is primarily determined by the sediment transport capacity of flow, under which erosion occurs, otherwise deposition occurs. In modelling river morphodynamics, the bed change process is essential in channel morphologic evolution. The deposition and erosion related to suspended load and bed load have been incorporated into bed morphologic change equations (e.g. Wu, 2007). The size composition of bed material may vary along the vertical direction due to historical sedimentation. To consider this vertical variation, the bed above the non-erodible layer is often divided into multiple layers, with the top layer being the mixing layer. Nevertheless, this multiple layer concept has rarely been used in the present braided river models.

The effect of bank erosion is important for the braided pattern generation. As river develops and channel widens with an erodible bed and banks, local bank erosion causes the emergence of bars and the initiation of meandering or braiding (Jang, 2005b). Previous studies examined the mechanical processes of channels with erodible banks theoretically (Ikeda et al., 1981; Parker et al., 1982), and have

proposed methods to reproduce lateral changes in the channel. Many of the present physics-based models for braided river simulation include the effect of bank erosion (e.g. Jang, 2005b; Nicholas, 2013), and have shown their important role in braiding evolution process.

The 2-D based shallow water equations were solved with the implicit scheme ADI (e.g. Williams et al., 2013; Wang et al., 2010a, 2010b), and some explicit schemes such as the CIP scheme (Jang and Shimizu, 2005a, 2005b) and TVD scheme (Takebayashi and Okabe, 2009). The effect of secondary flow was considered by different equations, sometimes in a simple way. With these models, the braided pattern and its continuum have been produced with many morphologic elements observed in natural rivers (e.g. Nicholas, 2013; Jang and Shimizu, 2005b). Suspended load and bed load have been considered in one model (e.g. Nicholas, 2013).

However, despite all these achievements, there are still limitations in braided river simulation. For example, few of the present calculation schemes for the solution of shallow water equations can solve supercritical flow, which exists in some shallow areas in natural rivers. In few of the present models, suspended sediment transport is considered in a full two dimensional advection-diffusion equation, and the transport of bed load is mostly calculated in an equilibrium way. Fractional method for sediments has rarely been used, yet sediment gradation plays an important role in calculating bed erosion and deposition. The changes in bed sediment distribution with channel evolution have rarely been studied. Few models consider the river bed in multiple bed layers while vertical bed material sorting is important for sediment

concentration and bed sediment distribution. Besides, white noise or disturbance sometimes plays important role in braiding process (Nicholas, 2013; Wang et al., 2010b; Schuurman and Kleinhans, 2011). Moreover, although some of these models produced similar braided patterns and channel avulsions observed in natural rivers (Singerland and Smith, 2004; Schuurman and Kleinhans, 2011), they have rarely quantitatively discussed the essential causes for braiding mechanisms and the consequential changes in sediment transport, morphology, and sediment fining and coarsening observed in natural rivers (Ashmore, 1991a; Leddy, 1993).

2.3.3 Methods for the Assessment of Numerical Models for Braided Rivers

Given that braided rivers in nature exhibit some intrinsic characteristics, several methods have been proposed to evaluate the simulation ability of physical and numerical models (e.g. Murray and paola, 1996; Doeschl et al., 2005). Generally, two main sets of characteristics identify and describe a braided river: the intrinsic spatial and temporal scales that distinguish a particular braided river from another, and the scale-invariant properties common to all braided rivers (Doeschl et al., 2006). Some of these characteristics have been used to compare the simulation results with natural rivers to evaluate simulation ability of numerical and physics-based models.

2.3.3.1 Intrinsic Spatial and Temporal Scales

Intrinsic spatial and temporal scales are normally described by braiding indices, sinuosity indices, the total or average width and the average confluence-confluence distance. Various braiding indices have been used to measure braiding intensity,

basically from the total channel length, the number of channels and bar dimensions and frequency in a given river length (Brice, 1960, 1984; Rust, 1978; Hong and Davis, 1979; Mosley, 1981; Ashmore, 1991b; Friend and Sinha, 1993). It has been demonstrated that some equivalent relationships may exist between these indices, such as a possible universal function with active braiding intensity and total braiding sinuosity, and they are sensitive to river stages (e.g. Bertoldi et al., 2006; Egozi and Ashmore, 2008, 2009).

Channel length indices

Total sinuosity was first proposed by Hong and Davis (1979), as an index defined by the total length of channels ($\sum L_L$, L_L= length of the Lth channel) divided by the reach length (L_r). It is a combined measurement of channel-segment sinuosity and degree of braiding. Ashmore and Sauks (2006) defined an effective width, which was calculated from the division of the water area by the total length of the visible river reach and equal to the average wetted width (AWW). Egozi and Ashmore (2008) used it to study the minimum channel length to obtain a stable estimate of reach-averaged braiding intensity and found that it was at least 10 times the average wetted width. Total sinuosity is a combined measure of channel-segment sinuosity and degree of braiding so that braided rivers with relatively large numbers of channel segments of low sinuosity can have a similar total sinuosity to those with fewer, higher sinuosity channel segments (Bridge, 1993). Therefore, it is necessary to define the braiding index separately by average sinuosity.

Average sinuosity is defined as either channel thalweg length/valley length,

channel length/valley length, or channel length/channel-belt axis length (Bridge, 1993). As suggested by Rust (1978), the sinuosity of a multiple-channel river can be defined as average thalweg length of channel segments of a given order at a given flow stage. Friend and Sinha (1993) used the centreline length of the widest channel in a braided river to define sinuosity. Bridge (1993) summarised the definition of average sinuosity as either channel thalweg length/valley length (Rust, 1978), channel length/valley length (Brice, 1984; Schumm, 1985), or channel length/channel-belt axis length (Brice, 1964).

Channel count index

Frequent joining and separating channels are the key characteristics of braided rivers. The number of links or braids (confluence and bifurcation) for a certain distance can reflect the frequency of this activity, or in other words, the intensity of braiding. Howard et al. (1970) and Hong and Davis (1979) proposed two related channel count indices, including the mean number of links intersected by a number of cross-sections and the total number of links in the measured reach. Others also have used number of channels in cross-section (Hong and Davies, 1979; Chew and Ashmore, 2001) or mean number of active channels per transect or mean number of active channel links in braided network (Ashmore, 1991b).

Braiding intensity

Total braiding intensity (BI_T) and active braiding sinuosity (BI_A) have been proposed to measure the channel intensity in braided rivers (Ashmore, 1991b, Egozi

and Ashmore, 2009). Total braiding intensity is defined as the number of wetted channels counted and averaged over a number of cross-sections. Active braiding intensity is conceived as referring to the network of channels that is transporting bed material load, i.e., that portion of the network that is actively involved in the channel morphodynamics at a given time and flow level. The relationship between total braiding intensity (BI_T) and active braiding intensity (BI_A) has been analysed by Egozi and Ashmore (2009).

2.3.3.2 Scale-invariant Properties

Scale-invariant properties indicate that although braided rivers are characterised by continually unstable and evolving morphology, the overall average morphology is statistically stable (Paola, 2000; Doeschl et al., 2006). These properties present statistical scale invariance in the spatial structure of braided rivers. They might indicate the presence of universal features (statistical similarities) between braided rivers of different scales that result from the same underlying mechanical processes inherent in all braided rivers (Sapozhnikov and Foufoula-Georgiou, 1997). Therefore, a model that claims to represent the mechanical processes of braided rivers should reproduce these scale-invariant properties. The scale-invariant properties have been mainly evaluated by state-space plots and spatial scaling (e.g. Sapozhnikov et al., 1998). Moreover, some transect topographic properties, such as the transect bed elevation feature and the elevation and the cumulative frequency of the link length or slope, were also used to analyse the scale-invariant property (Doeschl et al., 2006).

State-space plots

State-space plots have been used to evaluate the sequential organisation of the river pattern by plotting sequences of some characteristic variables, such as river widths and sequential scour depths or heights of bars and assessing the properties of the planform geometry and topography, respectively. These plots mainly have been used to study the periodical characteristics of the overall morphology in braided rivers. This method has been applied to natural rivers and physical and numerical models, and some common features among them were found (Murray and Paola, 1996; Rosatti, 2002). In natural braided rivers, patterns of wide shallow sections and narrow deep channels often occur alternatively. Consequently, the sequential channel widths may form some loops, shown in Figure 2.6.

Traditional statistical methods miss some information available in the spatial relationships among the elements of a pattern, and it is very important in a system such as braided rivers that the ordering be quite sensitive to the underlying mechanics. Therefore, a method based on the statistical analysis of "state-space plots" was developed to evaluate the spatial patterns of braided rivers (Murray and Paola, 1996). In these types of plots, the position of the system is plotted in a state space that has an axis or dimension for each important variable except time. If only one of the variables that are important for a system can be measured, the state-space pattern can be reconstructed using a series of values of that variable by plotting each value versus the previous values. When the state plot moves from one point to the successive points and eventually forms a closed loop, it records the information on special ordering. The

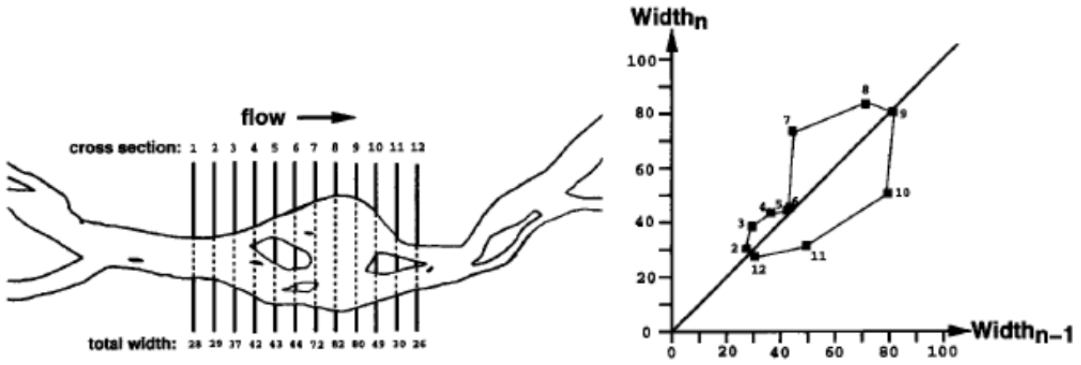

(a)

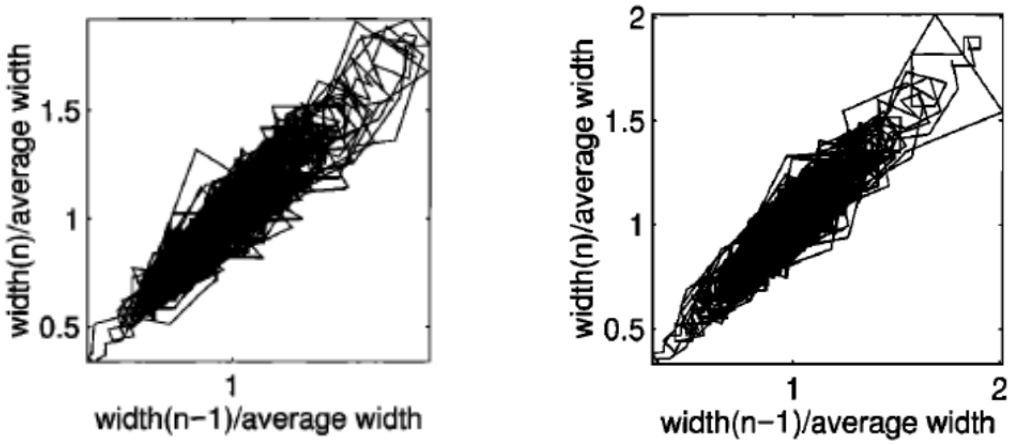

(b)

Figure 2.6 Signification and examples of state-space plots: (a) how a state space plot is constructed (Murray and Paola, 1996); and (b) state-space plots of the Aichilik River and a river produced by a cellular model (Sapozhnikov et al., 1998).

state-space plots have been applied to study spatial characteristics of braided rivers in nature, laboratories, numerical models and some sequential space features. Sapozhnikov et al. (1998) applied it to compare braided rivers from nature with results produced by cellular model, and found it can reveal and quantify subtle characteristics of the river pattern and permit to test a model. Moreover, Rosatti (2002) used state-space plots combined with some other methods to validate a physical model and concluded that main features of braided rivers can be correctly reproduced

in experimental channels if the laboratory tests are carefully performed. Doeschl et al. (2006) proposed some new parameters to test morphologic properties with topographic and dynamic data, such as sequential scour depths or bed elevations below and above a certain reference level instead of wet and dry pixels as criteria.

Self-scaling

Scaling properties have been investigated in natural braided rivers and models and were demonstrated to be valid in a wide range and type of rivers (Korvin, 1993; Sapozhnikov et al., 1998; Rosatti, 2002; Kelly, 2006). Scaling characteristics exist in the channel patterns of real braided rivers, which means within some scales, if a small part of a braided river is stretched in a certain way, it will look statistically the same as a bigger part of the river. How do braided rivers show scaling and whether they are self-similar or self-affine were studied in the past twenty years (Nykanen, 1998; Foufoula-Georgiou and Sapozhnikov, 2001; Rosatti, 2002; Walsh and Hicks, 2002). The results showed that braided rivers including natural, experimental and numerical rivers are self-affine, though their scaling coefficients vary in a wide range. Some natural rivers exhibiting spatial scaling characteristic are shown in (Sapozhnikov and Foufoula-Georgiou, 1996). The scaling exponents of rivers from nature, laboratory and numerical model are shown in Figure 2.7.

The anisotropic analysis follows the procedure proposed by Sapozhnikov and Foufoula-Georgiou (1996). It includes the following steps (Rosatti, 2003): 1) A rectangular box of size X*Y, where X and Y are odd multiples of the pixel width, is centered on a black pixel; 2) the number of black pixels inside the box are counted

and the mass is computed by multiplying the number by the area A of the pixel; and 3) Steps 1 and 2 are repeated, centering the box on all black pixels.

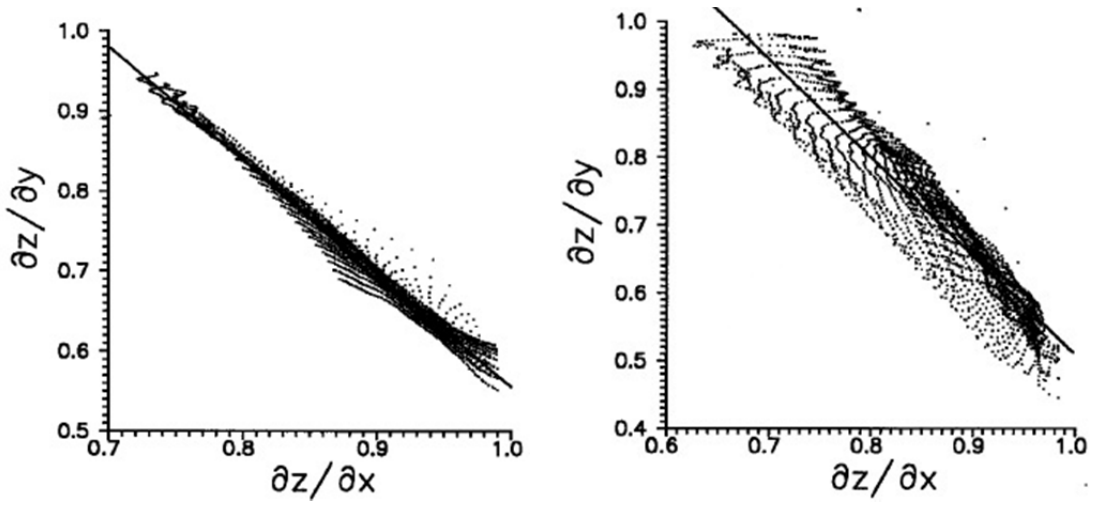

Figure 2.7 Spatial scaling examples of real rivers: the Aichilik River and the Brahmaputra River (Sapozhnikov and Foufoula-Georgiou, 1996).

Table 2.1 Scaling parameters of different rivers

Authors	River model	v_x	v_y	v_x / v_y
Sapozhnikov,1996	Three natural rivers	0.72–0.74	0.51–0.52	1.41–1.45
Nykane et al., 1998	The Tana River	0.70–0.77	0.47–0.50	1.54–1.57
Rosatti, 2002	Laboratory model	0.645	0.424	1.52
Sapozhnikov,1998	Cellular model	0.75–0.97	0.47–0.52	1.46–1.95

The mean mass M(X, Y), associated with the box size X*Y, is then given by

$$M(X,Y)=\frac{1}{N_b}\sum_{j=1}^{N_b} A\cdot n_j(X,Y) \qquad (2.\ 1)$$

where N_b = number of black pixels in the picture; and n_j (X, Y) = number of black pixels contained in the box (X*Y), centered at the pixel *j*. Boxes extending outside the inflow-outflow boundaries were disregarded.

According to Sapozhnikov and Foufoula-Georgiou (1995), considering mass M as a self-affine object within an X*Y rectangular, there is a mathematical relationship which can be expressed as

$$\mathrm{M(X,Y)}\sim \mathrm{X}^{\frac{1}{v_x}}\sim \mathrm{Y}^{\frac{1}{v_y}} \tag{2. 2}$$

where v_x, v_y = scaling exponents in the x and y directions, respectively. The logarithmic function $z(x,y) = logM(X,Y)$, where $x = logX$ and $y = logY$, satisfies the equation

$$v_x\left(\frac{\partial z}{\partial x}\right)+v_y\left(\frac{\partial z}{\partial y}\right)=1 \tag{2. 3}$$

or in another form

$$\frac{\partial z}{\partial y}=\frac{1}{v_y}-\frac{v_x}{v_y}\frac{\partial z}{\partial x} \tag{2. 4}$$

Equation (2.4) can be treated as a linear equation, which defines a linear relationship between the partial derivatives of the function $z(x,y)$ that can be used to estimate the fractal exponents.

The estimate can be obtained by two steps: (1) The correlation integral of the partial derivatives $\partial z/\partial x$ and $\partial z/\partial y$ can be computed by centred finite difference method, obtaining a couplet of values for each location (x, y); (2) Each couplet defines a point in a graph of $\partial z/\partial x$ versus $\partial z/\partial y$ and thus the parameters $1/v_x$ and $-v_{x/}v_y$ can be computed by the best fitting method (Rosatti, 2002).

However, caution has been proposed by Doeschl et al. (2006) that, fractal properties of a channel network can be attributed only to the self-organising nature of flow and sediment flux, but do not specify the particular fundamental processes and their degree of influence on these properties. So even if a model produces the

specified fractal properties, it is not guaranteed to incorporate all the essential processes contributing to a realistic braiding behaviour.

Bar scaling

Bars are a key expression of river behaviour and characterised by relatively high stream power, rapid rates of erosion and deposition and frequent channel and braid belt avulsions (Best et al., 2003; Rice et al, 2009). Scaling characteristics in real braided rivers and physical and numerical models have been analysed by many researchers (e.g., Sapozhnikov and Foufoula-Georgiou, 1996; Rosatti, 2002). As for bar scaling, Kelly (2006) studied the statistical significance from a dataset of modern and ancient braided rivers with both of suspended load and bed load and suggested that scale exists in bars characterised by hierarchy; therefore, it is possible to predict bar size when some channel characteristics are known. In addition, scaling in islands was also found and characterised by α in the perimeter-area relationship of $P \sim A^{\alpha}$ (Korvin, 1993; Rosatti, 2002).

2.4 Summary

The occurring environment, braiding mechanisms and morphologic processes in braided rivers have been investigated by many studies. However, the knowledge of river morphodynamics is still limited, such as the erosion and deposition processes during channel avulsions, the bed sediment distribution during river evolution process and so on. Moreover, it is useful for predicting channel changes during flood periods.

With the development of computing techniques, many numerical models have

been proposed for studying the complex morphodynamics in braided rivers, among which cellular models and physics-based models play important roles. Fruits have been achieved by cellular models for its ability in exploring the processes in long reaches and large catchment processes over useful time. Yet they have limitations such as the unrealistic braided planform and topographic patterns, and most morphologic changes being concerned nearly in one or two cells.

Compared with cellular models, physics-based models have showed their advantages in simulating the complex flow and morphologic changes in rivers, yet their development is just in an early stage. Although some models have been used to model the processes and morphologic changes in braided rivers, many deficiencies exist, such as the solution of supercritical flow, the transport of non-uniform sediments, vertical sorting effect and so on. Moreover, they have rarely quantitatively discussed the essential causes for braiding mechanisms and the consequential changes in sediment transport, morphology, and sediment fining and coarsening observed in natural rivers.

Further study needs to be undertaken to enhance model capability in the simulation of braided rivers. Firstly, since braided rivers are characterised by high flow energy with supercritical flow existing in local areas, it is important to model trans-critical flows. Secondly, though bed load plays a dominant role in bed morphology, the effect of suspended load cannot be neglected and should be included in bed deformation, especially in modelling large rivers on plains. Thirdly, as non-uniform sediment transport is essential in influencing the processes of coarsening

and fining in local units, it is important to apply the fractional method to the river models. Fourthly, to model the interaction between sediments and river bed, multiple bed layers should be considered for the vertical sorting process in bed. Most importantly, due to the difficulties in measuring flow and morphologic changes in natural rivers, it is meaningful to study the processes in braided rivers quantitatively by modelling work. The present study tries to develop a physics-based model including these effects, and analyse the braiding mechanisms and morphologic processes in braided rivers.

Chapter 3 Governing Equations for Hydrodynamics and Numerical Solution

3.1 Introduction

The morphologic evolution of a river is determined by the hydrodynamic condition and its interaction with sediment transport and bed morphology. The primary processes relating to river morphology are usually classified as hydrodynamic and morphodynamic processes, thus these two processes can be numerically treated separately. In this chapter, theories of hydrodynamics and solutions of its governing equations are presented.

For river flows, a 2-D hydrodynamic model is applied to describe the hydrodynamic process. The 2-D hydrodynamic equations and the significance of each term are first introduced in detail in this chapter. Then two solution methods are proposed for different hydrodynamic conditions. The ADI method is used to solve the hydrodynamic equations when the Froude number is less than unity. Meanwhile, the TVD method is integrated into the original model for solving the hydrodynamic equations when the Froude number approaches or exceeds unity.

3.2 Governing Equations for Hydrodynamics

3.2.1 Governing Equations

The numerical modelling of fluid flow is based on the principles of continuity of mass and conservation of momentum. Reynolds equations can describe the three-dimensional turbulent motion of incompressible fluid. The 3-D Reynolds equations for mass and momentum conservation can be derived from these principles in a Cartesian coordinate system (Falconer, 1993; Falconer et al., 2001). Furthermore, in the case where the horizontal length scale is much greater than the vertical length scale, the vertical velocity of the fluid is small. Under this condition, it is common to determine the velocity field using a 2-D depth-integrated numerical model. The 3-D Reynolds equations for incompressible and unsteady turbulent flow can be integrated over water depth ($h+\xi$) (Figure 3.1), resulting in the 2-D hydrodynamic equations of motion for flow. These equations are also called shallow water equations (SWEs), in which vertical velocity is removed by the integration over water depth.

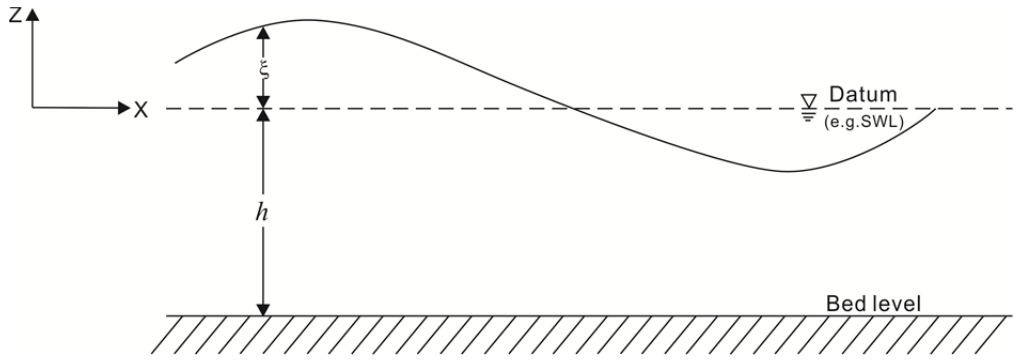

Figure 3.1 Coordinate system for depth-integrated equations.

The 3-D continuity equation can be integrated over flow depth to give the depth-integrated continuity equation, which can be written as

$$\frac{\partial \xi}{\partial t} + \frac{\partial p}{\partial x} + \frac{\partial q}{\partial y} = 0 \tag{3. 1}$$

where p, q = discharges per unit width in the x and y directions, respectively; and ξ = water surface elevation above datum.

Similarly, the depth-integrated momentum equations can be written as

$$\begin{aligned} \frac{\partial p}{\partial t} + \frac{\partial \beta p U}{\partial x} + \frac{\partial \beta p V}{\partial y} = {} & fq - gH\frac{\partial \xi}{\partial x} + \frac{\rho_a}{\rho} C_w W_x \sqrt{W_x^2 + W_y^2} \\ & - \frac{gp\sqrt{p^2+q^2}}{H^2 C^2} + \varepsilon\left[2\frac{\partial^2 p}{\partial x^2} + \frac{\partial^2 p}{\partial y^2} + \frac{\partial^2 q}{\partial x \partial y}\right] - F_x \end{aligned} \tag{3. 2}$$

$$\begin{aligned} \frac{\partial q}{\partial t} + \frac{\partial \beta q U}{\partial x} + \frac{\partial \beta q V}{\partial y} = {} & -fp - gH\frac{\partial \xi}{\partial y} + \frac{\rho_a}{\rho} C_w W_y \sqrt{W_x^2 + W_y^2} \\ & - \frac{gq\sqrt{p^2+q^2}}{H^2 C^2} + \varepsilon\left[\frac{\partial^2 q}{\partial x^2} + 2\frac{\partial^2 q}{\partial y^2} + \frac{\partial^2 p}{\partial x \partial y}\right] - F_y \end{aligned} \tag{3. 3}$$

where U,V = depth-averaged velocity components in the x and y directions, respectively; β = momentum correction factor for a non-uniform vertical velocity profile; f = Coriolis parameter due to the Earth's rotation; g = gravitational acceleration (= 9.806 m/s^2); H = water depth = $h+\xi$ with h = water depth below datum and ξ = water surface elevation above datum; ρ_a = density of air (≅ 1.292 kg/m^3); ρ = density of fluid; C = Chézy coefficient; C_w = wind resistance coefficient; W_x, W_y = wind velocity components in the x and y directions, respectively; ε = depth-averaged turbulent eddy viscosity; and F_x, F_y = drag force components induced by hydraulic obstructions per unit area in the x and y directions, respectively.

3.2.2 Denotation of Each Term

Advective terms

The advective terms describe the changes of momentum in the direction of flow. The non-cross term u∂u/∂x contains information of the velocity gradient in the same direction with flow, whereas the cross term v∂u/∂x contains information of the velocity gradient in the vertical co-ordinate direction. The more they are important, the larger the Reynolds number of the flow is. Due to their non-linearity, they may result in computational instability so that it is meaningful to neglect them under low Reynolds conditions.

The momentum correction factor

For an assumed logarithmic vertical velocity profile, the momentum correction factor β can be calculated by

$$\beta = 1 + \frac{g}{C^2 \kappa^2} \tag{3. 4}$$

where C = Chézy coefficient; and κ = von Karman's constant (= 0.4). The value of β is 1.016 for an assumed seventh power law velocity profile and 1.20 for an assumed quadratic velocity profile, respectively (Falconer and Chen, 1991).

Coriolis term

The Coriolis term represents the effect of the earth's rotation on flow. It is dependent on the latitude and flow velocity and acts at right angle to the flow. It deflects currents in channel and can indirectly influence river pattern and sediment transport, which can be expressed as

$$f = 2\omega_e \sin\theta_e \tag{3. 5}$$

where ω_e = 2π/(24×3600) = angular rotation speed of the earth; θ_e = geographical angle of latitude.

Surface slope term

This term represents the effect of gravity and takes into account both the topography and the water elevation. In the present study, the nonlinear term contains the mean depth (h) plus water elevation (ξ) and the derivative of water elevation ($\partial\xi$).

The effect of wind

Wind exerts a drag force on the flow by blowing over water surface. The shear stress at the air-water interface is calculated by assuming that it is proportional to the square value of the wind speed at a particular height above the water surface. Various empirical formulae have been proposed to calculate the air-water resistance coefficient in turbulent flow. In water bodies with strong currents such as estuaries and rivers, wind stress is often small compared with bottom shear stress. Nevertheless, it usually plays a predominant role in the open sea and lakes.

Turbulence

The turbulent shear stress presents the flow resistance associated with the random fluctuation of flow in space and time. The momentum exchange brought about by turbulence causes the velocity-depth distribution to be more uniform than that under laminar conditions. The turbulence model relates to Boussinesq's approximation for the mean shear stress τ_e in turbulent flow, giving

$$\tau_e = \varepsilon \frac{dv}{dy} \tag{3. 6}$$

where ε = eddy viscosity, which is dependent on the turbulence characteristics of flow and may be thousands of times larger than the molecular viscosity. Assuming the turbulent shear stress is dominated by bottom friction, a relationship between the Chézy coefficient and the eddy viscosity exists. The depth-integrated eddy viscosity ε is calculated (Fischer, 1979) from

$$\varepsilon = C_e \frac{H}{C} \sqrt{g(U^2 + V^2)} \tag{3. 7}$$

where C_e = eddy viscosity coefficient; H = water depth; C = Chézy coefficient; and U,V = depth-averaged velocity components in the x and y directions, respectively.

The turbulence model indicates the impact of bed generated turbulent momentum exchange on the overall time-averaged flow profile. This approach assumes that the turbulent shear stress is dominated by the turbulence near the bottom and is equal in the x and y directions. It cannot describe the turbulent fluctuation of velocity or specific flow features, yet its effect is to smooth velocity gradients and enhance the stability of the numerical solution.

Hydraulic obstruction Resistance

Hydraulic obstruction retards flow in a similar way to the bottom roughness, but is usually much larger than ordinary bottom friction. Many hydraulic obstructions exist in floodplains where natural vegetation and urban structures play an important role. In the present study, the effects of vegetation are ignored.

3.2.3 Bottom Friction

Bottom friction exerts a nonlinear, retarding effect on flow. It is very important for sediment transport due to its close interaction with sediment particles, which is presented here specifically. This effect is presented by the Chézy coefficient, which is a semi-empirical bottom friction coefficient. Under rough turbulent flow (Re >>1000) and an assumed logarithmic velocity-depth profile, the Chézy coefficient is assumed to be independent of flow and varies only with the relative roughness of the bed, giving (Falconer et al., 2001)

$$C = -18.0 * \log_{10}\left(\frac{k_s}{12H}\right) \tag{3. 8}$$

While under transitional flow conditions (R_e = 2000~4000), the Chézy coefficient varies with flow conditions, which can be calculated by

$$C = -18.0 * \log_{10}\left(\frac{k_s}{12H} + \frac{5C_0}{18.0 * R_e}\right) \tag{3. 9}$$

where k_s = roughness height; H = water depth; R_e = Reynolds number; and C_0 = the value of C in Equation 3.8.

The coefficient k_s denotes the equivalent roughness height of Nikuradse. It is a factor to describe the roughness degree of the river bed, and is important for sediment transport process, especially for bed load. Particle saltation length can be reduced by increasing the roughness height as it decreases the local flow velocity and thus the lift and drag forces. Coarse particles play a dominant role in determining bed roughness as they are more important than fine sediments in influencing the roughness height.

Different values of k_s have been stated by many researchers such as Engelund (1966) of $2.5D_{65}$, van Rijn (1984a) of $3D_{90}$ and Maynord (1991) of $2D_{90}$.

3.3 Numerical Solution for Hydrodynamic Equations

Usually the shallow water equations are solved with the alternating direction implicit (ADI) method. The ADI has been tested to work well for slow flow when the Froude number is much less than unity. However, it has difficulties in the solution of flows with the Froude number approaching or exceeding unity. Instead, the TVD scheme has been tested to solve trans-critical flow well. Thus it is chosen to solve the momentum and mass conservation equations of this kind of rivers.

3.3.1 ADI Method

3.3.1.1 Grid System and Finite Difference Form for ADI Scheme

The alternating direction implicit (ADI) technique is used in the finite difference scheme. It involves the sub-division of each time step into two half time steps, and only considers one dimension implicitly for each half time step instead of the solution of a full two-dimensional matrix. A space-staggered grid system is used in it (Figure 3.2). In the first half time step the water depth H, the unit width discharge p and the solute concentration S are solved implicitly in the x direction, while the other variables are represented explicitly. Similarly, in the second half time step, H, q and S are solved implicitly in the y direction, with other variables being represented explicitly. An explicit illustration for the calculation of the parameters, including ξ, ε,

C, *S*, *p*, *q*, *U*, *V*, etc., is shown in Figure 3.3.

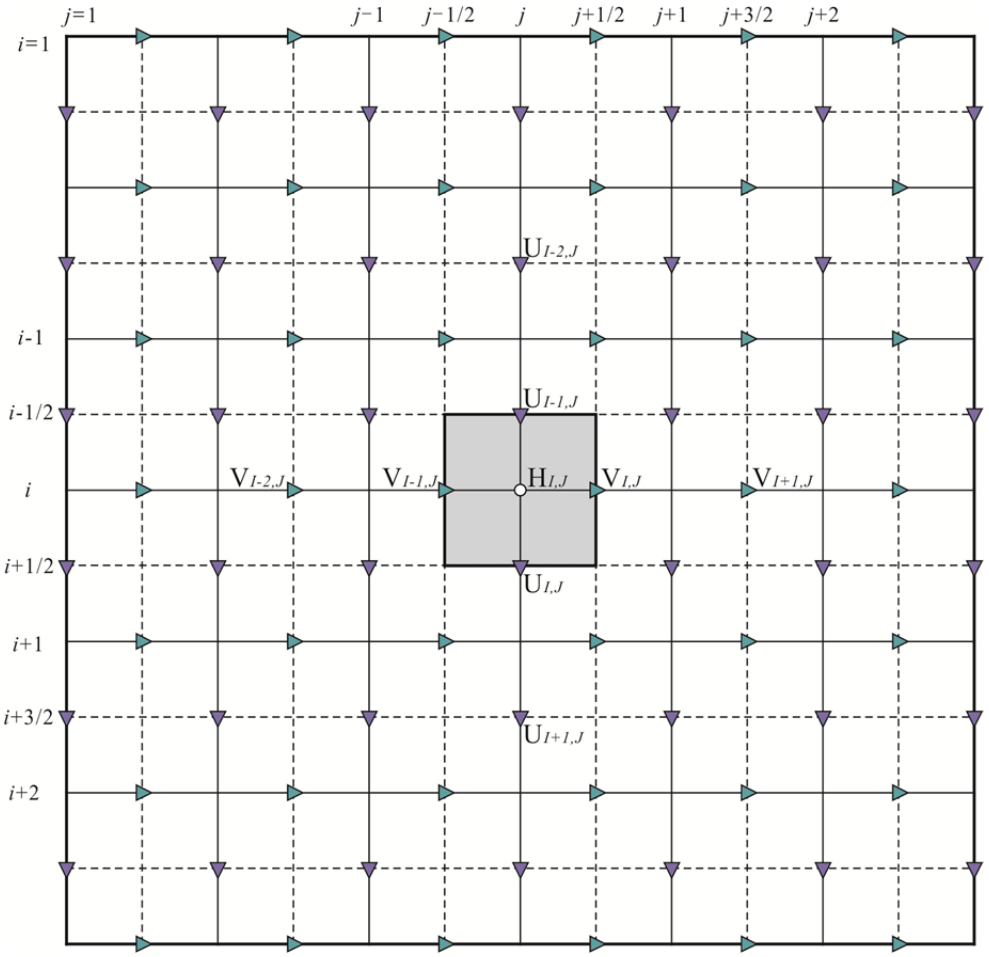

Figure 3.2 Velocities and depth points on computer grid with finite difference scheme.

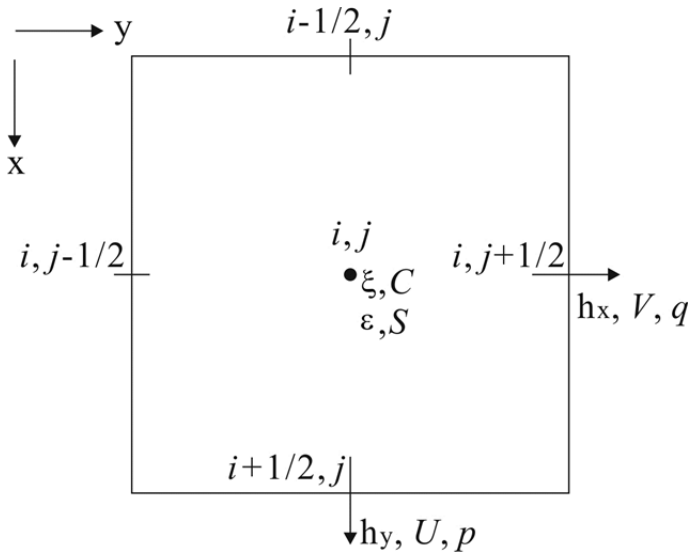

Figure 3.3 Finite difference grid notations with locations of parameters.

Note: h_x = depth below datum in the x direction at i+1/2, j; h_y = depth below datum in the y direction at i, j+1/2; and S = solute concentration at i, j.

The continuity equation (3.1) can be expressed in the first and second half time steps in the following forms, respectively

$$\frac{2}{\Delta t}\left(\xi_{i,j}^{n+1/2}-\xi_{i,j}^{n}\right)+\frac{1}{\Delta x}\left(p_{i+1/2,j}^{n+1/2}-p_{i-1/2,j}^{n+1/2}\right)+\frac{1}{\Delta y}\left(q_{i,j+1/2}^{n}-q_{i,j-1/2}^{n}\right)=0 \qquad (3.10)$$

$$\frac{2}{\Delta t}\left(\xi_{i,j}^{n+1}-\xi_{i,j}^{n+1/2}\right)+\frac{1}{\Delta x}\left(p_{i+1/2,j}^{n+1/2}-p_{i-1/2,j}^{n+1/2}\right)+\frac{1}{\Delta y}\left(q_{i,j+1/2}^{n+1}-q_{i,j-1/2}^{n+1}\right)=0 \qquad (3.11)$$

where i, j = grid point locations in the x and y directions, respectively; superscripts n, n+1/2, n+1 = variables evaluated at time $n\Delta t$, (n+1/2)Δt and （n+1）Δt, respectively; Δt = computational time step; and Δx, Δy = computational spatial steps in the x and y directions, respectively.

The momentum equation in the x direction (Equation 3.2) can be written in the following formation for the first half time step

$$\frac{p_{i+1/2,j}^{n+1/2}-p_{i+1/2,j}^{n-1/2}}{\Delta t}+\beta\left[\frac{\left(\hat{U}\hat{p}\right)_{i+3/2,j}^{n}-\left(\hat{U}\hat{p}\right)_{i-1/2,j}^{n}}{2\Delta x}+\frac{\left(\overline{\vec{V}}\vec{p}\right)_{i+1/2,j+1/2}^{n}-\left(\overline{\vec{V}}\vec{p}\right)_{i+1/2,j-1/2}^{n}}{\Delta y}\right]$$
$$=f\overline{q}_{i+1/2,j}^{n}-gH_{i+1/2,j}^{n}\frac{\left(\frac{\xi_{i+1,j}^{n+1/2}+\xi_{i+1,j}^{n-1/2}}{2}\right)-\left(\frac{\xi_{i,j}^{n+1/2}+\xi_{i,j}^{n-1/2}}{2}\right)}{\Delta x} \qquad (3.12)$$
$$+\frac{\rho_a}{\rho}C_wW_xW_s\sin\phi-\frac{g\cdot\frac{p_{i+1/2,j}^{n+1/2}+p_{i+1/2,j}^{n-1/2}}{2}\cdot\sqrt{\left(\hat{p}_{i+1/2,j}^{n}\right)^2+\left(\overline{q}_{i+1/2,j}^{n}\right)^2}}{\left[(HC)_{i+1/2,j}^{n}\right]^2}$$
$$+\varepsilon\left(\frac{\hat{p}_{i+3/2,j}^{n}-2\hat{p}_{i+1/2,j}^{n}+\hat{p}_{i-1/2,j}^{n}}{\Delta x^2}+\frac{\hat{p}_{i+1/2,j+1}^{n}-2\hat{p}_{i+1/2,j}^{n}+\hat{p}_{i+1/2,j-1}^{n}}{\Delta y^2}\right)$$

where $\hat{p}$ denotes a term that is updated by iterations, giving

$$\hat{p}^{n}=\begin{cases}p^{n-1/2} & \text{for the first iteration}\\ \frac{1}{2}\left(p^{n-1/2}+p^{n+1/2}\right) & \text{for the second and remaining iteration}\end{cases} \qquad (3.13)$$

$\hat{U}$ denotes a value corrected by iterations, giving

$$\hat{U}^{n}=\begin{cases}U^{n-1/2} & \text{for the first iteration}\\ \frac{1}{2}\left(U^{n-1/2}+U^{n+1/2}\right) & \text{for the second and remaining iteration}\end{cases} \qquad (3.14)$$

$\overline{q}$ and $\overline{V}$ represent flux and velocity values obtained by averaging corresponding values at surrounding grid points, giving

$$\overline{q}_{i+1/2,j}^{n}=\frac{1}{2}\left(q_{i,j}^{n}+q_{i+1,j}^{n}\right) \qquad (3.15)$$

$$\overline{V}_{i+1/2,j+1/2}^{n}=\frac{1}{2}\left(V_{i,j+1/2}^{n}+V_{i+1,j+1/2}^{n}\right) \qquad (3.16)$$

and $\vec{p}$ denotes a value obtained from the upwind algorithm where

$$\vec{p}_{i+1/2,j}^{n}=\begin{cases}p_{i+1/2,j-1}^{n} & if\ V_{i+1/2,j}^{n}>0\\ p_{i+1/2,j+1}^{n} & if\ V_{i+1/2,j}^{n}<0\end{cases} \qquad (3.17)$$

Similarly, the momentum equation in the y direction can be written for the second half time step, giving

$$
\begin{aligned}
&\frac{q_{i,j+1/2}^{n+1}-q_{i,j+1/2}^{n}}{\Delta t}+\beta\left[\frac{\left(\hat{V}\hat{q}\right)_{i,j+3/2}^{n+1/2}-\left(\hat{V}\hat{q}\right)_{i,j-1/2}^{n+1/2}}{2\Delta y}+\frac{\left(\overline{U}\hat{\overline{q}}\right)_{i+1/2,j+1/2}^{n+1/2}-\left(\overline{U}\hat{\overline{q}}\right)_{i-1/2,j+1/2}^{n+1/2}}{\Delta x}\right]\\
&=-fp_{i,j+1/2}^{n+1/2}-gH_{i,j+1/2}^{n+1/2}\frac{\left(\frac{\xi_{i,j+1}^{n+1}+\xi_{i,j+1}^{n}}{2}\right)-\left(\frac{\xi_{i,j}^{n+1}+\xi_{i,j}^{n}}{2}\right)}{\Delta y}\\
&+\frac{\rho_a}{\rho}C_wW_yW_s\sin\phi-\frac{g\cdot\frac{q_{i,j+1/2}^{n+1}+q_{i,j+1/2}^{n}}{2}\cdot\sqrt{\left(\hat{q}_{i,j+1/2}^{n+1/2}\right)^2+\left(\overline{p}_{i,j+1/2}^{n+1/2}\right)^2}}{\left[(HC)_{i,j+1/2}^{n+1/2}\right]^2}\\
&+\varepsilon\left(\frac{\hat{q}_{i+1,j+1/2}^{n}-2\hat{q}_{i,j+1/2}^{n}+\hat{q}_{i-1,j+1/2}^{n}}{\Delta x^2}+\frac{\hat{q}_{i,j+3/2}^{n}-2\hat{q}_{i,j+1/2}^{n}+\hat{q}_{i,j-1/2}^{n}}{\Delta y^2}\right)
\end{aligned}
\tag{3.18}
$$

3.3.1.2 Thomas Algorithm for ADI Scheme

Take the solution of the shallow water equations in the x direction as an example, the finite difference form of the momentum equation in the x direction, Equation (3.10), can be written as

$$
-a_i\xi_{i,j}^{n+1/2}+b_ip_{i+1/2,j}^{n+1/2}+c_i\xi_{i+1,j}^{n+1/2}=B_i^n \tag{3.19}
$$

where

$$
a_i=c_i=\frac{g\Delta t}{2\Delta x}H_{i+1/2,j}^{n};
$$

$$
b_i=1+\frac{g\Delta t\sqrt{\left(\hat{p}_{i+1/2,j}^{n}\right)^2+\left(\overline{q}_{i+1/2,j}^{n}\right)^2}}{2\left[(HC)_{i+1/2,j}^{n}\right]^2};
$$

$$
\begin{aligned}
B_i^n=&\left(1-\frac{g\Delta t\sqrt{\left(\hat{p}_{i+1/2,j}^{n}\right)^2+\left(\overline{q}_{i+1/2,j}^{n}\right)^2}}{\left[(HC)_{i+1/2,j}^{n}\right]^2}\right)p_{i+1/2,j}^{n-1/2}-\frac{g\Delta tH_{i+1/2,j}^{n}\left(\xi_{i+1,j}^{n-1/2}-\xi_{i,j}^{n-1/2}\right)}{2\Delta x}\\
&-\beta\Delta t\left[\frac{\left(\hat{U}\hat{p}\right)_{i+3/2,j}^{n}-\left(\hat{U}\hat{p}\right)_{i-1/2,j}^{n}}{2\Delta x}+\frac{\left(\overline{V}\hat{\overline{p}}\right)_{i+1/2,j+1/2}^{n}-\left(\overline{V}\hat{\overline{p}}\right)_{i+1/2,j-1/2}^{n}}{\Delta y}\right]\\
&+\varepsilon\Delta t\left(\frac{\hat{p}_{i+3/2,j}^{n}-2\hat{p}_{i+1/2,j}^{n}+\hat{p}_{i-1/2,j}^{n}}{\Delta x^2}+\frac{\hat{p}_{i+1/2,j+1}^{n}-2\hat{p}_{i+1/2,j}^{n}+\hat{p}_{i+1/2,j-1}^{n}}{\Delta y^2}\right)\\
&+\Delta tf\overline{q}_{i+1/2,j}^{n}+\frac{\rho_a}{\rho}\Delta tC_wW_xW_s\sin\phi
\end{aligned}
.
$$

The finite difference form of the continuity equation in the x direction can be written as

$$-d_i p_{i-1/2,j}^{n+1/2} + e_i \xi_{i,j}^{n+1/2} + f_i p_{i+1/2,j}^{n+1/2} = A_i^n \tag{3. 20}$$

where

$d_i = f_i = \dfrac{\Delta t}{2\Delta x}$;

$e_i = 1$;

$A_i^n = \xi_{i,j}^n - \dfrac{\Delta t}{2\Delta x}\left(q_{i,j+1/2}^n - q_{i,j-1/2}^n\right)$.

Equations (3.19) and (3.20) are rewritten for each time step, thus the water elevation and depth-integrated velocity are next obtained for $i = i_{\max}, \cdots\cdots 1$, giving

$$p_{i\max+1/2,j}^{n+1/2} = -R_{i\max}\xi_{i\max+1,j}^{n+1/2} + S_{i\max} \tag{3. 21}$$

$$\xi_{i,j}^{n+1/2} = -P_i p_{i+1/2,j}^{n+1/2} + Q_i \quad \text{for } i = i_{\max},\ldots\ldots 1 \tag{3. 22}$$

$$p_{i+1/2,j}^{n+1/2} = -R_i \xi_{i+1,j}^{n+1/2} + S_i \quad \text{for } i = i_{\max\text{-}1},\ldots\ldots 1 \tag{3. 23}$$

where for $i = 1, \cdots\cdots, i_{\max}$, parameters in these equations can be calculated by

$$R_1 = \frac{c_1}{b_1};\ S_1 = \frac{B_1^n + a_1 \xi_{1,j}^{n+1/2}}{b_1} \tag{3. 24}$$

$$P_i = \frac{f_i}{e_i + d_i R_{i-1}};\ Q_i = \frac{A_i^n + d_i S_{i-1}}{e_i + d_i R_{i-1}} \quad \text{for } i = 2,\ldots\ldots, i_{\max} \tag{3. 25}$$

$$R_i = \frac{c_i}{b_i + a_i P_i};\ S_i = \frac{B_i^n + a_i Q_i}{b_i + a_i P_i} \qquad \text{for } i = 2,\ldots\ldots, i_{\max} \tag{3. 26}$$

Combining the boundary equations (Equations 3.21 and 3.24) with the rotation equations (Equations 3.22, 3.23, 3.25 and 3.26), time series of water elevation and flow discharge per width in the x direction can be calculated. Similarly, time series of water elevation and flow discharge per width in the y direction can be obtained.

3.3.2 TVD-MacCormack Method

The TVD-MacCormack Scheme applied in the present study is outlined by Liang et al. (2006, 2007) and has been compared with the ADI scheme, showing its good shock-capturing capability which is particularly necessary for modelling dam-break, levee-breach and steep riverine flows.

3.3.2.1 Governing Equations for TVD Scheme

In the shallow water equations (Equations 3.1–3.3), the water surface gradient term can be written in the following forms

$$-gH\frac{\partial \xi}{\partial x}=-\frac{\partial\left(\frac{g\xi^2}{2}+gh\xi\right)}{\partial x}+g\xi\frac{\partial h}{\partial x} \tag{3. 27}$$

$$-gH\frac{\partial \xi}{\partial y}=-\frac{\partial\left(\frac{g\xi^2}{2}+gh\xi\right)}{\partial y}+g\xi\frac{\partial h}{\partial y} \tag{3. 28}$$

Correspondingly, the momentum equations, Equations (3.2) and (3.3), can be changed to give

$$\begin{aligned}\frac{\partial p}{\partial t}+\frac{\partial\left(\frac{\beta p^2}{H}+\frac{g\xi^2}{2}+gh\xi\right)}{\partial x}+\frac{\partial\left(\frac{\beta pq}{H}\right)}{\partial y}&=fq+g\xi\frac{\partial h}{\partial x}+\frac{\rho_a}{\rho}C_wW_x\sqrt{W_x^2+W_y^2}\\&\quad-\frac{gp\sqrt{p^2+q^2}}{H^2C^2}+\varepsilon\left[2\frac{\partial^2 p}{\partial x^2}+\frac{\partial^2 p}{\partial y^2}+\frac{\partial^2 q}{\partial x\partial y}\right]\end{aligned} \tag{3. 29}$$

$$\begin{aligned}\frac{\partial q}{\partial t}+\frac{\partial\left(\frac{\beta pq}{H}\right)}{\partial x}+\frac{\partial\left(\frac{\beta q^2}{H}+\frac{g\xi^2}{2}+gh\xi\right)}{\partial y}&=-fp+g\xi\frac{\partial h}{\partial y}+\frac{\rho_a}{\rho}C_wW_y\sqrt{W_x^2+W_y^2}\\&\quad-\frac{gq\sqrt{p^2+q^2}}{H^2C^2}+\varepsilon\left[\frac{\partial^2 q}{\partial x^2}+2\frac{\partial^2 q}{\partial y^2}+\frac{\partial^2 p}{\partial x\partial y}\right]\end{aligned} \tag{3. 30}$$

3.3.2.2 TVD-MacCormack Finite Difference Scheme

The 2-D SWEs can be decomposed into two sets of 1-D equations and solved separately. Take the variance in the x direction as an example, the 1-D equations can be generalized by (Liang et al., 2007)

$$\frac{\partial E}{\partial t}+\frac{\partial F}{\partial x}=S_a \tag{3. 31}$$

where $E=\xi$, p or q; and F, S_a = flux and source terms in the corresponding equations, respectively.

An explicit TVD-MacCormack finite difference scheme is used to solve Equation (3.31). To remove the numerical oscillations near sharp gradients, a five point symmetric TVD term is added to the correction step. Two steps in each time marching are included in the overall scheme, giving

$$\overline{E_i^{n+1}}=E_i^n-\frac{(F_i^n-F_{i-1}^n)\cdot\Delta t}{\Delta x}+S_a{}^n\cdot\Delta t \tag{3. 32}$$

$$E_i^{n+1}=0.5\cdot\left[\overline{E_i^{n+1}}+E_i^n-\frac{(\overline{F_{i+1}^{n+1}}-\overline{F_i^{n+1}})\cdot\Delta t}{\Delta x}+\overline{S_a{}^{n+1}}\cdot\Delta t\right]+TVD_i \tag{3. 33}$$

where superscripts n, n+1 and subscript i = temporal and spatial indices, respectively, and

$$TVD_i=\left[G(r_i^+)+G(r_{i+1}^-)\right]\cdot\Delta E_{i+1/2}^n-\left[G(r_{i-1}^+)+G(r_i^-)\right]\cdot\Delta E_{i-1/2}^n \tag{3. 34}$$

in which

$$\Delta E_{i+1/2}^n=E_{i+1}^n-E_i^n \tag{3. 35a}$$

$$\Delta E_{i-1/2}^n=E_i^n-E_{i-1}^n \tag{3.35b}$$

$$r_i^+=\frac{\left\langle\Delta E_{i-1/2}^n,\Delta E_{i+1/2}^n\right\rangle}{\left\langle\Delta E_{i+1/2}^n,\Delta E_{i+1/2}^n\right\rangle} \tag{3. 36a}$$

$$r_i^- = \frac{\left\langle \Delta E_{i-1/2}^n, \Delta E_{i+1/2}^n \right\rangle}{\left\langle \Delta E_{i-1/2}^n, \Delta E_{i-1/2}^n \right\rangle} \tag{3. 36b}$$

where $\langle , \rangle$ indicates the usual scalar product (Mingham et al., 2001).

The function G() in Equation (3.34) is defined as

$$G(x) = 0.5 * \Gamma * [1 - \phi(x)] \tag{3. 37}$$

where the flux limiter function $\phi(x)$ is given as

$$\phi(x) = \max(0, \min(2x, 1)) \tag{3. 38}$$

and variable Γ is defined as

$$\Gamma = \begin{cases} C_r * (1 - C_r), & C_r \le 0.5 \\ 0.25, & C_r > 0.5 \end{cases} \tag{3. 39}$$

where C_r is the local Courant number and is defined as

$$C_r = \frac{(|q_x / H| + \sqrt{gH})\Delta t}{\Delta x} \tag{3. 40}$$

More detailed description about this method can be found in Liang et al. (2006, 2007).

3.4 Summary

In this chapter, the 2-D depth-integrated hydrodynamic theories, including the continuity and momentum conservation equations and their solution methods have been presented in detail. The ADI scheme which is normally used in the solution of shallow water equations has been introduced. Meanwhile, as the ADI method is not applicable in trans-critical flow, the TVD method is integrated into the original model for solving the flow with fast and shallow water, in which the Froude number approaches or exceeds unity. They are the foundation of the solutions of sediment transport and bed evolution.

Chapter 4 Governing Equations for Morphodynamics and Numerical Solution

4.1 Introduction

According to their transport modes, sediments carried with flow can be divided into two categories including suspended load and bed load. It is widely accepted that bed load is essential for bed morphology change in braided rivers in mountain areas, but for large braided rivers on plains with mild slopes, suspended load plays an important role in river morphodynamics (Sarma, 2005; Ashworth et al., 2000). Physics-based models have made significant advances in simulating morphologic changes in braided rivers during the past decades. However, their ability in presenting realistic braiding mechanisms and morphodynamic processes in natural rivers still remains to be improved.

In the present study, an integrated 2-D numerical model based on non-equilibrium equations is applied to simulate the transport of suspended load and bed load in rivers, as sediment transport in natural rivers is usually in the state of non-equilibrium under varying flow conditions. Due to the important role of sediment gradation in bed deformation calculation, sediment transport is simulated by a

fractional method. The erosion or deposition quantity of each size fraction is first calculated and then they are added up to give the total bed variation mass. To consider the variation of size gradation in bed material in the vertical direction, the bed is divided into several layers to describe its interaction with sediments in transport.

This chapter develops a module for simulating bed load transport and introduces a module for suspended load transport. It explains the governing equations for sediment transport and bed evolution and the boundary conditions applied in the model, and gives an illustration for the solution of these equations.

4.2 Bed Load Transport Equations

4.2.1 Governing Equations

The 2-D governing equations for bed load transport and bed deformation of the *k*th size fraction can be described as (Wu, 2007)

$$\frac{\partial(q_{bk}/u_{bk})}{\partial t}+\frac{\partial(\alpha_{bx}q_{bk})}{\partial x}+\frac{\partial(\alpha_{by}q_{bk})}{\partial y}=\frac{1}{L_s}(q_{b*k}-q_{bk}) \tag{4. 1}$$

$$(1-p')\left(\frac{\partial z_b}{\partial t}\right)_k=\frac{1}{L_s}(q_{bk}-q_{b*k}) \tag{4. 2}$$

where q_{bk} = bed load transport rate of the *k*th size fraction; u_{bk} = bed load transport velocity of the *k*th size fraction; k = sediment fraction; p' = porosity of bed material; L_s = non-equilibrium adaptation length, which will be introduced in Section 4.2.2; q_{b*k} = equilibrium bed load transport rate of the *k*th size fraction, which be introduced in Section 4.2.2; and $(\partial z_b/\partial t)_k$ = bed elevation change rate releted to the *k*th size fraction of bed load.

In Equation (4.1), α_{bx} and α_{by} denote the direction cosines of bed load movement, which are usually assumed to be along the direction of bed shear stress, giving

$$\alpha_{bx} = u_{bx} / \sqrt{u_{bx}^2 + u_{by}^2}\ , \alpha_{by} = u_{by} / \sqrt{u_{bx}^2 + u_{by}^2} \tag{4. 3}$$

where u_{bx}, u_{by} = bed load transport velocities in the x and y directions, respectively.

As bed load particles transport in a layer of near-bed flow, the bed load transport velocity can be related to flow velocity at a reference level (level *a*). The vertical velocity profile in the main flow direction is assumed to be logarithmic (Duc et al., 2004)

$$\frac{u(z) - \overline{u}}{u_*} = \frac{1}{\kappa}\left(1 + 2.3\log\frac{z - z_b}{H}\right) \tag{4. 4}$$

where z = vertical coordinate above datum; $\overline{u}$ = depth-averaged flow velocity; u_* = bed shear velocity; κ = von Karman constant (in the range of 0.4–0.55, in the current study 0.4 is used); and z_b = bed elevation above datum. van Rijn (1987) and Duc et al. (2004) related level a to grain size by choosing $a = 3D_{90}$. The bed sediment transport velocity has been represented by the flow velocity at $z - z_b = 0.08H$ (H = water depth, Blanckaert and Graf, 2001). van Rijn (1984a) also gave an equation for bed load particle transport velocity u_b which is expressed as

$$u_b = 1.5\left[(s-1)gD_{50}\right]^{0.5} T^{0.6} \tag{4. 5}$$

where s = sediment specific density (ρ_s/ρ); D_{50} = median diameter of sediment mixture; and T = dimensionless transport stage parameter, which will be introduced in Section 4.2.2.

In the present study, the flow velocity at level *a*, which is related to bed load transport velocity, is determined by Equation (4.4) referring to Equation (4.5). When

taking into consideration the influence of secondary flow and slope, it is necessary to correct the sediment transport velocity with some item, which will be introduced in Section 4.2.3.

4.2.2 Characteristic Parameters

Bed load transport rate

The bed material in natural rivers usually consists of non-uniform sediments. The selective transport process for different size fractions is important and has been studied by many researchers (e.g. Einstein, 1950; Cui et al, 1996; van Rijn, 2007). The present study applies van Rijn's equation (1993) for bed load transport, and the size-selective transport for fractional sediments is considered by including the hiding and exposure effect. Based on a verification study using 580 flume and field data, assuming the motion of bed load particles is determined by particle saltation, the bed load transport rate q_{b*k} (in m^2/s) of the kth size fraction for particles in the range of 0.2–2 mm can be computed as (van Rijn, 1984a)

$$q_{b*k} = p_{bk} * 0.053\left[(s-1)g\right]^{0.5} d_k^{1.5} \frac{T^{2.1}}{D_*^{0.3}} \tag{4. 6}$$

where p_{bk} = percentage of the kth size fraction in the mixing layer of the bed; s = sediment specific density (ρ_s/ρ), and d_k = representative particle diameter of the kth size fraction. In our model, a simple equation is applied, which is expressed as

$$d_k = \frac{D_k + D_{k+1} + \sqrt{D_k D_{k+1}}}{3} \tag{4. 7}$$

where D_k, D_{k+1} = lower and upper limits of the kth size fraction.

van Rijn (1993) found that Equation (4.6) overpredicts the transport rate for $T \geqslant 3$ and proposed a modified expression for this range

$$q_{b*k} = p_{bk} * 0.1\left[(s-1)g\right]^{0.5} d_k^{1.5} \frac{T^{1.5}}{D_*^{0.3}} \tag{4. 8}$$

The bed load transport rate q_{b*k} is assumed to be described by two parameters including a dimensionless particle parameter (D_*) and a dimensionless transport stage parameter (T). D_* is defined as

$$D_* = d_k \left[\frac{(s-1)g}{\nu^2}\right]^{1/3} \tag{4. 9}$$

where ν = kinematic viscosity coefficient. And T is defined as

$$T = \frac{\tau_b' - \tau_c}{\tau_c} \tag{4. 10}$$

where $\tau_b' = \rho u_*'^2 =$ bed shear stress related to grains; $u_*' = \left(g^{0.5}/C'\right)\overline{u} =$ bed shear velocity related to grains; $C' = 18 * \log_{10}\left(12H/3D_{90}\right)$ = Chézy coefficient related to grains with H = water depth; $\overline{u} =$ depth-averaged flow velocity; and $\tau_c =$ critical shear stress for incipient motion, which can be expressed as

$$\tau_c = \rho\theta_c(s-1)gd_k \tag{4. 11}$$

where the critical particle mobility parameter θ_c can be obtained according to the shields curve (van Rijn, 1984a)

$$\theta_c = \begin{cases} 0.24D_*^{-1} & D_* \leq 4 \\ 0.14D_*^{-0.64} & 4 < D_* \leq 10 \\ 0.04D_*^{-0.10} & 10 < D_* \leq 20 \\ 0.013D_*^{0.29} & 20 < D_* \leq 150 \\ 0.055 & D_* > 150 \end{cases} \tag{4. 12}$$

However, Equations (4.6) and (4.8) are applicable for sediment particles in the range of 0.2–2 mm. Parker (1990) gave the bed load transport rate equation for

gravel-bed rivers with sediment sizes larger than 2 mm. Wu (2007) developed the fractional transport rate equation for non-uniform bed load from laboratory data measured by some researchers and field data from five natural rivers. These data covered a wide range of sediment sizes from 0.062 to 128 mm. The bed load transport rate q_{b*k} (in m^2/s) of the kth size fraction can be expressed as

$$q_{b*k} = p_{bk}\Phi_{bk}\sqrt{\left(\frac{\gamma_s}{\gamma_m}-1\right)gd_k^3} \tag{4. 13}$$

The dimensionless bed load transport rate Φ_{bk} can be shown as

$$\Phi_{bk} = 0.0053\left[\left(\frac{n'}{n}\right)^{3/2}\frac{\tau_b}{\tau_c}-1\right]^{2.2} \tag{4. 14}$$

where γ_s = specific weight of sediment; γ_m = specific weight of water and sediment mixture; d_k = representative particle diameter of the kth size fraction; $n' = D_{50}^{1/6}/20$ = roughness coefficient related to grains; n = Manning roughness coefficient = $R_h^{1/6}/C$ with R_h = hydraulic radius; $C = 18*\log_{10}(12H/k_s)$ = Chézy coefficient with H = water depth; $\tau_b = \rho u_*^2$ = bed shear stress; $u_* = \left(g^{0.5}/C\right)\overline{u}$; and τ_c = critical shear stress.

The critical shear stress τ_c in Equation (4.14) for a given sediment size can be obtained according to Shields curve, which can be approximated by (Wu and Wang, 1999)

$$\frac{\tau_c}{(\gamma_s-\gamma)d_k} = \begin{cases} 0.126D_*^{-0.44}, & D_* < 1.5 \\ 0.131D_*^{-0.55}, & 1.5 \le D_* < 10 \\ 0.0685D_*^{-0.27}, & 10 \le D_* < 20 \\ 0.0173D_*^{0.19}, & 20 \le D_* < 40 \\ 0.0115D_*^{0.30}, & 40 \le D_* < 150 \\ 0.052, & D_* \ge 150 \end{cases} \tag{4. 15}$$

Non-equilibrium adaptation length

In Equations (4.1) and (4.2), L_s denotes the non-equilibrium adaption length. It is a characteristic distance for the sediment in transport to adjust from non-equilibrium to equilibrium state. Different values have been adopted by previous researchers (e.g. Rahuel et al. 1989; Wu et al. 2000), since bed load movement is closely related to bed forms. In laboratory experiments the sediment transport processes are mainly based on small scales such as sand saltation, ripples and dunes, while in nature sediment transport processes occur usually at larger scales with longer periods (Wu et al., 2000). In the present study, it is calculated using an empirical formula of van Rijn (1987)

$$L_s = 3d_k D_*^{0.6} T^{0.9} \tag{4. 16}$$

4.2.3 Bed Roughness

The hydraulic roughness can be caused by grain and the river form. In the present study, the equivalent roughness height of Nikuradse, k_s is related to the D_{90} of the bed material as van Rijn (1984a)

$$k_s = 3D_{90} \tag{4. 17}$$

Equation (4.17) denotes the roughness caused by the grain. Besides, the form roughness is also a part of the hydraulic roughness of a movable bed surface. van Rijn (1984c) related this form roughness to bed form length and water depth. By adding the river form roughness, Equation (4.17) can be expressed as

$$k_s = 3D_{90} + 1.1\Delta(1 - e^{-25\psi}) \tag{4. 18}$$

where $\psi = \Delta/\lambda$ = bed form steepness. The bed form height Δ is calculated for $0 \leq T \leq$

25 as

$$\frac{\Delta}{\lambda} = 0.015\left(\frac{D_{50}}{H}\right)^{0.3}\left(1-e^{-0.5T}\right)(25-T) \tag{4. 19}$$

It is assumed that, for $T \leq 0$ or $T \geq 25$, no bed form exists. The bed form length λ is expressed as

$$\lambda = 7.3H \tag{4. 20}$$

where H = water depth.

4.2.4 Areal Fraction and Sheltering Effect for Non-uniform Sediments

In the process of sediment transport, the drag force and the lift force exerted on the particle are essential for the initiation of sediment transport. These forces are proportional to the projected areas of particles exposed to the flow. However, normally the volumetric percentage of the upper layer exposed to flow is used to calculate sediment transport rate. Karim (1998) proposed that the volumetric percentage in the mixing layer of the bed, p_{bk}, can be converted into the areal percentage p_{ak} by the following expression

$$p_{ak} = \frac{\frac{p_{bk}}{d_k}}{\sum_{k=1}\frac{p_{bk}}{d_k}} \tag{4. 21}$$

For a river bed composed of a mixture of various sediment sizes, smaller particles tend to remain immobile for a certain time due to the sheltering effect from larger particles. van Rijn (2007) proposed that the degree of exposure of non-uniform sediment particles can be modelled by two methods, including modifying the critical

shear stress or the effective grain shear stress through a correction factor. And he found that the hiding factor can be well represented by a linear expression $(d_k / D_{50})^{-1}$. Wilcock (1993a) also gave an indication of this linear effect. In the present model, the liner expression of van Rijn (2007) is applied to correct the critical shear stress τ_c for the initiation particle motion, which is expressed as

$$\tau_c' = \tau_c (d_k / D_{50})^{-1} \tag{4. 22}$$

4.2.5 Influences of Slope and Secondary Flow

The channel slopes of natural rivers are normally gentle and thus the effect of gravity on sediment transport is usually ignored. However, when river bed is steep, gravity may change the sediment transport capacity and influence bed deformation significantly. Bed slope affects the shear stress (τ) and sediment transport rate (q_s) in longitudinal and transverse direction. The transport rates show some increase at steep bed slopes. A relationship between the transport rate on a sloping bed and on a horizontal bed can be derived as (van Rijn, 1993)

$$q_{b,s} = \alpha_s q_b \tag{4. 23}$$

where $q_{b,s}$ = bed load transport rate on a sloping bed; q_b = bed load transport rate on a horizontal bed; $\alpha_s = \tan\theta / [\cos\delta_s (\tan\theta \pm \tan\delta_s)]$ = Bagnold slope factor, "+" for upsloping flow, "-" for downsloping flow; θ = sediment repose angle, 30° is adopted in the present study; and δ_s = longitudinal slope angle.

Bed load transport rate is also influenced by secondary flow. To consider the effect of secondary flow and transverse slope, the deviation angle (φ) between bed

flow and sediment transport rate is integrated into the bed load transport rate. Combined the methods of Jang (2005a) and van Rijn (1993), the deviation is presented as

$$tan\varphi = \frac{H}{r_s} N_* + \epsilon \left(\frac{\tau_{c,o}}{\tau_b}\right)^{0.5} tan\delta_n \qquad (4.24)$$

where φ = deviation angle between flow and bed load transport velocity; H = water depth; r_s = radius of curvature of the stream line; N_* = coefficient of the strength of secondary flow, with a value of 7.0 adopted (Engelund, 1974); ϵ = mixing coefficient =1.5 based on measured data along a straight channel (van Rijn, 1993); $\tau_{c,o}$ = critical shear stress for median particle $= \rho\theta_c(s-1)gD_{50}$; $\tau_b = \rho u_*^2$ = bed shear stress; $u_* = \left(g^{0.5}/C\right)\overline{u}$; and δ_n = transverse slope angle. In Equation (4.24), the first term denotes the effect of secondary flow and the second term represents the effect of transverse slope.

The longitudinal and cross-sectional slopes will also change the critical shear stress for the incipient motion of sediments. According to van Rijn (1993), the shear stress with the consideration of slope effect can be expressed by

$$\tau_{c,s} = k_{\delta,s} k_{\gamma,n} \tau_c \qquad (4.25)$$

where $k_{\delta,s}$ = coefficient of longitudinal slope, $k_{\delta,s} = \sin(\theta - \delta_s)/\sin\theta$ for downsloping flow ($k_{\delta,s} < 1$), $k_{\delta,s} = \sin(\theta + \delta_s)/\sin\theta$ for upsloping flow ($k_{\delta,s} > 1$); δ_s = longitudinal slope angle; θ = sediment repose angle, with 30° adopted in the present study; $k_{\delta,n}$ = coefficient of transverse slope = $\cos\delta_n(1-\tan^2\delta_n/\tan^2\theta)^{0.5}$, in the model $k_{\delta,n}$ approximately equals to $\cos\delta_n$; and δ_n = transverse slope angle.

4.2.6 Bank Erosion

Bank erosion is accounted into bed deformation in the model. As rivers develop, flow scours the river bank and bed, resulting in local erosion. When the bank slope (δ) becomes steeper than the sediment repose angle (θ), the sediments will slide to the neighbourhood areas immediately. This process will continue until the bank slope is equal to or lower than the sediment repose angle (Figure 4.1a). The amount of sediments deposited on the neighbourhood areas is supposed to be equal to what is eroded from the bank. The sediments deposited on the river bed will be mixed with the upper layer of the bed (to be introduced in Section 4.3). Consequently, the formation and composition of the river bed are renewed. The amount of sediments from bank erosion is redistributed in four directions by choosing a direction with the steepest slope (Figure 4.1b).

Supposing $z_{ix,j} = \min\left(z_{i-1,j}, z_{i+1,j}\right)$, $z_{i,jy} = \min\left(z_{i,j-1}, z_{i,j+1}\right)$, then

$$\tan\delta_x = \frac{z_{i,j} - z_{ix,j}}{\Delta x} \tag{4. 26a}$$

$$\tan\delta_y = \frac{z_{i,j} - z_{i,jy}}{\Delta y} \tag{4.26b}$$

$$\tan\delta = \sqrt{\tan\delta_x + \tan\delta_y} \tag{4.26c}$$

If $\tan\delta > \tan\theta$, then bed elevation changes in the x and y directions Δz_x and Δz_y are given as

$$\Delta z_x = \frac{\left(\tan\delta - \tan\theta\right)\tan\delta_x}{\tan\delta}\frac{\Delta x}{2} \tag{4. 27a}$$

$$\Delta z_y = \frac{\left(\tan\delta - \tan\theta\right)\tan\delta_y}{\tan\delta}\frac{\Delta y}{2} \tag{4.27b}$$

The new bed elevations $z'_{ix,j}$, $z'_{i,jy}$, and $z'_{i,j}$ come out to be

$$z'_{ix,j} = z_{ix,j} + \Delta z_x \tag{4. 28a}$$

$$z'_{i,jy} = z_{i,jy} + \Delta z_y \tag{4. 28b}$$

$$z'_{i,j} = z_{i,j} - \Delta z_x - \Delta z_y \tag{4. 28c}$$

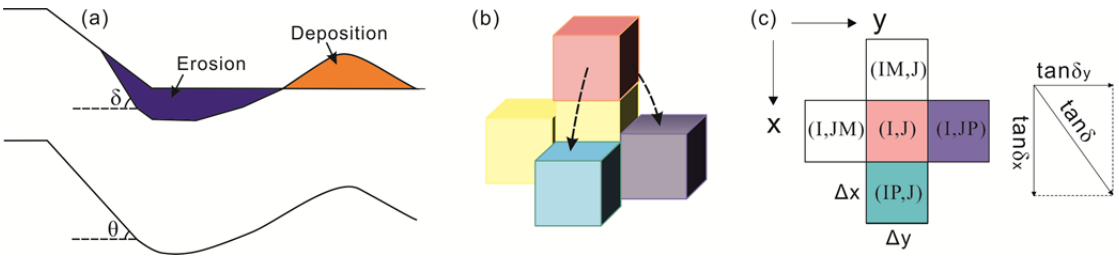

Figure 4.1 Bed deformation process with bank erosion: (a) bed degradation and bank erosion; (b) and (c) sediment redistribution between neighbourhood cells.

4.3 Suspended Load Transport Equations

4.3.1 Governing Equations

Assuming that the graded suspended load can be divided into N fractions, the transport of fraction *k* can be described by the following Equation (Zhou and Lin, 2008)

$$\frac{\partial Hs_k}{\partial t} + \frac{\partial HUs_k}{\partial x} + \frac{\partial HVs_k}{\partial y} = -\alpha_k \omega_k (s_k - \phi_k) + \frac{\partial}{\partial x}\left(D_{xx} H \frac{\partial s_k}{\partial x} + D_{xy} H \frac{\partial s_k}{\partial y} \right) + \frac{\partial}{\partial y}\left(D_{yx} H \frac{\partial s_k}{\partial x} + D_{yy} H \frac{\partial s_k}{\partial y} \right) \tag{4. 29}$$

where U, V = depth-averaged velocities in the x, y directions, respectively; H = water depth; k = sediment fraction; s_k = suspended load concentration for the kth size fraction; D_{xx}, D_{xy}, D_{yx}, D_{yy} = depth-averaged dispersion-diffusion coefficients in the x, y directions, respectively; ϕ_k = suspended load transport capacity for the kth size fraction;

ω_k = fall velocity for the *k*th size fraction; and α_k = adjustment coefficient for the *k*th size fraction.

The dispersion-diffusion terms can be shown as follows (Preston, 1985)

$$D_{xx} = \frac{\left(k_l U^2 + k_t V^2\right) H\sqrt{g}}{\sqrt{U^2 + V^2}\, C} + D_w$$

$$D_{yy} = \frac{\left(k_l V^2 + k_t U^2\right) H\sqrt{g}}{\sqrt{U^2 + V^2}\, C} + D_w \qquad (4.30)$$

$$D_{xy} = D_{yx} = \frac{\left(k_l - k_t\right) UVH\sqrt{g}}{\sqrt{U^2 + V^2}\, C}$$

where k_l = longitudinal depth-averaged dispersion constant; k_t = depth-averaged turbulent diffusion constant; D_w = wind-induced dispersion coefficient; C = Chézy coefficient; and g = gravitational acceleration.

The river bed deformation is given as

$$\left(1 - p'\right)\left(\frac{\partial z_b}{\partial t}\right)_k = \frac{1}{\gamma_s}\alpha_k \omega_k \left(s_k - \phi_k\right) \qquad (4.31)$$

where p' = porosity of bed layer; γ_s = specific weight of sediment; and $\left(\partial z_b / \partial t\right)_k$ = bed elevation change rate related to the *k*th size fraction of suspended load.

In Equations (4.29) and (4.31), the source term $\alpha_k \omega_k \left(s_k - \phi_k\right)$ is a key term for sediment transport and bed deformation. It controls the rate of bed erosion and deposition. In this term the transport capacity ϕ_k and adjustment coefficient α_k for each fraction are the main parameters to be determined.

4.3.2 Fall Velocity

The fall velocity ω_k of the *k*th size fraction in Equations (4.29) and (4.31) applies

the equations developed by van Rijn (1984b). In clear and still fluid, fall velocity ω_k for solitary sand particle smaller than about 0.1 mm can be described by

$$\omega_k = \frac{1}{18}\frac{(s-1)gd_k^2}{\nu} \tag{4. 32}$$

For sand particles in the range of 0.1–1.0 mm, the following equation is applied

$$\omega_k = 10\frac{\nu}{d_k}\left\{\left[1+\frac{0.01(s-1)gd_k^3}{\nu^2}\right]^{0.5}-1\right\} \tag{4. 33}$$

For sand particles larger than about 1.0 mm, the following equation is used

$$\omega_k = 1.1[(s-1)gd_k]^{0.5} \tag{4. 34}$$

where s = sediment specific density; $d_k = \left(D_k + D_{k+1} + \sqrt{D_k D_{k+1}}\right)/3$ = representative particle diameter of the kth size fraction; and ν = kinematic viscosity coefficient.

For the transport of high concentration sediment, the influence of sediment concentration on fall velocity should also be considered. Under this situation the fall velocity ω_{mk} can be calculated by an equation (Richardson and Zaki, 1954) giving

$$\omega_{mk} = \omega_k(1 - S_t/\gamma_s)^{\chi} \tag{4. 35}$$

where γ_s = specific weight of sediment; and S_t = total suspended load concentration. The value of χ was set to 7.0 based on some flume experimental work.

4.3.3 Suspended Load Transport Capacity

Many formulas can be found in computing sediment transport capacity, such as Einstein (1950) and Arkers and White (1973). However, most of the existing formulas are developed for bed load transport. As for large rivers on plains with high fine sediment concentration, suspended load is also very important for bed evolution and

river pattern change. Zhou and Lin (2008) proposed a simplified formula for calculating total suspended load transport capacity, giving

$$\Phi = K_1 \frac{\gamma_m}{\gamma_s - \gamma_m} \frac{\overline{u}^3}{gH\omega} \tag{4. 36}$$

In Equation (4.36), only the coefficient K_1 is to be determined, which can be approximately expressed as

$$K_1 = 0.102 \left(\frac{\overline{u}^3}{gH\omega} \right)^{0.6346 - 0.2161 * \log_{10}\left(\frac{\overline{u}^3}{gH\omega} \right)} \tag{4. 37}$$

where Φ = total suspended load transport capacity; γ_s , γ_m = specific weights of sediment and water mixed with sediment, respectively; $\overline{u}$ = depth-averaged flow velocity; H = water depth; $\omega = \sum p_k \omega_k$ = average fall velocity of suspended load; and p_k = percentage of the kth size fraction of suspended load .

In Equation (4.29), suspended load transport capacity for the kth size fraction ϕ_k can be calculated according to an energy theory which is related to the total sediment transport capacity Φ and the percentage of fractional sediments in suspension and bed layer. More details of its calculation can be found in (Zhou and Lin, 2008).

4.3.4 Adjustment Coefficient

The adjustment coefficient α given in Equations (4.29) and (4.31) is a basic parameter for non-equilibrium transport of suspended load. Its value is determined by the vertical profiles of sediment concentration. In some models α is set to a constant, while in some others this coefficient is treated as a calibration constant, which is

different for each study. In the present study, erosion and deposition processes are considered separately.

Zhou and Lin (1998) showed that the adjustment coefficient can be determined by

$$\alpha = \frac{R}{4} + \frac{\sigma_1^2}{R} \tag{4. 38}$$

where $R = 6\omega/\kappa u_*$; $\omega = \sum p_k \omega_k$ = average fall velocity of suspended load; κ = von Karman constant; u_* = bed shear velocity; σ_i = the ith positive root of equations $\tan(\sigma) = -\sigma/R$ (for erosion) and $\cot(\sigma) = \sigma/R - R/4\sigma$ (for deposition). Figure 4.2 illustrates the distribution of α (Zhou and Lin, 1998). Zhou et al. (2003) tested this method and stated that it agrees well with the laboratory data.

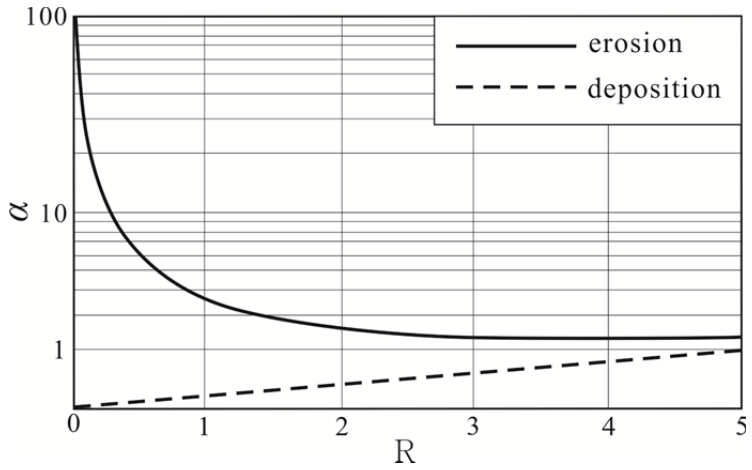

Figure 4.2 Distribution of the adjustment coefficient α (Zhou and Lin, 1998).

4.4 Bed Deformation and Composition Changes

During river evolution process, the amount of sediments in transport is primarily determined by the sediment transport capacity of flow. Erosion occurs when sediment concentration is lower than sediment transport capacity. Otherwise deposition occurs.

Erosion and deposition of sediments will change the bed elevation and composition, and consequently change the local hydraulic conditions and river pattern. They can change the amount of deposit to river bed and their properties, such as fall velocity, friction resistance and incipient velocity. In turn, the changes in bed morphology and composition will influence the flow velocity and sediment transport rate. Then erosion or deposition occurs again. According to the bed deformation equations (4.2) and (4.31) for suspended load and bed load, the total bed deformation can be described as

$$(1-p')\frac{\partial z_b}{\partial t} = \sum \frac{1}{\gamma_s}\alpha_k \omega_k (s_k - \phi_k) + \sum \frac{1}{L_s}(q_{bk} - q_{b*k}) \tag{4. 39}$$

The sediments come from the river bed, which will deposit or get eroded from the bed and will consequently change the bed form and composition. Therefore, it is meaningful for numerical models to consider the influence of bed sediment composition. Consequently, numerical models should be capable of resolving the spatial and temporal variation of sediment gradations over the loose layers of a river bed. One such method is to divide the river bed into several vertical sediment layers. As shown in Figure 4.3, the loose bed is divided into three layers of upper, middle and lower, with their thicknesses and volumetric fractions being defined as H_U, H_M, H_L and P_{Uk}, P_{Mk} and P_{Lk}, respectively. Due to a bed-level change, ΔZ_B, caused by sediment deposition or erosion, the upper layer becomes $H_U+\Delta Z_B$. The fractional percentage of sediment fraction k can be computed by

$$P_{Uk}^{*} = \frac{H_U P_{Uk}^{0} \Delta Z_{Bk}}{H_U + \Delta Z_B} \tag{4. 40}$$

where ΔZ_{Bk} = scoured or deposited thickness of an individual fraction; and the

superscripts 0 ,* = values from the last time step and the present tiem step.

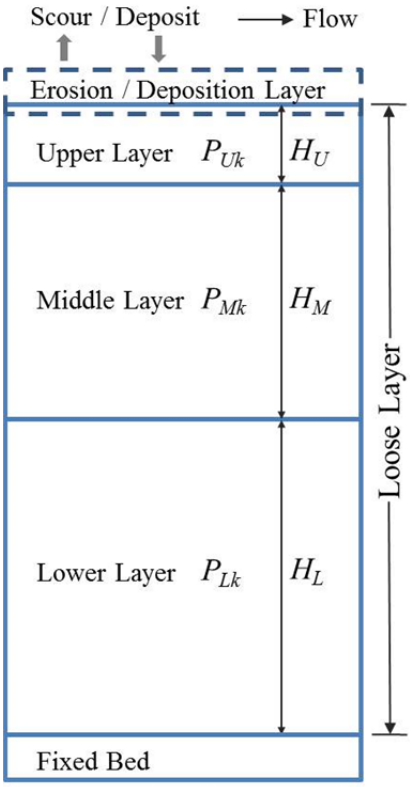

Figure 4.3 Multiple layers of bed material sorting.

The lower layer is adjustable according to bed deformation, with the upper and middle layer thickness H_U, H_M being set constant. The fractional sediment composition is computed using the formula given below.

a) For the case of deposition ($\Delta Z_B > 0$)

Upper layer $$P_{Uk} = P_{Uk}^{*} \tag{4. 41}$$

Middle layer $$P_{Mk} = \frac{\Delta Z_B P_{Uk}^{*} + (H_U - \Delta Z_B) P_{Mk}}{H_M} \tag{4. 42}$$

Lower layer $$P_{Lk} = \frac{\Delta Z_B P_{Mk}^{0} + H_L^{0} P_{Lk}^{0}}{H_L^{0} + \Delta Z_B} \tag{4. 43}$$

b) For the case of erosion ($\Delta Z_B < 0$)

Upper layer
$$P_{Uk} = \frac{(H_U + \Delta Z_B)P^*_{Uk} - \Delta Z_B P^0_{Mk}}{H_U} \tag{4. 44}$$

Middle layer
$$P_{Mk} = \frac{(H_M + \Delta Z_B)P^0_{Mk} - \Delta Z_B P^0_{Lk}}{H_M} \tag{4. 45}$$

Lower layer
$$P_{Lk} = P^*_{Lk} \quad \text{and} \quad H_L = H^0_L + \Delta Z_B \tag{4. 46}$$

where it is assumed that $\Delta Z_B < H_U$. The above method has not been restricted to three layers, and can be extended to more layers when necessary.

4.5 Numerical Solution for Morphodynamic Equations

The sediment transport equations of bed load (4.1) and suspended load (4.29) are solved with an ULTIMATE QUICKEST SCHEME, which is applied to simulate two-dimensional solute transport in coastal and estuarine waters by Lin and Falconer (1997). A conventional discretization (splitting) algorithm has been used to solve the solute transport advective-diffusion equations. Furthermore, in this solution, to avoid the occurrence of numerical oscillations, the ULTIMATE algorithm and the third-order accurate QUICKEST scheme are used to represent the advective terms.

For the conformal boundary-fitted mesh used in this study, the continuity equation of the hydrodynamic model can be expressed as

$$\frac{\partial \xi}{\partial t} + \left[\frac{\partial (HU)}{\partial x} + \frac{\partial (HV)}{\partial y} \right] = 0 \tag{4. 47}$$

The solute transport equation can be given as

$$\frac{\partial S}{\partial t}+\frac{\partial US}{\partial x}+\frac{\partial VS}{\partial y}=\frac{1}{H}\frac{\partial}{\partial x}\left(D_{xx}H\frac{\partial S}{\partial x}+D_{xy}H\frac{\partial S}{\partial y}\right)+\frac{1}{H}\frac{\partial}{\partial y}\left(D_{yx}H\frac{\partial S}{\partial x}+D_{yy}H\frac{\partial S}{\partial y}\right)+S_a+S_s \quad (4.48)$$

where S_a = source term; and $S_s=S\left(\frac{\partial U}{\partial x}+\frac{\partial V}{\partial y}\right)$, which is shown to be vital for the conservation of mass in modelling solutes.

The finite difference formulation for Equation (4.48) is written in the following form

$$S_{i,j}^{n+1}=S_{i,j}^{n}+\text{advection terms}+\text{dispersion terms}+\text{source term} \quad (4.49)$$

For bed load, only the source term is included and Equation (4.49) is given as

$$S_{i,j}^{n+1}=S_{i,j}^{n}+\text{source term} \quad (4.50)$$

where i, j = grid square locations in the x and y directions, respectively. For consistency, the advection term in Equation (4.49) is again formulated using the ULTIMATE QUICKEST SCHEME, with the dispersion terms being represented using the explicit second-order central scheme. The source and decay terms are represented by Euler method. The definition of terms for two-dimensional QUICKEST Algorithm is shown in Figure 4.4. For simplicity, only the discretization of the advection terms is given here. The solution of the advection terms in Equation (4.49) can be expressed as the sum of the four face values, giving

$$\text{advection terms}=\left[(C_r)_e S_e-(C_r)_w S_w\right]+\left[(C_r)_n S_n-(C_r)_s S_s\right] \quad (4.51)$$

where subscripts w, e, s and n = west, east, south and north face grid values respectively, as shown in Figure 4.4; C_r = Courant number; and S = solute

concentration. More detailed explanation for this method can be found in Lin and Falconer (1997).

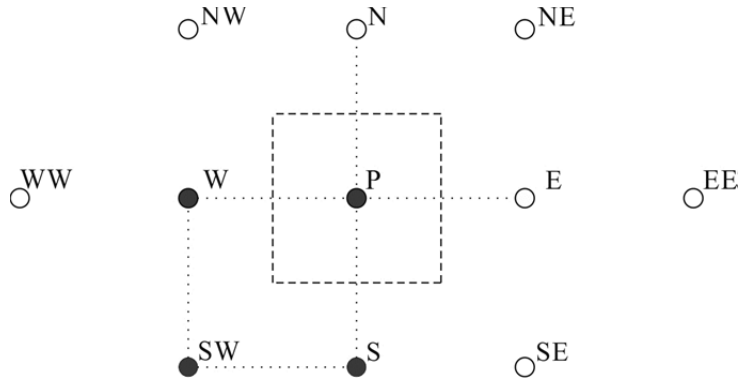

Figure 4.4 Compass-point notation in the QUICKEST SCHEME (Lin and Falconer, 1997).

4.6 Summary

This chapter introduces the theories of morphodynamics in the present model and the solution method. Referring to the physics-based equations describing bed load movement from the previous studies in real rivers, a module for simulating the bed load transport in rivers is developed and integrated into the original model. It considers the non-equilibrium equations, bank erosion and sheltering effect for graded sediments, and applies the fractional sediment method and multiple bed layers to count the vertical sorting process in river bed deformation. The effects of slope and secondary flow are also included in the model by altering the sediment transport rate on slope and the critical shear stress for the initiation of particle motion.

Besides, the theories of suspended load transport are also introduced in this chapter. Similar configuration is included in suspended load transport such as graded

sediments and sheltering effect. Due to the different transport mode with bed load, the suspended load transport is described by different theories. And then the solution method of the QUICKEST SCHEME is given a schematic illustration. Nonetheless, in specific modelling cases, it is important to consider the practical situation, ignore some less important factors and make appropriate simplification, which will enhance the model stability and simulation ability.

Chapter 5 Braided River Modelling with Bed Load

5.1 Introduction

Braided rivers often occur in mountain areas with abundant bed load, steep valley slope and frequent channel configuration changes. They are characterised by high flow energy and large sediment particles with supercritical flow existing in local areas. Bank erosion is important for braiding evolution, in which secondary flow plays an important role. With some natural rivers as prototypes, experiments have been used to study the morphologic processes and compared with natural rivers, and one main channel theory has been proposed by some researchers (Egozi and Ashmore, 2008, 2009; Bertoldi et al., 2009), which suggests that, though there are multiple channels in braided rivers, one dominant channel exists and conveys a large part of the total load.

In this chapter, the newly developed model is first validated by two test cases, one involving dam-break flow, and the other involving bed aggradation. The former is used to test the ability of the TVD scheme in simulating trans-critical flows. The latter is to test the model in simulating sediment transport and deposition. Then a laboratory

river is predicted by the model, with the Sunwapta River in Canada as a prototype. Essential morphologic changes in the braiding evolution process and the response to increased discharge are analysed and compared with those from the laboratory and natural rivers. Channel braiding mechanisms, mainly relating to channel avulsions, are investigated based on local morphodynamic behaviours. Moreover, the statistical characteristics of the predicted river are analysed and the simulation ability of the model is assessed by employing several methods.

5.2 Model Verification and Calibration

5.2.1 Dam-break Flow Test

The test case is a 2-D dam-break problem, which has been widely used for model calibration (e.g. Louaked and Hanich, 1998; Liang et al., 2006). Its computation was undertaken in an area of 200 m long and 200 m wide. A dam located at x = 100 m divided the simulation domain into two equal regions with still water of 10 m and 5 m deep initially. The grid size was set to 5 m and the time step was set to 0.2 s. At time t = 0 s, part of the dam was suddenly removed, so that a breach of 75 m formed, extending from y = 95 m to 170 m.

The dam-break process has been shown in Figure 5.1. After the dam was removed, the water crushed quickly downstream in a very short time. The changes of the water surface show similar profile with previous studies (e.g. Mingham and Causon, 1998; Louaked and Hanich, 1998; Wang et al., 2000; Rogers et al., 2001). The water depth contours at 7.2 s generally agree well with the result from some

previous study (Figure 5.2). The condensed contour lines illustrate the model is good at presenting the rapid changes of water surface.

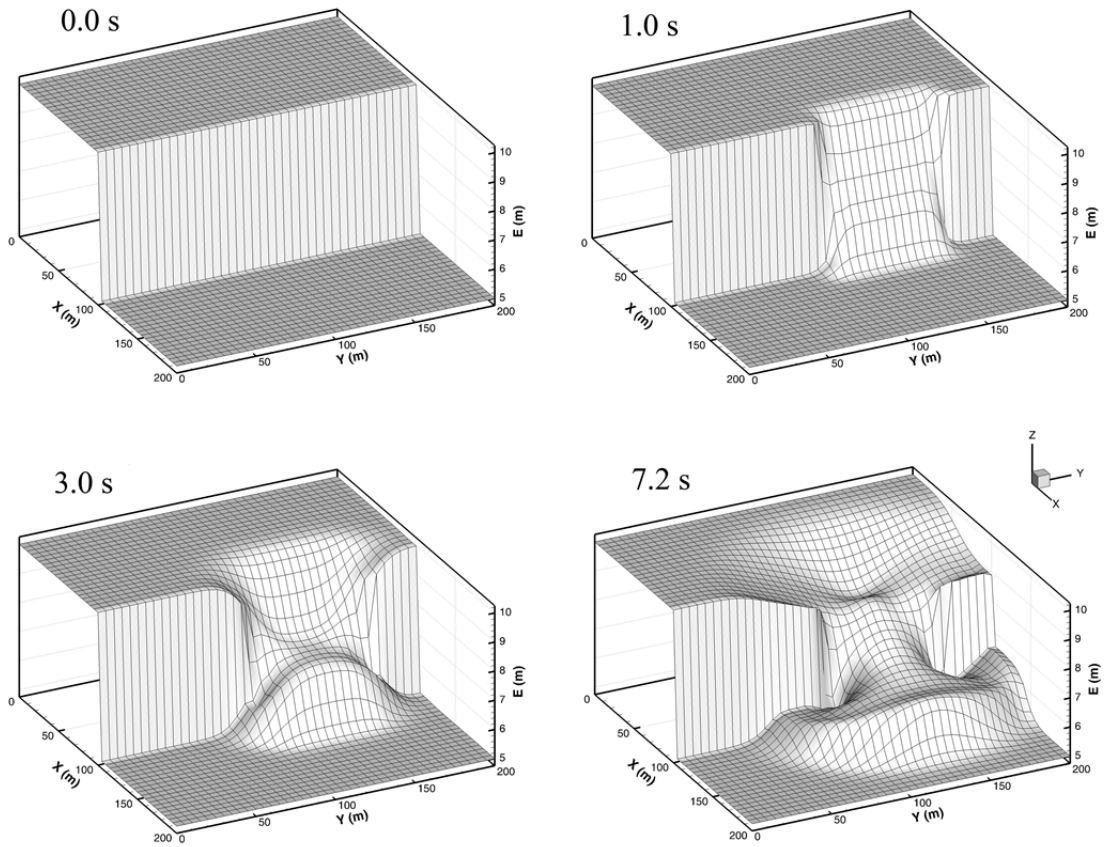

Figure 5.1 Water surface elevation of the 2-D dam-break simulation.

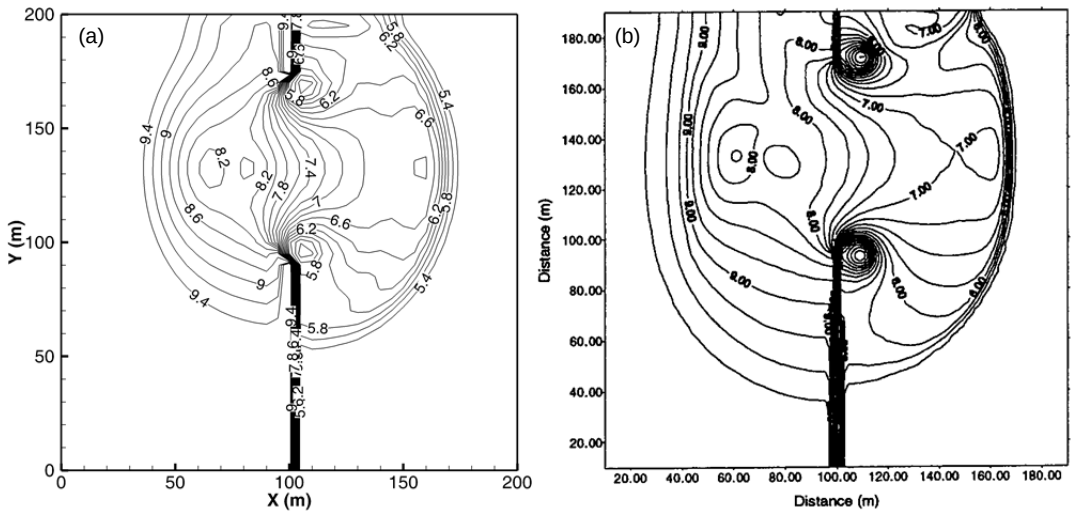

Figure 5.2 Water depth contours at 7.2 s by: (a) present model; (b) Rogers et al. (2001).

5.2.2 Bed Load Transport Test

The model for bed load transport was validated with a laboratory experiment which wasundertaken by Seal et al. (1997) and Paola et al. (1992). The experiment has been modelled by Cui et al. (1996) to investigate bed aggradation and downstream fining, and by Wu (2004) to test model reliability for simulating bed deformation. In the current study this case was used to test the reliability of the bed load transport module, and prepare for the following application.

Details of the Experiment

The experiment was carried out in a flume, with the test reach being 45 m long and 0.305 m wide and with an initial channel slope of 0.002 (Seal, 1997). A pond located at the downstream end was blocked by a weir, forming a free overfall (Figure 5.3). The water elevation at the tailgate was set to 0.4 m. The sediment distribution was originated from two natural rivers, which was poorly sorted and weakly bimodal. The grain size was in a range from 0.125 mm to larger than 64 mm, with two main modes at 0.35 mm and 16 mm. The flow discharge was set to 0.049 m^3/s with sediment feed rate being 11.3 kg/min. The sediment was fed into the channel manually at 1 m downstream the headgate for 16 hours and 50 minutes. In the upstream reach, the Froude number (Fr) was only modestly above unity. An undular hydraulic jump occurred just beyond the front.

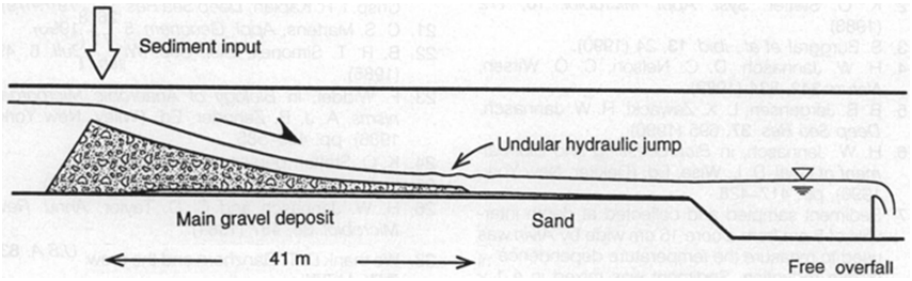

Figure 5.3 Schematic diagram of the experimental channel at 16.8 h.

Numerical Model Setup

The modelled river was 45 m long and 0.3 m wide, which started from the sediment input location in the experiment (Figure 5.4). It included 900*8 cells, with each cell size being 0.05*0.05 m^2. The initial bed was set to 0.1 m at the headgate and 0.0 m at the tailgate with a bed slope of 0.002.

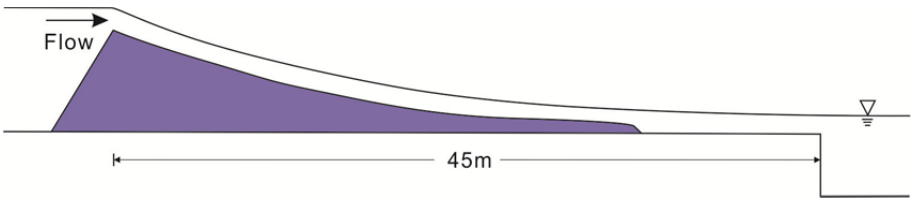

Figure 5.4 Schematic diagram of the model configuration.

Flow discharge was set to 0.049 m^3/s. The sediments were divided into eight groups (Figure 5.5 and Table 5.1). The adaption length was set to 1.0, and the bed roughness height was $3D_{90}$. As the Froude number was near unity, the TVD-MacCormack Method was applied to solve the hydraulic equations. The time steps were set to 0.005 s and 0.01 s for the hydrodynamic and sediment computations, respectively. The minimum water depth used to resolve the drying and flooding

processes of the floodplain was set to 1 mm. The simulation lasted 17 hours.

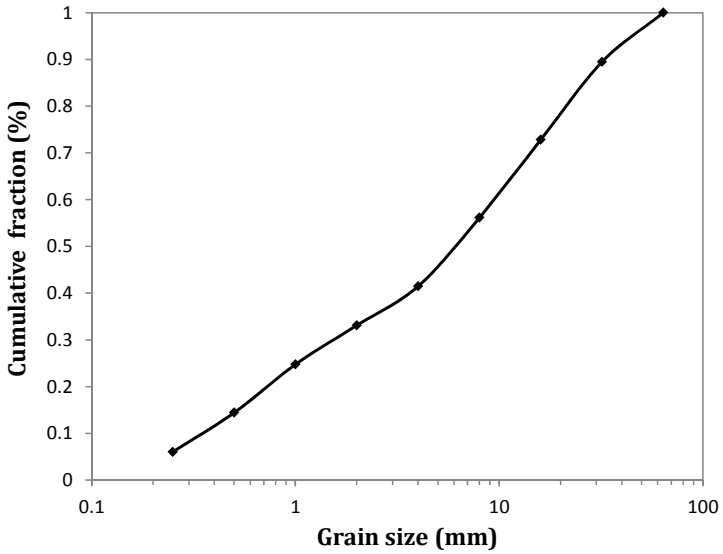

Figure 5.5 Sediment distribution in the numerical model.

Table 5.1 Sediment fractions and percentages in the numerical model

Sand Groups	1	2	3	4	5	6	7	8	
Grain Size (mm)	0.25	0.5	1.0	2.0	4.0	8.0	16.0	32.0	64.0
Percentage (%)	6.03	8.38	10.33	8.36	8.36	14.67	16.68	16.68	10.51
Finer than (%)	6.03	14.41	24.74	33.10	41.46	56.13	72.81	89.49	100.0

Model Result Analysis

The predicted result is shown in Figure 5.6. Generally, the model predicts the bed elevation and water surface well. As water with sediment flowed into the channel, sediment particles deposited on to the bed and caused it to aggrade quickly. The predicted bed slope at 2 h is a little lower than the experiment, whereas they correspond to each other well at 8 and 16.8 h. The water elevation at 16.8 h was simulated generally well. A hydraulic jump could be seen at the downstream end of

the main bed deposit, which was also observed in the experiments. As the bed aggraded, bed slope changed from 0.002 to about 0.022. Due to the lack of more detailed measured data, it is difficult to determine the exact shapes of the bar head. Nevertheless, it still can be seen that the bar head extends downstream a little further than the experiment for the entire simulation period. A rough bed exists at the bar head, which may result from the hydraulic jump there.

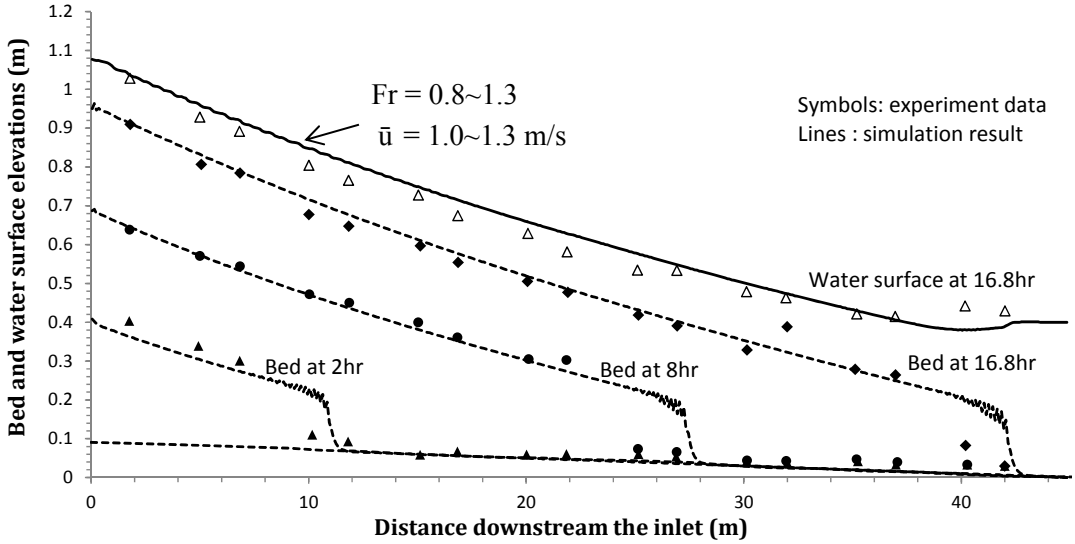

Figure 5.6 Predicted bed elevation and water surface.

Figure 5.7 shows the changes of flow velocity, water depth and the Froude number with time at 10 m to 40 m with an interval of 10 m. It illustrates the local hydraulic changes as the bed aggrades. As shown in Figure 5.6, sediments deposited on the bed and when the bed slope increased to 0.022, most of the sediments could be transported downstream on the new bed. A bar exists in the front of the new bed, which is extending downstream with time. Near the bar there is a hydraulic jump,

with the Froude number suddenly increased from 0.2 to 0.9. It illustrates that the model can predict sudden hydraulic changes well.

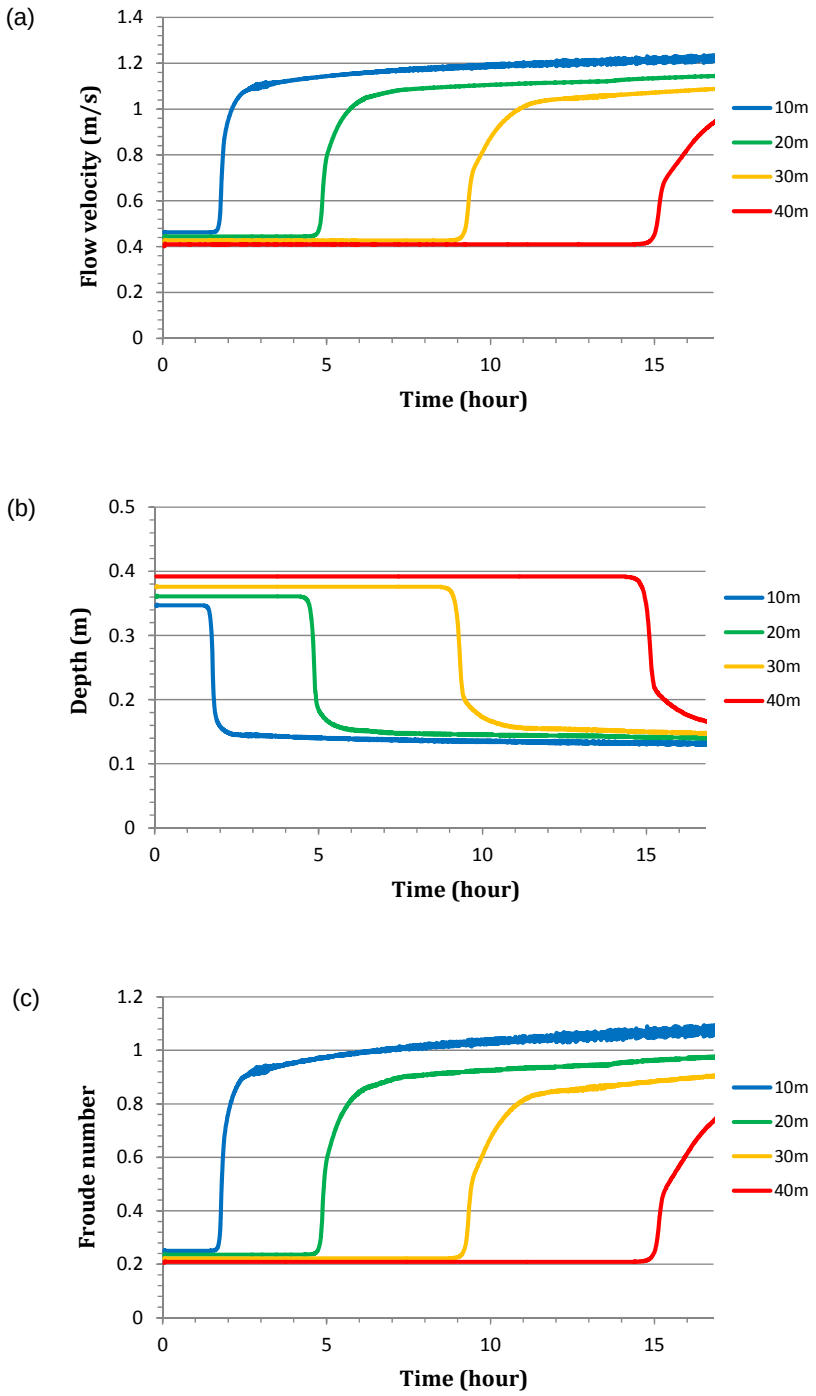

Figure 5.7 Changes of flow velocity, water depth and Froude number with time at different locations.

It has been found that the value of the roughness height (k_s) is a key factor in

determining the bed slope by affecting the bed load transport rate and distance. The ADI scheme has also been applied to solve this case. Compared with the well predicted result by the TVD scheme, the result by the ADI scheme is poor, with a milder bed slope and a deeper and slower flow, which has not been shown here.

5.3 Model Application to an Experimental Braided River

After the tests with dam-break flow and bed aggradation, the model was applied to predict the morphodynamics of a braided river in laboratory with the Sunwapta River as its prototype.

5.3.1 Physical Model

The laboratory experiment was conducted by Egozi and Ashmore (2008, 2009) and their data are used in the present study. The physical model adopted the overall gradient, discharge and grain-size characteristics of the Sunwapta River in Canada. Bed load transportation is dominant in this river. It is a generic Froude-scaled model which satisfies the same Froude number (Fr) with natural rivers, yet relaxes the Reynolds similarity criterion for flows that are hydraulically rough and turbulent. Froude similarity defines the relation between all the other variables so that some factors are unaltered from prototype to model (e.g. bed slope), some are linearly scaled (e.g., grain size), whilst others are reduced by a fractional proportion (e.g. flow velocity) (Moreton et al., 2002). This kind of model has been widely used in geomorphologic studies of gravel braided rivers (e.g. Davies, 1987; Ashmore, 1991b;

Hoey and Sutherland, 1991).

The physical experiments were conducted in a flume of 3 m wide, 18 m long and 0.3 m deep with a sand layer of 0.15 m thick (Figure 5.8). The sediment gradation was similar to that of the Sunwapta River but truncated at the equivalent of coarse sand size (2.8 mm) (Figure 5.9). The grain sizes range from 0.1 mm to 8 mm with D_{50} of 1.2 mm, D_{84} of 3.0 mm and D_{90} of 3.6 mm, respectively. The sand leaving the end of the flume was recirculated from the tail tank and fed back into the flume via a vibrating mesh tray that drained the remaining water so that only sand was fed back to the flume. The time lag from the tail tank to the sand feed was about 25 s. By this kind of circulation, the sediment feed rate varies naturally and over the long-term matched the sediment transport rate in the flume (Egozi and Ashmore, 2009).

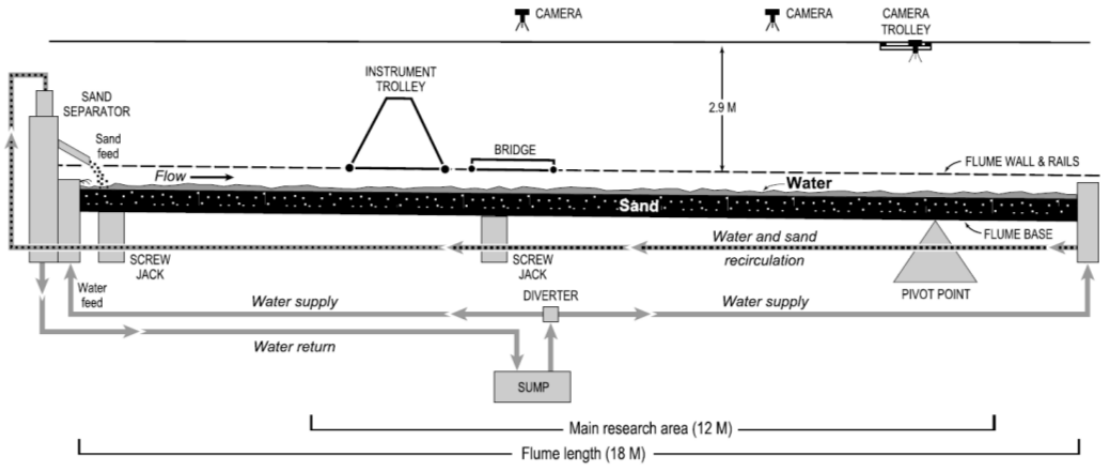

Figure 5.8 Side view of the experimental flume (Egozi and Ashmore, 2009).

Three consecutive experiments were conducted with different constant discharges but an identical flume slope of 0.015. The sequential discharges increase

gradually with values of 1.4 l/s (experiment 7), 2.1 l/s (experiment 8) and 2.8 l/s (experiment 14). Initially the flume bed was leveled with fully mixed sediments. A straight channel with a trapezoidal cross-section was cut with a top width of 0.5 m and depth of 0.015 m along the centre of the flume. To simulate the topography response to the increased discharge in an established braided pattern, the experiments were run in a sequence without bed flatting. Each experiment was run for about 70 hours. The experimental data were collected in a section of 12 m ranging from 5 to 17 m in the flume so as to minimise any entrance or sediment feed effect on the channel pattern. The experiment parameters and the main hydraulic parameters of the main channel are shown in Table 5.2. Figure 5.10 shows the variations of the total braiding intensity and active braiding intensity in the experiment. More detailed information on the experiment and data can be found in Egozi and Ashmore (2008, 2009).

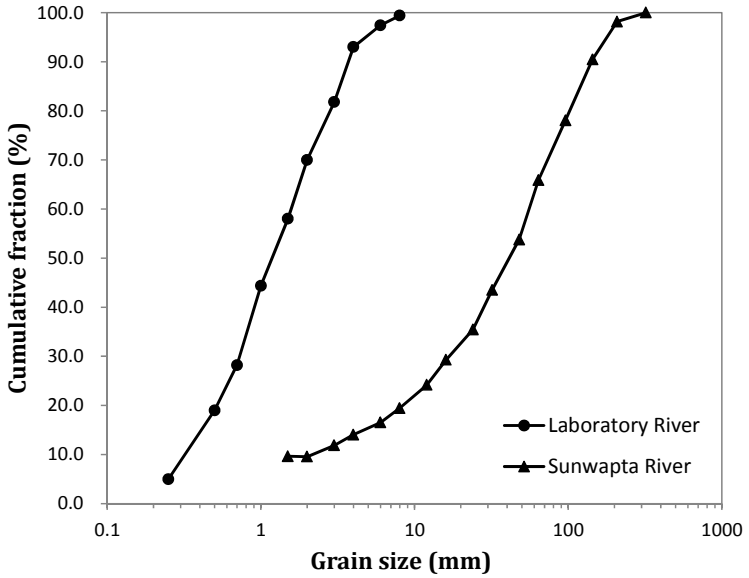

Figure 5.9 Sediment distributions in the experiment and the Sunwapta River (Varkaris, 2002).

Table 5.2 Parameters of the experiment and the main channel (Mch)

	Experimental Parameters							Hydraulic parameters of the Mch					
Exp.	T (hrs)	Q (l/s)	S_F (%)	D_{50} (mm)	D_{90} (mm)	Mean BI_A	Mean BI_T	S_B (%)	H (m)	w/H	$\overline{u}$ (m/s)	F_r	R_e
7	71.5	1.4	1.5	1.2	3.6	1.00	2.80	1.5	0.006	63	0.21	0.86	1260
8	73	2.1	1.5	1.2	3.6	1.40	3.80	1.5	0.007	61	0.24	0.91	1680
14	64.5	2.8	1.5	1.2	3.6	1.87	4.35	1.5	0.009	55	0.30	0.97	2700

BI_A and BI_T denote the active and the total braiding intensity, respectively; and S_F denotes the initial bed slope. S_B denotes the main channel bed slope; d denotes water depth; *w*/*H* denotes width-depth ratio; $\overline{u}$ denotes average velocity; Fr is the Froude number defined as $\overline{u}/\sqrt{gH}$; and Re is the flow Reynolds Number defined as $\overline{u}\,H/\nu$.

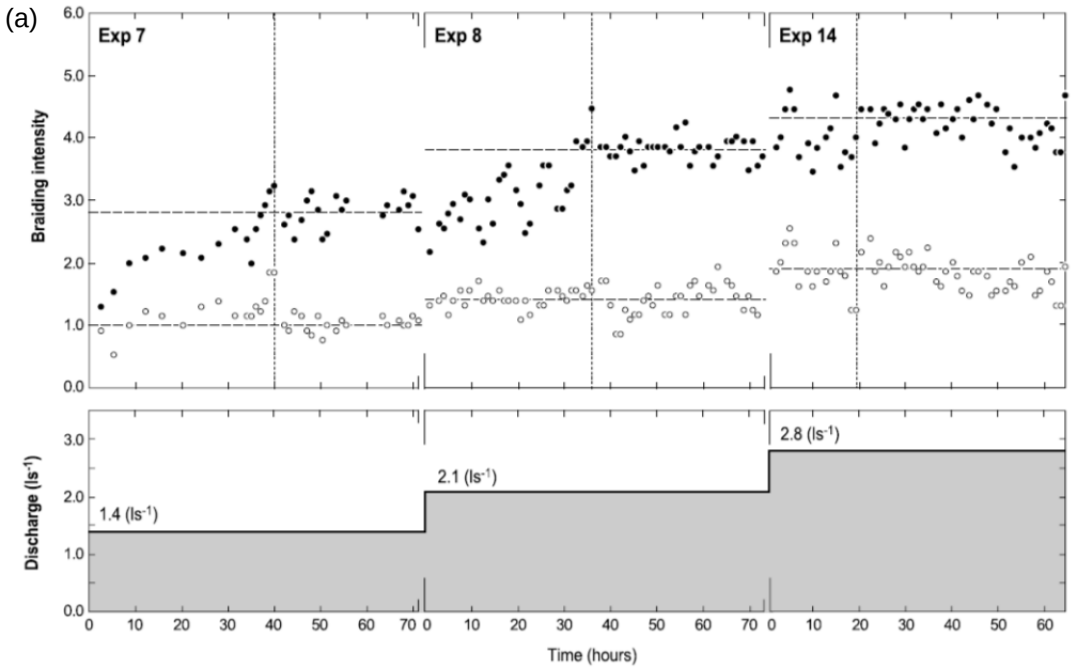

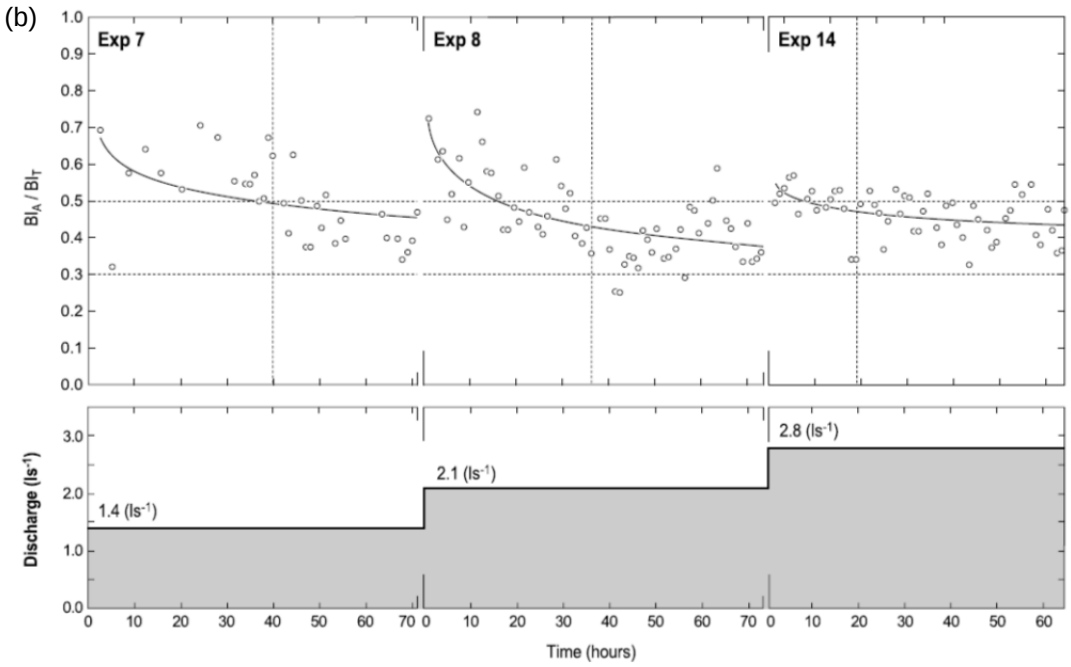

Figure 5.10 Variations of braiding intensity during each constant discharge experiment and in response to step increases in discharge between experiments: (a) mean BI_T and BI_A; and (b) BI_A/BI_T (Egozi and Ashmore, 2009).

5.3.2 Model Setup

A numerical model was set up by adopting the original experimental conditions. The flume was 18 m long and 3 m wide with a constant slope of 0.015 (Figure 5.11a). Basic parameters for the model are shown in Table 5.3. The sand distribution was identical to the experiment data which is shown in Figure 5.9. The sediments were divided into nine groups with size boundaries and percentages illustrated in Table 5.4. Three bed layers were adopted with the thicknesses of the upper layer 0.01 m, the middle layer 0.01 m and the lower layer 0.1 m. Initially the bed was assumed to be flattened and uniform, with a trapezoidal straight channel in the middle which was 0.015 m deep and 0.5 m wide (Figure 5.11b). Some immovable points spacing equivalent distances were set along the side walls of the flume. They were used to

represent the nails on the walls of the physical model (Figure 5.14). The water discharges were set to 1.4 l/s and 2.1 l/s. The aim of the simulation is not to produce a river same to the experimental river or the natural river. Instead, it is focused on improving our understanding of the braiding mechanisms and morphologic changes in the river evolution process, the essential factors for braiding generation, and the stage response for discharge. The two discharge stages adopted by the present research were enough for investigating these phenomena and mechanisms.

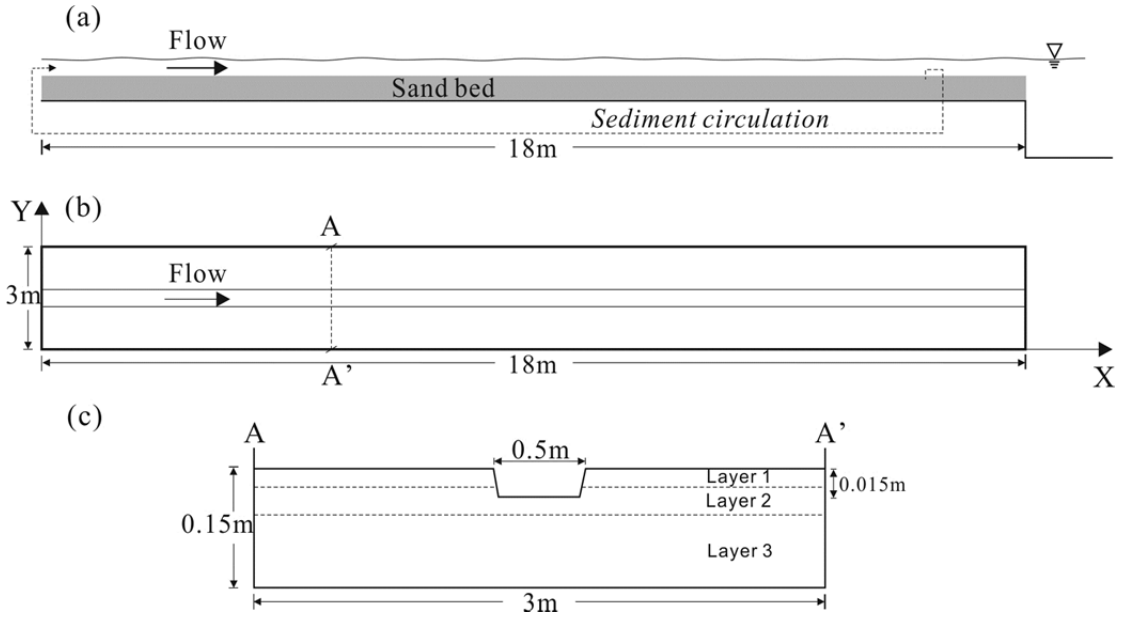

Figure 5.11 Schematic diagrams of the river flume: (a) schematic flume; (b) horizontal plan; and (c) cross-section A–A'.

The model consists of 900*150 cells, with a cell size of 0.02*0.02 m^2. To avoid the influence of the outlet, the sediments were collected at the location 2 m up the outlet, and then loaded to each cell in the upstream boundary averagely. The Coriolis effect was neglected. The momentum correction factor β was set to 1.0. The eddy

viscosity coefficient was set to 0.15 or 1.0 in different cases to analyse the influence of turbulence situation. The bed roughness coefficient (k_s) was set to $3D_{90}$ plus a correction term related to water depth (shown in Section 4.2.3). The repose angle was set to 30º both for under and above water. The time steps were set to 0.001 s and 0.01 s for hydrodynamic and sediment calculations, respectively.

Table 5.3 Initial parameters for flow and channel in the numerical model

Basic Parameters in Numerical Model							
Flume	Length	18	m	Initial Channel	Depth	0.015	m
	Width	3			Top width	0.5	
	Slope	1.5	%		Bottom width	0.46	
Sand	D_{50}	1.2	mm	Discharge	1	1.4	l/s
	D_{84}	3			2	2.1	
	D_{90}	3.6		Duration	1	71.5	hour
	Specific weight	2.65	kg/m^3		2	61.5	
Bed Layer	1	0.01	m	Model Set	Length	900	cell
	2	0.01			Width	150	cell
	3	0.15			dx (dy)	0.02	m
	Porosity	0.35			dt	0.001	s

Table 5.4 Sediment fractions and percentages in the numerical model

Sand Groups	1	2	3	4	5	6	7	8	9	
Grain Size (mm)	0.25	0.5	0.7	1.0	1.5	2.0	3.0	4.0	6.0	8.0
Percentage (%)	4.95	14.05	9.20	16.16	13.64	12.00	11.78	11.22	4.42	2.58
Finer than (%)	4.95	19.00	28.20	44.36	58.00	70.00	81.78	93.00	97.42	100.0

The simulation lasted 133 hours, with a discharge increase at hour 71.5. During this period, important hydraulic and sediment parameters, such as the flow velocity, water depth, flow discharge, Manning coefficient, Froude number, bed load transport rate, bed roughness, bed shear stress, erosion depth, bed D_{50} and D_{90} in different bed

layers, were calculated. In the present study, the braiding mechanisms and activities in the river evolution process and river geometry characteristics are investigated. The results with eddy viscosity coefficient and the slip coefficient set to 1.0 are mainly discussed.

5.4 Model Results

A braided river was formed after 41 hours with an intertwining effect of a braid with a number of alluvial channels meeting and dividing again with bars between them (Figure 5.12). Channel nodes including bars, confluences and bifurcations, and X-shaped pairs of junctions and bifurcations can be seen in the river, which share some similarities with the experimental results. Series of sequential pool-bar units have been found (Figure 5.12a). One major channel formed in the flume. Froude number was calculated by $\bar{u}/\sqrt{gd}$, which was closely related to the flow condition. For most of the active channels, Froude number was between 0.6 and 0.7 (Figure 5.12b). In some local areas, especially in the areas where confluence and bifurcation occurred, Froude number was greater than 0.7. High values did not occur in deep or shallow areas, yet often occurred at the bifurcations where the flow bifurcates and becomes shallower.

In the present model, bed shear stress is shown to be related to bed grain size distribution and water depth. High shear stress occurred mainly in the main channel and bifurcation areas with high Froude number, and sometimes existed on channel edges (Figure 5.12c). This can be related to the bed sediment distribution in the upper

layer (Figure 5.12e). Due to the special sediment load method in the experiment that "the sand leaving the end of the flume was recirculated from the tail tank and fed back into the flume", finer sediments were more involved in the circulation as it is easier for them to be transported under the same flow condition. Therefore, after some time when the river domain did not change too much, sediments in transportation should be finer than those in the beginning as more fine sediments tended to be transported and loaded back to the inlet than coarse sediments. This is also closely related to the vertical sorting effect in bed layers.

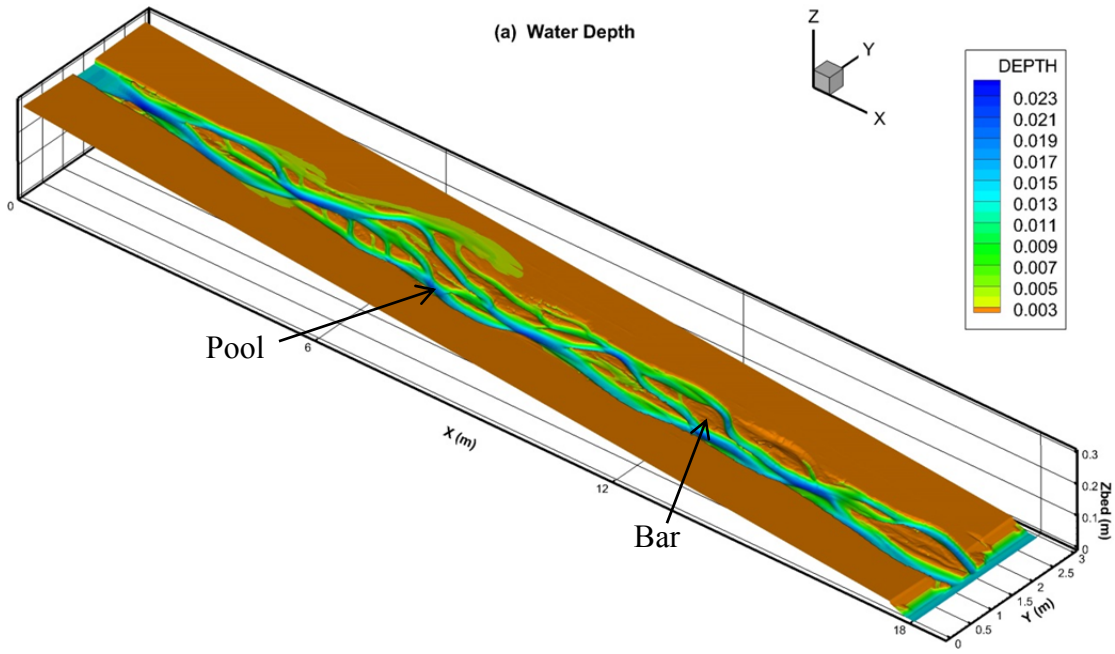

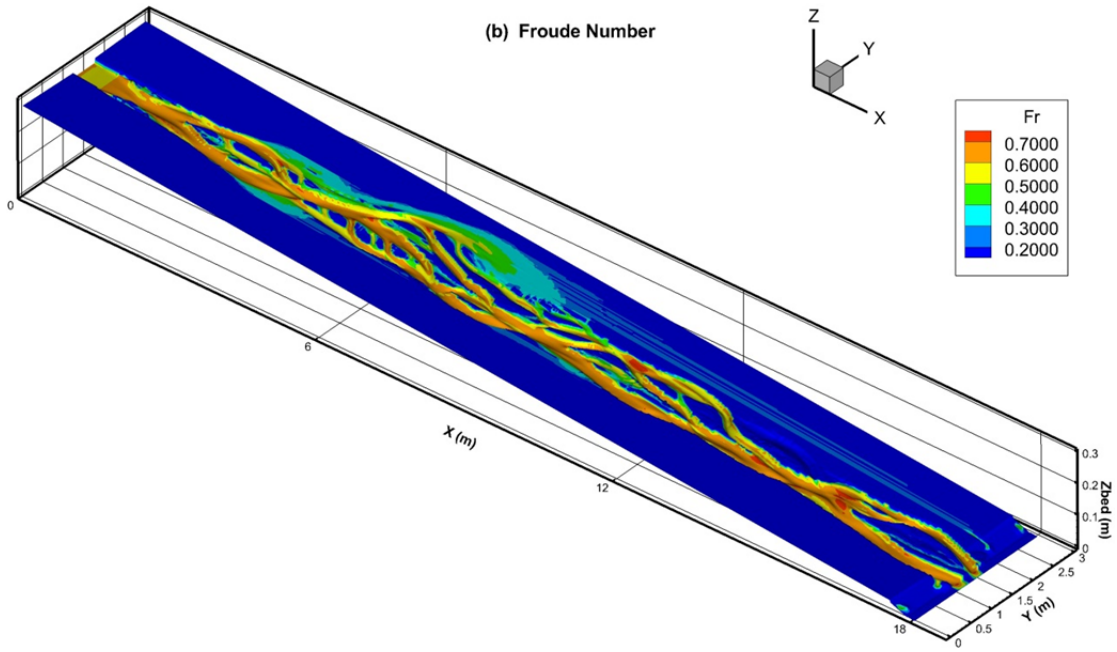
(b) Froude Number
Z
Y
X
Fr
0.7000
0.6000
0.5000
0.4000
0.3000
0.2000
0
6
12
18
X (m)
0
0.5
1
1.5
2
2.5
3
Y (m)
0
0.1
0.2
0.3
Zbed (m)

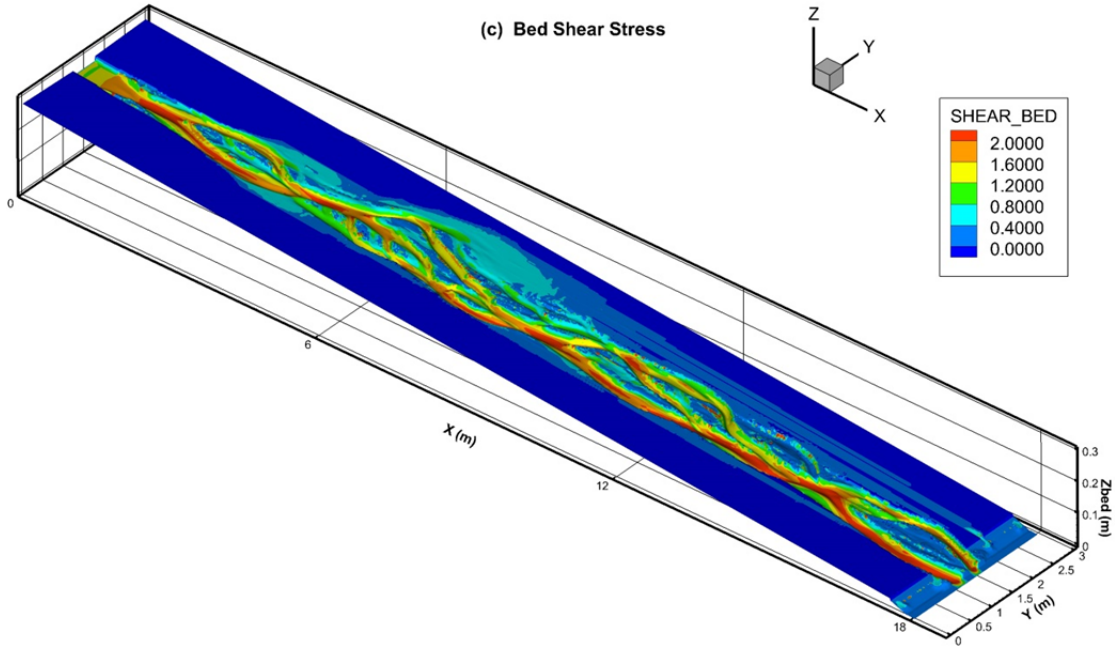
(c) Bed Shear Stress
Z
Y
X
SHEAR_BED
2.0000
1.6000
1.2000
0.8000
0.4000
0.0000
0
6
12
18
X (m)
0
0.5
1
1.5
2
2.5
3
Y (m)
0
0.1
0.2
0.3
Zbed (m)

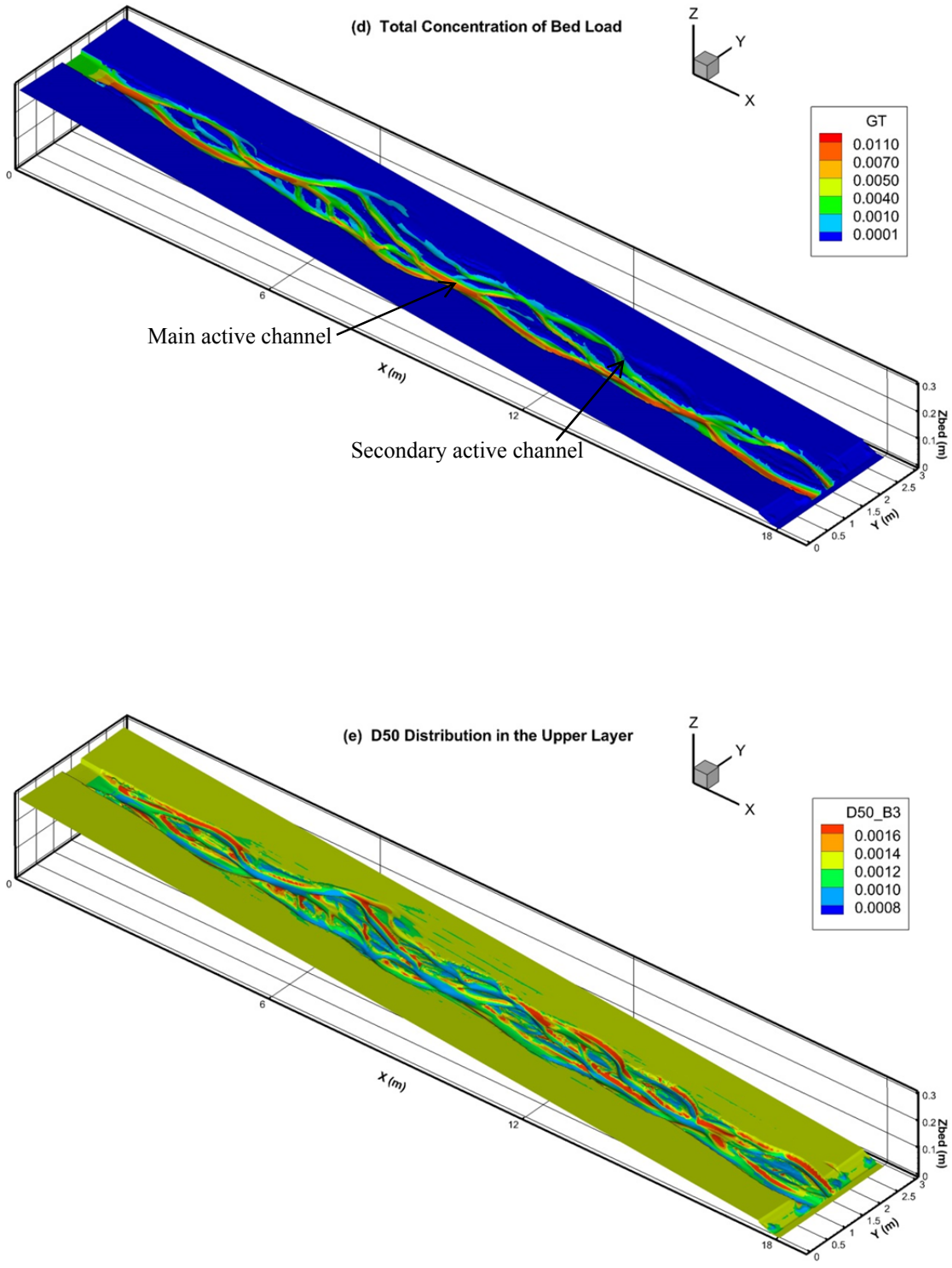

Figure 5.12 3-D images of the modelled braided river after 41 hours.

Active channel is defined as a channel with visible bed material movement (Egozi and Ashmore, 2009). In the modelled river, if the bed load transport rate is

higher than a certain value (e.g. 0.001 kg/(m·s) or some higher value), then it can be considered as “active”, otherwise as “non-active”. Referring to the bed load transport rate, a main active channel formed in the river with the highest bed load, and other active channels were joining and bifurcating from it (Figure 5.12d). Generally for channels with water depth below 4 mm, little bed load was in transport. There is a close relationship between bed load transport rate and shear stress, yet difference also exists between them. Specially, in the bifurcation areas with high shear stress, high bed load does not necessarily occur.

5.5 Braiding Processes and Morphologic Changes

5.5.1 Initiation and Development of Braiding

The evolution processes of the simulated river are analysed and compared with those of the experiments. Figure 5.13 illustrates the evolution of the modelled river. In these pictures, the colour in the areas with water depth lower than 3 mm was cut off. The reach between 3 m and 17 m is shown in these figures to present a clearer overview of the river. The river first developed in the initially cut channel and then the network continually changed its configuration by local switching of the main channel and formation or abandonment of secondary channels. Typical braiding mechanisms in natural rivers were observed in this process, including avulsion by incision, avulsion by progradation and avulsion by annexation, accompanied by frequent increases and decreases in channel sinuosity.

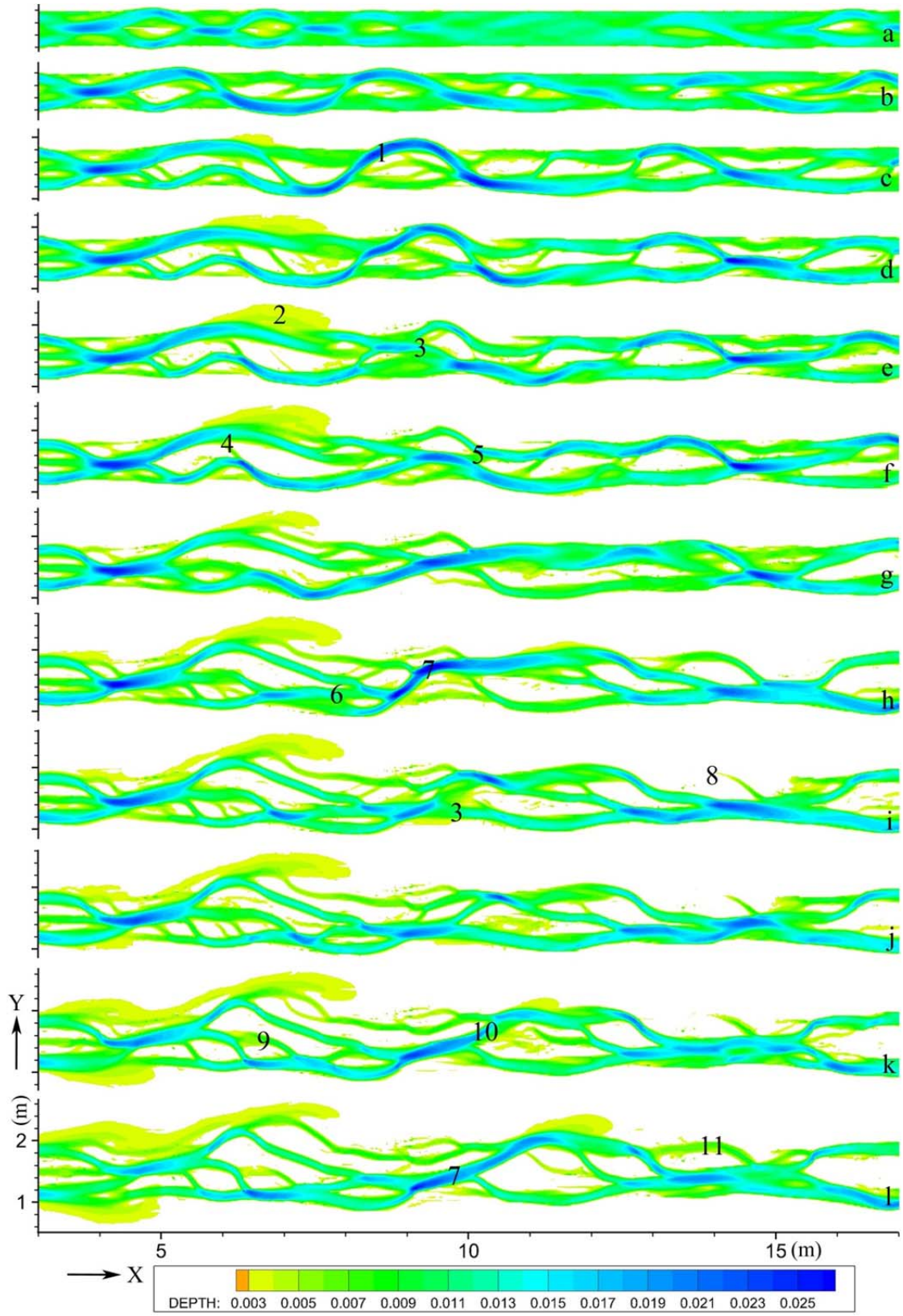

Figure 5.13 Morphologic changes and activities during the braiding evolution process of the modelled river in the reach of 3–17 m (water depth/m): (a) 8; (b) 12; (c) 19; (d) 22; (e) 24; (f) 27; (g) 30; (h) 36; (i) 38; (j) 40; (k) 44; and (l) 47 (hour).

Note: 1: increasing sinuosity of the main channel (b–c); 2: generation and obliteration of pseudoanabranches (b–c); 3: avulsion by incision 2 (apex avulsion) (h–j); 4: abandonment of the secondary channel (e–g); 5: reconnecting of two active channels (e–f); 6: avulsion by incision 1 (constriction avulsion) (g–h); 7: concentration of the flow in the main channel (g–h); 8: avulsion by progradation (choking avulsion) (h–i); 9: water diversion from one secondary channel to the other or a new one (j–k); 10: shifting of the main channel (j–k); 11: regeneration of an abandoned channel (avulsion by annexation) (k–l).

Initially, alternate bars and channels first formed in the upstream reach, mainly distributed in the initial channel within a domain of 0.5 m wide (Figure 5.13a). Then one main channel took its shape under the strengthening connection of the alternate channels by incision, bank erosion and channel migration (Figure 5.13b). Flow concentrated further in this main channel with channel sinuosity getting higher (Figure 5.13c, 1). Under the effect of secondary flow, some part of the channel migrated outside the original channel with intense bank erosion (Figure 5.13c). As the channel was getting more sinuous, at some local bend, water overflowed outside the channel and spread in the unchannelled margins downstream the bend (Figure 5.13e, 2). This activity could be viewed as an avulsion by incision. Meanwhile, at some nearby bend, the flow was dissected into several parts by the upstream flow in different directions and one of them connected with some other downstream channel in neighbourhood and avulsions occurred (Figure 5.13e, 3). This could also be classified to avulsion by incision, but with a little difference with the previous one (Figure 5.13e, 2). At the bifurcation of the newly avulsed areas, the discharge in the original main channel was decreasing yet the discharge in the new channel was increasing. Consequently, the new channel might become dominant whist the old

channel died out gradually. By avulsions the channels tend to find a straighter pathway.

The braiding configuration has been fully developed by hour 27 (Figure 5.13f). Some dissected channels reconnected with each other again by overflow or new channel erosion (Figure 5.13f, 5), while some secondary channels were gradually abandoned (Figure 5.13f, 4). The overflowed channel at one bend of the main channel was eroded and exaggerated further with its sinuosity getting lower (Figure 5.13g). Again the flow concentrated in the main channel and then it formed another channel bend (Figure 5.13h, 7), at which an avulsion occurred consequently by channel interception (Figure 5.13i, 3). Some channels were choked by channel progradation (Figure 5.13i, 8). More avulsions by incision occurred accompanied by the abandonment of some other secondary channels (Figures 5.13h and i).

By hour 40, the upstream reach had widened a lot by extending downstream and to the original margin areas, evolving to a new stage (Figure 5.13j). As it developed, the bifurcated channels allocated a large amount of flow from one of the original channels around the bar and finally evolved into a deep channel, followed by the disappearance of the original channel (Figure 5.13k, 9). The main channel shifted to another tributary as the upstream flow condition was changing (Figure 5.13k, 10). Some of the channels generated by avulsions disappeared while some previous abandoned channels were regenerated by channel annexation (Figure 5.13l, 11). The main channel was getting more sinuous again and a new circulation of straight channel to sinuous channel and then to avulsions might occur in future.

The initiation of braiding in the physical model shared similarities with the numerical model (Figure 5.14, experiment 7, q = 1.4 l/s, with the activity number identical to Figure 5.13). Some alternate bars and channels were first originated and then one main channel was generated (Figure 5.14, 1-1, 1-3). With its sinuosity getting higher, channel avulsions occurred and then more secondary channels were formed (Figure 5.14, 1-5, 1-7). The main channel migration and the abandonment of secondary channels left some abandoned channels without any flow (Figure 5.14, 1-24). Figure 5.13 and Figure 5.14 illustrate that the evolutions of the modelled river and the physical model share similar initiation processes and braiding activities. Some of the activities observed in the numerical model were also found in the laboratory river (Egozi and Ashmore, 2009).

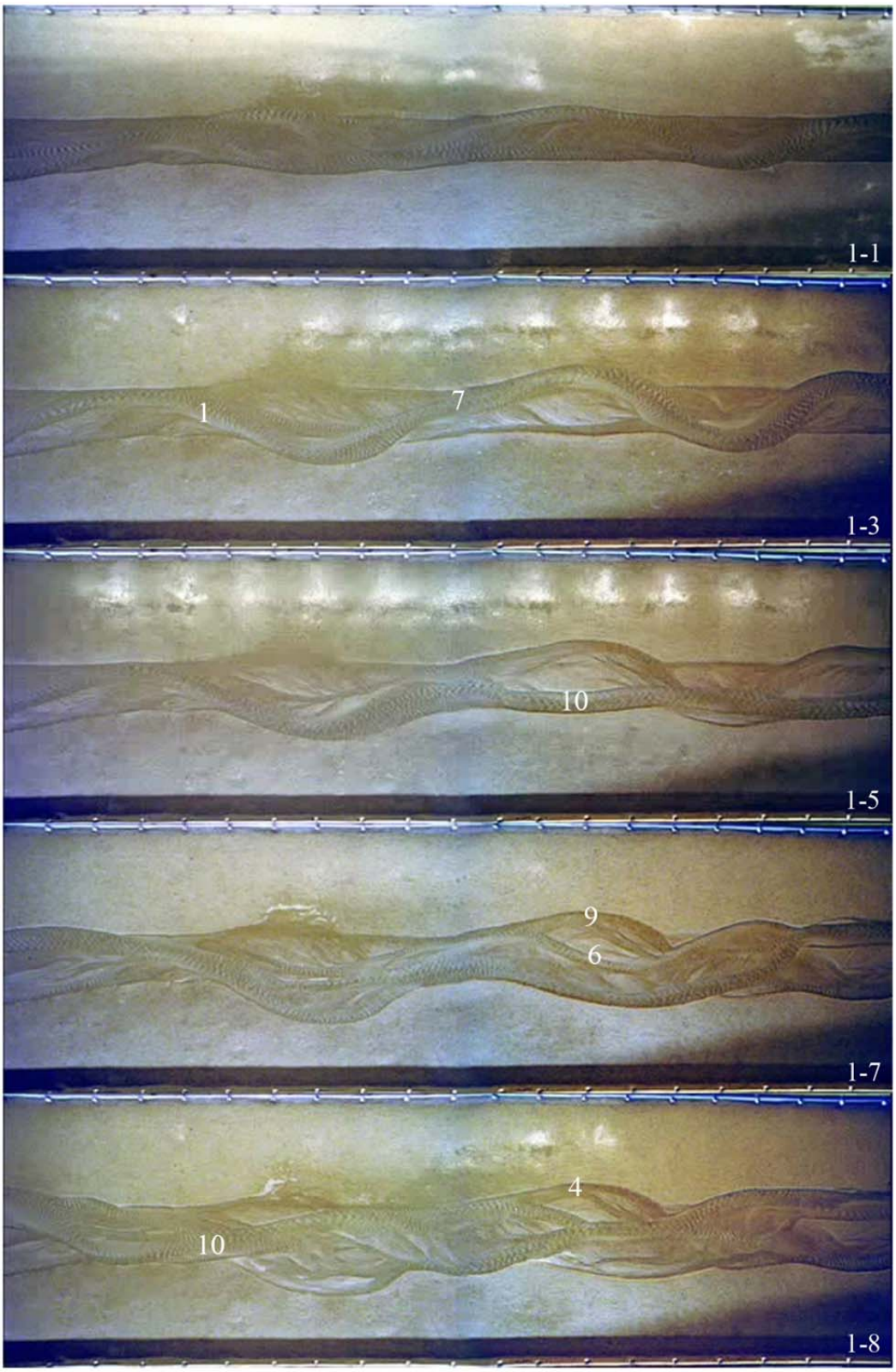

(to be continued)

(continued)

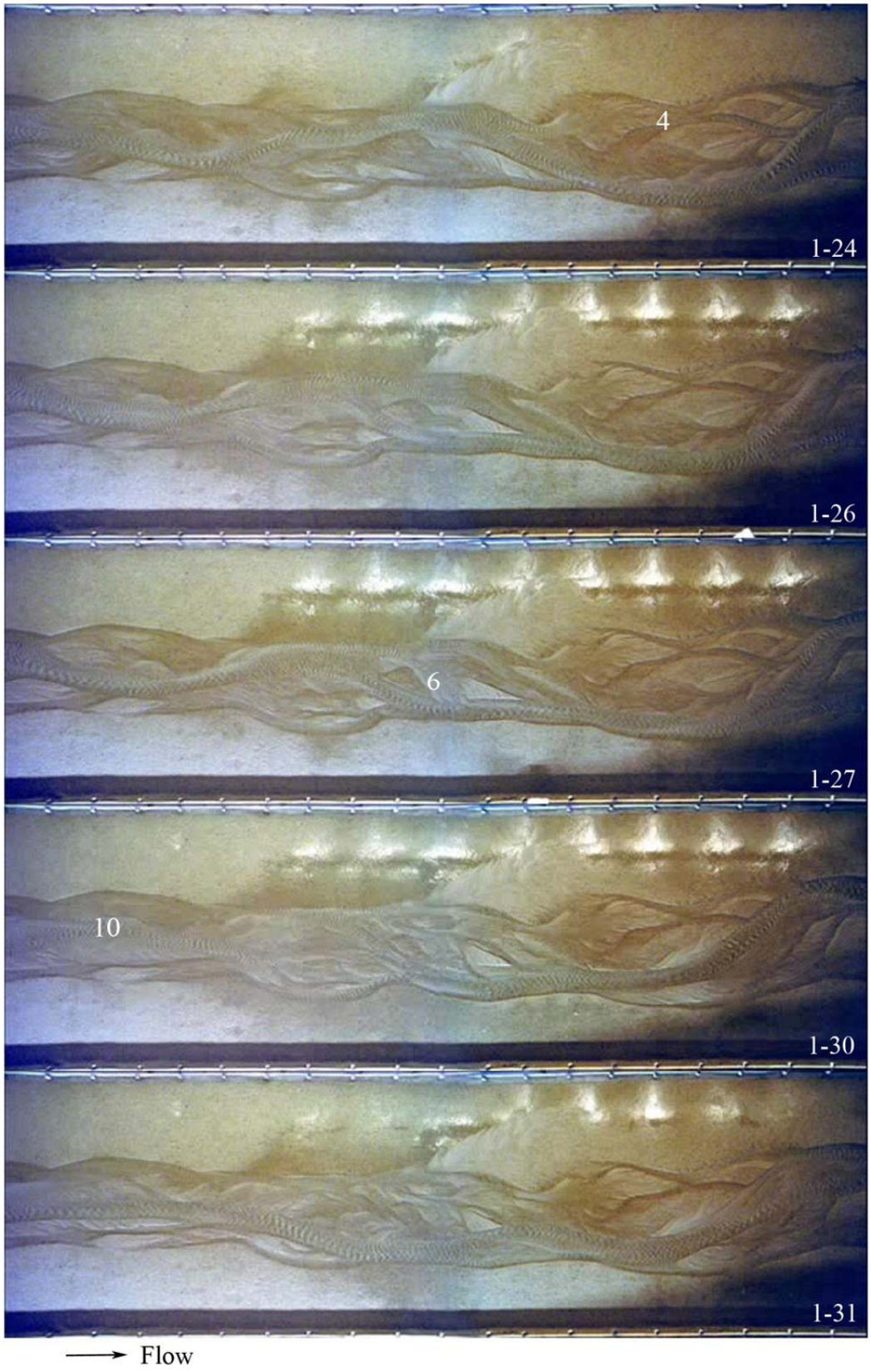

Figure 5.14 Morphologic evolution process of the laboratory river in the reach of 6–17 m.

5.5.2 Response to Increased Discharge

Figure 5.15 shows the regime response of the braided pattern to a step increase in discharge from hour 71 to hour 113. As the discharge increased from 1.4 l/s to 2.1 l/s at hour 71.5, the channels responded by increases in sinuosity and total channel number, channel widening and frequent channel avulsions. The alternation of the development and disappearance of some secondary channels is a typical characteristic during this period. As found in the experiment (Egozi and Ashmore, 2009), the total number of bifurcations gradually increased and then became stable with the given discharge.

The braided pattern at the end of the first stage (1.4 l/s) is shown in Figure 5.15a, which has entered a stable stage by hour 71. Multiple channels including confluences and bifurcations exist in the upstream reach, compared with the relatively simple channel pattern in the downstream reach (Figure 5.15a). As flow discharge increased, the main channels widened and became deeper and more sinuous (Figure 5.15b). Some secondary tributaries disappeared with the development of the main channels (e.g. Figure 5.15a, 1), which were thought mainly due to choking avulsions. Some water overflowed the channel bank and spread across the unchannelled margins of the river, which was called “pseudoanabranches” (Figure 5.15c, 2). Some of them grew into new channels while others did not. As the channels became more sinuous (Figure 5.15c, 3), some bends got curved enough for the occurrence of avulsions, or for the generation of more pseudo-anabranches (Figure 5.15e, 5). The main channel migrated frequently between its tributaries (Figure 5.15d, 4). After channel avulsions occurred,

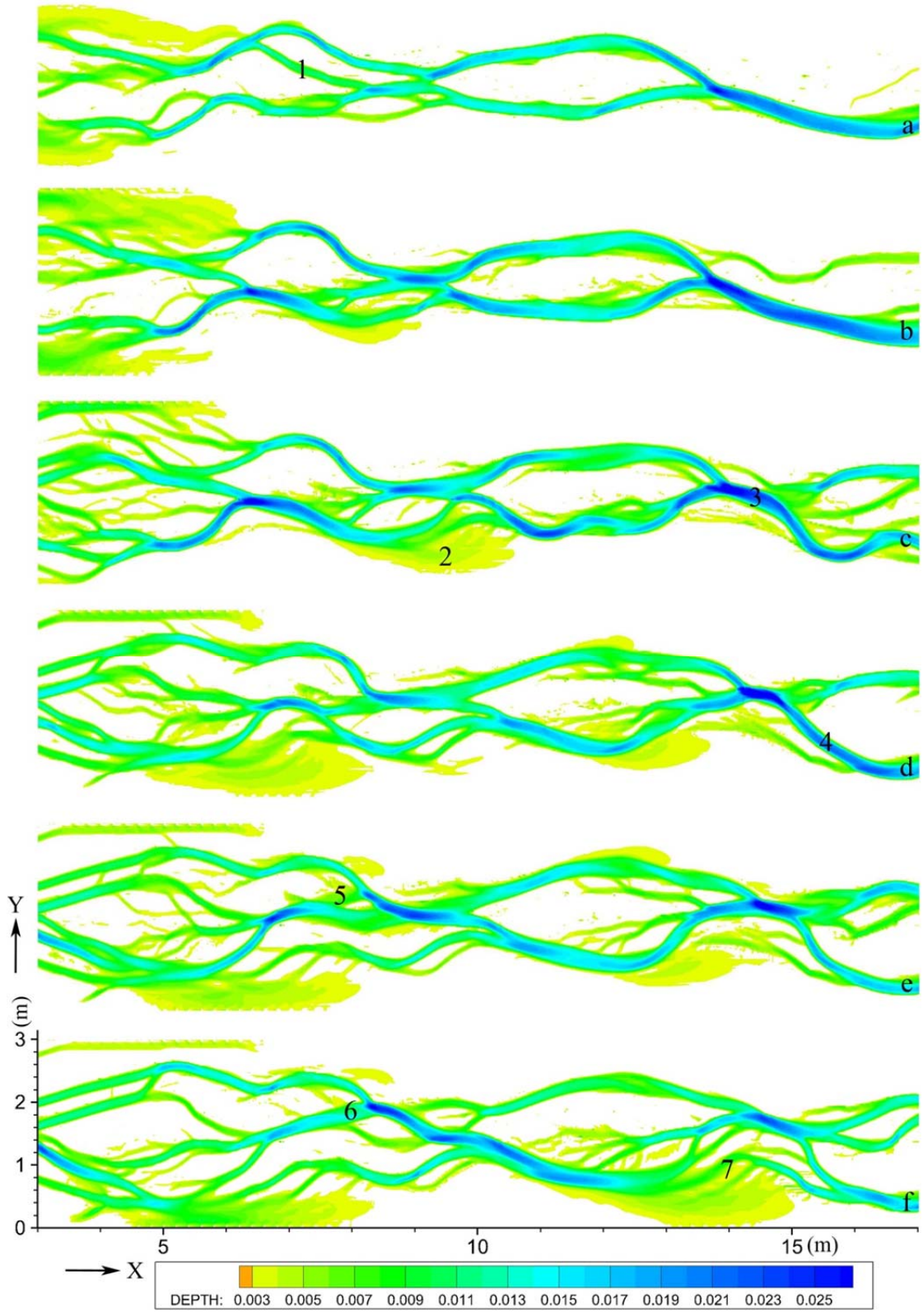

(to be continued)

(continued)

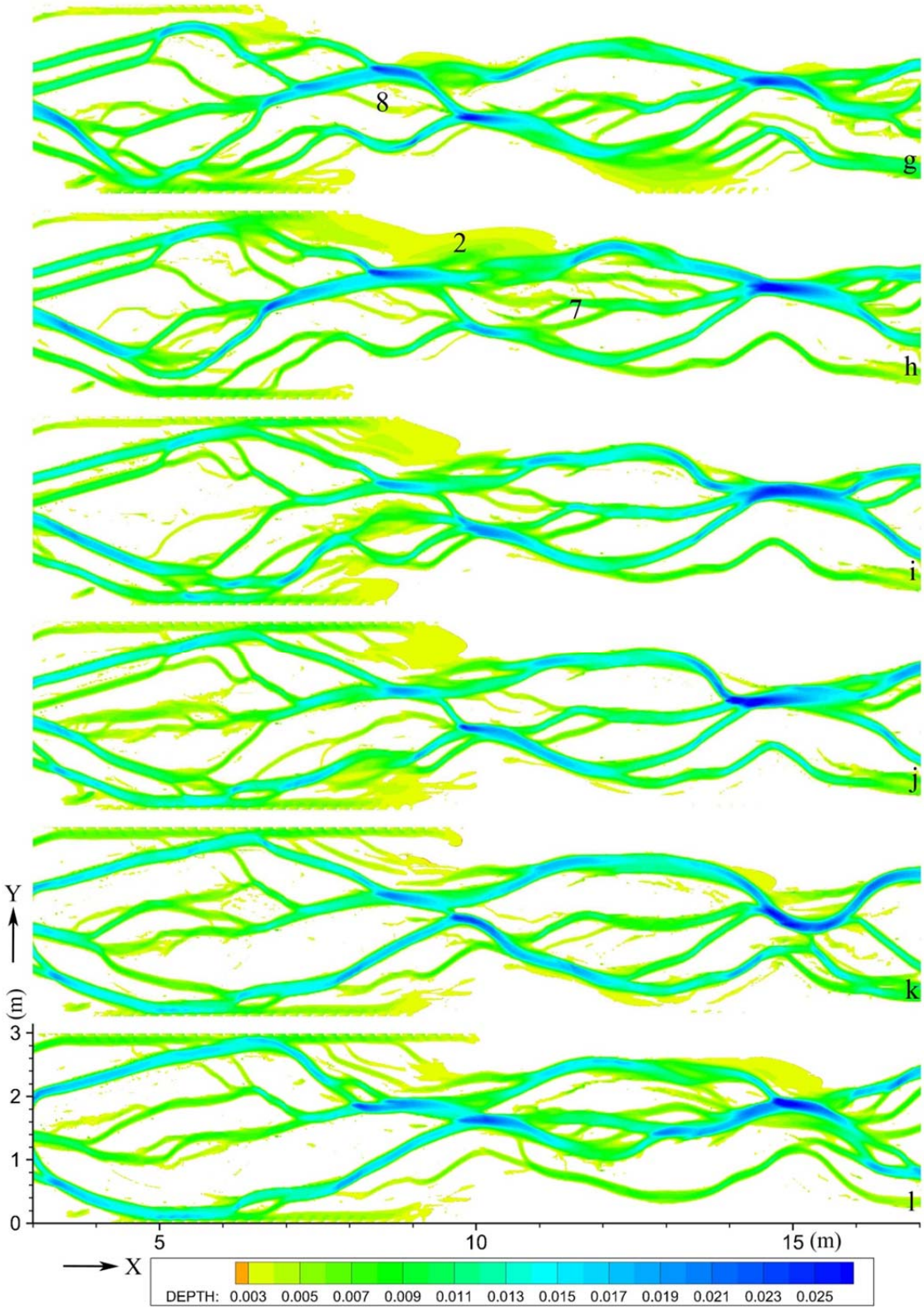

Figure 5.15 Morphodynamic response to the increased discharge from 1.4 l/s to 2.1 l/s in the reach of 3–17 m (water depth/m): (a) 71; (b) 76; (c) 81; (d) 86; (e) 88; (f) 91; (g) 94; (h) 98; (i) 102; (j) 105; (k) 110; and (l) 116 (hour).

Note: 1: abandonment of secondary channel (avulsion by progradation, or choking avulsion) (a–b); 2: generation and obliteration of pseudoanabranches (c–e); 3: increasing sinuosity of the main channel (b–c); 4: lateral migration of the main channel (c–d); 5: avulsion by incision 1 (constriction avulsion) (d–e); 6: water diversion from one secondary channel to the other or a new one (e–f);7: generation of more secondary channels (f and h); 8: abandonment of the avulsion channel (f–h).

a large amount of water at the bifurcation was diverted from the original channel to the new channel (Figure 5.15f, 6). Consequently, the old channel died out gradually (Figure 5.15g, 8). The spreading water outside the channels eroded the river bed to form some new secondary channels (Figure 5.15f, 7).

The number of total channels did not increase with the flow immediately. Instead, this effect could be seen clearly after approximately 20 hours in the downstream reach (Figure 5.15f), compared with that of about 15 hours in the upstream reach (Figure 5.15d). Then channel changes occurred frequently, with the generation and obliteration of secondary channels and pseudoanabranches, and the migration of the main channel. The whole stream arrived at a considerable stable stage after approximately 30 hours (Figure 5.15h). After discharge increased, the main channel could be seen in the early stage, yet several channels were formed which were nearly equivalent to each other in the late stage. As the main channel migrated, more pseudoanabranches were generated in the river under the increased discharge.

5.6 Braiding Mechanisms

Braiding mechanisms in real braided rivers have been introduced in Chapter 2. The braiding mechanisms found in the evolution process of the modelled river have

been briefly introduced in Section 5.6. Generally, four typical avulsion processes are investigated herein, including avulsion by progradation (choking avulsion), avulsion by incision 1 (constriction avulsion), avulsion by incision 2 (apex avulsion), and avulsion by annexation.

5.6.1 Avulsion by Progradation (Choking Avulsion)

Choking avulsions occurred frequently in the evolution process of braiding. It belongs to the avulsion by progradation in the category of Slingerland and Smith (2004). One case (Figure 5.13i, 8) was chosen to analyse the development of this kind of avulsion. It occurred at a bifurcation area of two tributaries, namely, the left tributary (L) and right tributary (R) (Figure 5.16, areas with water depth below 2 mm are viewed as dry). In this process, as one channel disappeared which had been flowing into the bifurcation (channel 1, Figure 5.16c), continuous deposition occurred in the left tributary, resulting in the development of a bar (bar A, Figure 5.16f) and the death of the tributary. Finally, the bifurcation disappeared. This activity illustrates one mechanism of channel dying in braided rivers. Two lines were stretched across the left tributary and the right tributary, as shown in Figure 5.16. The sequential changes of the parameters in the two tributaries are shown in Figure 5.21 and Figure 5.22.

The left tributary gradually died out during the period of hour 34 to 39, when deposition dominated in the channel evolution process. Initially, the scour axis of the bifurcation was towards the left tributary, yet it transferred to the right tributary in about 0.5 hours (Figure 5.16b). In the channel, the flow talweg and maximum shear

stress were close to the right bank of the channel apparently (Figures 5.21b and c). However, the fastest flow was not in the talweg area. Instead, it was closer to the left bank, so was the bed load transport rate. In the next two hours, as channel 1 died out and channel 2 gradually grew, the discharge flowed into the bifurcation decreased. Consequently, the flow in the left tributary could not afford the wide channel and it was gradually divided into two parts. Sediments deposited quickly in the middle of the channel and accordingly, one bar appeared (Figure 5.16f). As the bar grew, the two small tributaries around it gradually died out. Finally, the left tributary disappeared.

The right tributary migrated towards channel 2 and eroded the bed to enlarge its domain. Initially the talweg of the channel existed close to the left bank (Figure 5.22b). Before hour 36.5, the main channel was eroded and a deeper region formed near the left bank. During this period, flow velocity and shear stress slightly increased. Nevertheless, as sediment transport capacity (q_b) became greater than the sediment transport rate (Total C, Figure 5.22d), flow carried more sediments, leading to an increase in bed load transport. River bed was eroded to a maximum value of 3 mm. The talweg migrated towards the left bank. After 36 hours, with the disappearance of channel 1, the channel began to migrate towards the right bank. Intense bank erosion occurred at the right bank, with bank sliding playing an important role. During this period, bed load transport rate was approximately equal to bed load transport capacity, indicating that sediment transport is in equilibrium.

Figure 5.18 illustrates the trends of bed load transport rate. Ashmore et al. (2011)

defined active channel as one channel with visible bed material movement. However, it is hard to give a definite criterion for the "visible bed material movement", since it can vary with some factors such as the sensitivity of different people. If 0.001 kg/(m·s) is taken as the boundary of active and nonactive, in the left tributary, bed load transport rate continued decreasing in the whole process, and the channel became nonactive from hour 36.5 (Figure 5.18f). Meanwhile, in the right tributary, bed load transport rate first kept increasing till hour 37, and then decreased gradually. In other words, the left tributary became less active, while the right tributary first became more active, and then less active.

Figure 5.19 and Figure 5.20 illustrate the bed load transport rate and bed elevation changes in the channel avulsion. In Figure 5.20, the elevation data excluded bed slope and the datum located on the edge of the flume, with u_b denoting bed load transport velocity. Different with the choking avulsion in braided rivers with suspended load (will be shown in Chapter 6), the position of the bar head and its sediment distribution nearly remained unchanged. The bar growth could be seen in Figure 5.19. After the avulsion occurred, the left channel did not disappear completely. Instead, most of its channel still remained alive except its head at the bifurcation was blocked. One abandoned channel could be seen in Figure 5.16i. As to the bed sediment distribution, fine sediments distributed on the bar with no flow passing and in channels with most flow passing, whereas coarse sediments distributed on the edges of the channels. The coarse edge of channels was also observed in the experiment of Egozi and Ashmore (2009). The sediments in bed were generally

coarser than those in transport (Figures 5.21f and 5.20g), indicating that the model presented the coarsening and fining effect correctly.

The incentive of the occurrence of the choking avulsion deserves to be investigated. In braided rivers, as the braiding configuration develops, channels may get more sinuous and thus the flow discharge redistributes among different channels. In the channel avulsion illustrated herein, the more and more sinuous upstream channel caused the discharge redistribution between the two tributaries. Different from the avulsion found by Slingerland and Smith (2004), it was related to the discharge changes in several channels, other than the change only occurred in the parent channel.

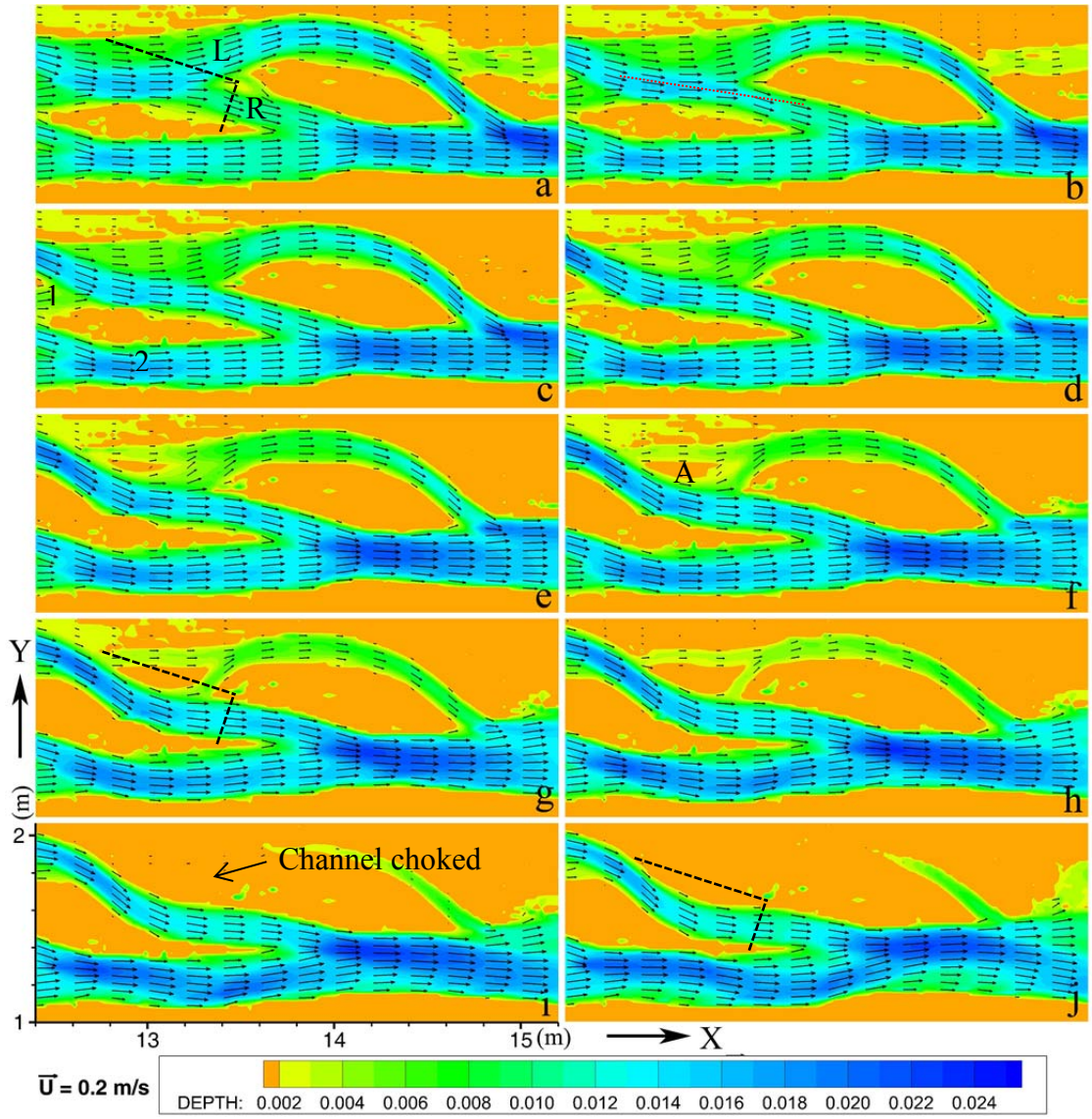

Figure 5.16 Water depth in the avulsion by progradation (m): (a) 34; (b) 34.5; (c) 35; (d) 35.5; (e) 36; (f) 36.5; (g) 37; (h) 37.5; (i) 38; and (j) 39 (hour).

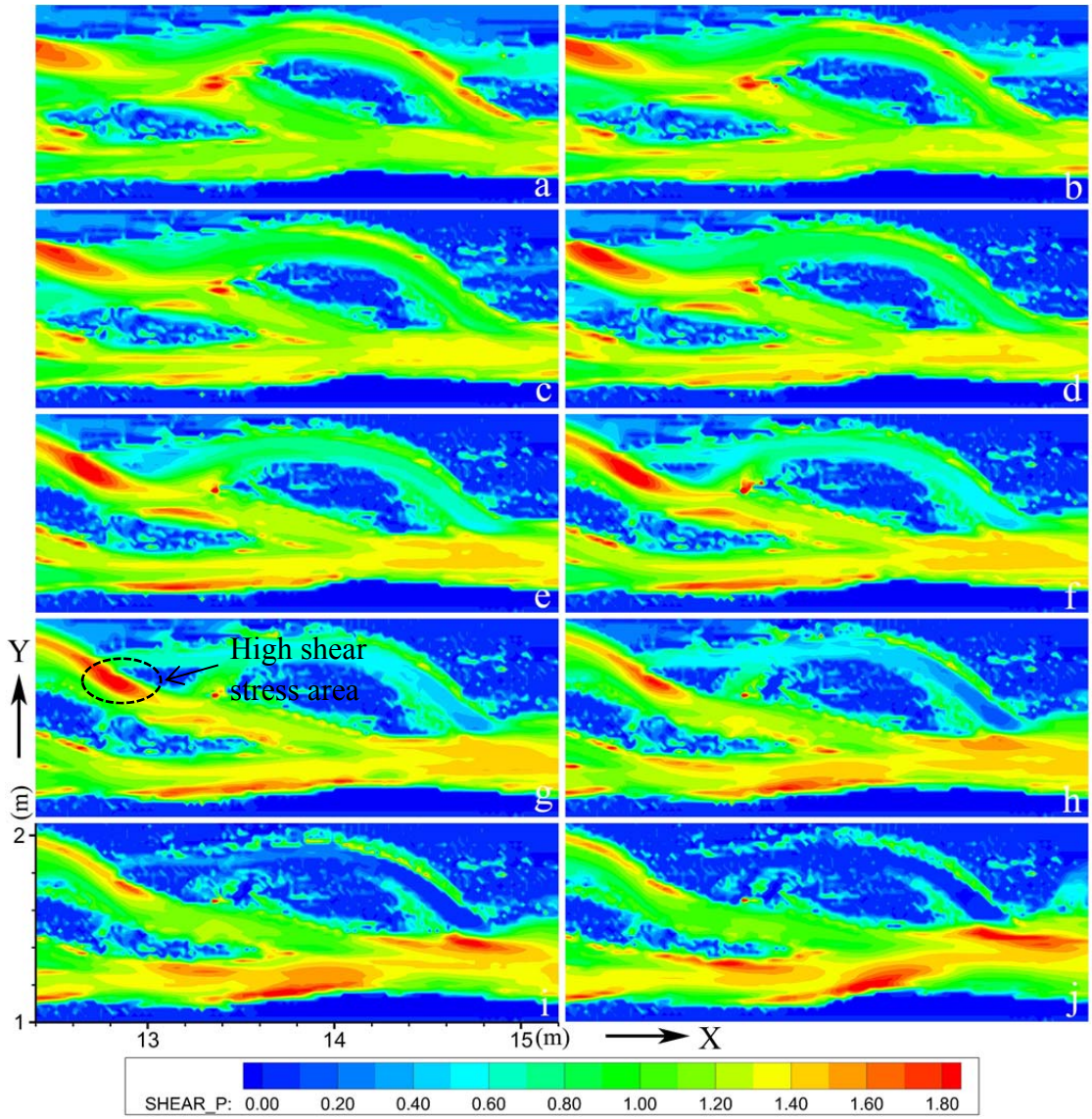

Figure 5.17 Shear stress in the avulsion by progradation (N/m^2): (a) 34; (b) 34.5; (c) 35; (d) 35.5; (e) 36; (f) 36.5; (g) 37; (h) 37.5; (i) 38; and (j) 39 (hour).

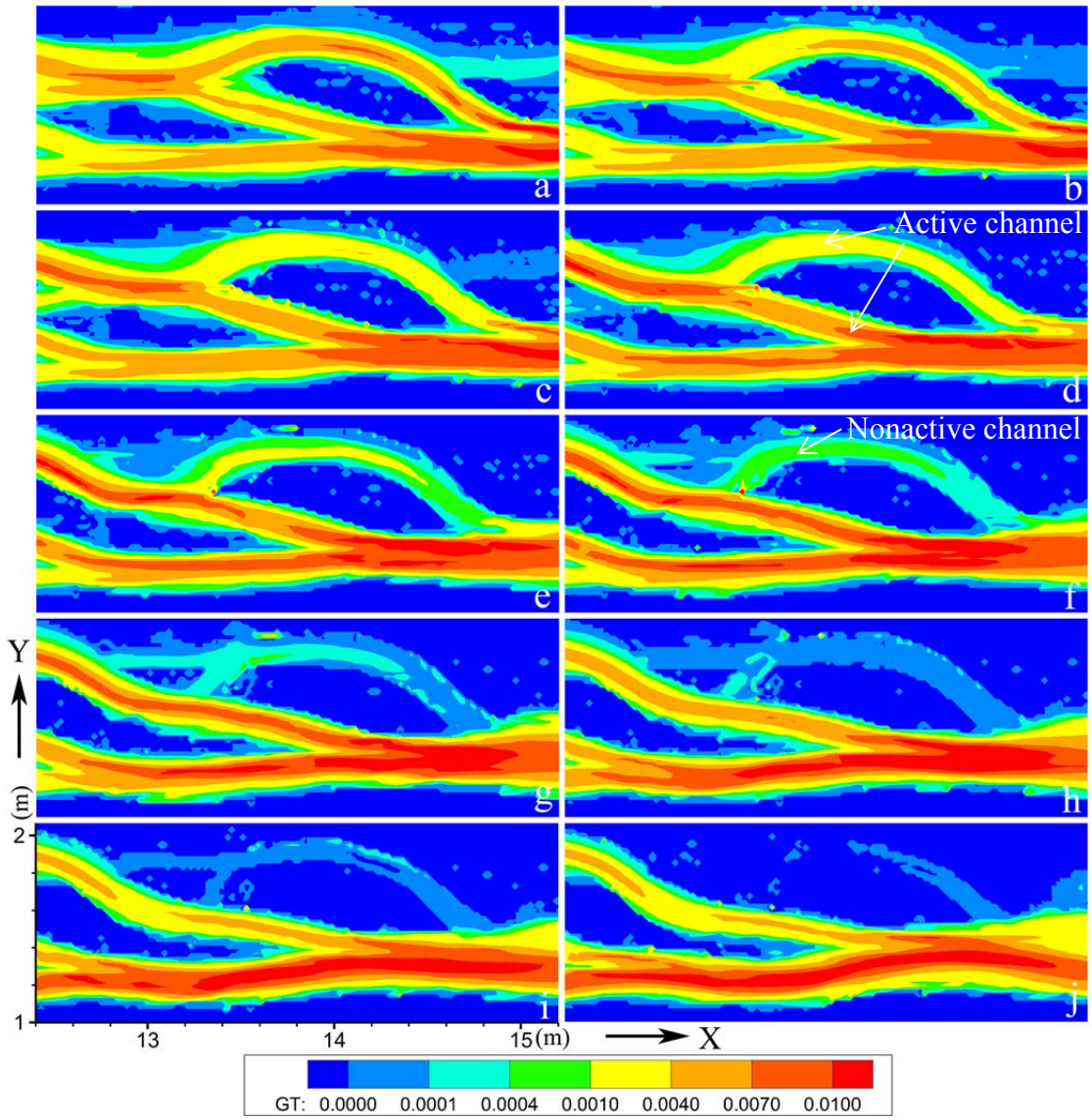

Figure 5.18 Bed load transport rate in the avulsion by progradation (kg/(m·s)): (a) 34; (b) 34.5; (c) 35; (d) 35.5; (e) 36; (f) 36.5; (g) 37; (h) 37.5; (i) 38; and (j) 39 (hour).

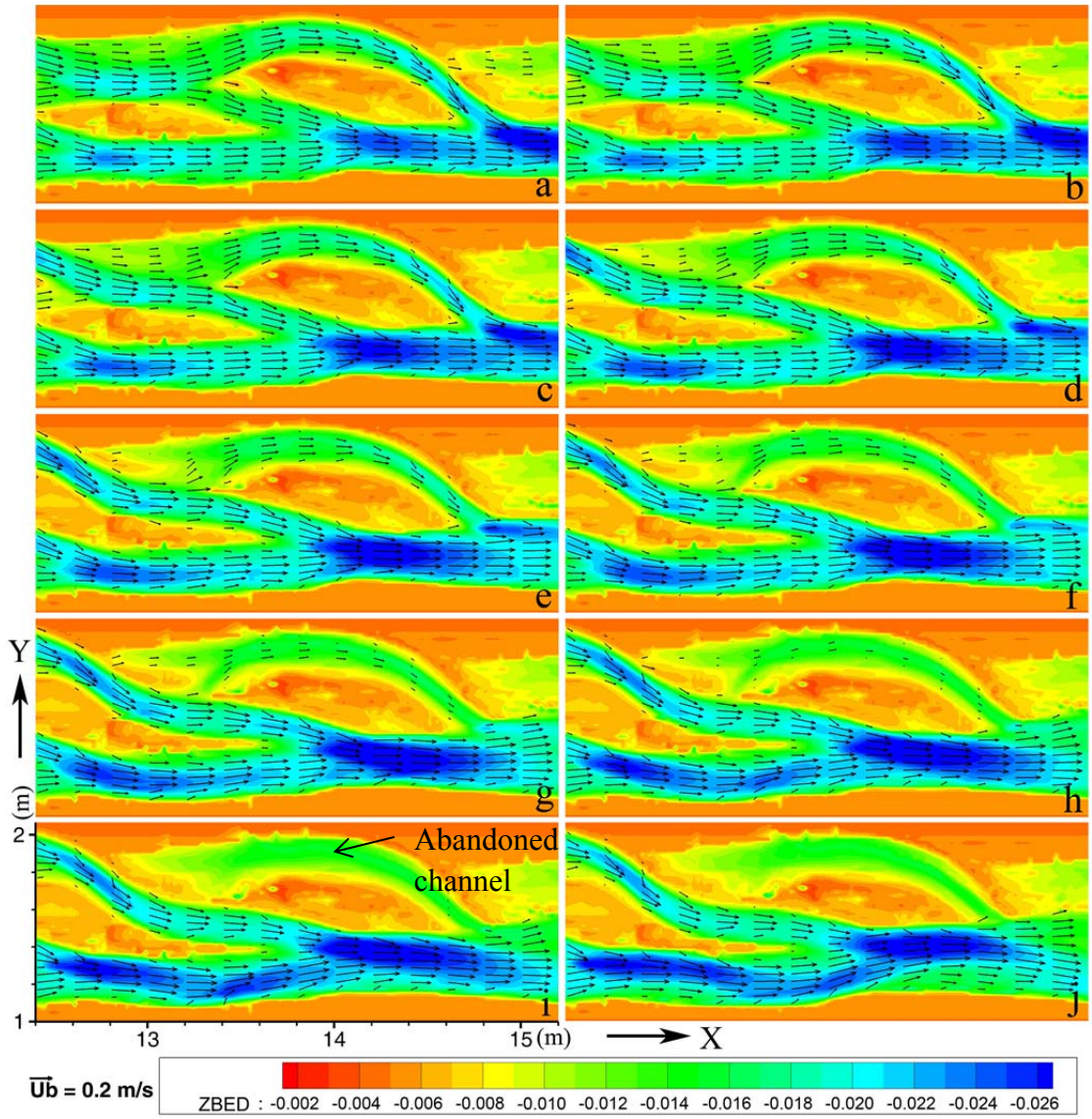

Figure 5.19 Bed elevation in the avulsion by progradation (m): (a) 34; (b) 34.5; (c) 35; (d) 35.5; (e) 36; (f) 36.5; (g) 37; (h) 37.5; (i) 38; and (j) 39 (hour).

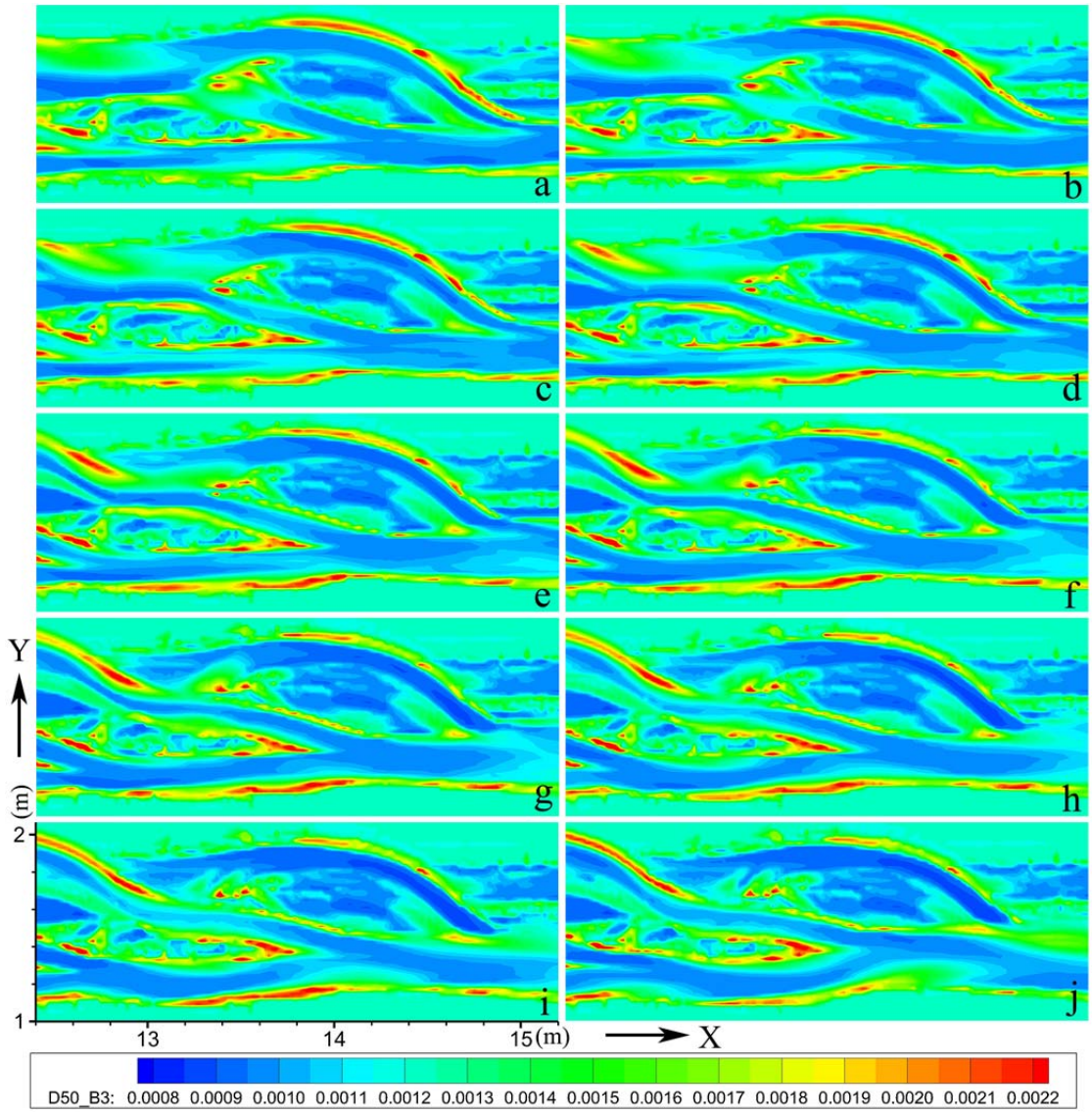

Figure 5.20 Sediment D_{50} distribution in bed in the avulsion by progradation (m): (a) 34; (b) 34.5; (c) 35; (d) 35.5; (e) 36; (f) 36.5; (g) 37; (h) 37.5; (i) 38; and (j) 39 (hour).

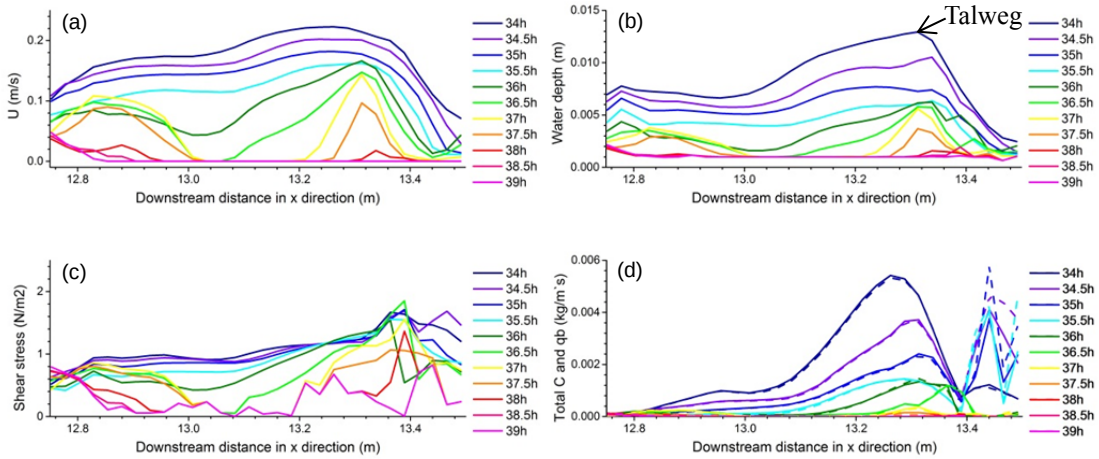

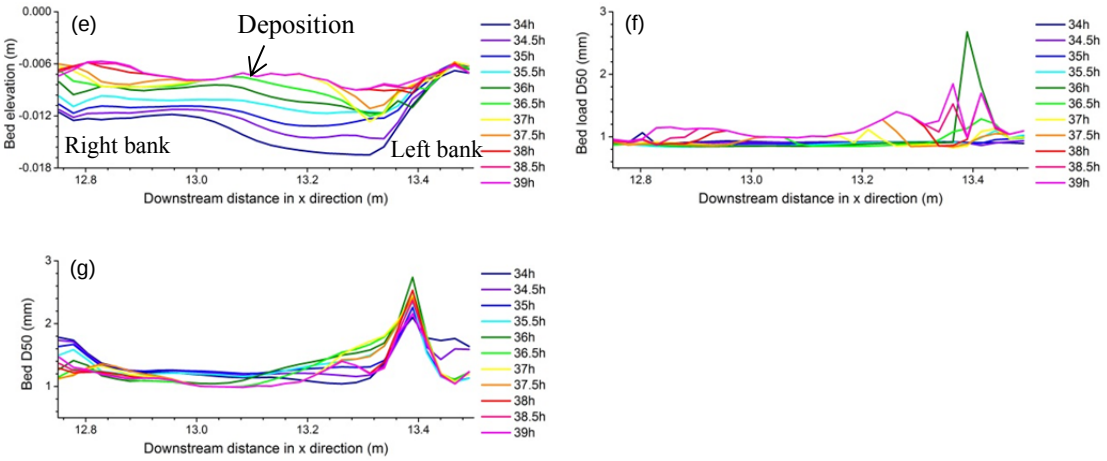

Figure 5.21 Hydraulic and morphodynamic changes in the left tributary during the avulsion by progradation.

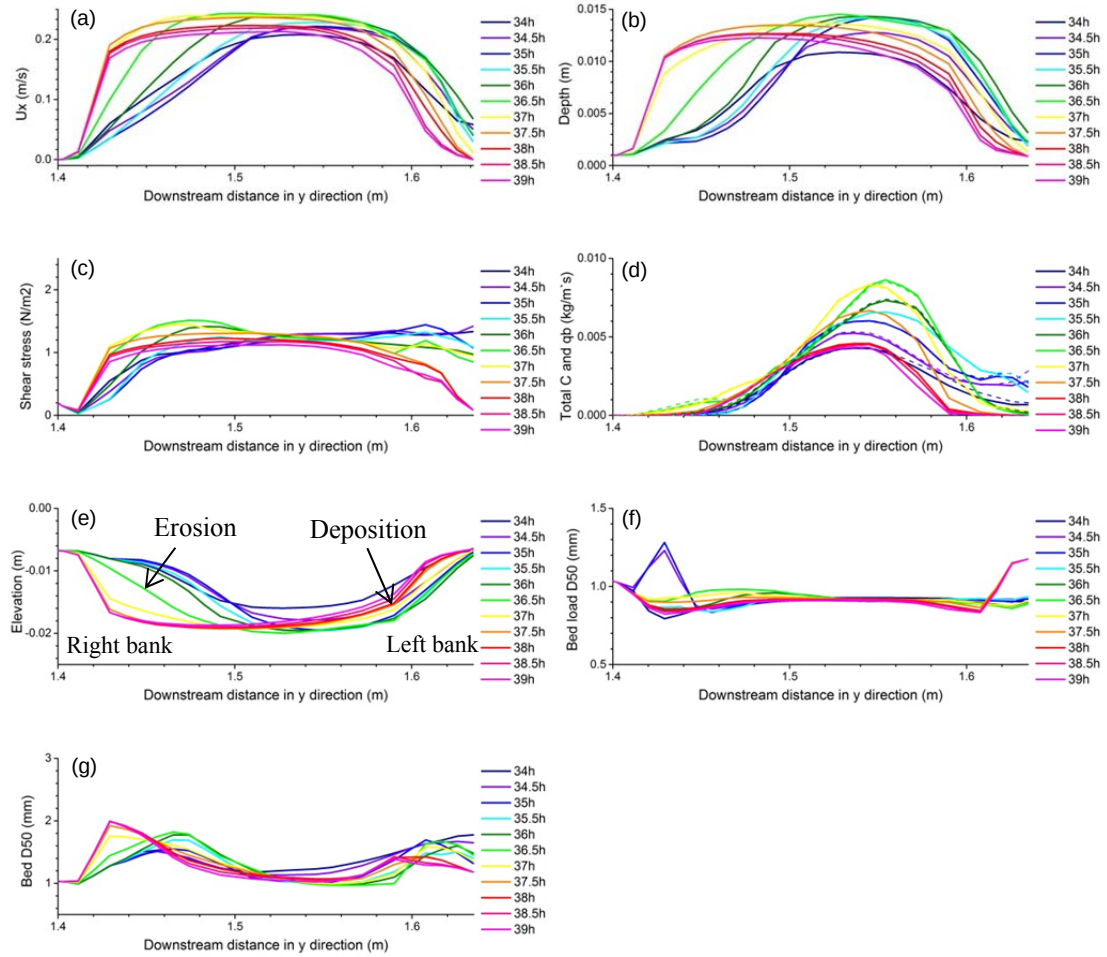

Figure 5.22 Hydraulic and morphodynamic changes in the right tributary during the avulsion by progradation.

5.6.2 Avulsion by Incision 1 (Constriction Avulsion)

Constriction avulsions can be found both in the braiding initiation stage and the response stage to the abruptly increased discharge. It is one situation of the avulsion by incision in the classification of Slingerland and Smith (2004). One case (Figure 5.15e, 5) was chosen to illustrate the evolution process of this kind of avulsion. In this process, with the development of the upstream channel configuration, the channel bend was getting more sinuous (Figure 5.23c), and then water overflowed from this channel bend to achieve a more straight course (Figure 5.23e). Consequently, a new channel was generated (Figure 5.23i). As the new channel grew, it branched a large amount of the discharge in the old channel (channel 1, Figure 5.23i) and finally caused it to die out. As stated by Slingerland and Smith (2004), this avulsion was driven by the initial irregular and inefficient pathway (more and more sinuous bend). One line was stretched across the new channel and one old channel (Figure 5.23e). The changes of the essential parameters along this line are shown in Figure 5.28.

As the parent channel grew, water ponded at its bend (Figures 5.26b and c). From hour 85.5 to 86, water overflowed from the channel bend and water depth increased by about 4 cm in the deepest area, and flow velocity increased to about 0.1 m/s from almost zero (Figures 5.28a and b). However, the bed elevation remained nearly unchanged. This indicates that, the overflowing activity occurred in such a short time that there was no opportunity for flow to erode out their channel. In the next half hour, more discharge flowed out and distributed in an unchannelled condition (Figure 5.23e). Flow velocity and shear stress increased apparently and thus

bed load erosion began to occur.

From hour 86.33 on, the new channel began to erode its way. Its development was accompanied by the dying of the old channel (channel 1). The left bank of channel 1 was eroded intensely from hour 86.17 to 86.5. Conversely, its talweg which was originally close to its right bank was quickly filled to a large content. Erosion at the left bank and deposition at the right bank continued in the next few hours. Consequently, a new channel formed (Figures 5.23 and 5.28e). Channel 1 gradually died out and its discharge was totally adopted by the new channel.

Shear stress in the new channel increased faster than water depth (Figures 5.27b and c). Bed load transport rate changed slower than other parameters (Figure 5.23). The total bed load transport rate would increase if it was greater than its transport capacity (q_b) and consequently erosion occurred. Otherwise, deposition would occur. Coarse sediments distributed mostly on the edge of the channels, especially near the areas of bifurcations (Figure 5.27). Sediments in transport were always finer than bed sediment distribution (Figures 5.28f and g).

Constriction avulsion is characterised by fact that water overflows out of the bank when there is no channel. This process allows the channel to obtain a straighter course with a reduced channel sinuosity. Its occurrence is driven by the more and more curved bend. In real rivers, the temporal alternation of increase and decrease of sinuosity in local channels is an important characteristic too.

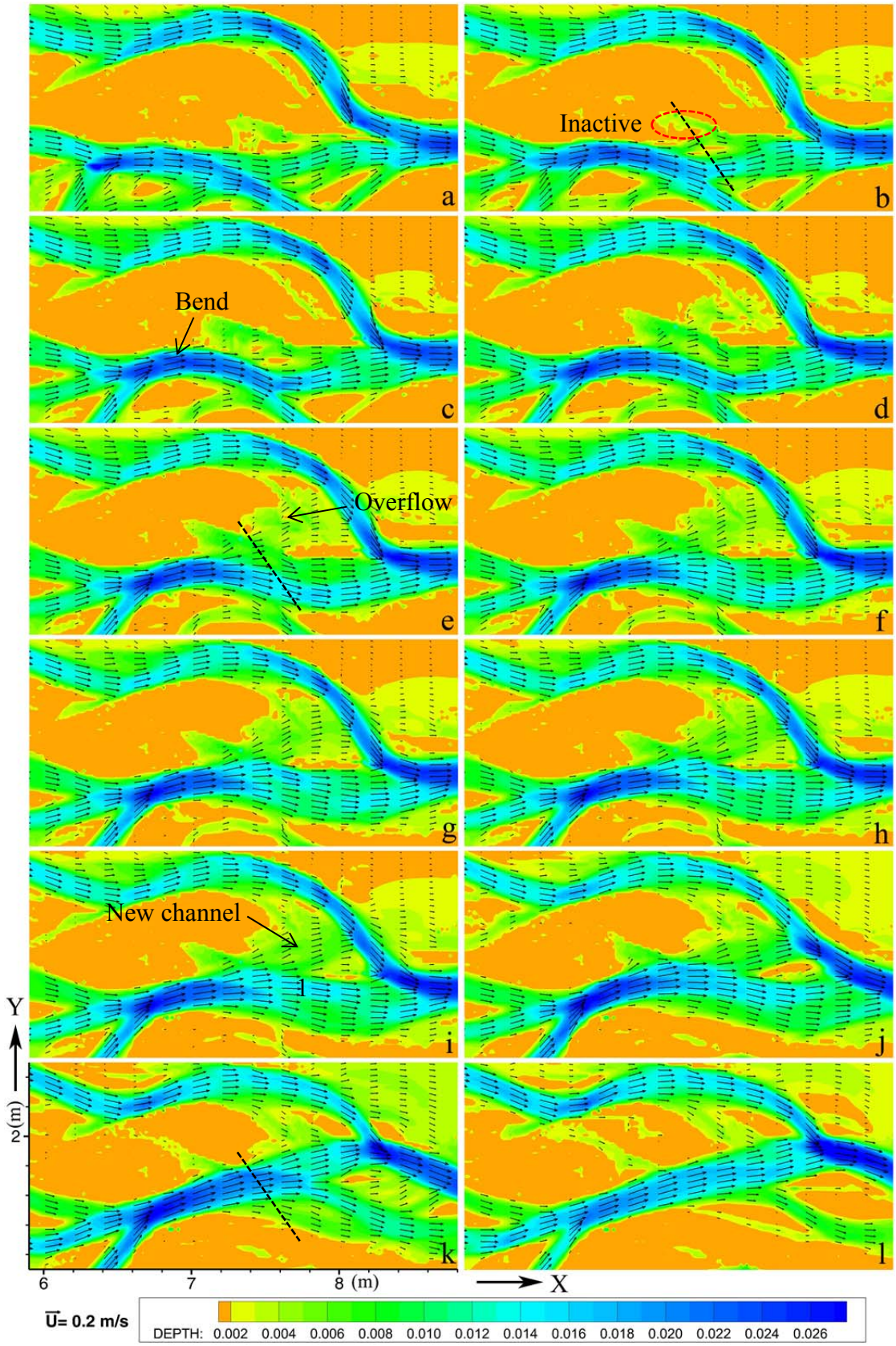

Figure 5.23 Water depth in the avulsion by incision 1 (m): (a) 84; (b) 85.5; (c) 86; (d) 86.17; (e) 86.33; (f) 86.5; (g) 86.67; (h) 86.83; (i) 87; (j) 88; (k) 90; and (l) 91 (hour).

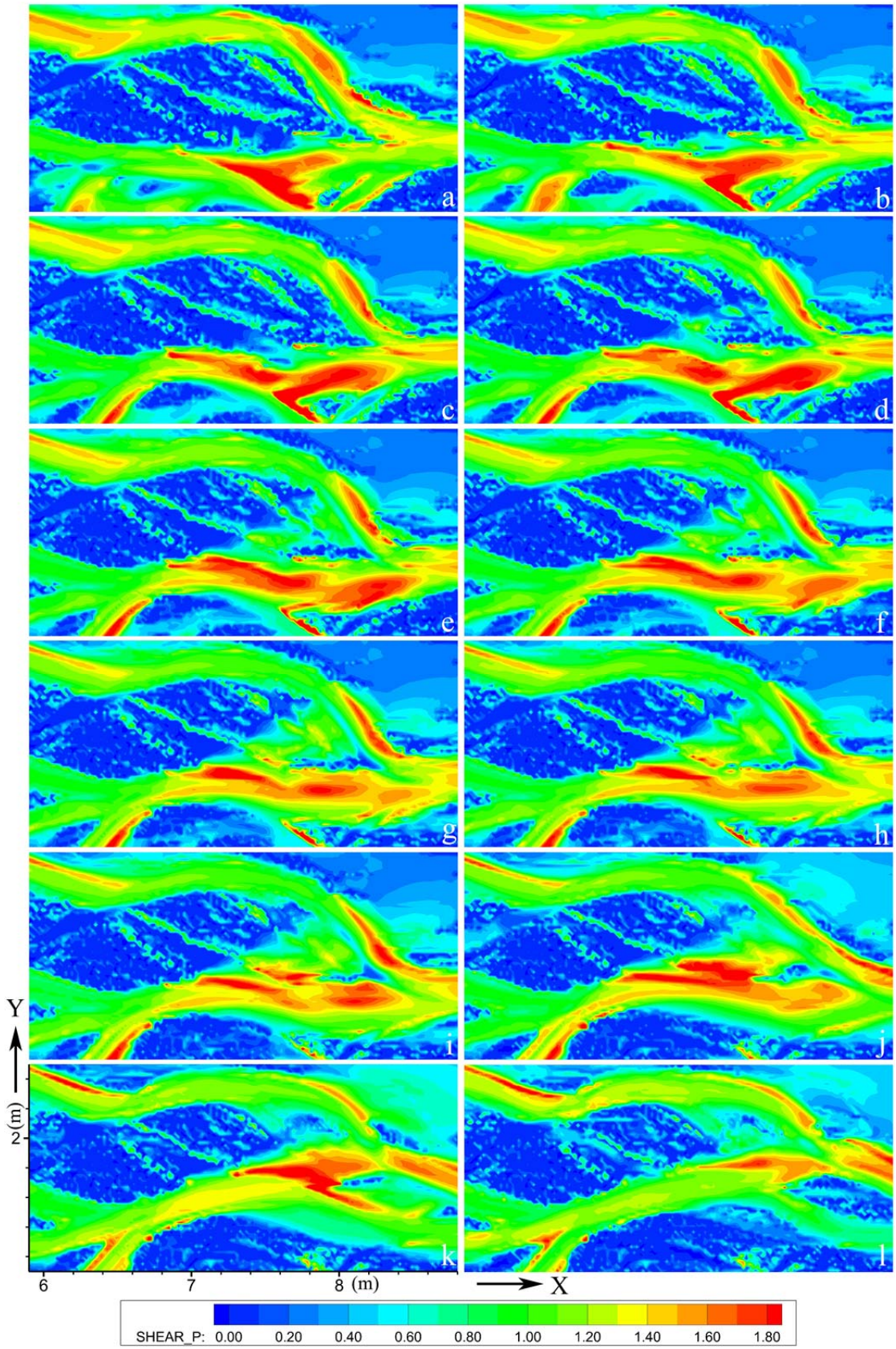

Figure 5.24 Shear stress in the avulsion by incision 1 (N/m^2): (a) 84; (b) 85.5; (c) 86; (d) 86.17; (e) 86.33; (f) 86.5; (g) 86.67; (h) 86.83; (i) 87; (j) 88; (k) 90; and (l) 91 (hour).

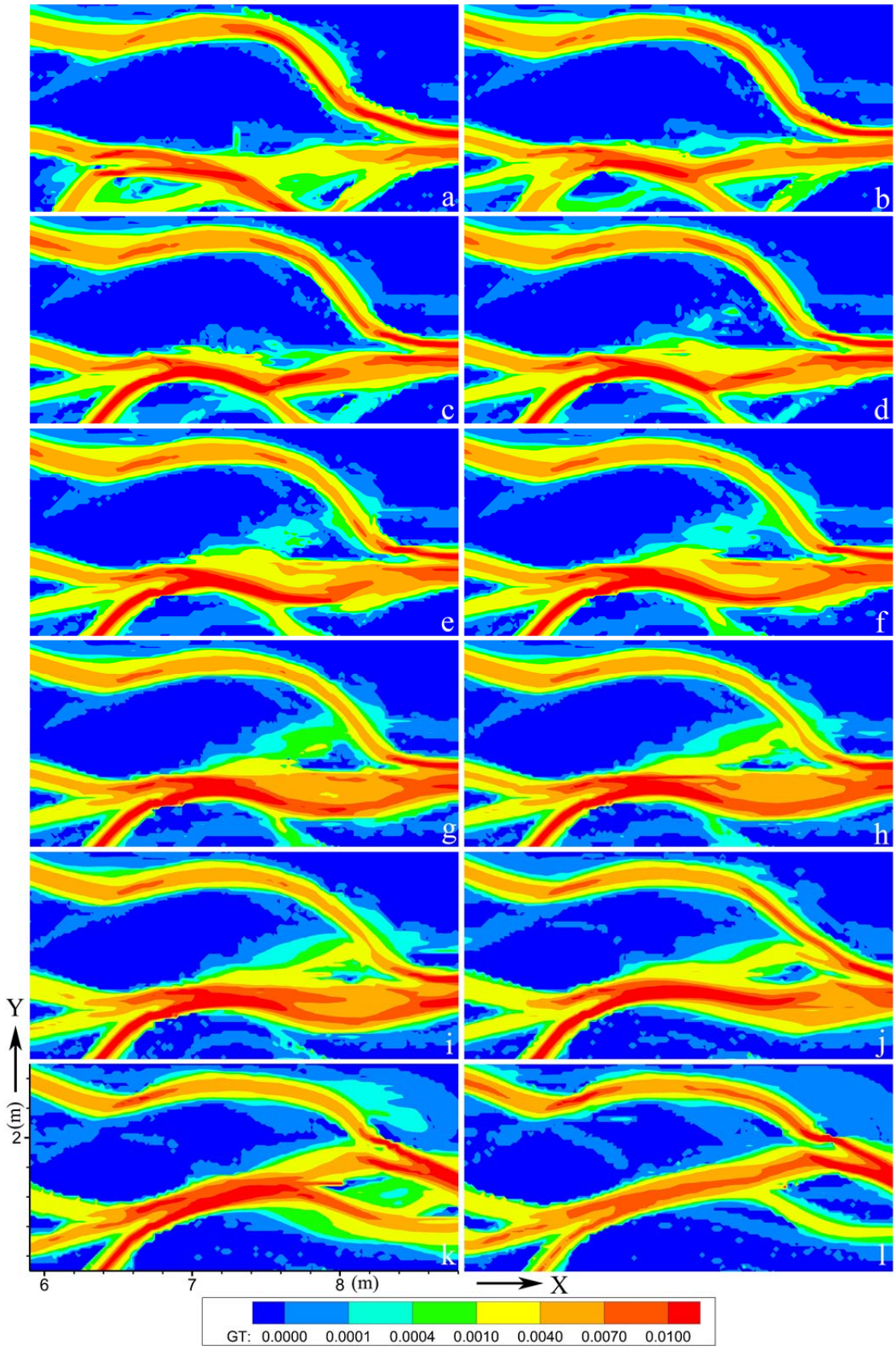

Figure 5.25 Bed load transport rate in the avulsion by incision 1 (kg/(m·s)): (a) 84; (b) 85.5; (c) 86; (d) 86.17; (e) 86.33; (f) 86.5; (g) 86.67; (h) 86.83; (i) 87; (j) 88; (k) 90; and (l) 91 (hour).

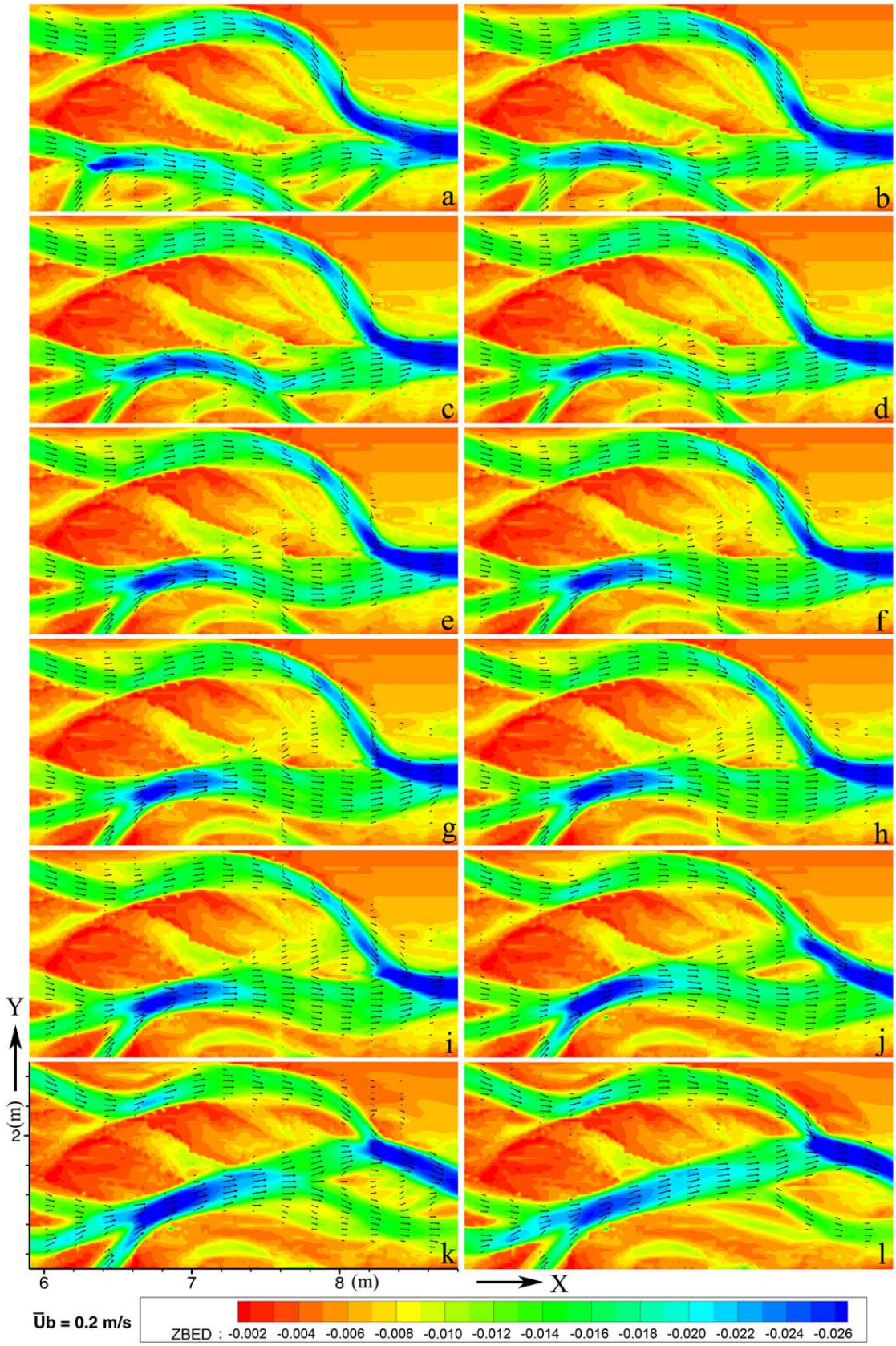

Figure 5.26 Bed elevation in the avulsion by incision 1 (m): (a) 84; (b) 85.5; (c) 86; (d) 86.17; (e) 86.33; (f) 86.5; (g) 86.67; (h) 86.83; (i) 87; (j) 88; (k) 90; and (l) 91 (hour).

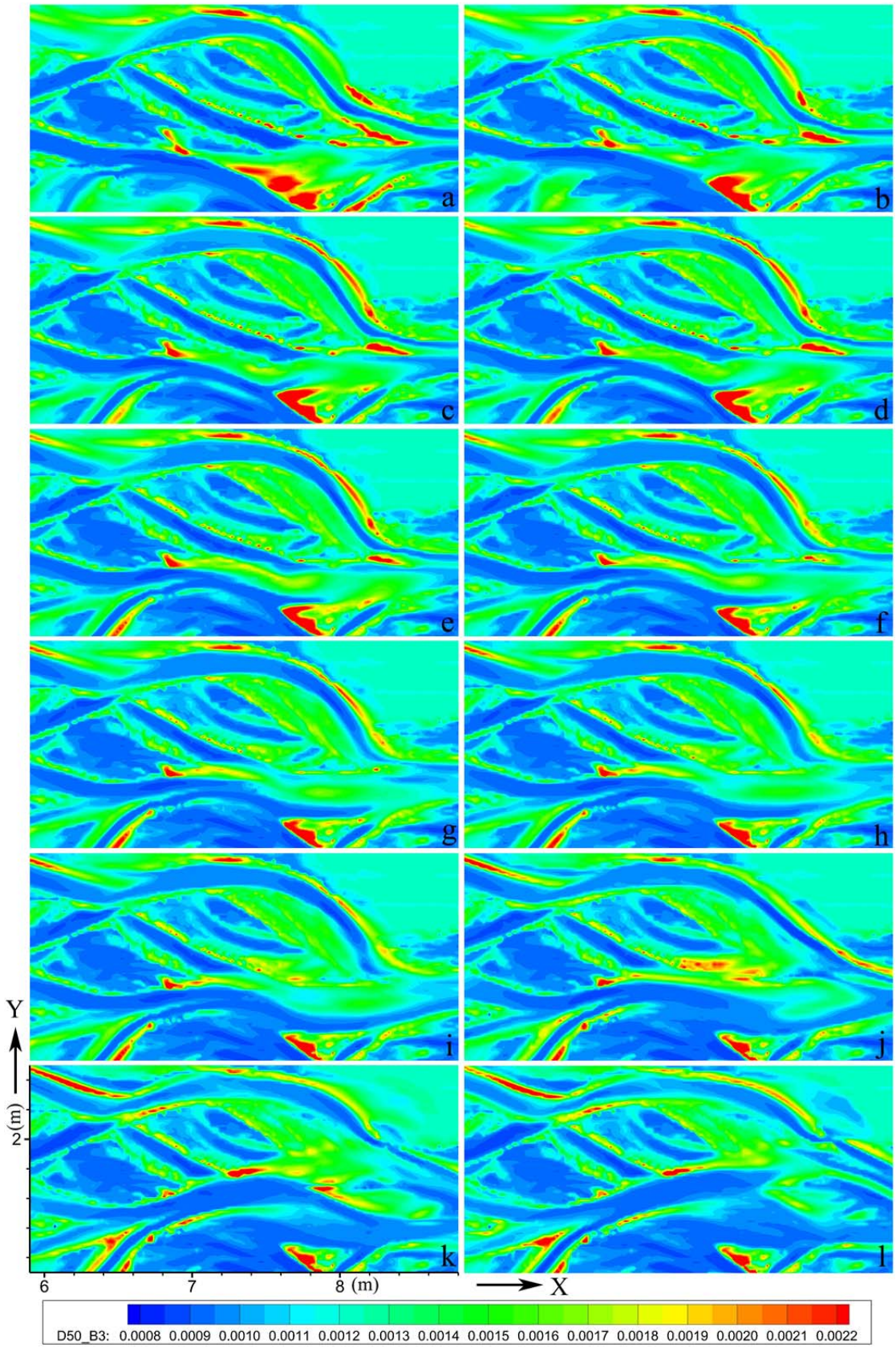

Figure 5.27 Sediment D_{50} distribution in bed in the avulsion by incision 1 (m): (a) 84; (b) 85.5; (c) 86; (d) 86.17; (e) 86.33; (f) 86.5; (g) 86.67; (h) 86.83; (i) 87; (j) 88; (k) 90; and (l) 91 (hour).

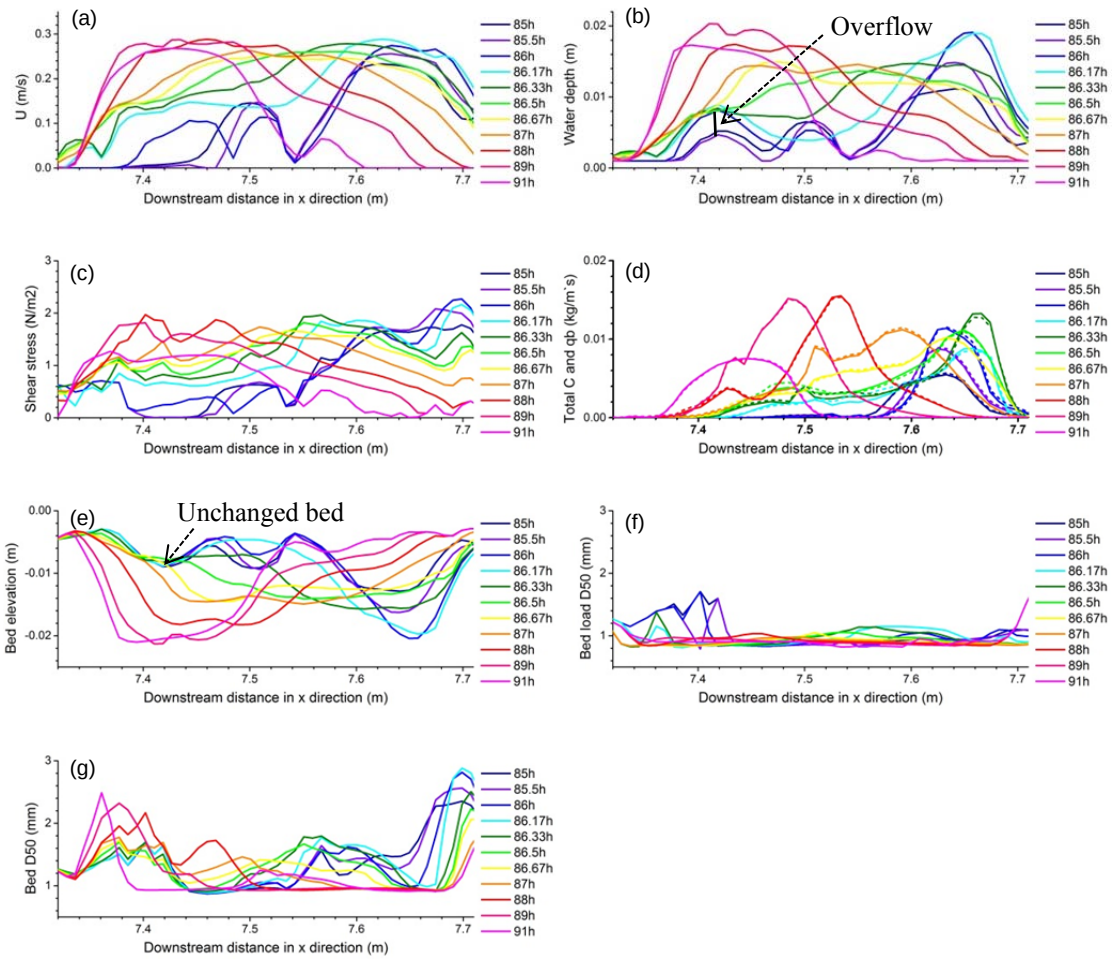

Figure 5.28 Hydraulic and morphodynamic changes during the avulsion by incision 1.

5.6.3 Avulsion by Incision 2 (Apex Avulsion)

Another case of avulsion by incision is illustrated here. Unlike the avulsion by incision introduced above which is promoted by the constricted water pathway, this avulsion is promoted by the interception of one upstream tributary (Figure 5.13i, 3). As the parent channel grew, it became more sinuous (Figure 5.29a). As one of its tributaries (channel 1 in Figure 5.29f) became stronger and stronger, it cut the bank of the parent channel and diverted most of its flow to a different direction, with a new channel being formed (Figure 5.29i). In this process, the parent channel moved with

the new channel. In order to catch up with this channel change, the crossing line also moved with the channel (Figure 5.29d).

Initially, the parent channel was nearly straight, with shear stress distributing close to the right bank, denoting the inertia effect of the flow (Figure 5.30a). However, sediment transport rate was roughly consistent with flow depth, with high value in the deep area. As the channel configuration was moving downstream, the channel was bent in its upstream reach and the shear stress increased there. As the bend got more sinuous, one of its upstream tributaries, tributary 1 grew quickly. Its increasing flow joined in the parent channel and finally flow spilled out of the right bank of the parent channel (Figure 5.29f). As the shear stress was high there, sediments were taken away quickly by the flow, and the new channel was formed by erosion. The talweg of the parent channel was changed, with most discharge branched to the new channel.

It can be seen that high shear stress usually occurred in the areas where flow was energetic and erosion activity was possible. Furthermore, in these areas, bed sand was usually coarse (Figure 5.33), which was supported by the fact that shear stress and bed D_{50} showed similar trends on the line (Figure 5.34). As the configuration changed in the whole river, the parent channel tended to move downstream. With the effect of the secondary flow, fine sediments were taken away and the bed became coarser on the channel edge. However, when flow was strong enough for supporting certain bed load transport rate, the bed became fine gain for the fine sediments in transport. Nonetheless, bed load D_{50} was always finer than bed D_{50}, indicating the sorting effect of flow on bed composition.

This kind of avulsion is very common in the evolution process of braiding in the predicted river. The straight channels were becoming more sinuous. When this effect reached some extent, the channels became irregular and inefficient. Then avulsion occurred by discharge diversion for the channel to get a more efficient way. After that the straight channel got sinuous again and another circulation began. The alternating circulation of straight and sinuous channels is the most important characteristic in the initiation and development of the predicted river.

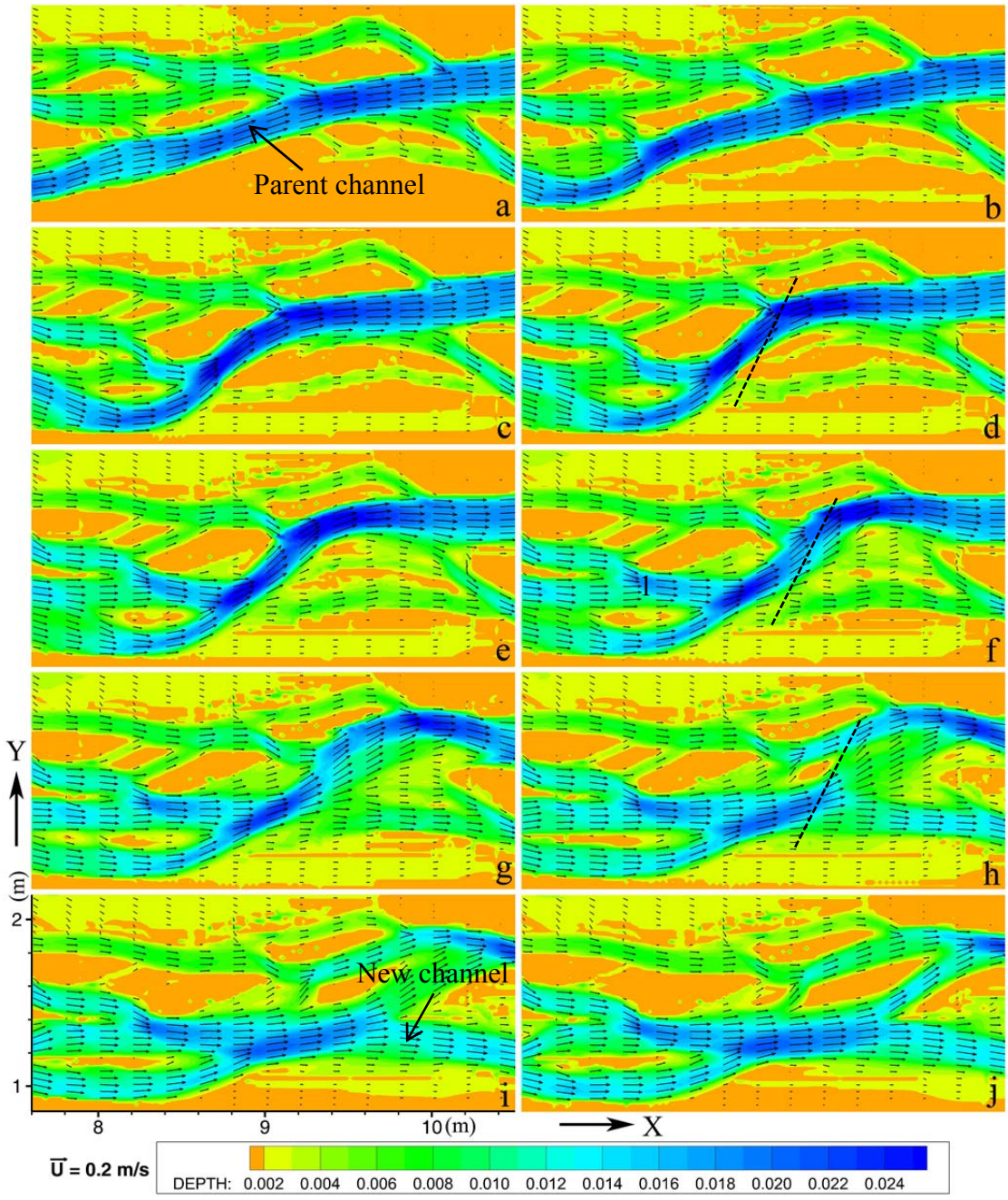

Figure 5.29 Water depth in the avulsion by incision 2 (m): (a) 30; (b) 32; (c) 34; (d) 35; (e) 36; (f) 36.5; (g) 37; (h) 38; (i) 39; and (j) 40 (hour).

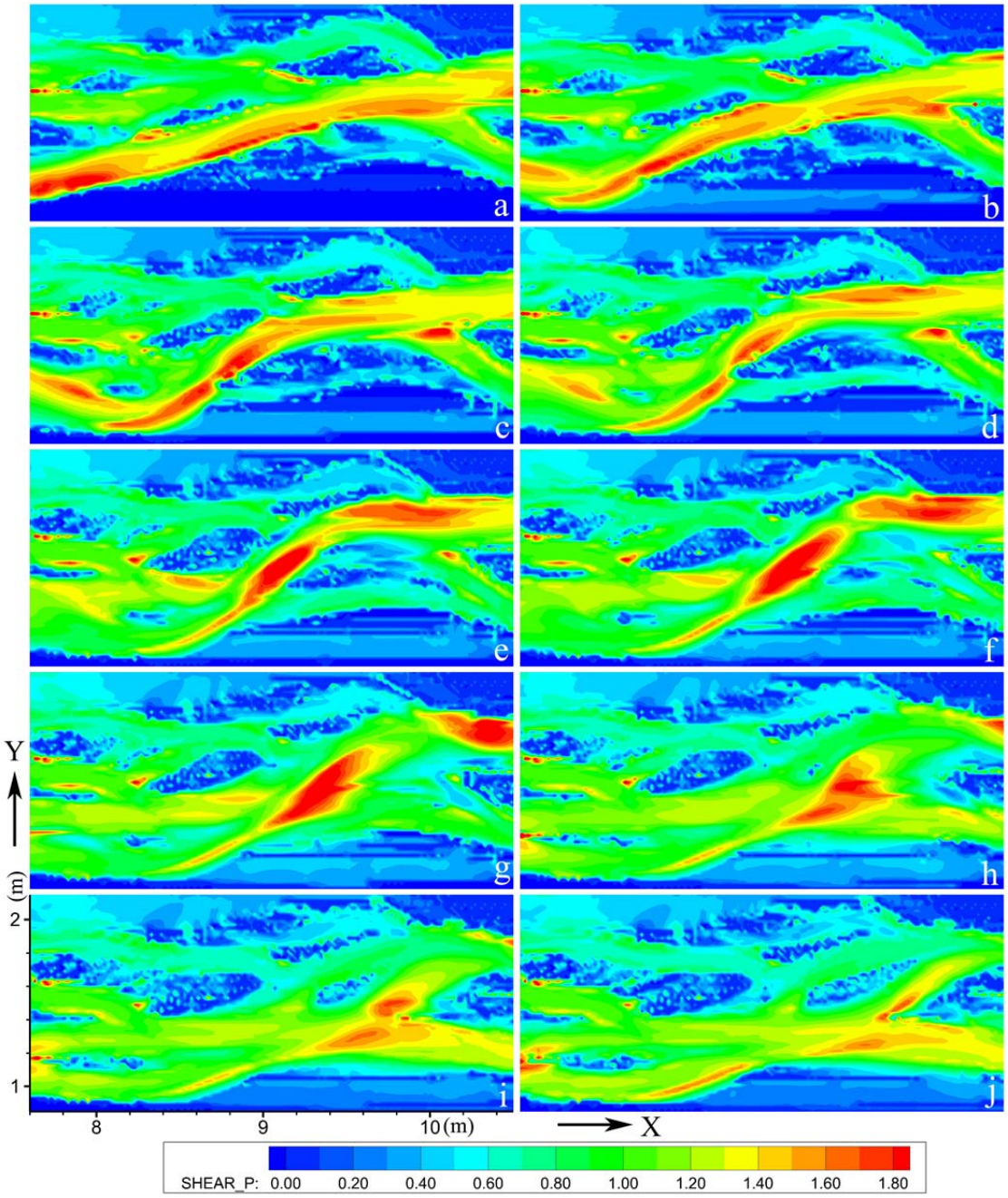

Figure 5.30 Shear stress in the avulsion by incision 2 (N/m^2): (a) 30; (b) 32; (c) 34; (d) 35; (e) 36; (f) 36.5; (g) 37; (h) 38; (i) 39; and (j) 40 (hour).

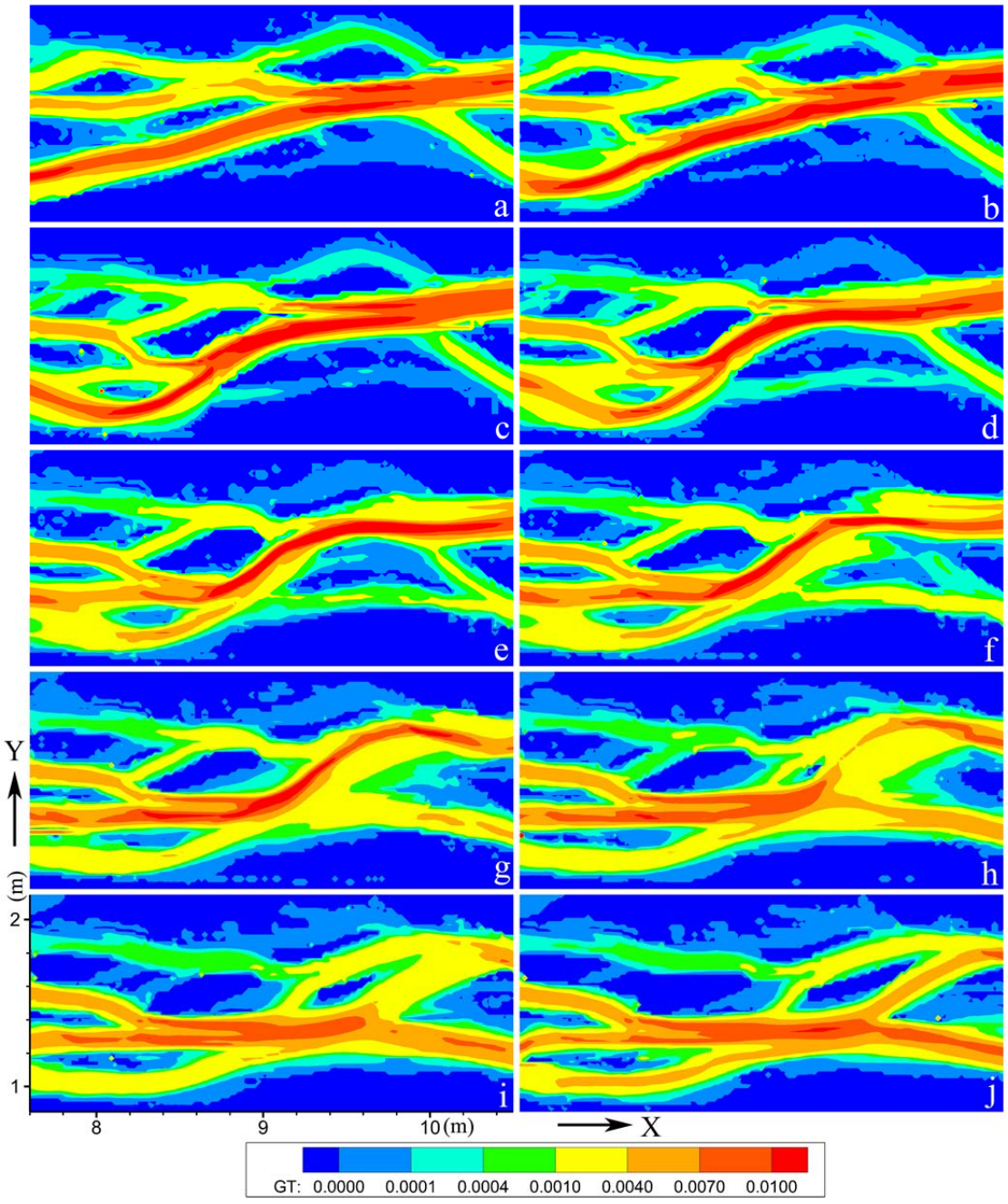

Figure 5.31 Bed load transport rate in the avulsion by incision 2 (kg/(m·s)): (a) 30; (b) 32; (c) 34; (d) 35; (e) 36; (f) 36.5; (g) 37; (h) 38; (i) 39; and (j) 40 (hour).

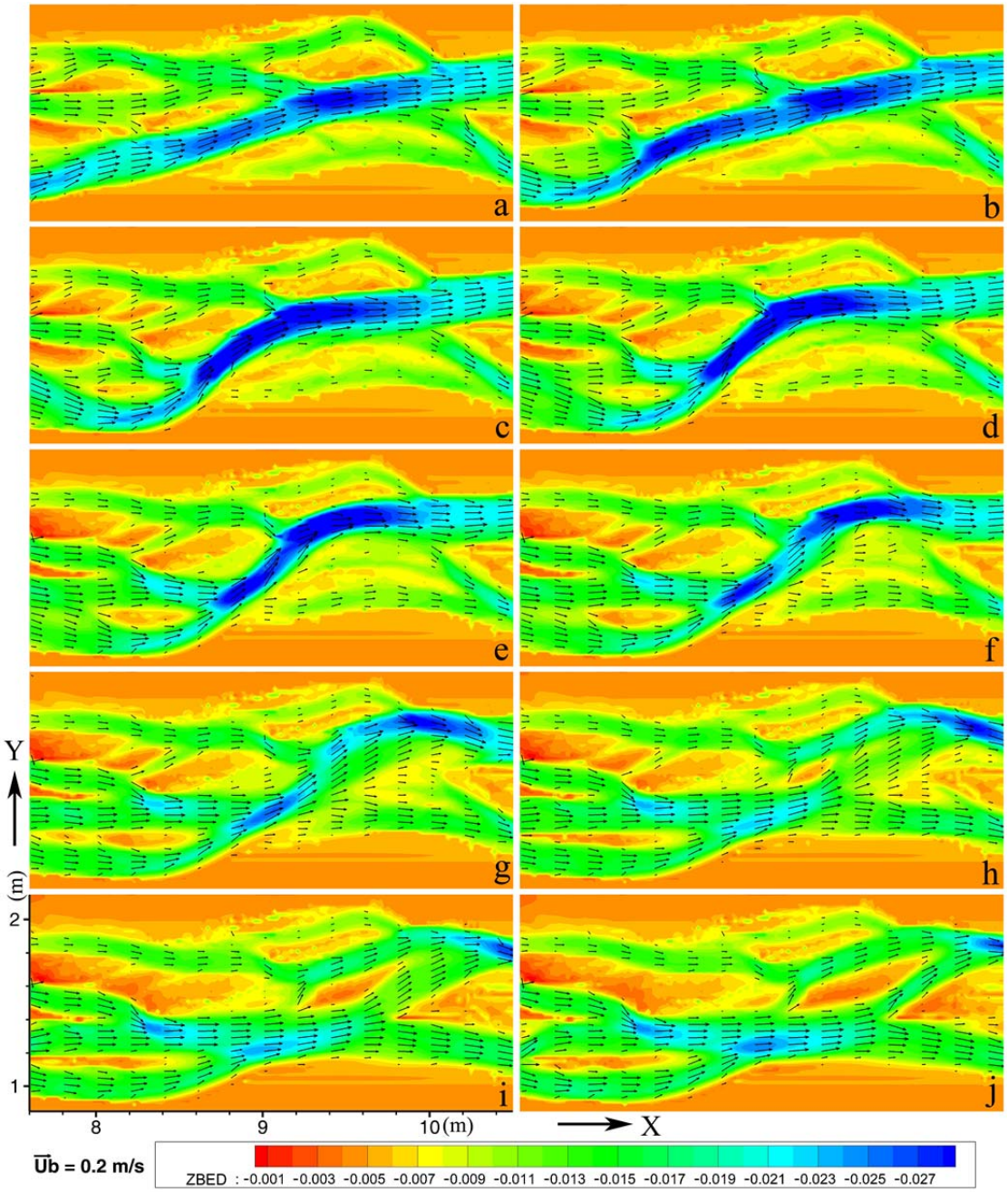

Figure 5.32 Bed elevation in the avulsion by incision 2 (m): (a) 30; (b) 32; (c) 34; (d) 35; (e) 36; (f) 36.5; (g) 37; (h) 38; (i) 39; and (j) 40 (hour).

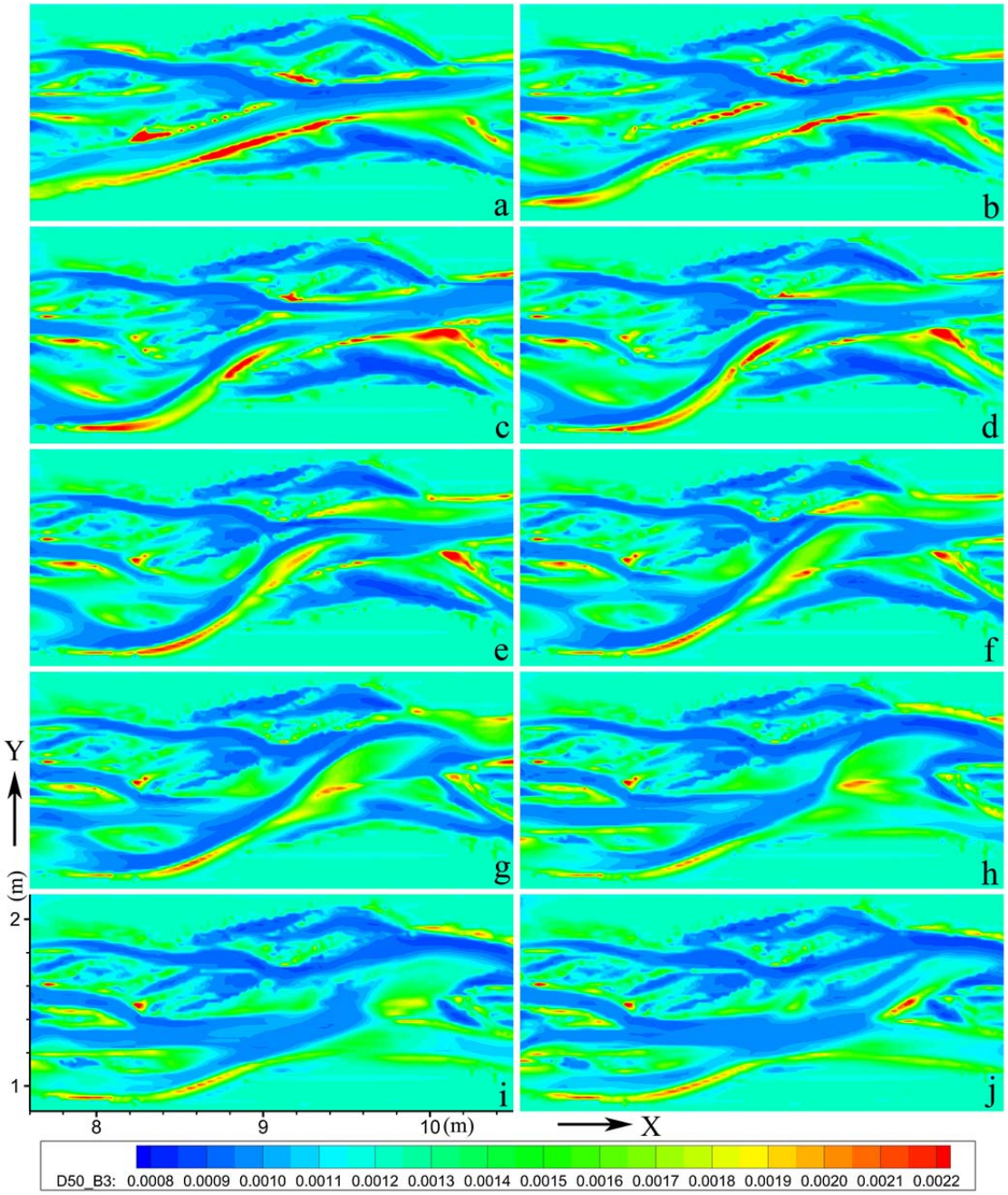

Figure 5.33 Sediment D_{50} distribution in bed in the avulsion by incision 2 (m): (a) 30; (b) 32; (c) 34; (d) 35; (e) 36; (f) 36.5; (g) 37; (h) 38; (i) 39; and (j) 40 (hour).

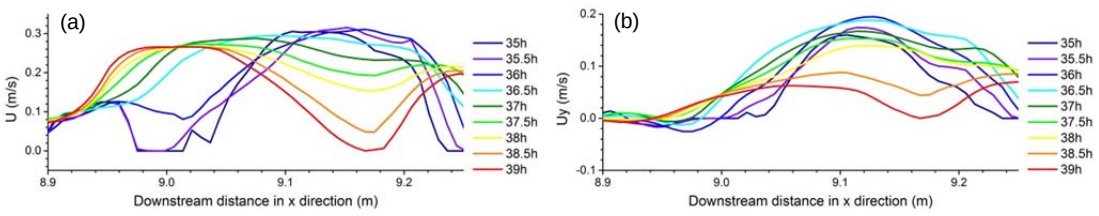

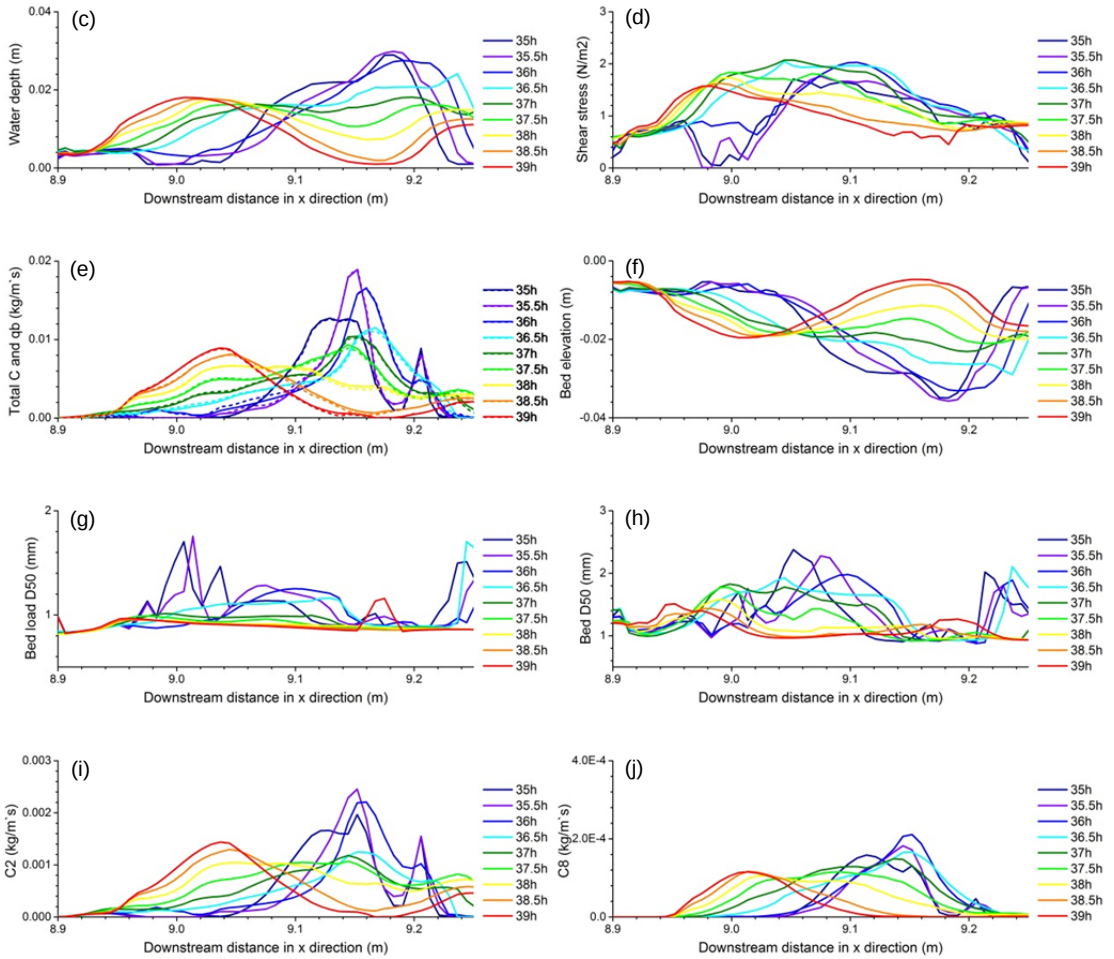

Figure 5.34 Hydraulic and morphodynamic changes in the avulsion by incision 2.

5.6.4 Avulsion by Annexation

The choked channel by progradation (introduced in Section 5.6.1) reconnected with the main channel again to accomplish an avulsion by annexation (see Figure 5.13l, 11). Figures 5.35 to 5.38 give an illustration of processes of this kind of avulsion. Initially, one tributary of the bifurcation was abandoned by choking avulsion. As the channel grew and its bend became sinuous, some water overflowed from the bend into the abandoned channel and it was reconnected to the main channel again (Figure 5.35c). After that it experienced channel advance and retreatment, and finally

died out again (Figure 5.35j).

When the upstream reach of the channel (channel 1, Figure 5.35a) became sinuous, the shear stress increased at the outer bank of the channel. Due to the inertia effect water overflowed to the abandoned channel and reconnected with its downstream part. As channel 1 was stretched, channel 2 was weakened again (Figure 5.35g). Then another bend came from upstream reach in channel 1 which caused channel 2 to grow again, thus a new circulation began. The braided river consumed its energy by channel scour and bank erosion, resulting in an increase in sinuosity. But when the channel was bent to some extent, avulsions would occur to make the channel straight, and another circulation would begin from straight to sinuous then to straight.

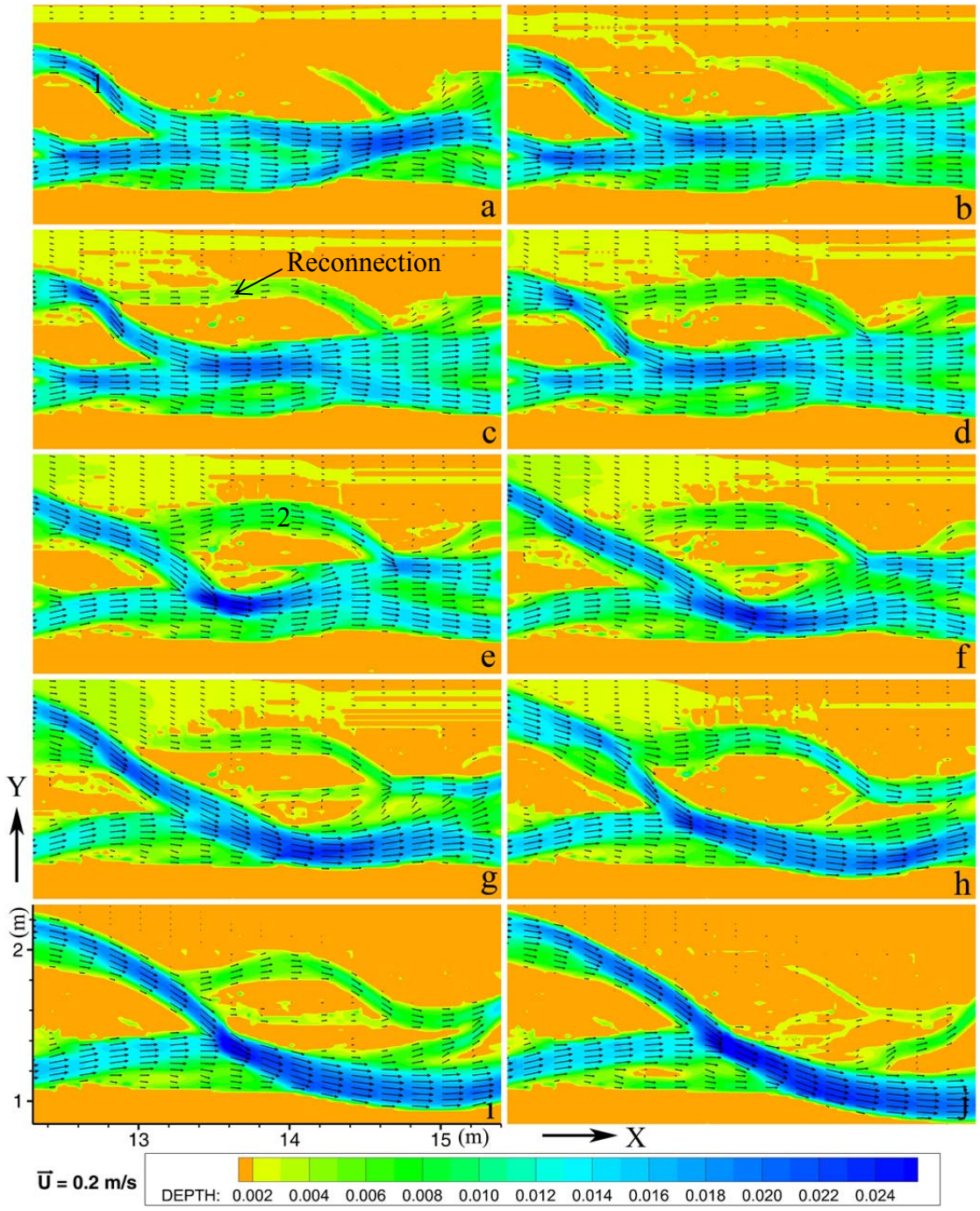

Figure 5.35 Water depth in the avulsion by annexation (m): (a) 42; (b) 45; (c) 46.5; (d) 47; (e) 48; (f) 49; (g) 50; (h) 52; (i) 55; and (j) 59 (hour).

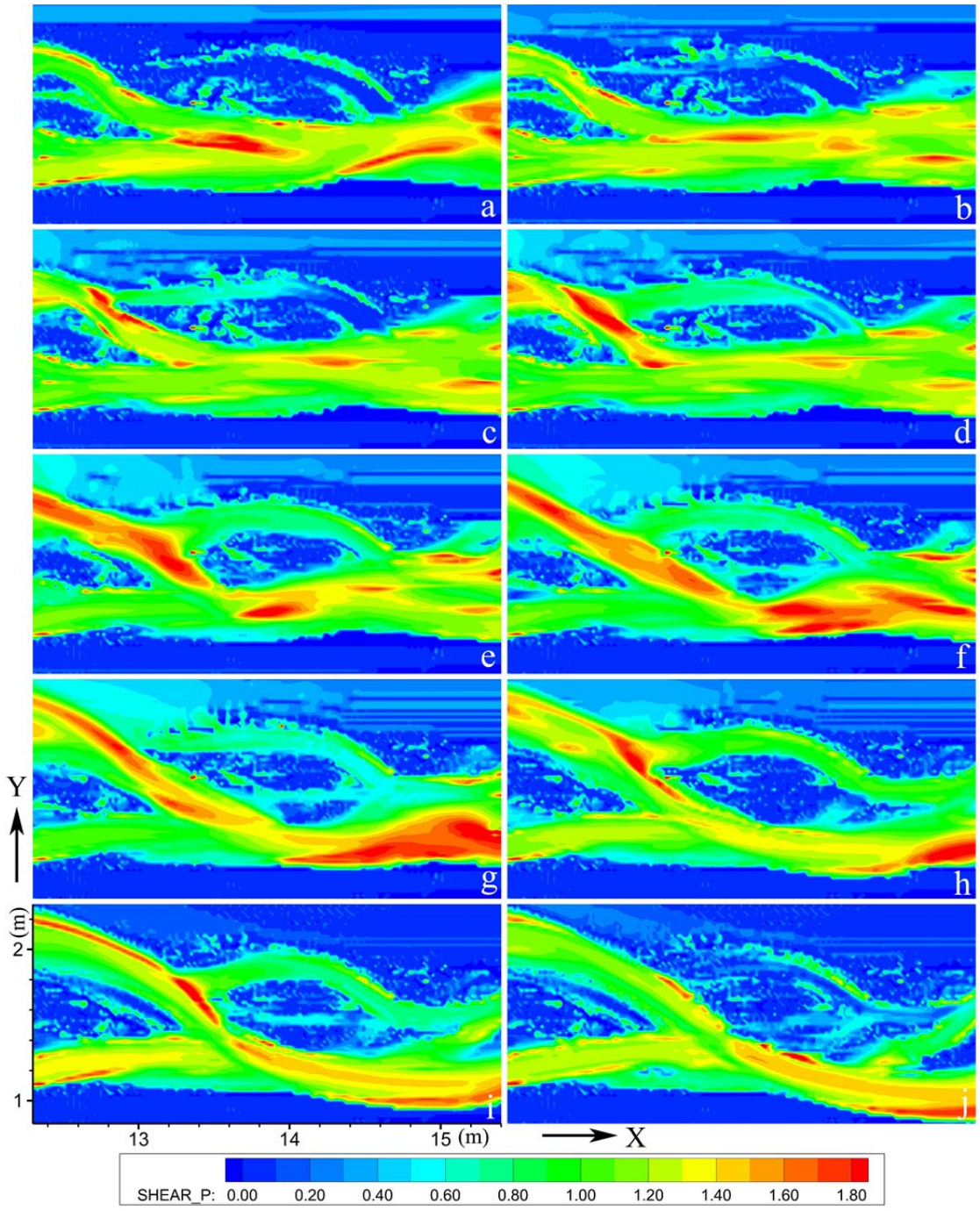

Figure 5.36 Shear stress in the avulsion by annexation (N/m^2): (a) 42; (b) 45; (c) 46.5; (d) 47; (e) 48; (f) 49; (g) 50; (h) 52; (i) 55; and (j) 59 (hour).

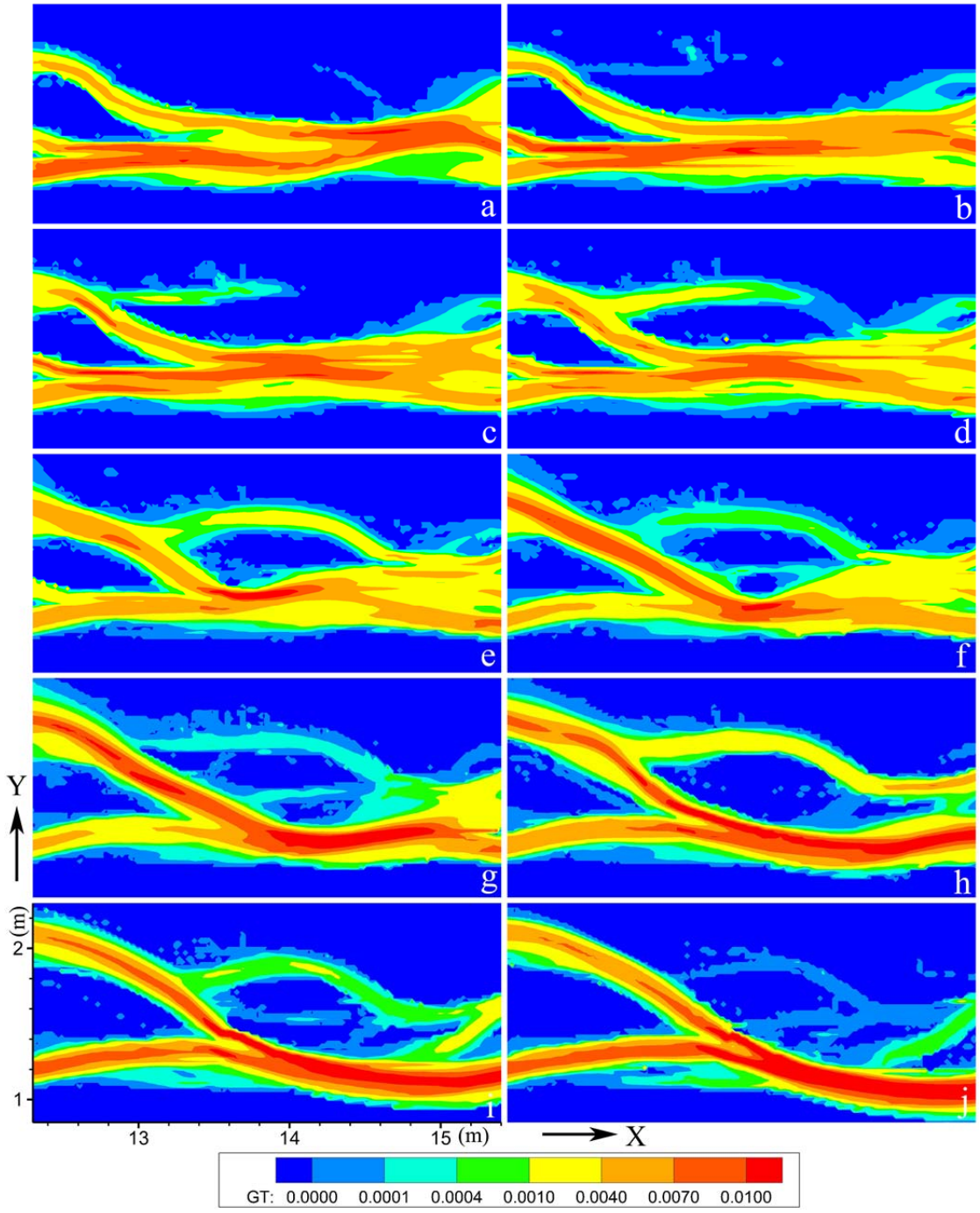

Figure 5.37 Bed load transport rate in the avulsion by annexation (kg/(m·s)): (a) 42; (b) 45; (c) 46.5; (d) 47; (e) 48; (f) 49; (g) 50; (h) 52; (i) 55; and (j) 59 (hour).

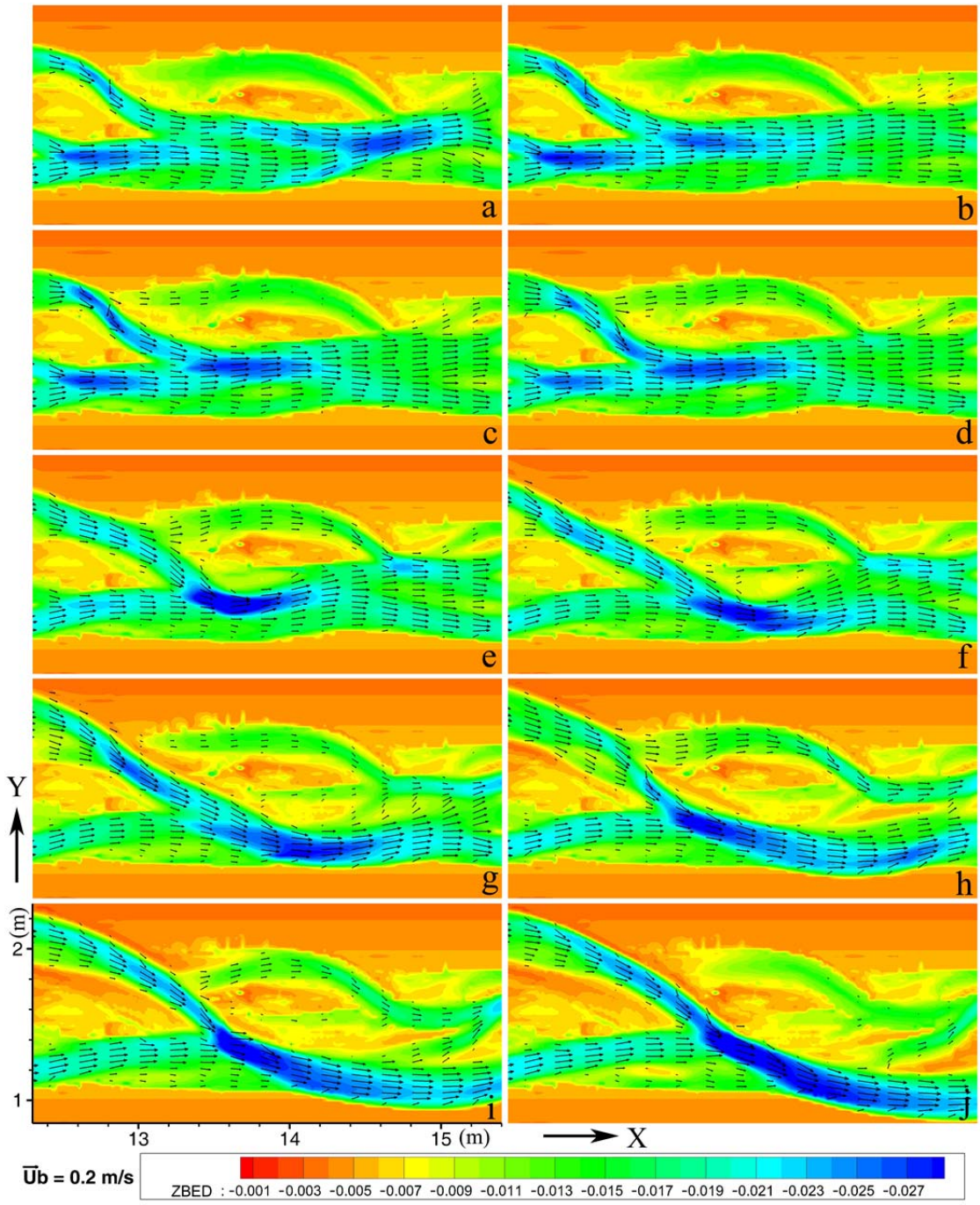

Figure 5.38 Bed elevation in the avulsion by annexation (m): (a) 42; (b) 45; (c) 46.5; (d) 47; (e) 48; (f) 49; (g) 50; (h) 52; (i) 55; and (j) 59 (hour).

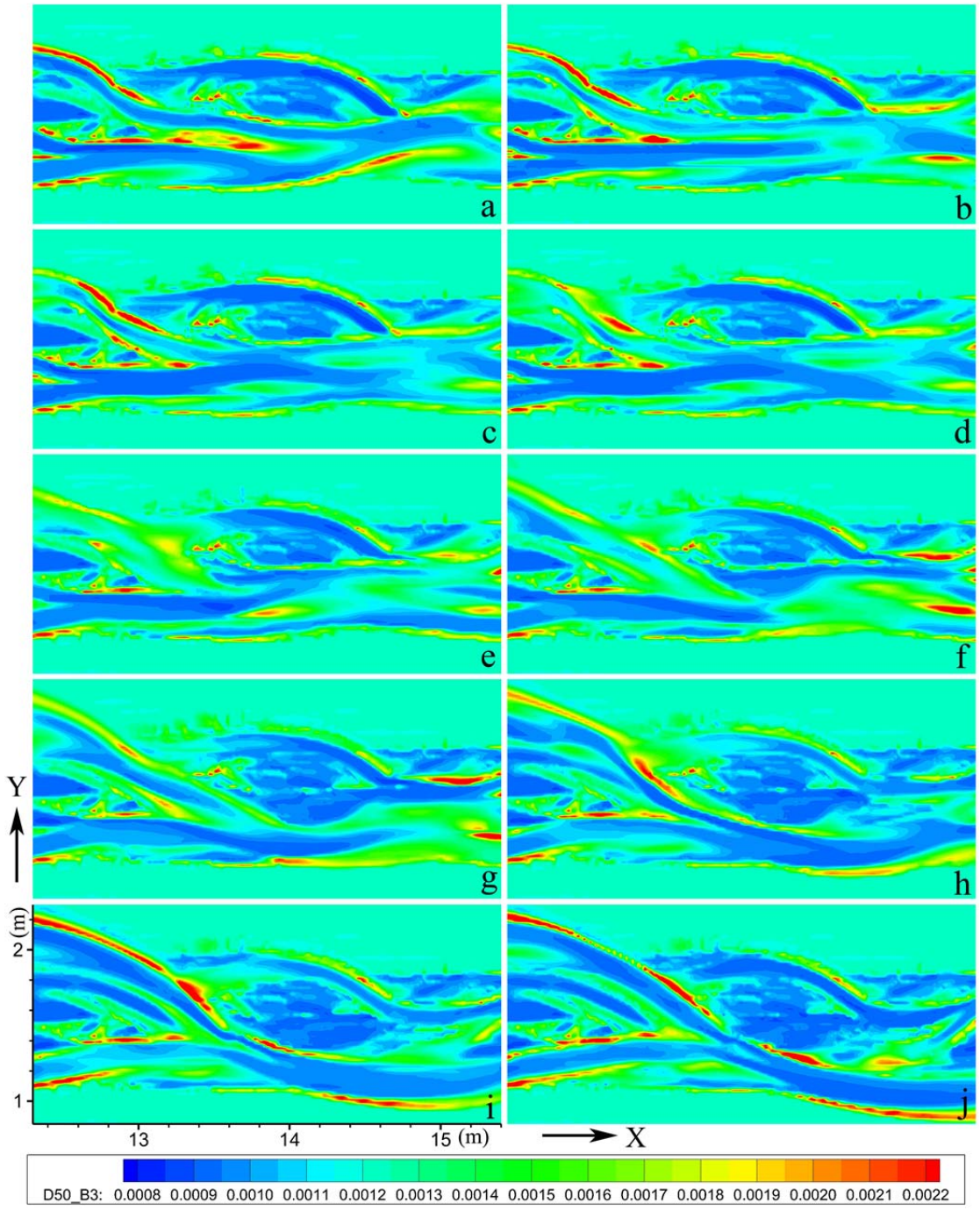

Figure 5.39 Sediment D_{50} distribution in bed in the avulsion by annexation (m): (a) 42; (b) 45; (c) 46.5; (d) 47; (e) 48; (f) 49; (g) 50; (h) 52; (i) 55; and (j) 59 (hour).

5.7 Braiding Characteristics

The predicted braided rivers show some typical braiding characteristics including intrinsic spatial and temporal scales and scale-invariant properties. In this section,

some methods including braiding intensity, state-space plots and spatial scaling were used to analyse the statistical characteristics of the predicted river.

5.7.1 Braiding Intensity

Total braiding intensity (BI_T), active braiding intensity (BI_A) and their ratio (BI_T/BI_A) in experiments 7 and 8 were calculated (Figures 5.40 and 5.41). BI_T and BI_A were compared with the experimental results shown in Table 5.5. The water depth of 3 mm is adopted as the boundary of channel and non-channel. Areas with water deeper than 3 mm (including at least two adjacent cells in the model) are viewed as channels. Total braiding intensity is calculated by

$$BI_T = \frac{\sum_{i=1}^{N_s} N_i}{N_s} \tag{5. 1}$$

where N_i = number of channels in the ith cross-section; and N_s = number of cross-sections. Bed load transport rate of 0.006 kg/(m·s) is adopted as the boundary of "active channel" and "non-active channel". Channels with bed load transport rate no less than 0.006 kg/(m·s) are viewed as active. Therefore, active braiding intensity BI_A can be calculated by

$$BI_A = \frac{\sum_{j=1}^{N_s} N_j}{N_s} \tag{5. 2}$$

where N_j = number of active channels in the jth cross-section; and N_s = number of cross-sections.

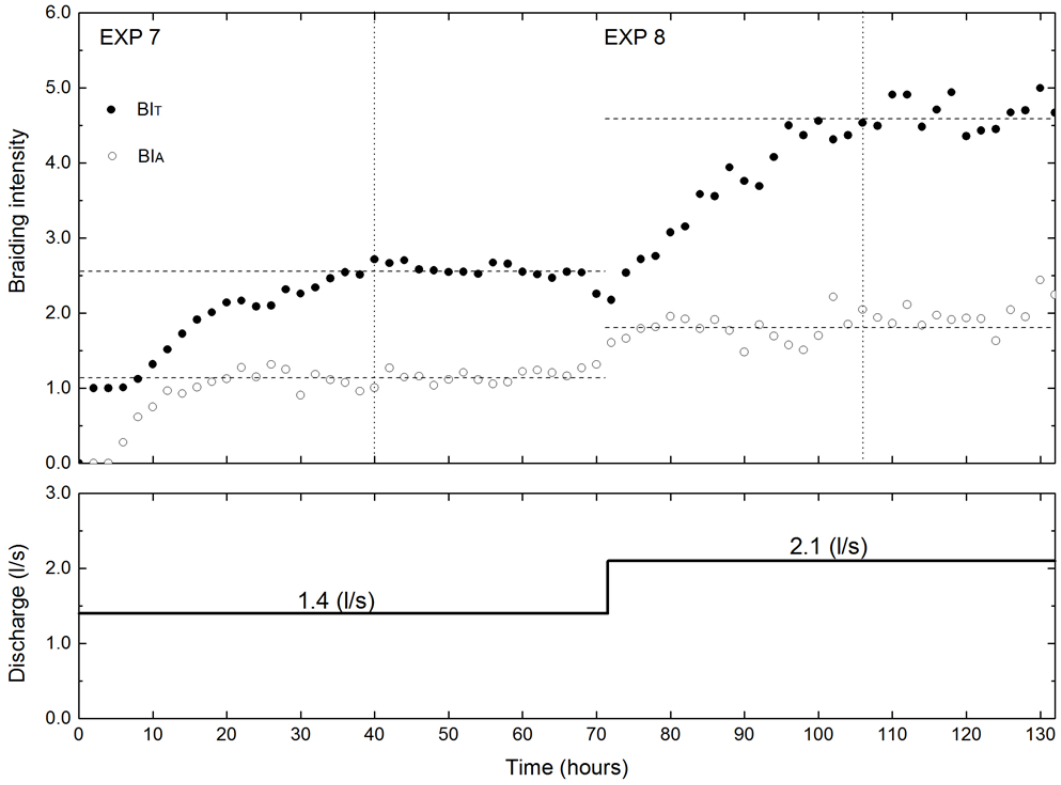

Figure 5.40 Variations of mean BI_T and BI_A during sequential flow stages.

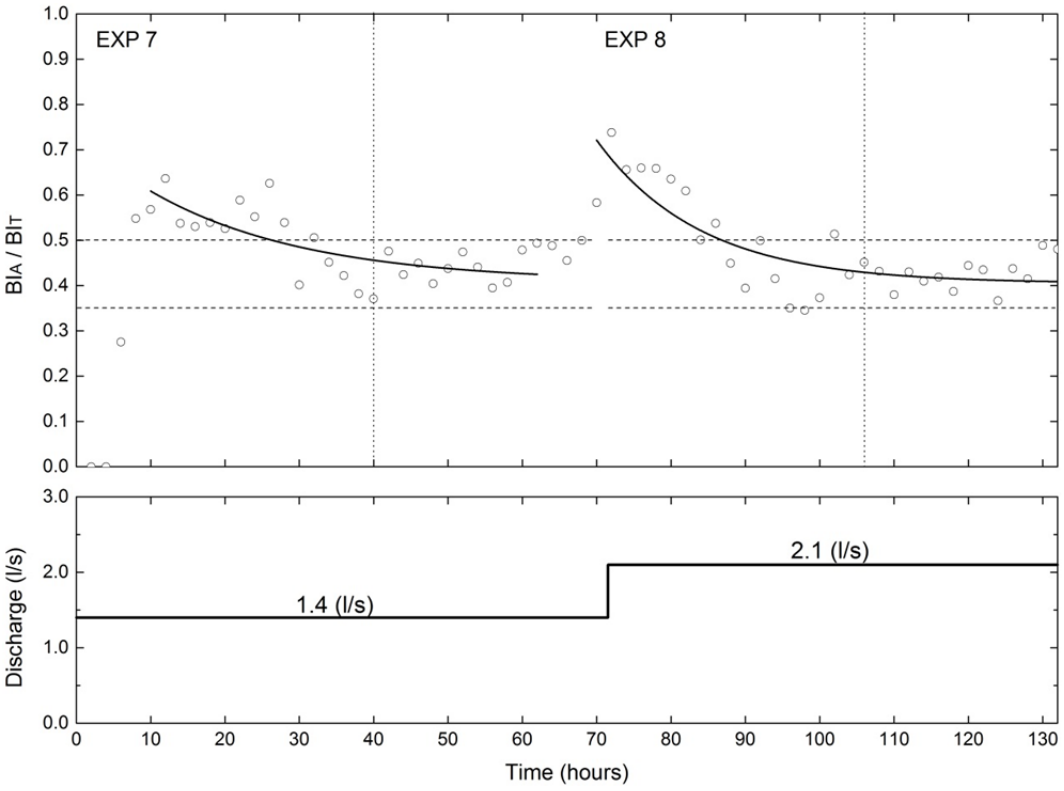

Figure 5.41 Variations of BI_A/BI_T during sequential flow stages.

Table 5.5 Braiding intensity of the modelled and laboratory rivers

	Modelled river			Laboratory river		
Parameters	BI_A	BI_T	BI_A/BI_T	BI_A	BI_T	BI_A/BI_T
Exp.7	1.1	2.55	0.35–0.5	1.1	2.8	0.3–0.5
Exp.8	1.8	4.56	0.35–0.5	1.3	3.8	0.3–0.5

In most cases, the maximum BI_T values were greater than twice of the maximum BI_A values, just as observed in the experiments. Compared with the laboratory river, the modelled river developed nearly the same BI_A and a little lower BI_T than those of experiment 7. Yet in experiment 8, it developed higher BI_A and BI_T values than those of the laboratory river. This results from the fact that, there was a main channel before hour 100 for both of the experiment and the model. But after hour 100, the main channel in the modelled river was not clear any more, which was replaced by several channels instead.

In both the two flow stages, active braiding intensity BI_A developed quickly to a stable value (Figure 5.40). In the first stage it took a little long time to stabilise but in the second stage, it took just a couple of hours. In contrast, BI_T increased to a stable state gradually. It took nearly 40 and 35 hours to reach a stable value in experiments 7 and 8, respectively. The longer time for the stabilization of both BI_A and BI_T during the first flow stage resulted from the fact that it took some time to develop a braided pattern from the initial straight channel. The quick stabilization of BI_A was explained by Egozi and Ashmore (2009) in this way. The increase in BI_A only requires a sufficiently large flow within an existing channel to mobilise the bed material and this can be accomplished very quickly. It involves very little adjustment in river

morphology. However, the increase in BI_T needs the time for the river to erode new channels.

The variation in BI_A/BI_T shows a consistent trend in which it gradually approaches to about 0.4 (Figure 5.41). The stable ratio results from the fact that BI_A reached a stable state quickly, yet BI_T took a much longer time. Zero values existed at the beginning because there was no main channel in the initial channel. The modelled river shared similar stable value of BI_A/BI_T with the experiment, while the variation range was between 0.35 and 0.5, compared with 0.3–0.5 in the experiment. It might be explained by the more movable river bed in the model than real rivers. Generally, it agrees well with the experiment results.

Egozi and Ashmore (2009) found that at any given time, only a subset of the total channels are actually conveying bed material and actively contributing to the formation of braided pattern and river morphology. Among these channels usually one main active channel exists. In the present study, in most cases one main channel with the largest discharge and bed load transport can be observed before hour 100 (Figure 5.42). The sinuosity of the main channel increased and decreased frequently by channel migrations and avulsions (Figure 5.13). Sometimes two equivalent channels existed during the exchange of the main channel from one tributary to another (Figure 5.42f). But after hour 100, the river wandered nearly in the overall flume and several channels played similar roles in the river, so that it was difficult to recognise a main channel (Figure 5.42h).

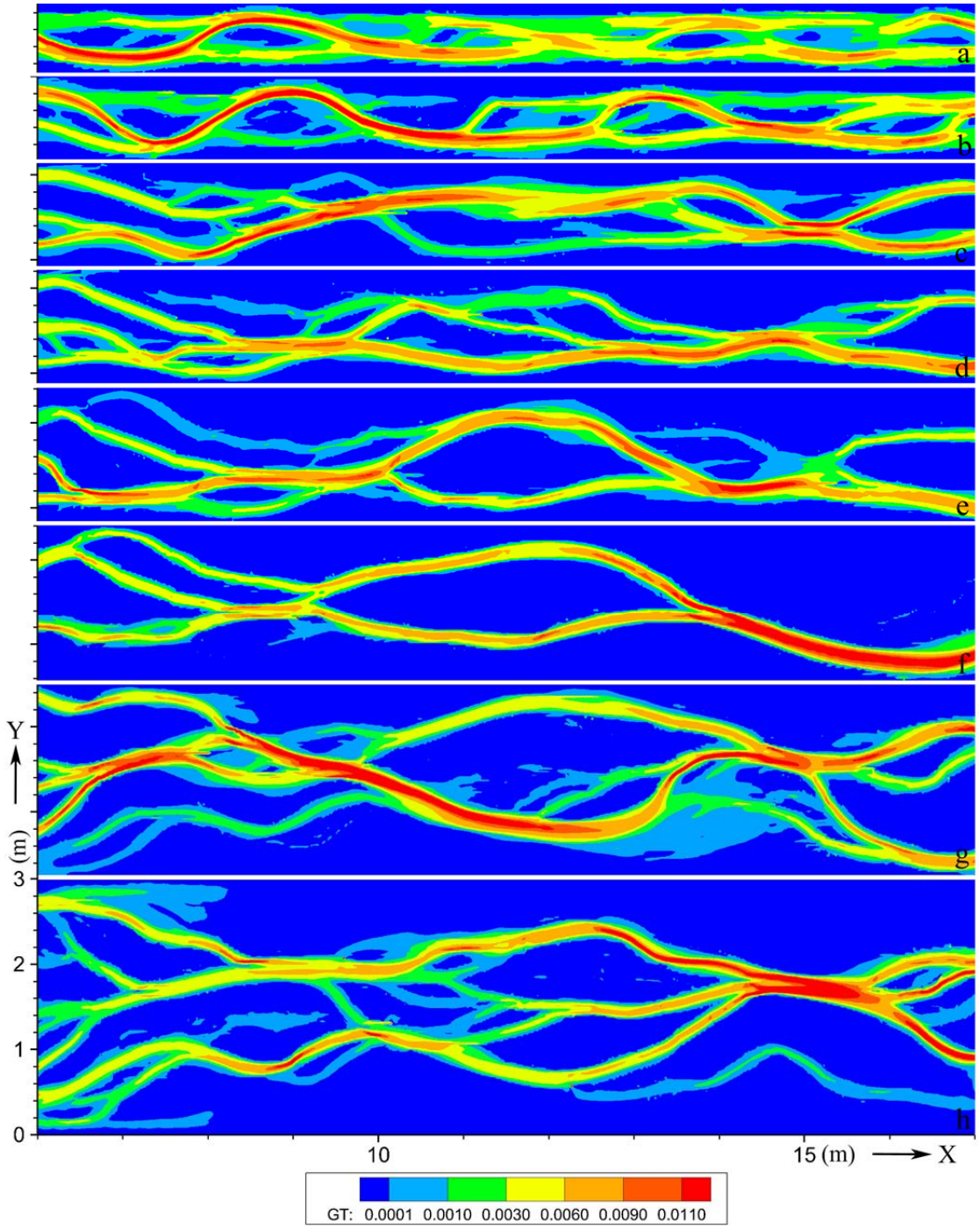

Figure 5.42 Distribution of bed load transport rate and active channels in the river evolution process: (a) 12; (b) 18; (c) 32; (d) 40; (e) 50; (f) 71; (g) 90; and (h) 100 (hour).

5.7.2 State-space Plots

The river at hour 41 is characterised by narrow and deep channels intercepted by wide and shallow reaches, with channel pattern shown in Figure 5.12. Its state-space plots with channel widths and maximum scour depths are shown in Figure 5.43. The plots of channel widths / average channel width vary approximately in a range of 0.5–1.8, with some cross lines in it. Compared with the state-space plots of real rivers (shown in Chapter 2), the loops of the modelled river are thinner. This indicates that the width of the modelled river change in a gentler way than real rivers.

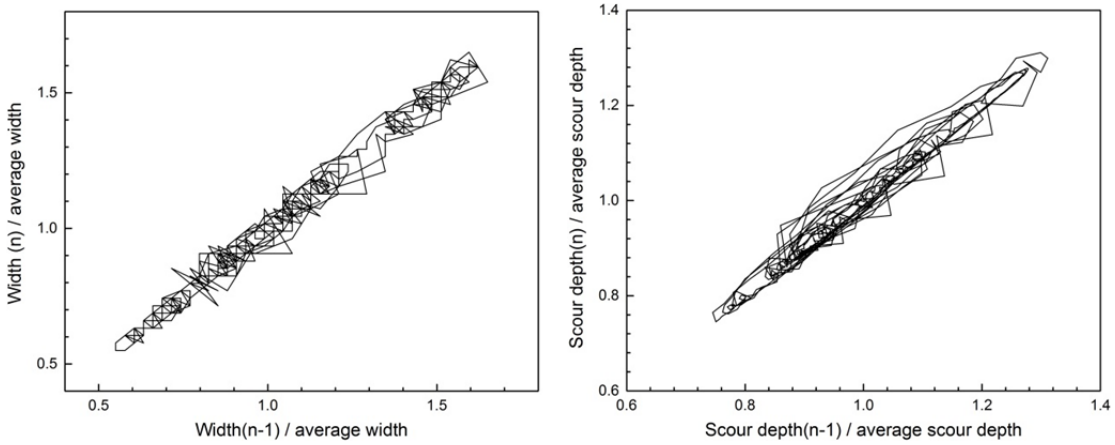

Figure 5.43 State-space plots of channel widths normalised by the average channel width and sequential maximum scour depths normalised by the average maximum scour depth at hour 41.

Compared with the result of channel widths, the state-space plots with maximum scour depths show a better record of the sequential pattern in braided river. The maximum scour depths in sequential cross-sections could present the scour depths in river bed. These plots show that, the maximum scour depth could present the

deterministic downstream effect in the modelled river.

5.7.3 Spatial Scaling

The river configuration at hour 41 (Figure 5.12) was analysed with the logarithmic correlation integral method (introduced in Section 2.3.3.2) and some scaling characteristics were observed (Figure 5.44). The goodness of fitting R^2 is 0.95, which indicates that the data agrees very well with the fitting line. The value of v_x/v_y 1.46 indicates that the modelled river is a self-affine object showing high degree of anisotropy. The values of the scaling exponents v_x and v_y are 0.7 and 0.47, respectively. Compared with the previous studies shown in Figure 2.7, it can be seen that the exponents are in a range similar to those of natural rivers. Actually, as stated by Nykane et al. (1998), the scaling exponents showed some variations with different data extraction methodologies.

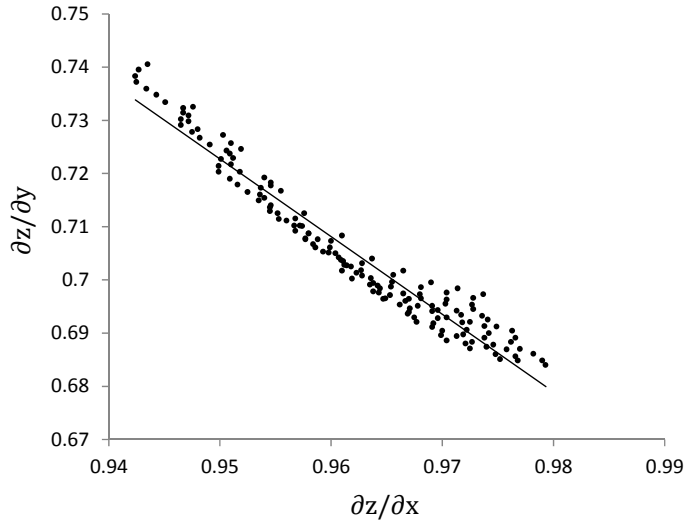

Figure 5.44 Dependence $\partial z(x,y)/\partial y$ versus $\partial z(x,y)/\partial x$ of the modelled river.

5.8 Model Sensitivity

A test with a different resolution was performed, with the flume consisted of 600*100 cells and a cell size of 0.03*0.03 m^2. Other parameters were the same with the river with a cell size of 0.02*0.02 m^2. A braided pattern formed after 40 hours with a main channel (Figure 5.45), yet developed fewer channels than the river with a cell size of 0.03*0.03 m^2 (Figure 5.13). The river broadened and developed more channels in response to increasing discharge. Compared with the results with a cell size of 0.02 *0.02 m^2 at the same time (Figures 5.13 and 5.15), it developed fewer but wider channels.

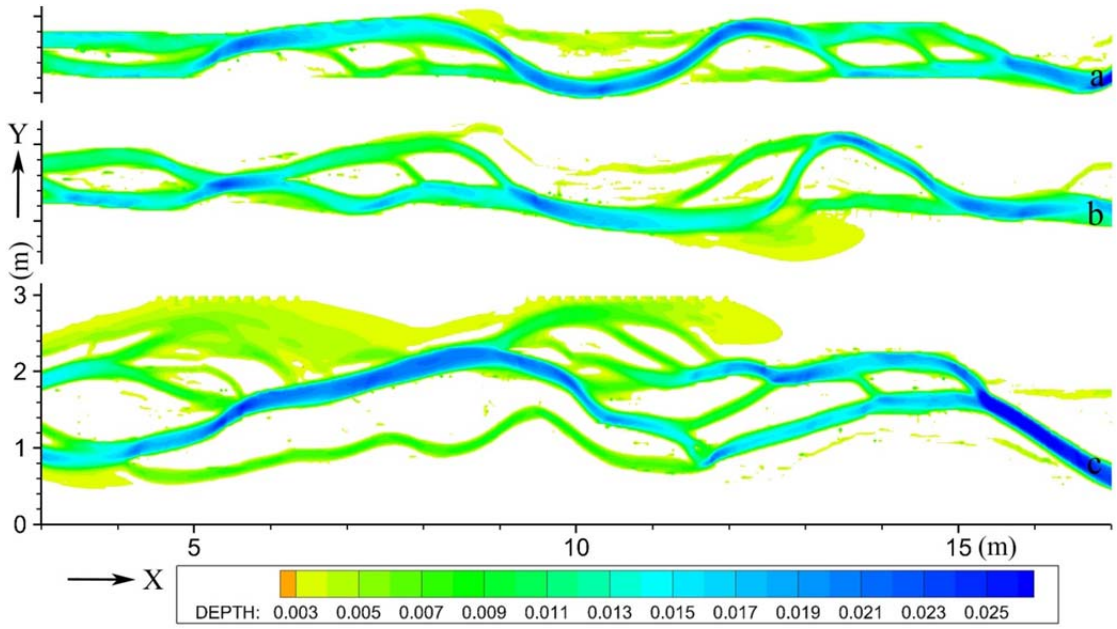

Figure 5.45 Braiding configuration with a cell size of 0.03 *0.03 m^2 (water depth/m): (a) 40; (b) 71; (c) 110 (hour).

5.9 Summary

In this chapter, the newly developed model was tested by a dam-break case and a

sediment aggradation case, and then was applied to simulate a laboratory braided river. The model has shown to be capable of predicting trans-critical flow and bed load transport process. With the same boundaries as an experimental river and no initial perturbation, the model well predicted the evolution process of braiding and channel pattern responses to increased discharge.

Some geomorphologic processes observed in the laboratory river and natural rivers have been found in the evolution process of the predicted river. Three kinds of avulsions have been analysed and found to show a close relationship to the temporal and spatial alternations of sinuous and straight channels, especially for the main channel. To consume its high energy the channel became more sinuous locally and then it adopted a new pathway by avulsion activities. The changes of braiding intensities illustrated trends similar to the laboratory river in the process of braiding generation and in response to increased discharge. Active braiding intensity developed quickly to a stable value, whereas total braiding intensity increased to a stable state gradually due to the time consumed by cutting new channels. Moreover, the river showed scaling characteristics, and maximum scour depths recorded the spatial geometry better than channel widths. The river presented anisotropic scaling properties with exponents similar to natural rivers. However, some braiding mechanisms in natural rivers, such as the central bar and chute cutoff, were not observed in the predicted river.

Generally, the model has shown to be capable of predicting some morphodynamic phenomena common in natural braided rivers. It well represents the

processes and morphodynamic changes in braided rivers. The items necessary for the prediction of the modelled river include: 1) basic hydraulic and sediment transport principles with bed morphology deformation; 2) a TVD scheme for solving trans-critical flow; 3) bank erosion and secondary flow, which are essential in channel migration and new channel generation; 4) consideration of graded sediments representing coarsening and fining effect with sheltering effect; and 5) a multiple layer arrangement with vertical sorting process. In these factors, bank erosion and bed deformation are essential for braiding generation in the predicted river.

Chapter 6 Braided River Modelling with Suspended Load

6.1 Introduction

Compared with those with bed load, braiding activities in rivers with suspended load have been less investigated. Actually, they occur mostly in some large rivers on plains with a less quantity. However, these rivers, such as the Yellow River and the Brahmaputra River, play important roles in our life due to their large catchments. In these rivers, braiding sometimes occurs under the water surface, which is different with the traditional definition of braiding. Due to the different flow conditions and sediment transport modes in these two kinds of rivers, their braiding mechanisms and morphodynamic changes may differ from each other.

In this chapter, a model was set up to simulate the processes of a large braided river dominated by suspended transport initially from an idealised river. The morphodynamics in the braided pattern and the fundamental morphologic units were investigated and compared with those from natural rivers. Furthermore, the braiding characteristics of this kind of river were analysed with some braiding indices and statistical methods. Finally, the results were compared with the predicted river with

bed load and natural rivers, and compared with the results produced by cellular models.

6.2 Model Setup

An idealised river with overloaded suspended load was set up to simulate the morphodynamic processes in large braided rivers. The input parameters are based on data collected from the Yellow River in China. Braiding is common in some parts of the Yellow River, such as the Ningxia-Inner Mongolia reaches and the Huayuankou reaches. For the former the river width ranges from 0.2 to 5.0 km, with some reaches showing typical braiding characteristics (Fan et al, 2012).

The modelled river was approximately 50 km long and 5 km wide (Figure 6.1a). Initially, it had a uniform bed slope of 0.000233 and a modified rectangular cross-section added with a cosine shape (Figure 6.1b). A cosine function was used to enable a more realistic channel cross-section. Sediments were divided into six fractions, with their sizes ranging from 0.0025 mm to 0.25 mm (Figure 6.2 and Table 6.1). Other than the actual grain sizes, these fractions are equivalent grain sizes, which have been corrected by considering the effect of cohesion (Xu et al., 2000). At the upstream boundary sediments were well mixed and initially homogenously laid on the river bed.

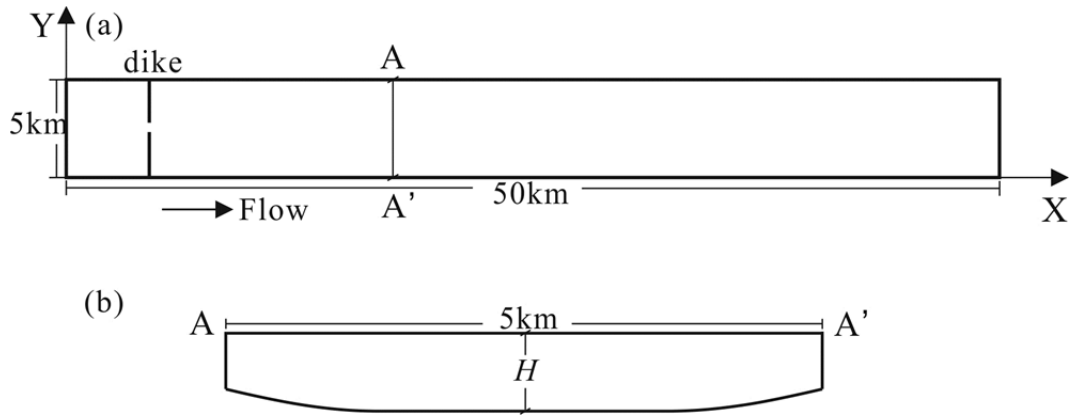

Figure 6.1 Schematic diagrams of initial river: (a) horizontal plan; and (b) cross-section A–A'.

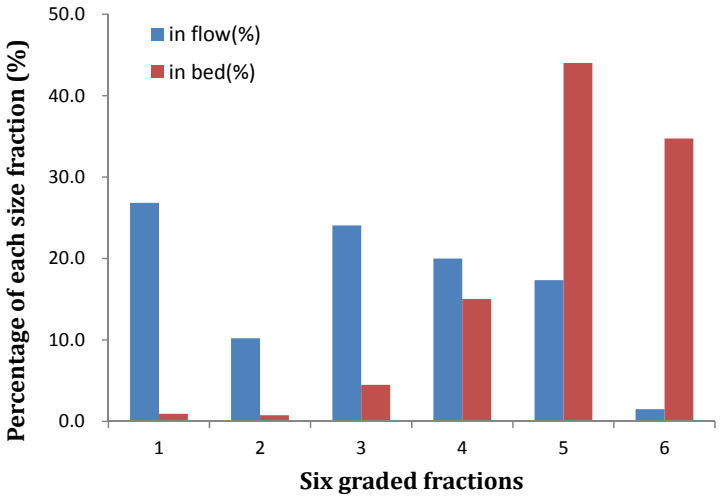

Figure 6.2 Sediment distributions in flow and bed layers.

Table 6.1 Sediment fractions and percentages in the numerical model

	Sand Groups	1	2	3	4	5	6
	Grain Size (mm)	0.0025	0.005	0.01	0.025	0.05	0.1	0.25
In flow	Percentage (%)	26.84	10.20	24.08	20.00	17.35	1.52	
	Finer than (%)	26.84	37.04	61.12	81.12	98.48	100.0	
In bed	Percentage (%)	0.95	0.75	4.50	15.05	44.00	34.75	
	Finer than (%)	0.95	1.70	6.20	21.25	65.25	100.0	

The model was set up with a total set of 557*58 cells, with the cell size being

90*90 m^2. Two spur dikes, one at each side, were set up at a location near the upstream boundary (4.32 km to the inlet) to create a local scour, which can reduce the evolution time for braiding pattern to develop. At the upstream boundary, flow discharge was specified as 6250 m^3/s, and at the downstream boundary, water level was specified. The sediment concentration was set to 44.5 kg/m^3. Three bed layers were adopted with the thickness of the upper layer 0.4 m, the middle layer 1.0 m and the lower layer 10.0 m. The time steps were set to 10 s for hydrodynamic and 20 s for sediment computations. The minimum water depth used to resolve the drying and flooding of the floodplain was 1.0 cm. The roughness height was set to 10 mm. The simulation time was 66 days, with principal hydrodynamic and morphologic data output once a day or shorter time intervals.

6.3 Model Results

After 33 days, due to sediment erosion and deposition, the river system experienced the formation and migration of bars and channels, and eventually formed a pattern similar to those observed from natural braided rivers (Figure 6.3). Repeated division and joining of channels with bars between them, presented an intertwining effect of a braided river, just as the braiding processes observed from many previous field and laboratory studies (Ashmore, 1991a, 1993; Rosatti, 2002; Egozi and Ashmore, 2009). From then on, the river evolution process obviously began to slow down, with fewer changes in the channel pattern.

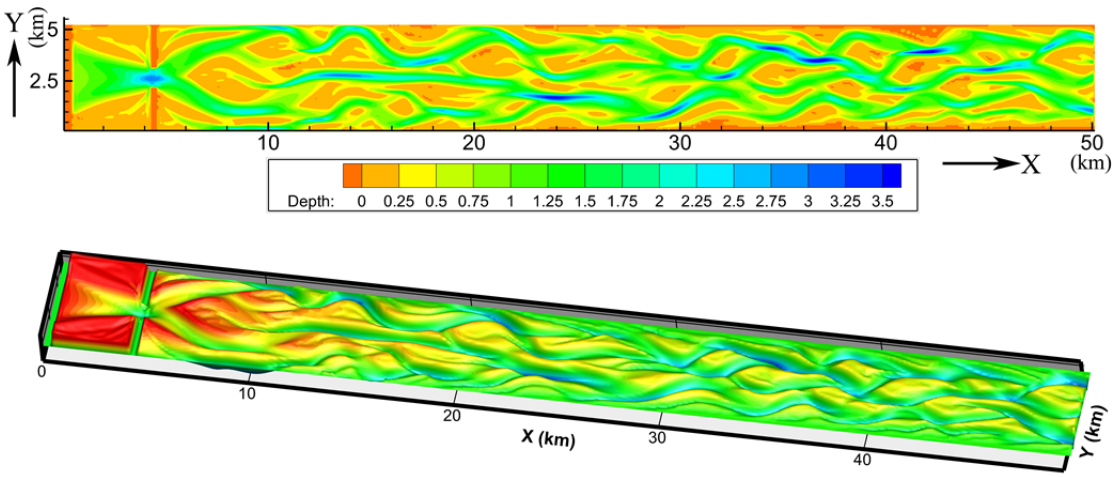

Figure 6.3 Channel pattern of the predicted braided river on day 33: (a) 2-D plain view of river bed (water depth/m); and (b) 3-D sketched river (erosion depth/m).

Notes: H: channel head; J: Y-shaped junction; B: reverse-Y-shaped bifurcation; X: X-shaped pairs of junction; a: pool; b: bar.

In addition, the analysis of the present study is based on the definition that braiding does not necessarily involve the exposure of inactive bars above the water surface, which is a classical view of braiding (Ashmore, 1991a). Instead, it can be defined as a distinct bifurcation of the flow and (or) bed-load flux around inactive (sensibly zero bed load) portions of the channel bed. In the modelled river, if a specific value of water depth is taken as the channel and bar boundary, flow velocity on bars is distinctively smaller than in channels, with some parts exposed. In this study, a water depth of 0.5 m was chosen as the channel and bar boundary in analysing the basic morphologic and statistical characteristics.

Channel nodes common in natural braided rivers, including channel heads, Y-shaped junctions, reverse-Y-shaped bifurcations, and X-shaped pairs of junctions and downstream bifurcations, can be seen in the prediction (Figure 6.3). Pool-bar units can be found in the predicted river, which are fundamental geomorphologic units

in a braided river (Ferguson 1993). Alternating channels and bars form pool-bar units and then form braided rivers. In the downstream river, pool-bar units occur alongside each other in two or more parallel rows (Figure 6.3). One typical pool-bar unit is circled in the rectangular. The pools are linked by talwegs which present two or more back to back meandering traces, alternately converging and diverging. Each braid bar is part of three pool units: the bar head is the distal part of one unit, and the left and right sides of the bar tail are lateral parts of two other units alongside each other. These phenomena were similar to those depicted by Bridge (1993).

6.4 Braiding Processes and Morphologic Changes

Generally, the evolution process of the predicted braided river can be divided into three stages, including the upstream channel pattern formation and downstream braiding initiation (Figure 6.4, a–b), the downstream channel pattern formation (Figure 6.4, c–d), and braided channel pattern evolution with avulsions (Figure 6.4, e–g).

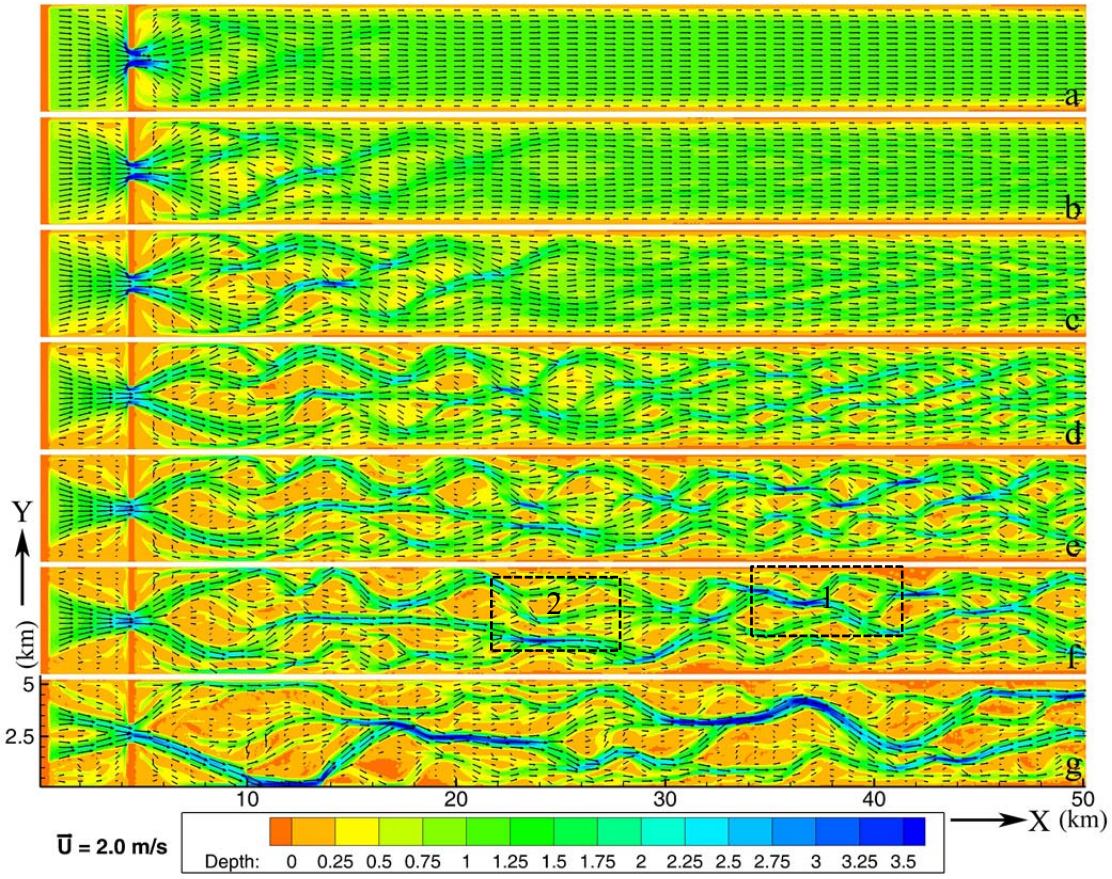

Figure 6.4 Development of braided channel pattern (water depth/m): (a) 4; (b) 9; (c) 14; (d) 20; (e) 27; (f) 33; and (g) 66 (day).

Zone 1 in (f): choking avulsion and constriction avulsion; zone 2: apex avulsion.

During stage one (Figure 6.4, a–b), braiding developed in the upstream flume. At the beginning, the depth of the loose sediment bed layer was uniform. After four days (Figure 6.4a), some limited changes occurred on the river bed, initially in the area near the spurs. Since the spurs narrowed the flow, the high flow velocity intrigued intense erosion and deposition. Consequently, channel pattern with alternative deep areas and shallow areas appeared in the upstream flume (Figure 6.4b, by day 5). This "deep-shallow alternating pattern" is normally referred to as "chute and lobe" (or pool and bar) in previous works (e.g. Ashmore, 1991a; Ferguson, 1992). The development

of chutes and lobes changed local hydraulic condition, with the braided configuration extending downstream. Erosion mainly occurred in chute areas and deposition occurred in lobe areas, and the differentiation between them continued to enlarge (Figure 6.4b).

The first stage was a period when river channels began to form. The braided pattern was initiated by sediment deposition and erosion in the form of lobes and wide shallow chutes. The river bed consisted of fine sands, so tiny perturbation of flow might cause local sediments to reach their critical shear stress and be carried away by flow. The energetic turbulent fluid motion near the bed might cause local erosion and deposition of a mound of sediment (a bed defect, Bridge, 2003). When the defect was sufficiently large, flow separation occurred on its lee side. Increased turbulence intensity in the zone of reattachment caused further erosion and further redeposition downstream as other defects. These defects developed progressively downstream and grew in size, until the whole bed was covered with pools and bars. The spurs strengthened the perturbation by first narrowing and then releasing the flow, promoting the development of the braided pattern.

During stage two (Figure 6.4, c–d), braided channel pattern formed downstream, while the upstream segment continued to evolve to a new morphologic geometry. Typical pool-bar units and some channel avulsions can be seen in this process. In the upstream reach, some important changes occurred. First, chutes and lobes developed and the channels were getting more sinuous. The young chutes deepened, constrained and connected with adjacent chutes, and grew into deep channels. The lobes grew in

size and elevation, taking the form of bars. As erosion and deposition developed, bars grew horizontally and consequently bent the channel flows. This resulted in a higher channel sinuosity. Second, the channel pattern moved downstream noticeably and confluence scour holes emerged. Third, sediment sorting effect occurred. Scour holes were often left with coarser sediments yet bars were composed of finer sediments. By day 14 (Figure 6.4c), the upstream channel pattern has been formed. In the next few days, the channels continued to become narrower and deeper as to form several major channels. At the end of this stage (Figure 6.4d), some parts of the upstream bars emerged from water surface.

During stage three (Figure 6.4, e–g), the upstream channels continued to constrain and migrated frequently. Channel avulsion is the most important braiding mechanism at this stage. In the midstream (between 22 and 30 km), intense channel diversion occurred. Channels separated from parent channels and connected with new ones frequently. In the downstream, flow is confined, moved downstream and some scour holes appeared at the confluence. Some channels disappeared and the two bars dissected by them merged together, forming more stable large bars, with some of them emerging from water surface. Sediment sorting effect continued and coarse channel and fine bars formed in the downstream reach. By day 33 (Figure 6.4f), a typical braided river had formed. The channel pattern evolution rate slows down after that. As channel avulsion occurred frequently, channels merged into each other, forming a large main channel in the whole flume (Figure 6.4g). In this situation, the river is still braided yet has fewer channels.

In the river evolution process some phenomena deserve our attention. First, the upstream and downstream braided patterns did not form simultaneously and showed different development mechanism. The upstream channels formed by downstream extension while the downstream channels appeared nearly simultaneously. Second, as to the sediment sorting, the changes of D_{50} were somewhat fast with local hydraulic conditions. This is due to the fine sediment load and bed structure. Third, the river seems to develop towards an equilibrium state. Many researchers consider that braiding can be a valid equilibrium even though individual channels might be transient (Knighton, 1998). This is supported by some studies from fieldwork and laboratory (Leopold and Wolman, 1957; Klaassen and Vermeer, 1988).

6.5 Braiding Mechanisms

Channel avulsion, an important braiding mechanism, is mainly introduced in this part. The three types of channel avulsions including chocking avulsion, constriction avulsion and apex avulsion have been observed and investigated in the predicted river. Take some typical processes as examples, the evolution process of these three types of avulsions are introduced in detail. Moreover, avulsions do not occur alone. Instead they are normally closely related to the channel and flow changes in surrounding areas. To illustrate the development of avulsions, a rectangular zone has been circled in Figure 6.4f (zone 1), including a pool-bar unit BA. It will be introduced first in which one constriction avulsion and one choking avulsion occur.

6.5.1 Pool-bar Unit BA

The pool-bar unit BA is composed by the bifurcation B and its two tributaries (L for left tributary and R for right tributary), bar A and its next confluence. The talweg in the two tributaries shows some interesting distribution. In the left tributary, flow talweg is apart from bar A in front of the channel curve, close to the bar at the curve, and apart from bar A behind it (Figures 6.5 and 6.7c, day 29). Yet in the right tributary, flow talweg is distributed in the middle of the channel nearly for the whole channel. The left tributary seems to be gentler with lower sinuosity than the right one. Compared with the talweg depicted by Bridge (1993), the left tributary shows similar talweg distribution at high flow stage, while the right tributary is similar to that at low flow stage. Actually, the discharge changes during days 25 to 40 (Figure 6.6) indicate that, the left tributary is at a stage when discharge continues decreasing, whereas the right tributary is at a different stage when discharge continues increasing.

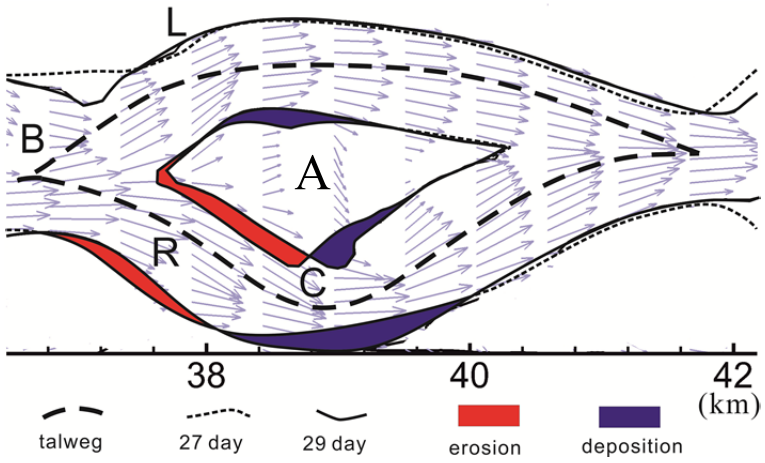

Figure 6.5 Flow velocity and talweg distributions in the pool-bar unit BA by days 27 (short dotted line) and 29 (solid line).

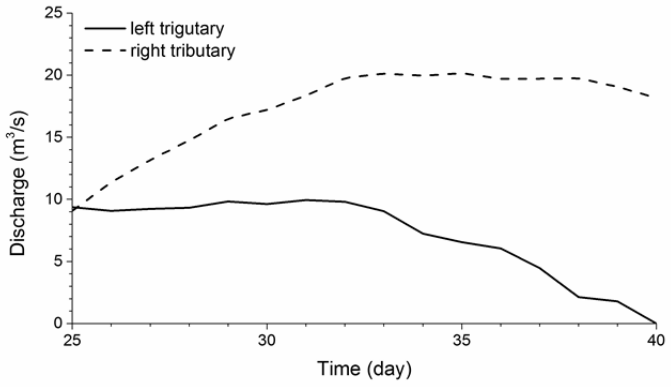

Figure 6.6 Discharge changes in the two tributaries of bifurcation B.

Initially the two tributaries were nearly equivalent to each other with similar water discharge. A scour hole was situated in front of the bifurcation, whose axis was deflected towards the right tributary (Figure 6.7a). As time passed, in the left tributary, flow velocity decreased continuously with deposition occurring. Eventually, the left tributary got blocked, which was considered as “choking avulsion” in braided river (Figure 6.7k). Meanwhile, a large amount of discharge at the bifurcation was diverted to the right tributary, causing it to become dominant and more sinuous. Finally, the channel got curved enough for the flow to overflow at the bend, resulting in the generation of a new channel, which was considered as “constriction avulsion”. Meanwhile, the scour hole in the right tributary moved downstream, extended into the right tributary and got filled to a great extent.

The deposition and erosion processes of the pool-bar unit are presented in Figure 6.5. In the right tributary, erosion occurred in front of bend C while deposition occurred behind it. On its outside, similar situation occurred. In the upstream part of the left tributary, as talweg was near the outside channel and flow velocity was not

high inside the channel, little erosion occurred on the face of bar A. Yet intense deposition occurred near the curve of bar. In its downstream part, little erosion took place both inside and outside the channel.

The movement of the pool-bar unit is accompanied by bed shear stress change, sediment concentration and bed D_{50}. Initially, flow discharge was similar for the two tributaries (Figure 6.6), but shear stress was lower in the left tributary than the right one (Figure 6.8a). High shear stress occurred at bifurcation B and curve C, whereas the zone with the highest sediment concentration occurred at the left part of the right tributary and bar A (Figures 6.7b and 6.9b). As constriction avulsion occurred at bend C (Figure 6.7d), the zone with high sediment concentration moved to the downstream part of the right channel (e.g. Figure 6.9g). In this area, flow kept decreasing and the channel got filled up to a large content. The zone with high sediment concentration still mostly occurred on bar A. Here, intense deposition occurred, but shear stress and flow velocity were low. In general, high sediment concentration is not necessarily related to high flow velocity and shear stress. Instead, it occurs in areas with intense erosion or deposition, usually on their boundaries.

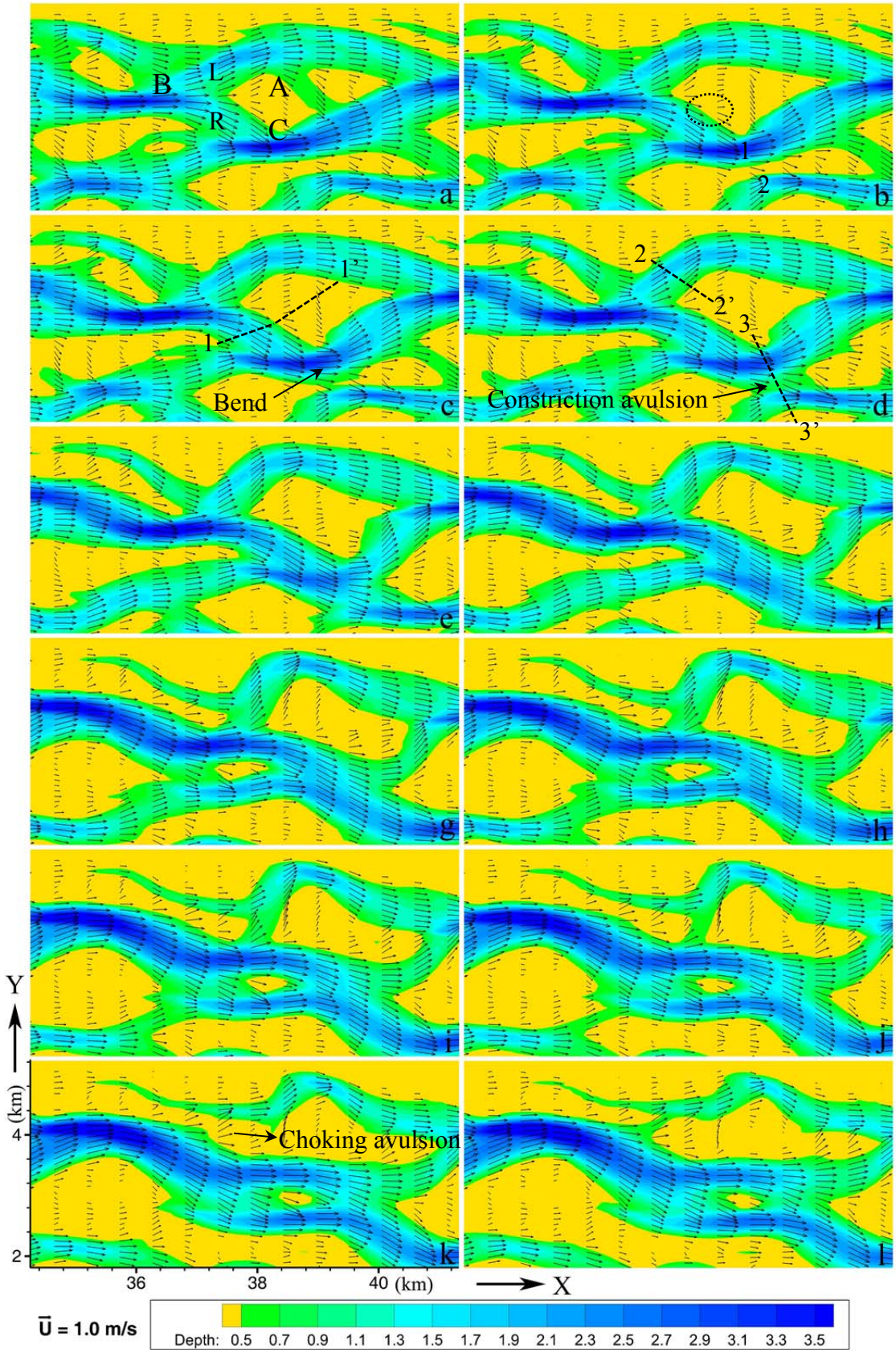

Figure 6.7 Water depth in the choking avulsion and constriction avulsion (m): (a) 25; (b) 28; (c) 29; (d) 30; (e) 32; (f) 34; (g) 36; (h) 37; (i) 38; (j) 39; (k) 40; and (l) 41(day).

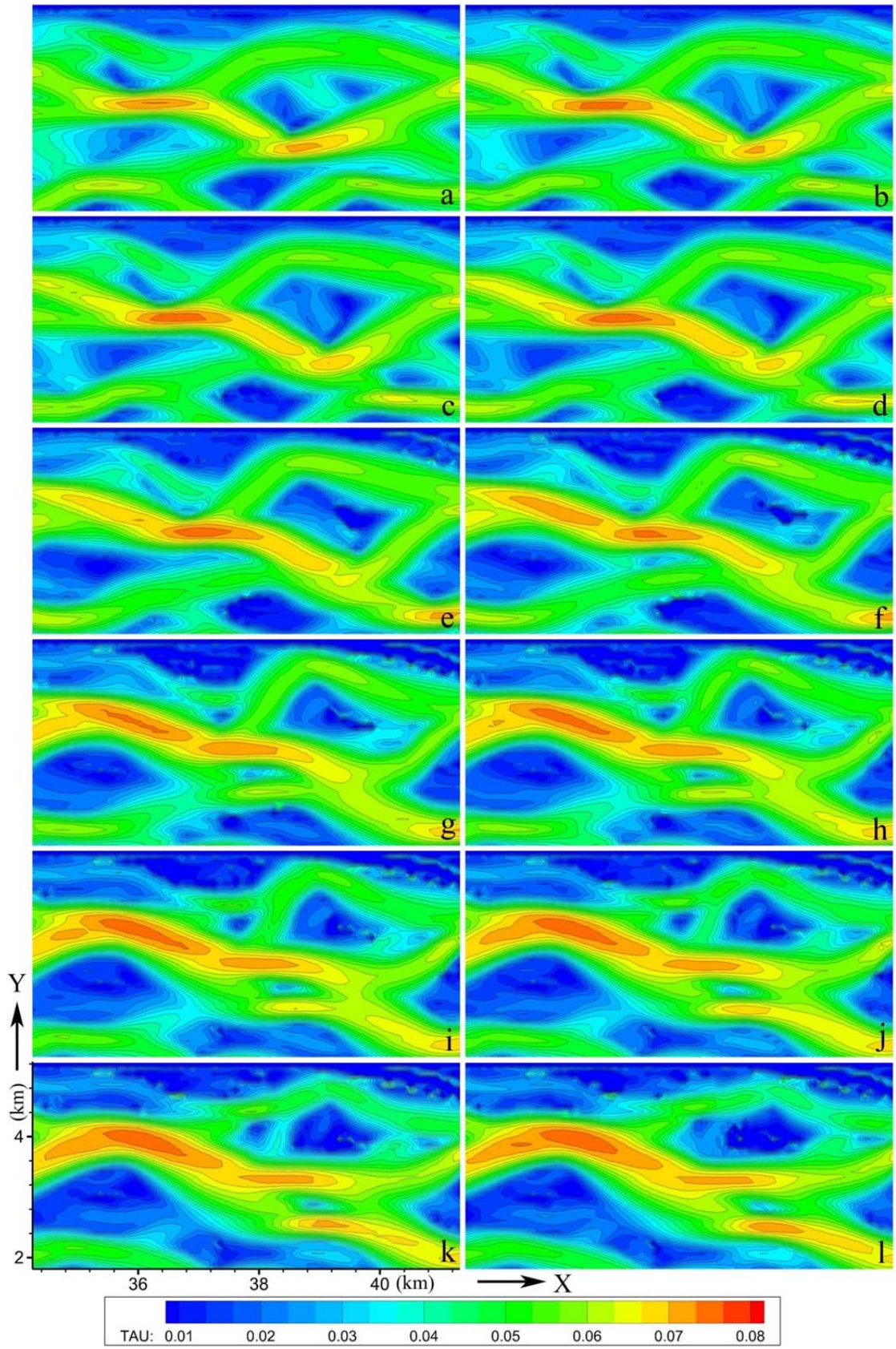

Figure 6.8 Shear stress in the choking avulsion and constriction avulsion (N/m^2): (a) 25; (b) 28; (c) 29; (d) 30; (e) 32; (f) 34; (g) 36; (h) 37; (i) 38; (j) 39; (k) 40; and (l) 41(day).

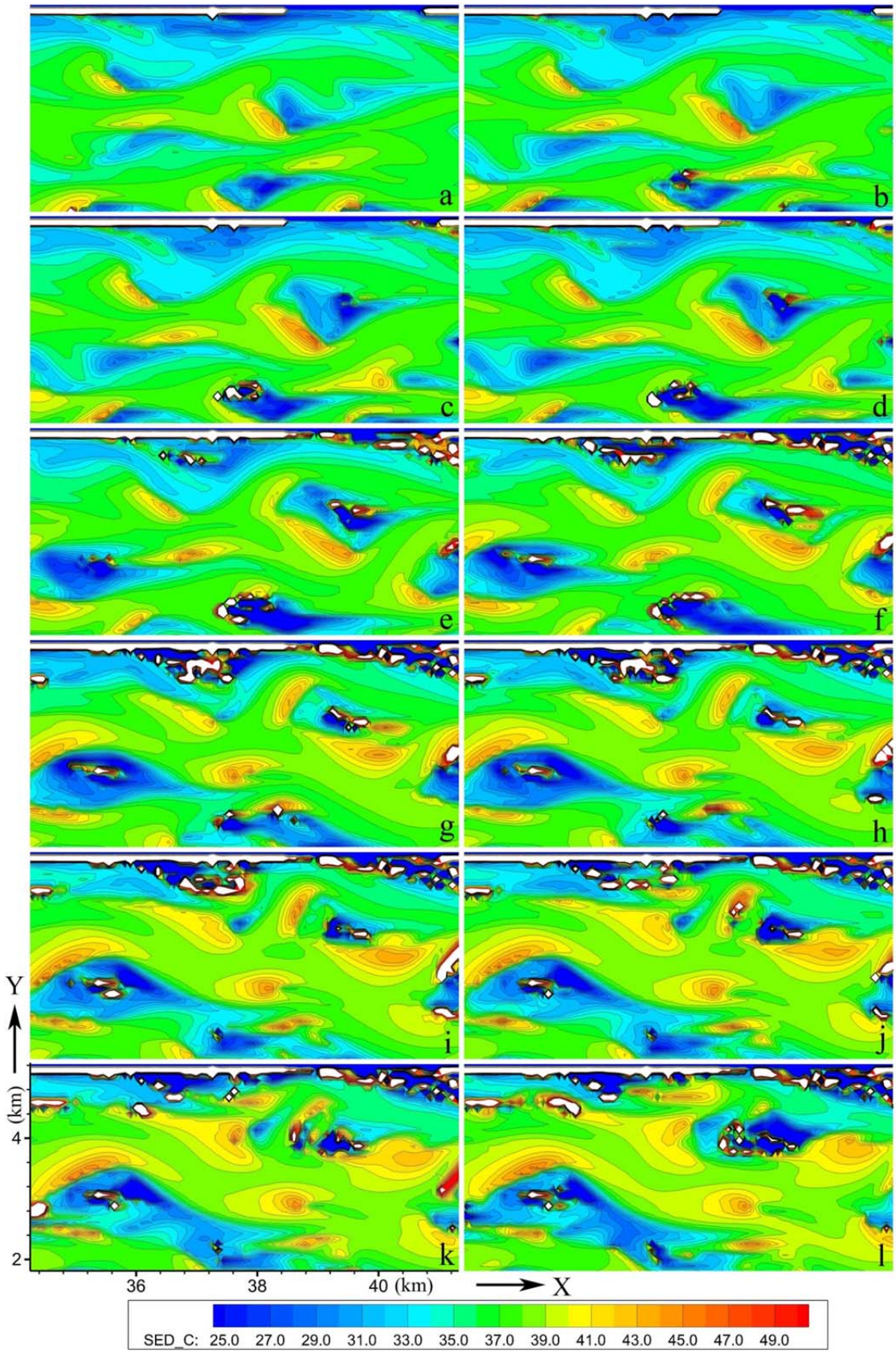

Figure 6.9 Sediment concentration in the choking avulsion and constriction avulsion (kg/m^3): (a) 25; (b) 28; (c) 29; (d) 30; (e) 32; (f) 34; (g) 36; (h) 37; (i) 38; (j) 39; (k) 40; and (l) 41(day).

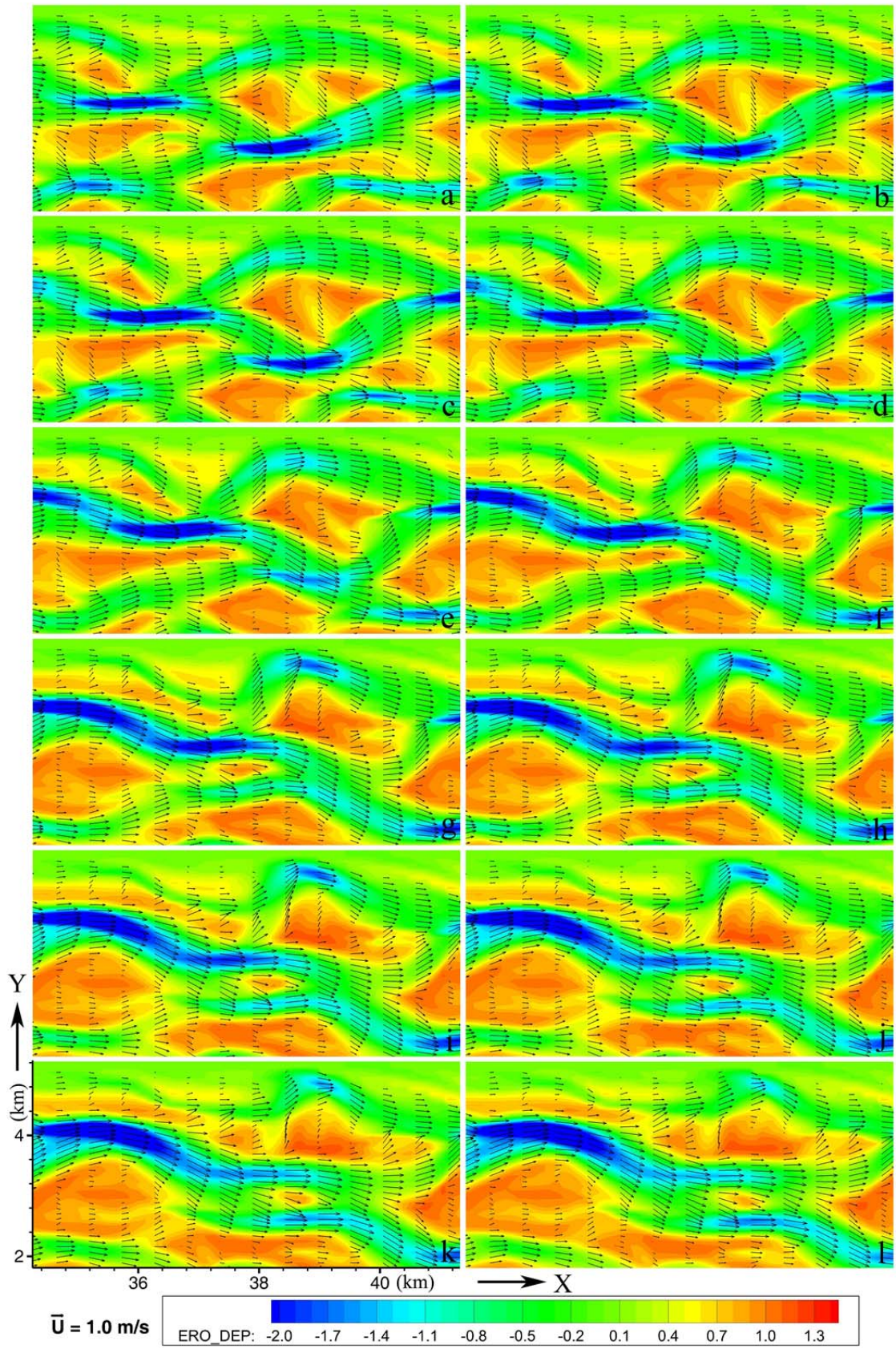

Figure 6.10 Erosion depth in the choking avulsion and constriction avulsion (m): (a) 25; (b) 28; (c) 29; (d) 30; (e) 32; (f) 34; (g) 36; (h) 37; (i) 38; (j) 39; (k) 40; and (l) 41(day).

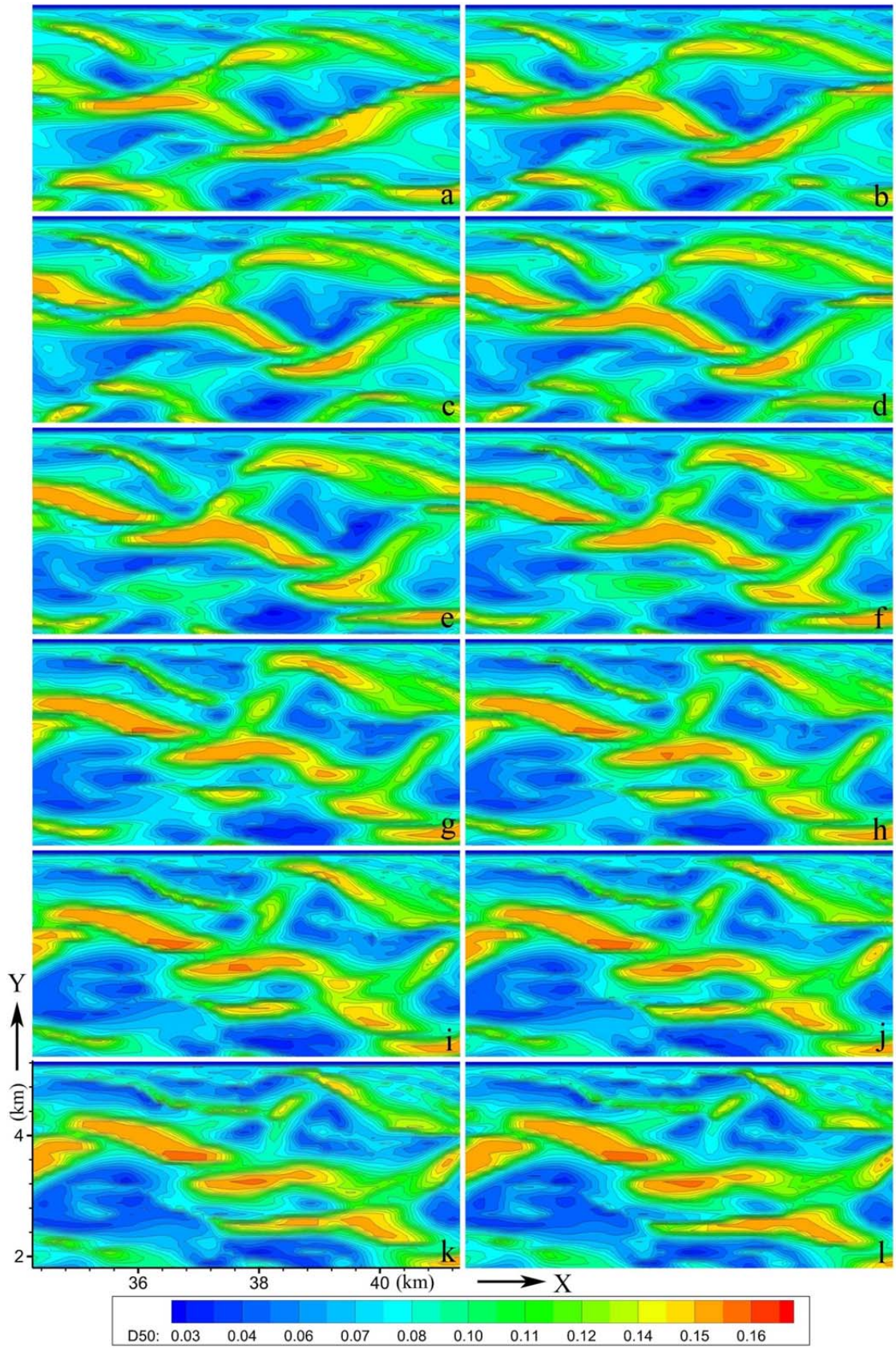

Figure 6.11 Sediment D_{50} distribution in bed in the choking avulsion and constriction avulsion (mm): (a) 25; (b) 28; (c) 29; (d) 30; (e) 32; (f) 34; (g) 36; (h) 37; (i) 38; (j) 39; (k) 40; and (l) 41(day).

Erosion and deposition mechanism

The evolution of the right tributary of bifurcation B shows the mechanism of channel erosion and deposition. Line 1-1' was stretched across the right tributary and bar A (Figure 6.7c). On day 29, in the right tributary, the talweg was near the channel centreline (Figure 6.12). Here the bed was the coarsest and erosion depth was the deepest. However, the maximum values of flow velocity and shear stress occurred near the left bank. Sediment concentration in suspension was not high. At the left bank, the high flow velocity contained high flow energy, generating high shear stress and thus sediments were carried away from the bed. Then erosion occurred here, resulting in high sediment concentration in suspension, deeper water and coarser sediments in bed. On the contrary, deposition occurred at the right bank, causing shallower water depth and finer sediments in bed. Bar A was eroded to move downstream with some upstream part changing into the channel. This activity proceeded quickly before the initiation of choking avulsion (started on day 29).

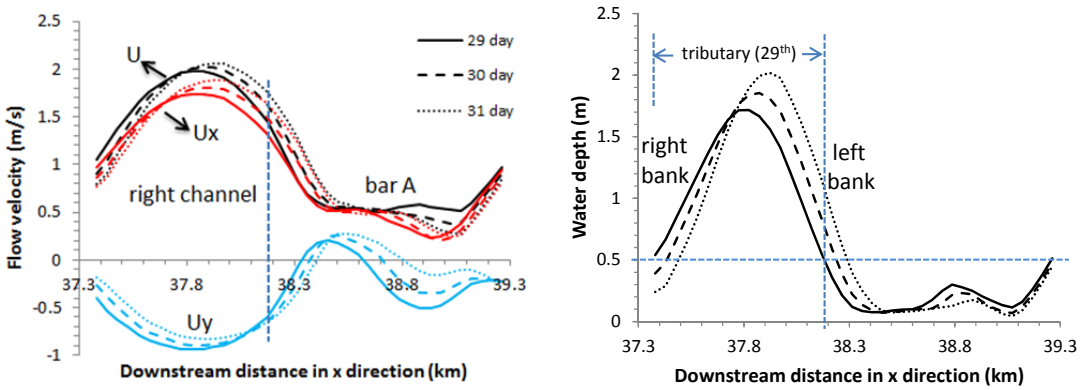

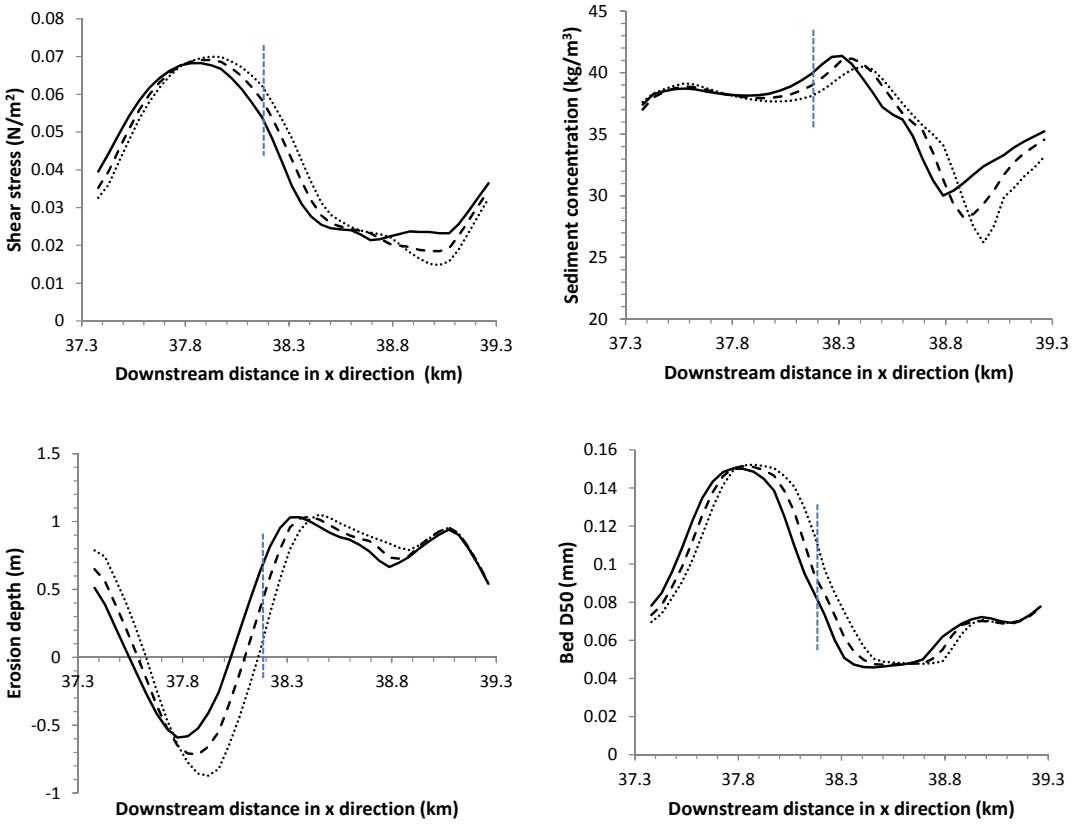

Figure 6.12 Changes in the right tributary of bifurcation B along the line 1–1' of Figure 6.7.

6.5.2 Chocking Avulsion

One choking avulsion occurred in the left tributary of bifurcation B. Line 2–2' was stretched across it (Figure 6.7d). Time serial charts of Hydraulic and morphodynamic parameters are shown in Figure 6.13.

Period 1

From day 25 to 33, the development of the tributary was relatively simple (Figure 6.13a). Initially, the talweg was close to the left bank, with the maximum flow velocity and shear stress slightly closer to the right bank yet with similar trend. But high concentration occurred near the right bank. As time passed, high values of flow

velocity and shear stress continued moving towards the right bank. Yet water depth did not change. Its talweg moved a little towards the left bank and became shallower with deposition occurred.

(a)

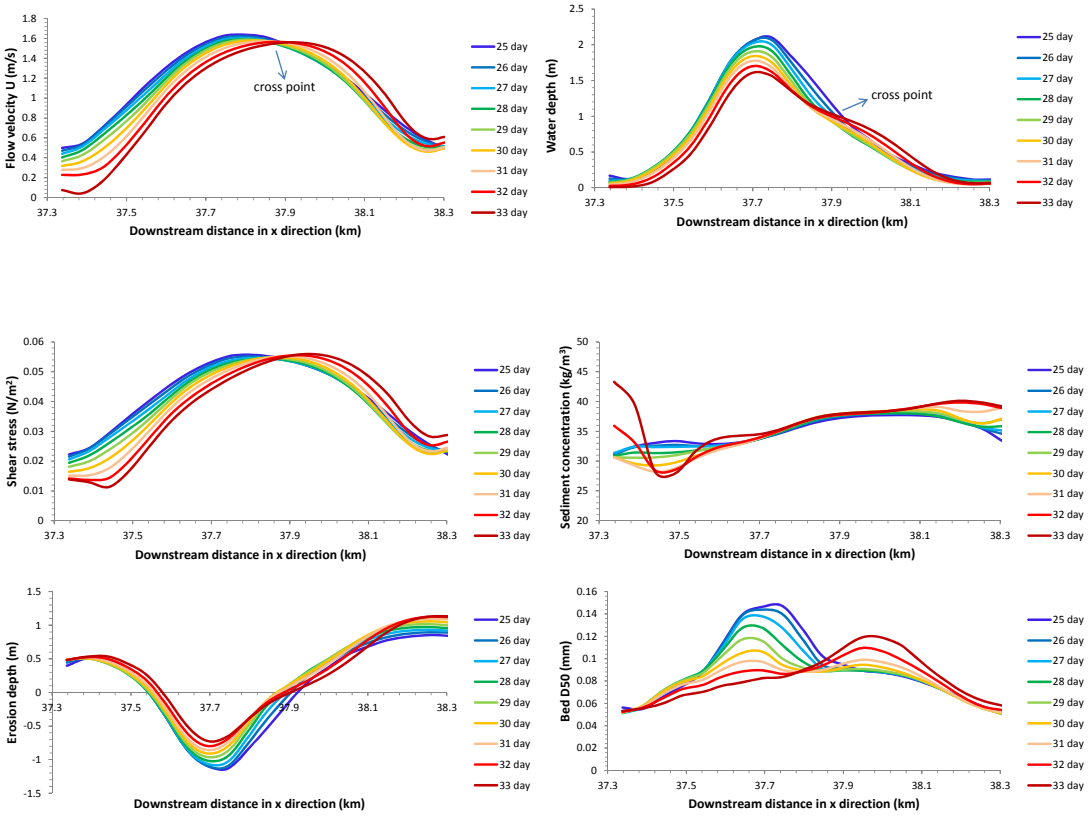

(b)

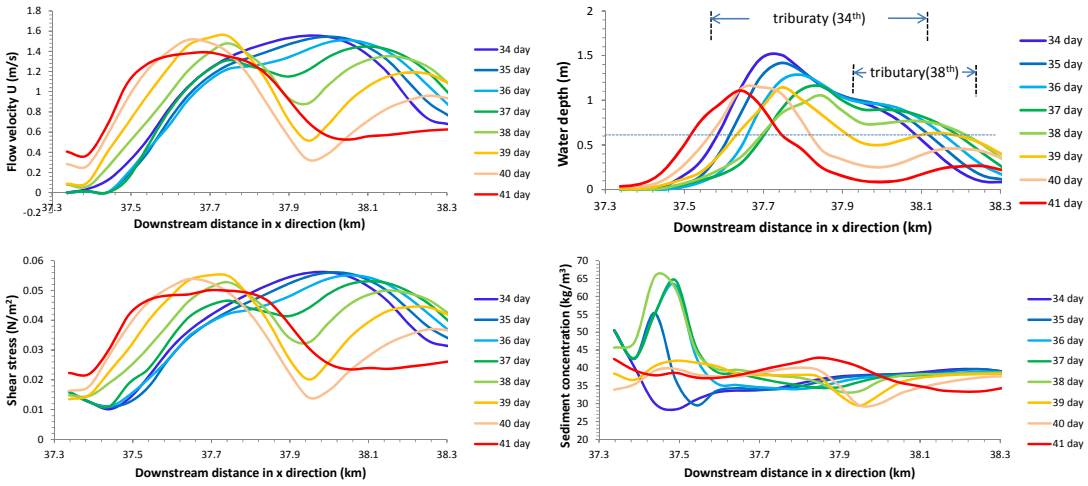

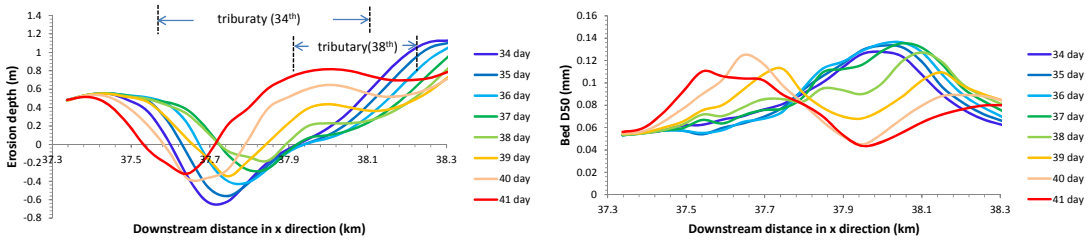

Figure 6.13 Hydraulic and morphodynamic changes in the left tributary during the choking avulsion: (a) 25–33; and (b) 34–41 (day).

During this period there was a "cross point" for these parameters (Figure 6.13a). To its left, flow velocity and shear stress continued decreasing, deposition occurred and fine sediments distributed in bed. To its right, flow velocity and shear stress continued rising, erosion occurred, fine sediments were carried away and river bed became coarser. The cross point of erosion occurred later than shear stress and flow velocity, indicating that changes of flow velocity and shear stress resulted in the variations of water depth, erosion depth and bed composition.

Period 2

The curves of erosion depth illustrate the deposition and erosion behaviours (Figure 6.13b, erosion depth). The bed evolution in the tributary could be divided into three zones. Near the left bank (zone 1), deposition occurred continuously. Maximum erosion occurred here and accordingly the talweg was here, too. However, as deposition went on, the left bank of the channel kept moving downstream continuously. By day 39, there was still some area deep in the precious left bank area, but it did not belong to the right tributary any more. Instead it was another sub-tributary which merged into this tributary.

Most of the middle part (zone 2) of the channel did not deposit sediments in the first three days. But in the next two days deposition occurred quickly, and by day 39 this area has become the left bank of the channel. The reason why the water depth was still higher than 0.5 m is that, line 2–2' was now at the confluence of a small channel. During days 38 to 40, large amounts of sediments were quickly deposited on zone 2, with relatively low sediment concentration in transport. Flow velocity and shear stress decreased fast. Bed D_{50} in this zone was the finest in the channel because of the large amount of quickly deposited sediments.

In zone 3 erosion first occurred near the right bank and caused the movement of the right bank towards downstream in the early four days. Flow velocity and shear stress increased during this period, especially near the right bank. High shear stress and flow velocity brought about intense consequent erosion near the right bank. Although the strongest erosion in this zone occurred near the right channel bank, here the sediment concentration was not the highest. From day 38 on, deposition started to occur in zone 3 and in the next three days the left tributary disappeared completely.

6.5.3 Constriction Avulsion

One constriction avulsion occurred at bend C in the right tributary. Figure 6.7 shows the two channels involved in the constriction avulsion, the right tributary of bifurcation B (channel 1) and one channel to its right (channel 2). A line 3–3' was stretched across these two channels (Figure 6.7d), which moved with channel 1 and 2 to make it always near the centre of the newly overflowed channel.

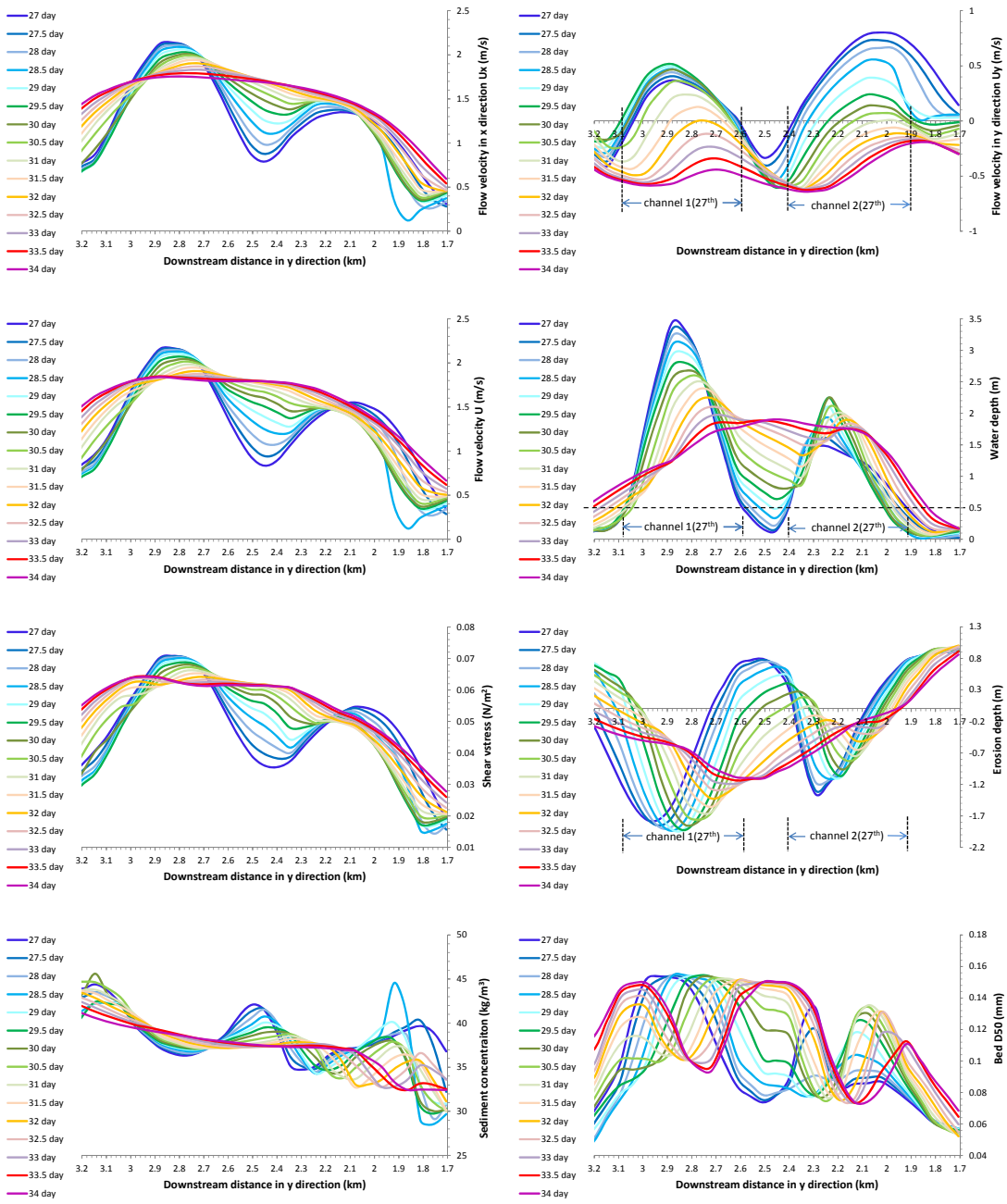

Figure 6.14 Hydraulic and morphodynamic changes during the constriction avulsion at bend C.

In channel 1 in front of bend C, continuous erosion occurred at the left bank yet deposition took place at the right bank. Consequently, channel 1 moved continuously towards channel 2. Meanwhile, the bar on the left of bend C aggraded continuously and extended horizontally. These two effects deflected the flow, and caused the

channel sinuosity to increase distinctively (Figure 6.7c). Consequently, the curvature radius of the streamlines decreased at bend C and water ponded there. Eventually, the water overflowed out of the bank to achieve a more straight flow, a new channel was born, which was called “constriction avulsion” (Figure 6.7c). From then on, channel 1 moved downstream and its bend pool was greatly filled.

Bed D_{50} tended to be coarser with erosion and finer with deposition. Sediment concentration was low in these two channels, while high value was observed between the areas of these two channels. With channel 1 gradually merging into channel 2, this difference decreased and finally got roughly averaged. Its trend was nearly opposite to the flow velocity. It can be seen that, high velocity is not necessarily followed by high sediment concentration. Instead, high sediment concentration often occurs in moving channel where intense erosion occurs.

What should be paid attention to is that why this process is considered as “constriction avulsion” other than “apex avulsion”. Both of constriction avulsion and apex avulsion are related to the avulsion into an adjacent inactive channel. The difference between them is the way how they get into the adjacent channel. In constriction avulsion, flow overflows out of its bank and joins the adjacent channel. However, in apex avulsion flow first erodes the bank to make its channel and then joins the adjacent channel.

6.5.4 Apex Avulsion

Apex avulsion is found in the evolution of midstream channels during stage three,

with a typical one circled in a rectangular zone in Figure 6.4f (zone 2). Figure 6.15 illustrates the evolution process of an apex avulsion. Line 4–4' was stretched along the talweg of the new channel, which was moving with the channel downstream in x direction (Figure 6.15h). Channels 3 and 4 are involved in this avulsion. Figure 6.16 shows the evolution process of the new channel.

Initially, channel 4 was one tributary of a bifurcation. It was disbranched from the bifurcation slowly and became inactive. Meanwhile, channel 3 gradually generated a new channel. The new channel eroded its new route, and connected to the inactive channel 4. It grew further and became one tributary of a bifurcation, with channel 3 as the other tributary. In this process, the location and sinuosity of channel 3 remained nearly unchanged. But in constriction avulsion, obvious erosion and deposition occurred with quickly decreasing sinuosity of corresponding channel 3.

Initially, there was no bifurcation in channel 3, yet high shear stress occurred at its left bank. Close to this area, the sediment concentration in channel 3 was apparently higher than the surrounding area. Flow eroded the bed and after four days, the new bifurcation began to form (Figure 6.15c). With the new channel eroding its route, channel 4 was shrinking behind quickly. By day 51, the new channel finally got connected with channel 4, by eroding its way continuously towards channel 4 during this period. The bed of the new channel was coarsening in this process, while it was finer than parent channel, channel 3.

Sediment concentration was changing in a much different way. Initially the highest sediment concentration distributed in the zone where the new channel would

begin, and kept growing in the next few days with high shear stress. Flow eroded the bed and more sediments were carried away and high sediment concentration occurred. This trend moved together with the development of the new channel, with maximum value usually occurring near the head of the new channel. It illustrates the fact that high sediment concentration is closely related to intense erosion activity.

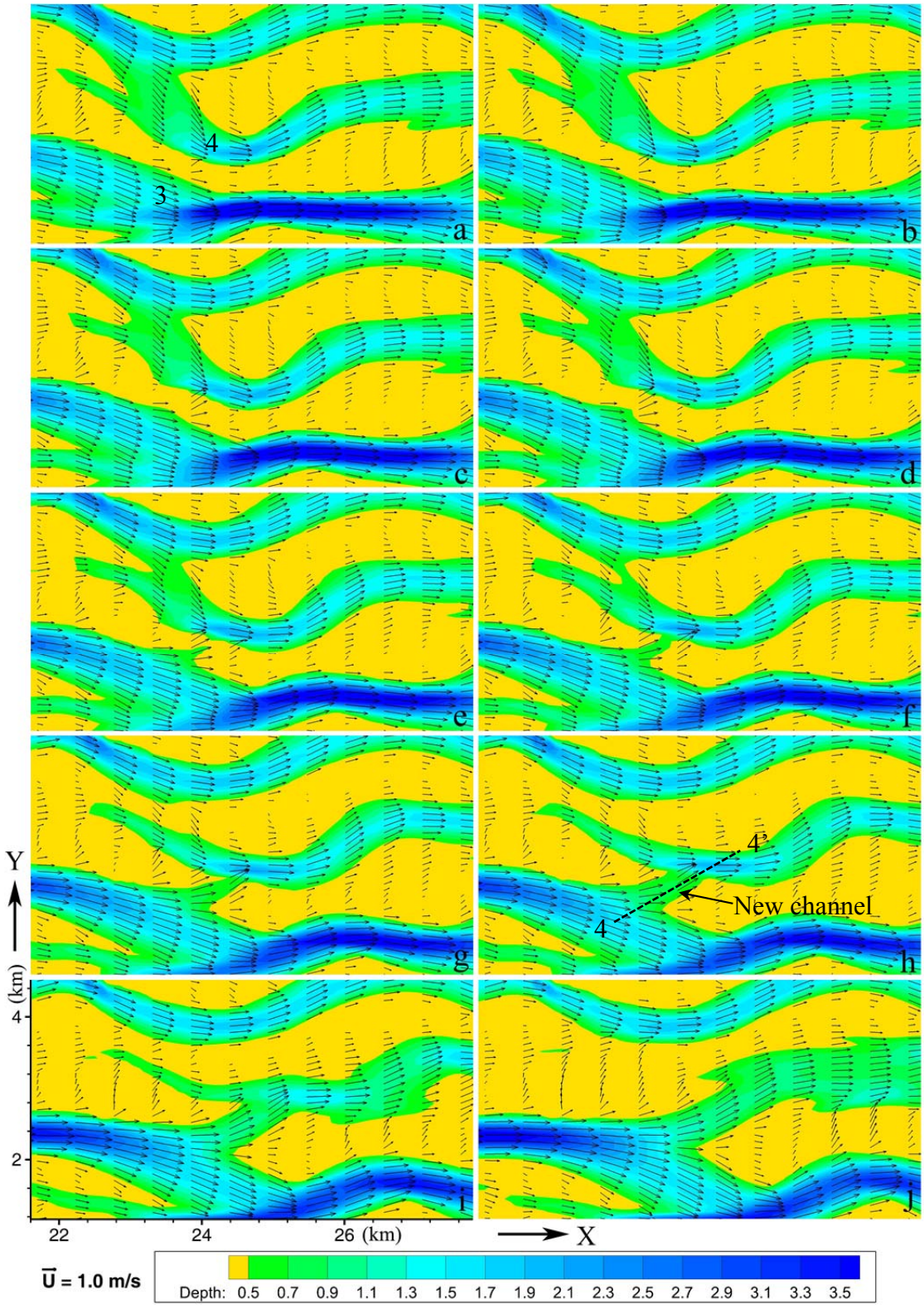

Figure 6.15 Water depth in the apex avulsion (m): (a) 45; (b) 46; (c) 48; (d) 49; (e) 50; (f) 51; (g) 52; (h) 53; (i) 56; and (j) 59 (day).

Note: Line 4-4' was stretched along the talweg of the new channel and moving with it.

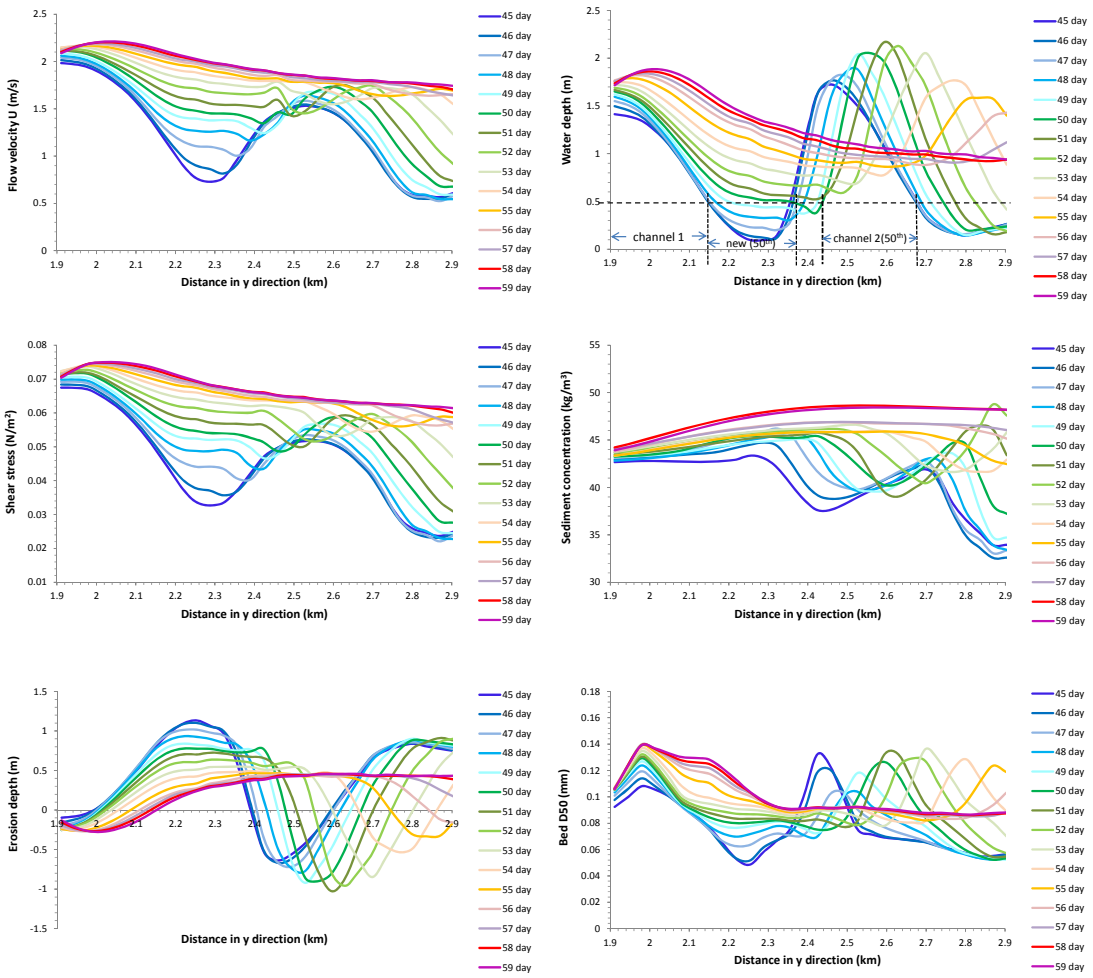

Figure 6.16 Hydraulic and morphodynamic changes during the apex avulsion.

6.6 Fundamental Morphologic Units

The braided river patterns are so complex that scientists sometimes identify basic units or building blocks and study them in isolation. Important processes at a confluence and a bar are discussed in detail in the following part.

6.6.1 Confluence

The evolution processes of confluence C and its two tributaries are shown in Figures 6.17—6.21 (L and R for left and right tributaries). The hydrodynamic changes in the left tributary are shown in Figure 6.22. Initially, the apexes of shear stress,

velocity, water depth were at the same site, with the talweg close to the right bank. In the next few days, for the left apex, shear stress increased continually until to be equivalent to the right one, flow velocity increased slightly, yet water depth remained nearly unchanged in the whole cross-section (Figures 6.17a and 6.22b). As flow velocity increased in the left apex, shear stress increased and more sediments were carried away from the channel bed. Consequently, erosion occurred and water depth increased near the left bank (Figure 6.17b). On the contrary, for the right apex, shear stress and flow velocity decreased, deposition occurred, and water depth became shallower. By day 26 (Figures 6.17c and 6.22c), the talweg had completely turned to the left bank and the right apex got diminished. However, this situation did not last a long time. In the next few days, increasing flow velocity and shear stress caused erosion in the original site of the right apex. Therefore, the right apex emerged again (Figure 6.17d). It can be summarised in this way. Increased shear stress and flow velocity caused local erosion, resulting in deepening of water depth. Importantly, there was a time lag between them.

In the left tributary, water discharge decreased from 889.4 m^3/s to 765.3 m^3/s until day 20, and then increased continually to 1151.4 m^3/s (Figure 6.23). The former trend might result from the initial channel constraint and increasing sinuosity (Figure 6.17b). The latter increase seemed to result partly from the disappearance of one middle channel between two adjacent bars enclosed by the two tributaries, and partly from the widening of the channel. For the right tributary, due to channel constraint and the disappearance of a small bifurcation, discharge increased from 1131.5 m^3/s to

1832.5 m^3/s. Simultaneously, the the curvature radius of the deflection decreased with the more and more sinuous channel. Flow scoured the outer bank intensely, causing serious erosion. Finally a bifurcation occurred at the channel bend, which branched off a large amount of discharge. Consequently, flow discharge of the right tributary decreased to 1037.6 m^3/s.

In this process, the orientation of the confluence was mainly controlled by the direction of the main channel. Initially the discharge into the right tributary was a little larger than that into the left one, when confluence orientation ($\theta_1 > \theta_2$) was close to its direction (Figure 6.17a). In the next four days, as the discharge increased in the right tributary and decreased in the left one, the right tributary became dominant. This caused the orientation of confluence C to change to a direction nearly parallel to the flow direction of the right tributary (Figure 6.17b). Due to the continual erosion and increasing sinuosity, the scour hole at confluence C enlarged and deepened dramatically (Figure 6.17c). The orientation of the confluence remained nearly parallel to the right tributary. However, as the discharge of the right tributary decreased abruptly in the last several days, the scour axis gradually rotated to the left again (Figure 6.17d). Finally, the flow discharges became comparable to each other, when the scour axis approximately bisected the scour angle (Figure 6.17f, $\theta_1' \approx \theta_2'$). As found in the experiment of Mosley (1976), the scour depth of the confluence increases with the angle of incidence θ where the upstream anabranches meet. The bed morphology of the confluence is related to a characteristic trough-shaped scour hole at the centre of the confluence.

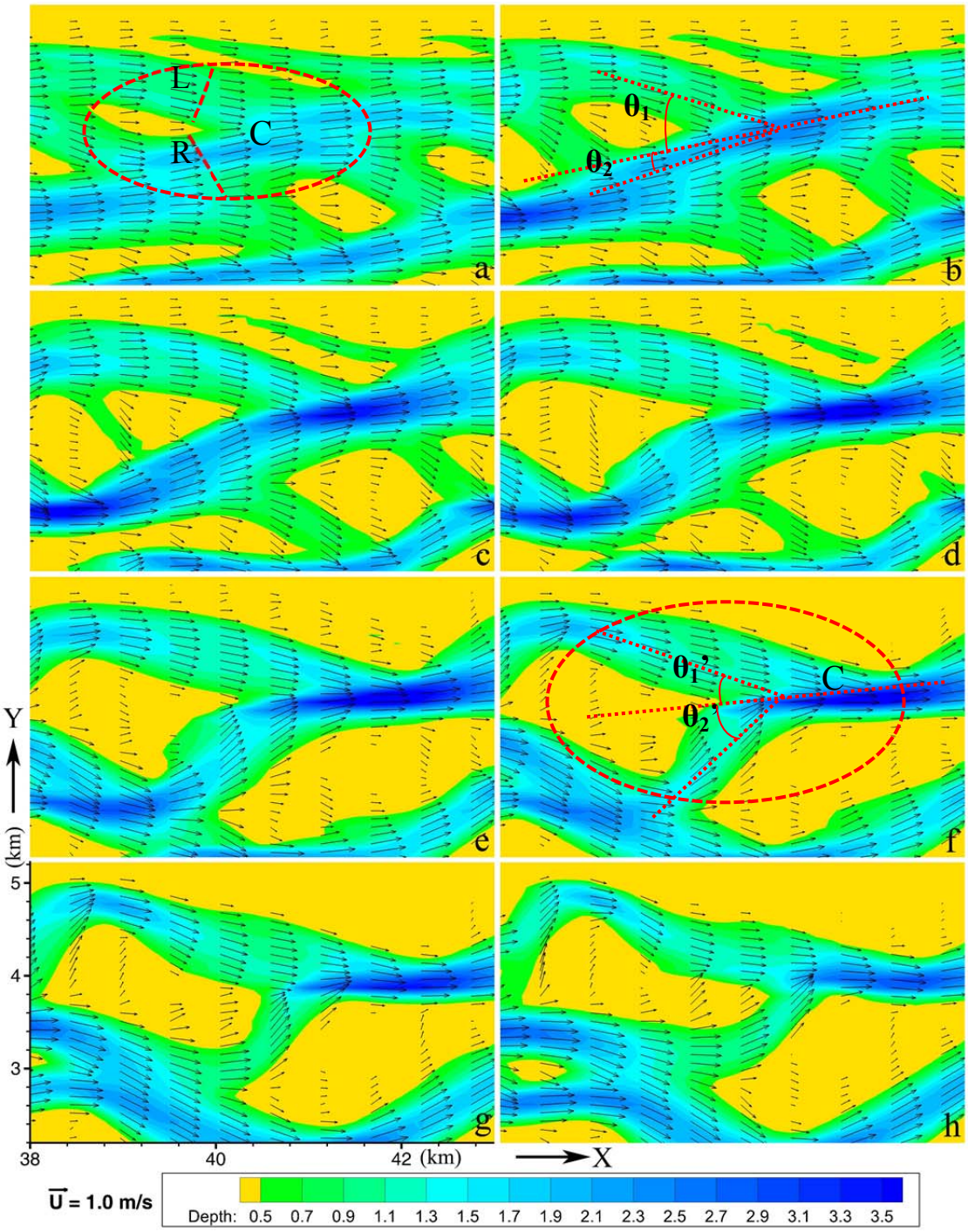

Figure 6.17 Water depth in the evolution process of confluence C (m): (a) 18; (b) 22; (c) 26; (d) 29; (e) 31; (f) 33; (g) 36; and (h) 39 (day).

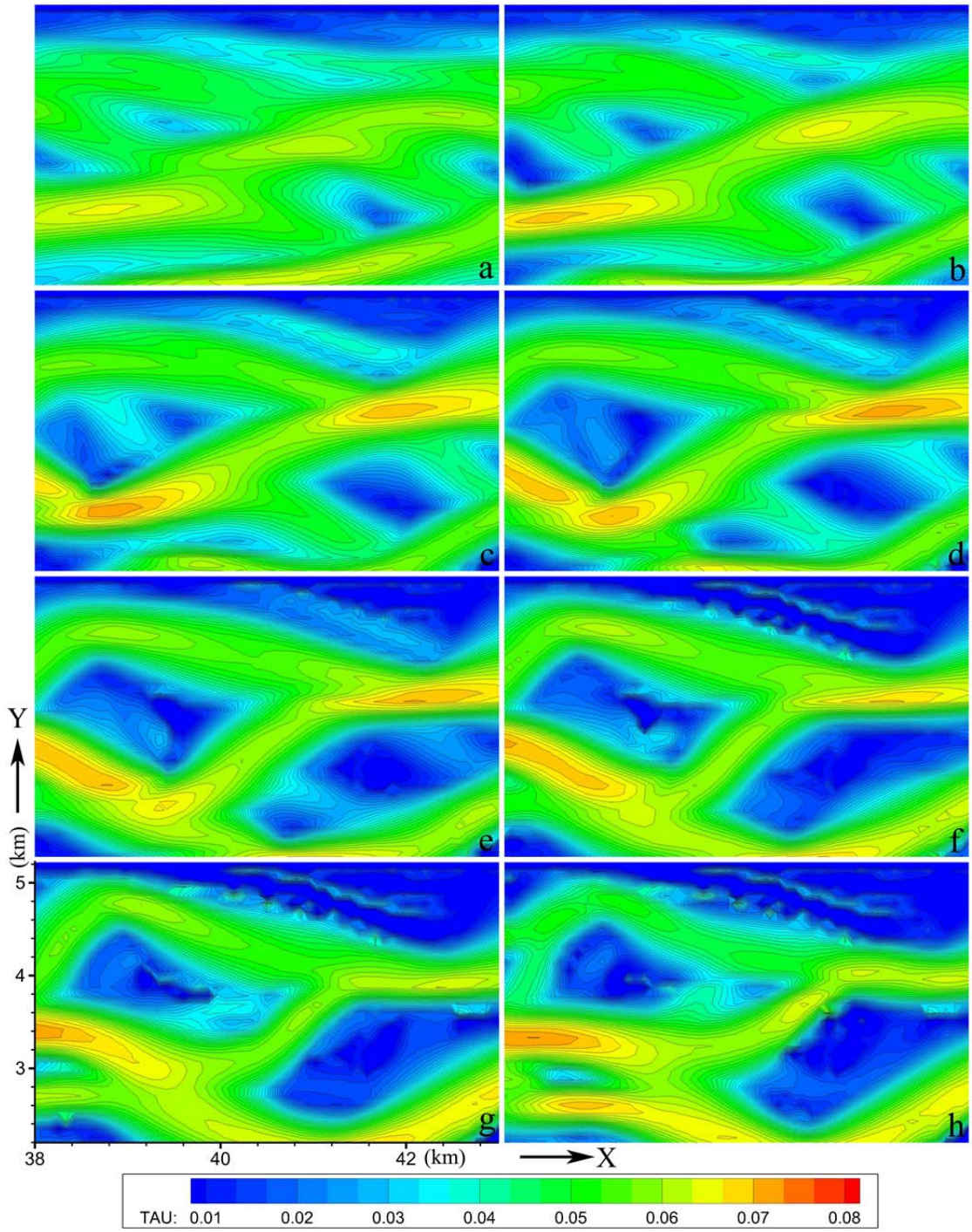

Figure 6.18 Shear stress in the evolution process of confluence C (N/m^2): (a) 18; (b) 22; (c) 26; (d) 29; (e) 31; (f) 33; (g) 36; and (h) 39 (day).

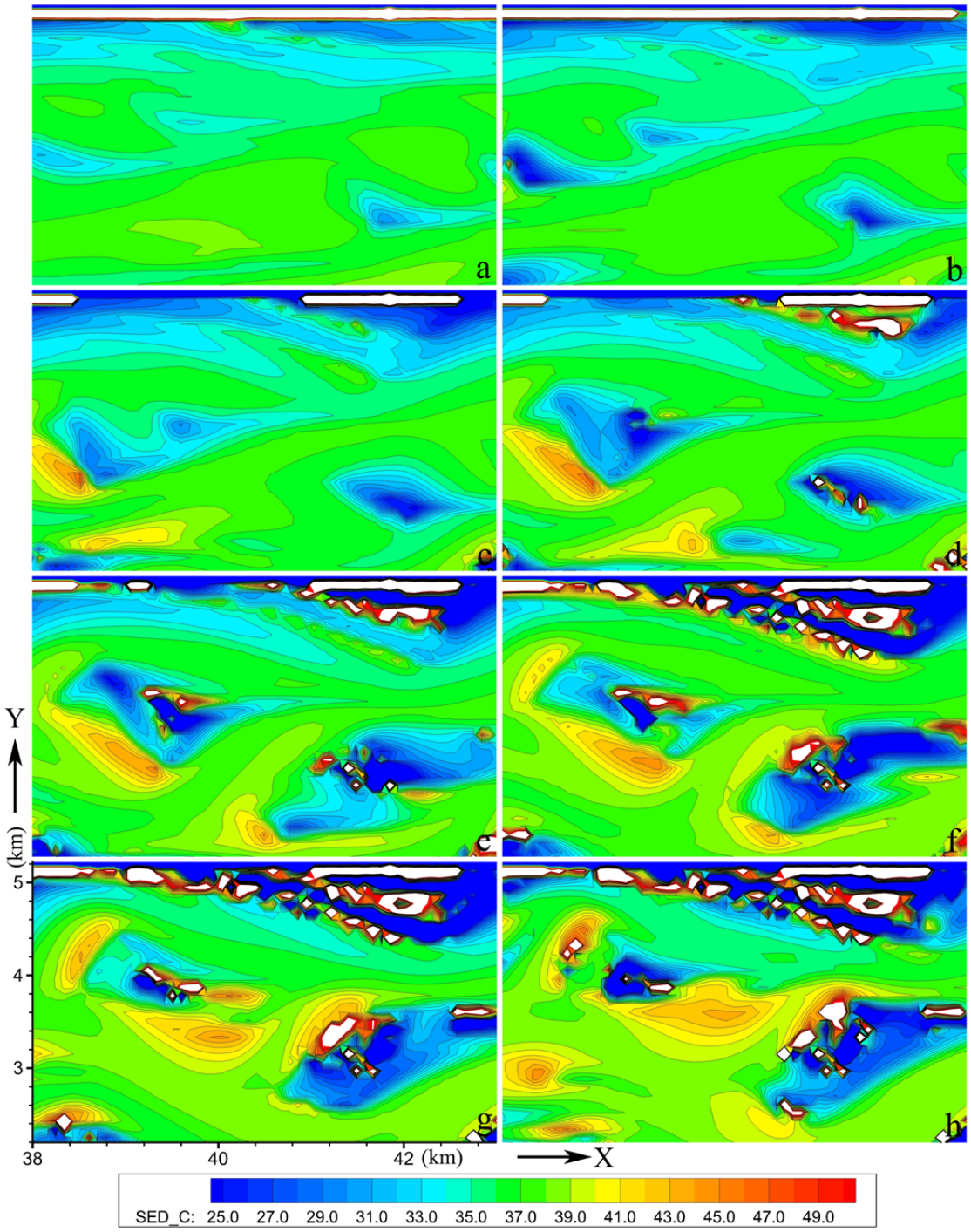

Figure 6.19 Seciment concentration in the evolution process of confluence C (kg/m^3): (a) 18; (b) 22; (c) 26; (d) 29; (e) 31; (f) 33; (g) 36; and (h) 39 (day).

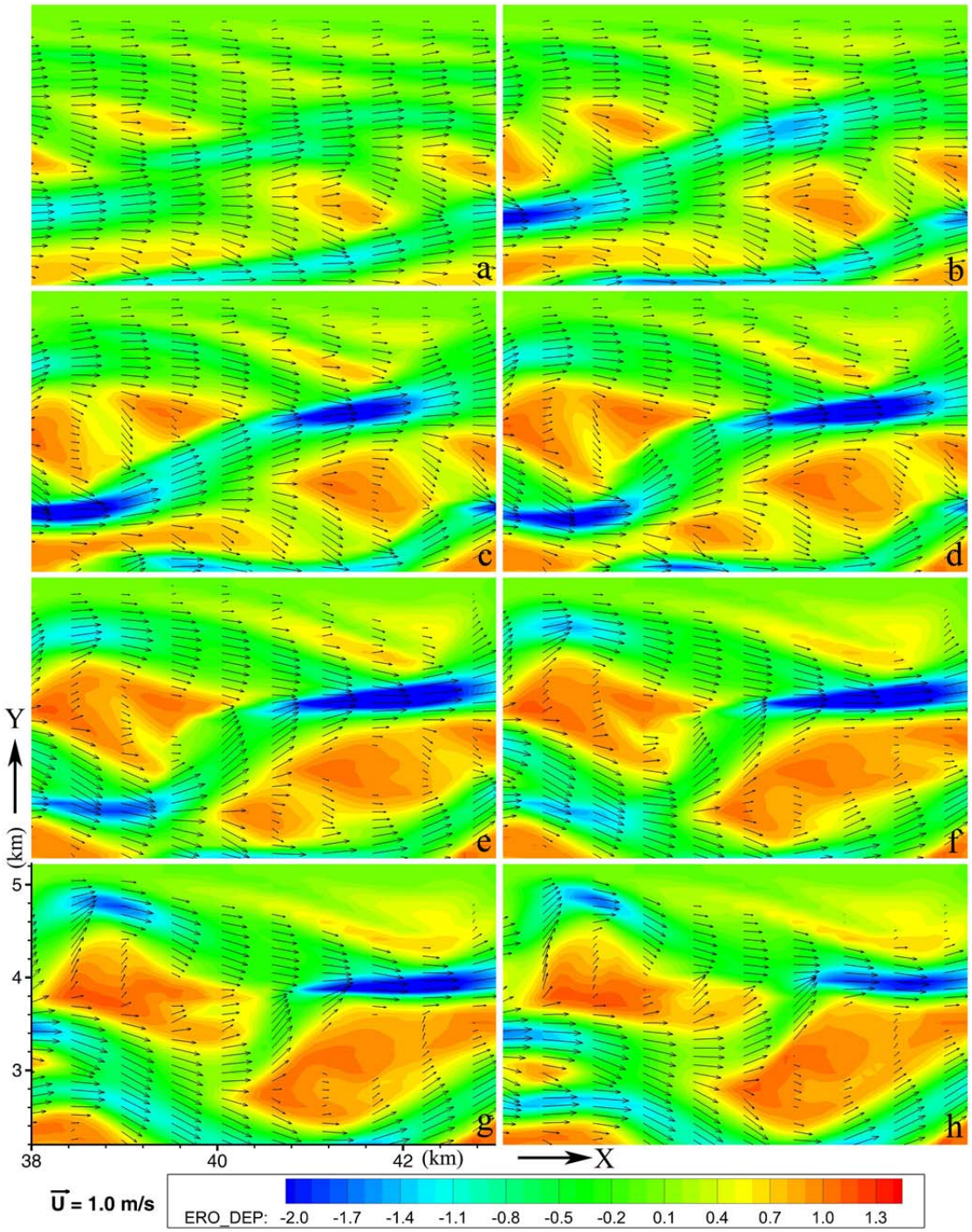

Figure 6.20 Erosion depth in the evolution process of confluence C (m): (a) 18; (b) 22; (c) 26; (d) 29; (e) 31; (f) 33; (g) 36; and (h) 39 (day).

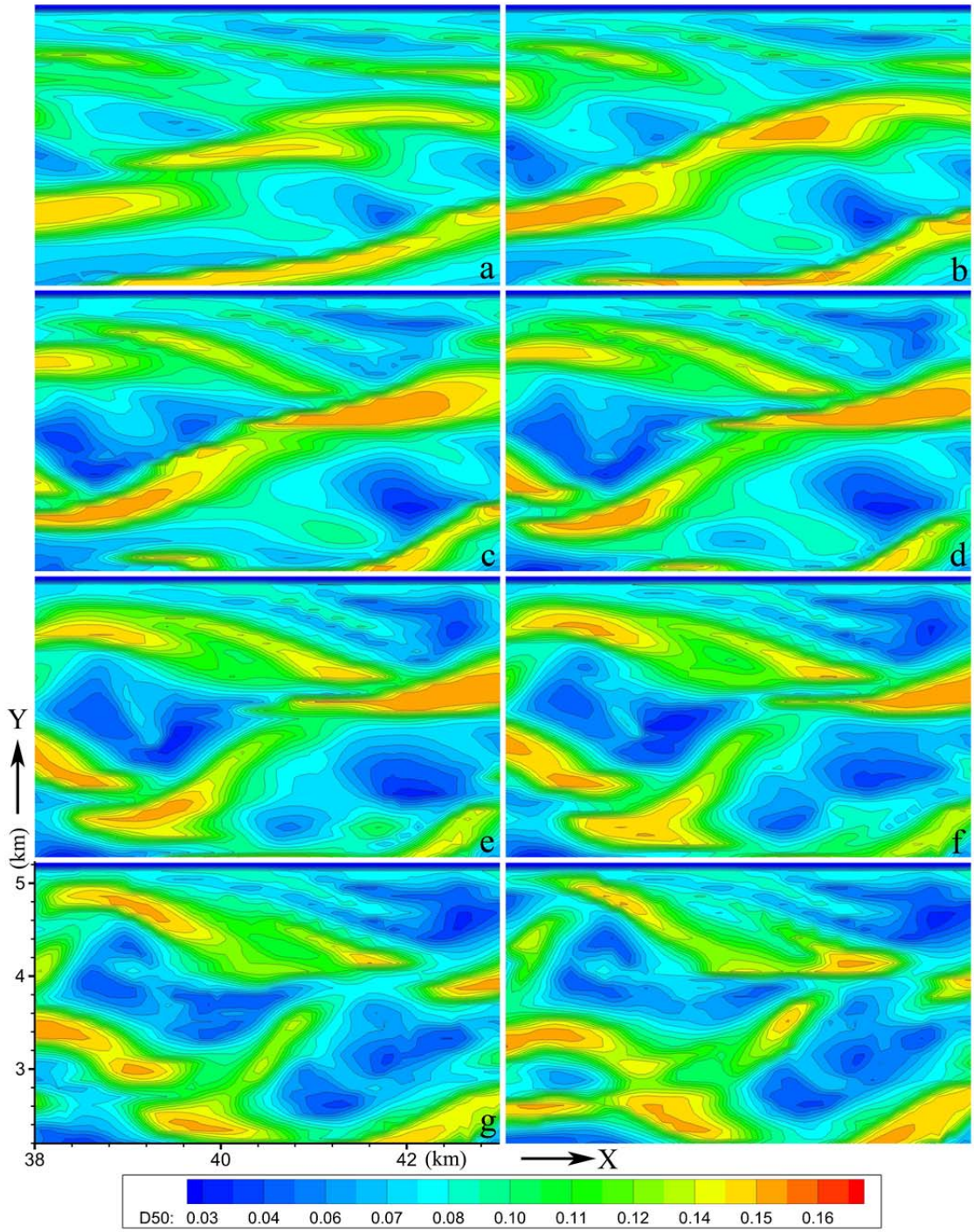

Figure 6.21 Sediment D_{50} distribution in bed in the evolution process of confluence C (mm): (a) 18; (b) 22; (c) 26; (d) 29; (e) 31; (f) 33; (g) 36; and (h) 39 (day).

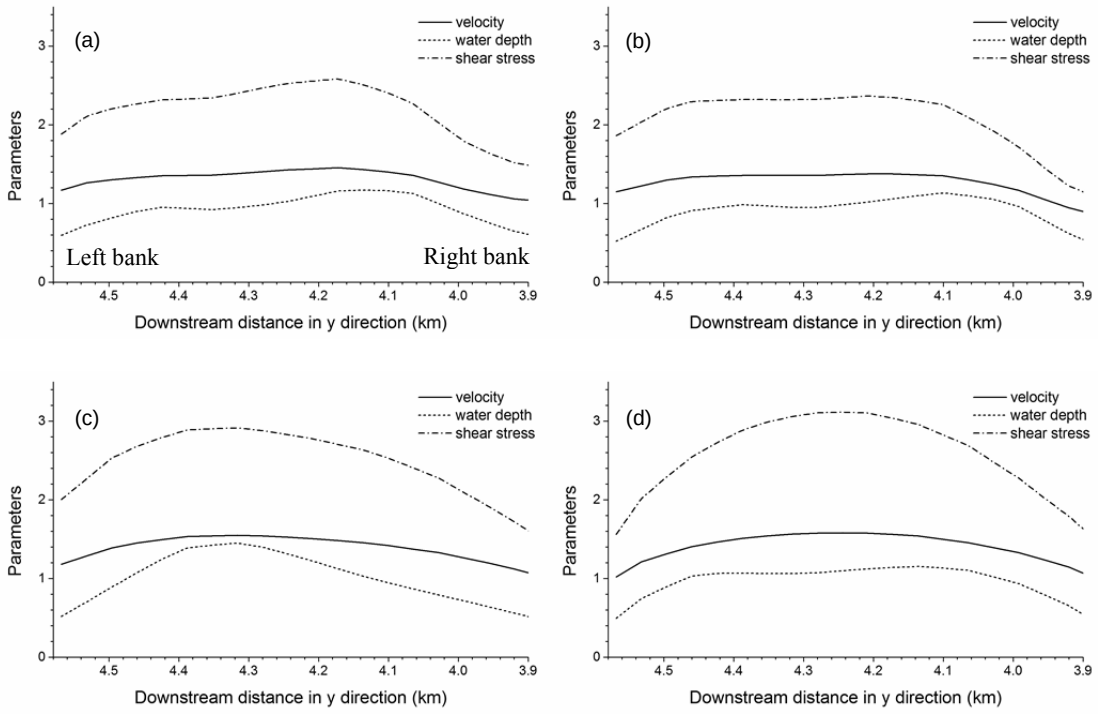

Figure 6.22 Spatial distributions of velocity (m/s), water depth (m) and shear stress (N/m^2) in the left tributary of confluence C: (a) 15; (b) 18; (c) 26; and (d) 33 (day).

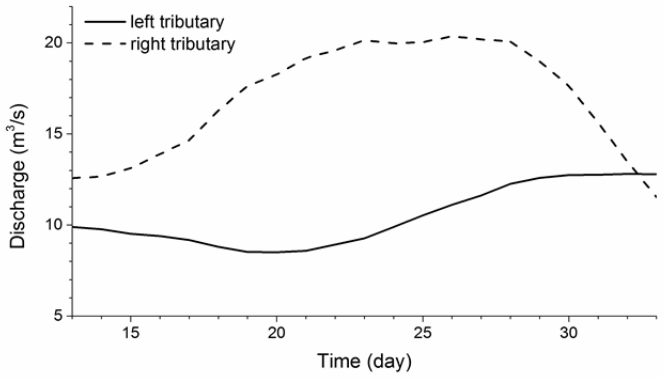

Figure 6.23 Discharge changes in the two tributaries of confluence C.

6.6.2 Bar

Figure 6.24 shows the formation process of a typical bar in the river. When the downstream pattern with pool-bar units formed bar D took its initial appearance. Then it grew by lateral and downstream accretion simultaneously, just as the growth of

many natural braided bars (Rice et al, 2009). The bar head was eroded and moved downstream obviously, while the bar tail moved downstream slightly and deposition occurred.

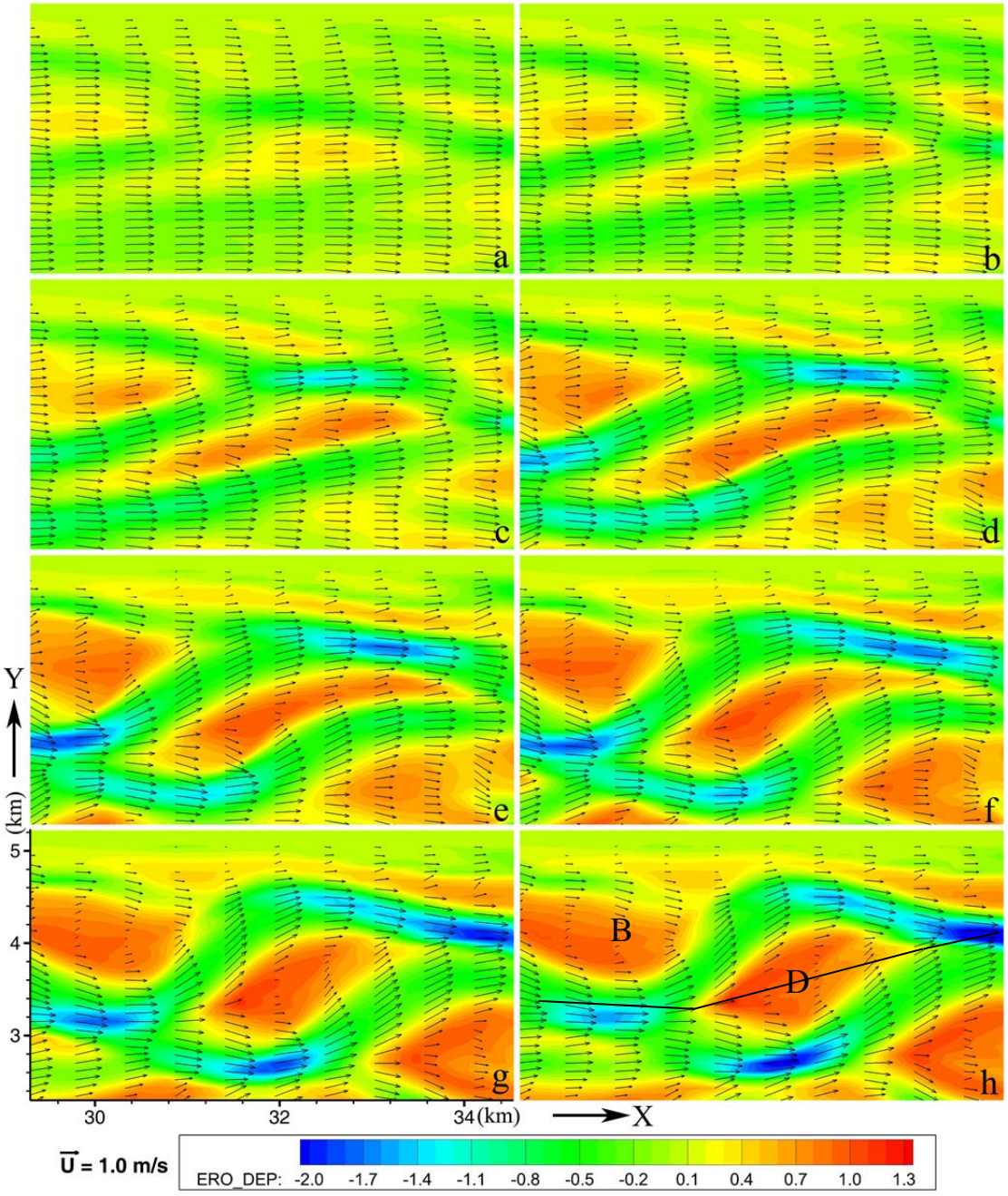

Figure 6.24 Erosion depth in the evolution process of bar D (m): (a) 13; (b) 16; (c) 19; (d) 22; (e) 25; (f) 28; (g) 31; and (h) 33 (day).

As channels migrated laterally and downstream, the deposits from different parts of the bar got vertically superimposed. For example, the bar-head deposits overlaid bar-tail deposits and upward bend deposits overlaid the downward bend deposits. Lateral accretion appears to be created by flow divergence and expansion at the bar head and inwardly moving flow and velocity reduction at the bar tail margins, just as observed by Ashworth et al. (2000). The bar shortened and broadened continuously, and took its final shape (Figure 6.24h). In a plain view of D_{50} distribution (Figure 6.25), it can be seen that the sediment tends to be coarser in the channels, especially in the pools, yet finer on the bars. Due to different flow directions, coarser sediment distributed in the downstream segment of the bend in the left tributary as also in the upstream segment of the bend in the right tributary.

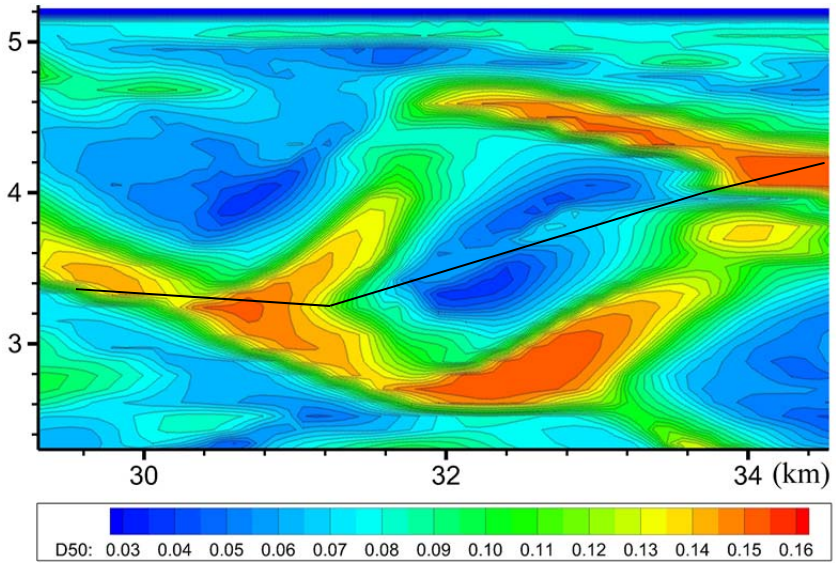

Figure 6.25 Sediment D_{50} distribution in bed on bar D and its surrounding areas by day 33 (mm).

During the growth of bar A, another bar (bar B in Figure 6.24h) developed on its

left upper course, too. Bar B grew horizontally with its right edge extending into the left tributary. Strong deposition occurred on the left bank of the channel. It deflected the flow and filled some part of the left tributary. Consequently, more discharge was directed into the right anabranch and progressive scour occurred in it. The right channel developed a deep thalweg with its riffle much lower than the left channel. The situation of the pools is different for the two channels, too. For the left channel, a small channel merged into it near the bend. The pool developed behind the bend, whose depth was not deep enough to see obviously. For the right channel, a deep pool developed just ahead of the anabranch bend. The relationship between discharge and orientation of tributaries indicated the two tributaries at a bifurcation might show similar orientation with those of a confluence discussed in Section 6.6.1.

A polyline was stretched across the pool-bar-pool unit (Figure 6.24h). The erosion depths of different times clearly showed the movement of the pool-bar unit (Figure 6.26). During these days, the bar head and tail moved downstream about 0.3 km and 0.1 km, respectively, with the bar shortened by 0.2 km. The upstream pool moved downstream yet deposition occurred. The bar head was eroded continually with a successive retreatment downstream. Meanwhile, deposition occurred at the downstream segment of the bar, generally behind the bar apex. The downstream pool was continuously eroded from –1.32 m to –2.31 m.

The flow velocity, erosion depth and sediment size distribution on the polyline are plotted in Figure 6.27. From the upstream pool to the bar, flow velocity decreased gradually to zero at the crown of the bar. Then it gradually increased to another high

value at the downstream pool. Flow at the bar head was faster than that at the bar tail. The faster flow at the bar head caused steeper slope in its upstream part. Sediment size variation shows similar trend with flow velocity. The sediment size (D_{50}) of the upstream pool, bar head, bar apex and bar tail are 0.15, 0.13, 0.08 and 0.07 mm respectively, showing that relatively coarse sediments were deposited on the bar head, whereas fine sediments were deposited on the tail. Periodic coarsening and fining of bed sediments occur along each side of the channel as the talweg swings around alternate bars. This phenomenon has been discussed by Ferguson (1993).

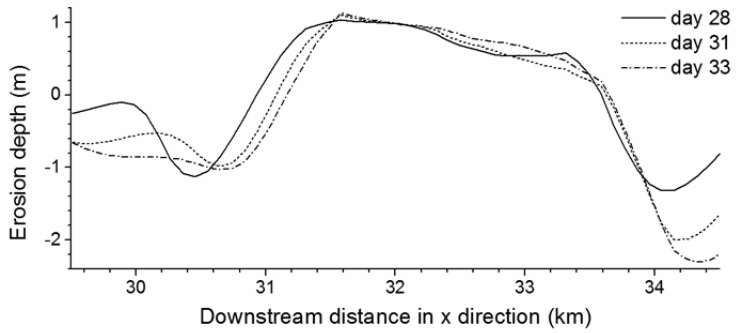

Figure 6.26 Morphologic variations along the line on bar D by day 33.

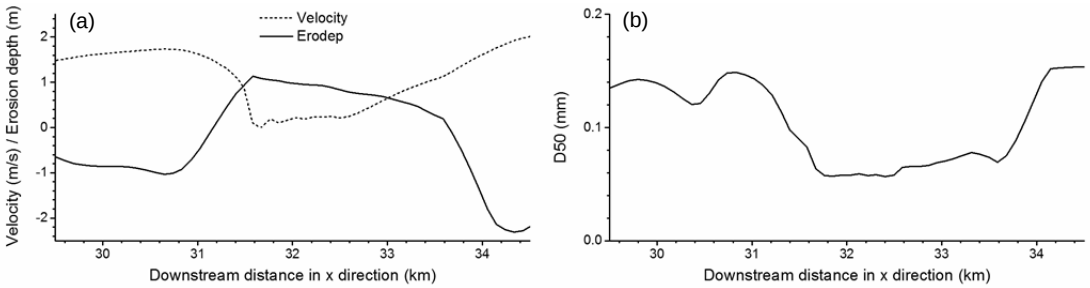

Figure 6.27 Time-lapse parameter changes along the line on bar D by day 33 (Figure 6.24h): (a) flow velocity and erosion depth; and (b) bed D_{50}.

6.7 Braiding Indices

In this study, three indices, including the average sinuosity, total sinuosity (P_T) and channel count index (BI_{T3}), were chosen to measure the degree of braiding. Statistical methods including the spatial space plots, transect topography, and bar parameters were also used to evaluate the essential braiding characteristics.

6.7.1 Average Sinuosity

In the current study, the average thalweg length/channel-belt axis length was chosen to calculate the average sinuosity of the modelled river (Figure 6.28). Two major channels in different evolution periods, with their velocity and depth values being generally larger than other channels (highlighted in dotted lines), were used for river sinuosity analysis. The thalwegs of the channels on days 23 and 33 are portrayed by dotted lines in Figure 6.28. The reaches were chosen in a 40-km long section of the river beginning from 10 km downstream of the entrance to minimise the influence of the upstream perturbation. The average sinuosity values on days 23 and 33 were found to be 1.077 and 1.095, respectively. Existing studies indicate that nearly all of natural braided rivers have sinuosity values below 1.3. In many cases, this value is treated as the criterion that distinguishes a braided river from a meandering river.

The trend of average sinuosity illustrates the evolution process of river channels. Braiding began with alternating chutes and lobes distributed in the upstream reach. Chutes connected with each other and formed initial channels with low sinuosity. As the river morphology developed, these channels were becoming more sinuous. The

lower sinuosity on day 23 compared with day 33 illustrates this trend. By day 33, the river was fully developed with high sinuosity. The relatively lower sinuosity than natural rivers might be related to the easily erosional bed layers. Rust (1978) used a mean sinuosity of 1.5 to separate 'low-sinuosity' rivers from 'high-sinuosity' rivers. Therefore, the modelled river belongs to the low-sinuosity category.

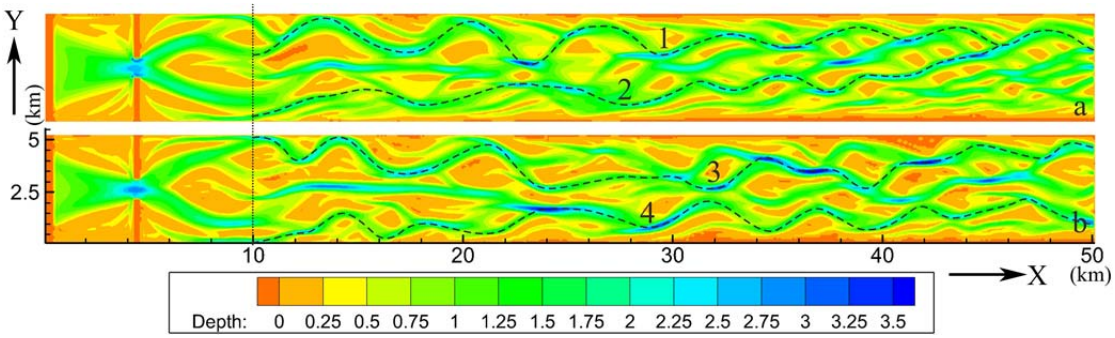

Figure 6.28 Channels for average sinuosity analysis calculation (water depth, m): (a) 23; (b) 33 (day).

6.7.2 Total Sinuosity

Based on the definition of Hong and Davis (1979) and Ashmore and Sauks (2006) for total sinuosity and effective channel width, the average wetted width of the modelled river was found to be 0.648 km. According to the method of Hong and Davis (1979), thirty cross-sections with the average wetted width as an interval were used to calculate the total sinuosity (Figure 6.29). As seen in Figure 6.30, the coefficient of variation decreases from over 50% to less than 10% as the sampled reach length increases from two times the AWW to over twelve times. The total sinuosity of the modelled river is 4.65 with all major and minor channels included (Figure 6.30).

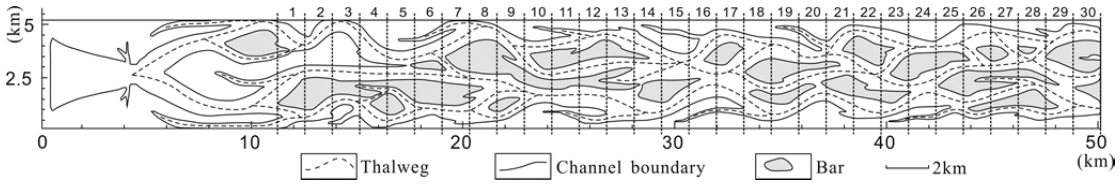

Figure 6.29 Cross-sections by per average wetted width in the river.

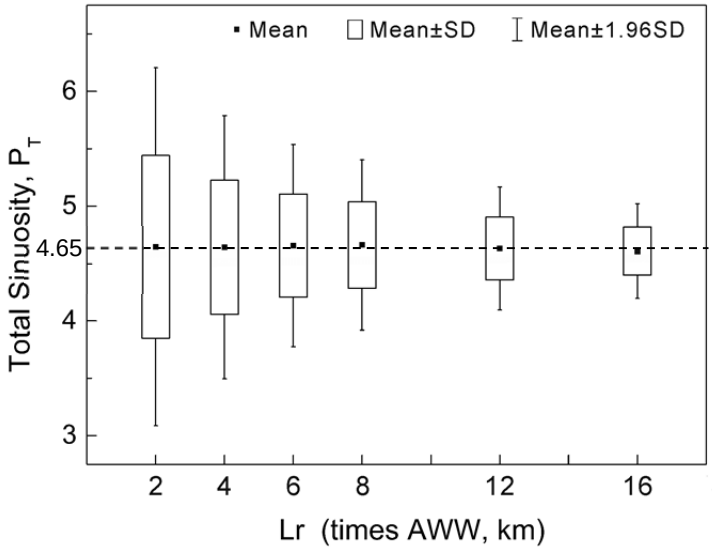

Figure 6.30 Mean and standard deviations of total sinuosity (P_T).

6.7.3 Channel Count Index

Howard et al. (1970) and Hong and Davis (1979) proposed two related channel count indices, including the mean number of links intersected by a number of cross-sections and the total number of links in the measured reach. To study changes of braids in different river segments, the total number of links in certain distances was studied. Twenty-two cross-sections (from 10 to 49.5 km) with a 1.8 km interval were used to calculate the link number (Figure 6.31). Generally, the link number changes can be divided into three segments. In the upstream segment (10 to 25 km), the

number of braids varies from 1 to 3. In the middle stream (25 to 37 km), the total braids fluctuate widely from 0 to 5, containing the smallest value and largest value in the river flume, respectively. In the downstream reach (37 to 49.5 km), the number of braids nearly remains stable.

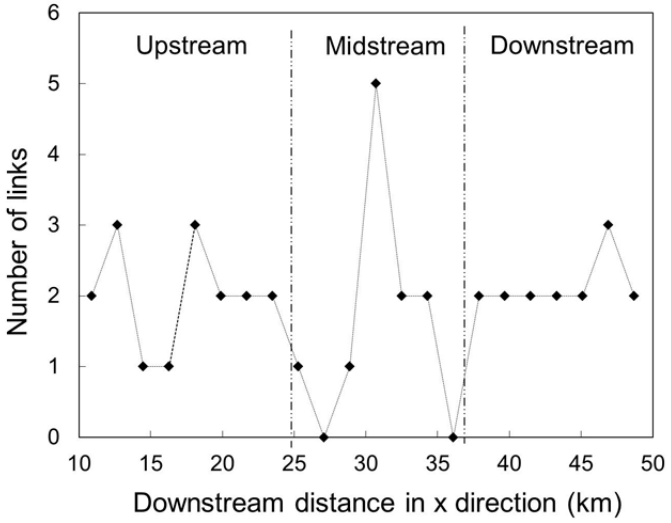

Figure 6.31 Braid numbers in 22 cross-sections along the river.

These variations in different river segments suggest different conditions along the river flume. In the upstream segment, significant differences in hydraulic conditions exist due to the influence of the two spurs, with frequent changing numbers of links produced. Simultaneously, a few small channels form and join in several major channels in this segment. They play an important role in determining the total number of links. In the midstream segment, the link number frequently changes, and the river is less influenced by the spurs. Thus, it develops more freely. The small channels are no longer important. Instead, braids are mostly from confluences and bifurcations in continual channels. River confluences and bifurcations appear

heterogeneously with both high density and low density. In the downstream segment, the averaged distribution of alternating confluences and bifurcations generated nearly uniform braid links.

6.8 Braiding Characteristics

6.8.1 State-space Plots

In the present study, the total widths (sum of the width of all the channels in a cross-section) were measured to parameterise the geometry of the modelled braided river. By plotting the current total width versus that of the preceding section, both normalised by the overall average width, state-space plots were constructed. Clusters of loops can be seen in the plots for days 18 and 33 (Figures 6.32a and b). Three parts exist in the plot of day 18, with one thick area in the middle and two sparse ones on each side, which is similar to the plots for natural and laboratory rivers (e.g. Murray and Paola, 1996; Sapozhnikov et al., 1998). These sequential circle lines present the spatial geometry pattern in real braided rivers: a narrow and deep channel is often followed by sedimentation zones in which wide shallow flows and bars occur (Ashmore, 1991b). The downstream changes in geometry reflect the downstream convergence and divergence of flow that are believed to drive erosion and redeposition, respectively, in braided streams (Murray and Paola, 1994, 1996).

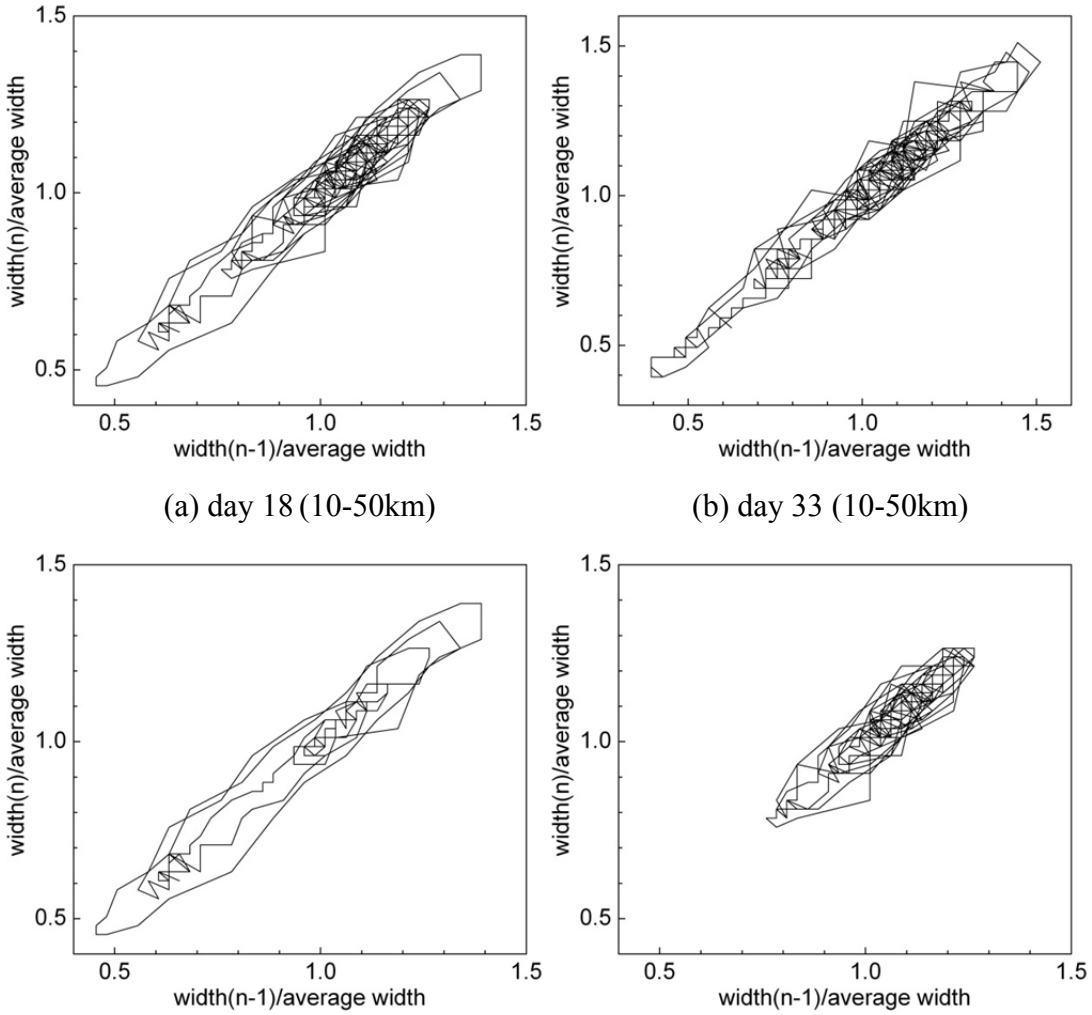

(a) day 18 (10-50km) (b) day 33 (10-50km)

(c) day 18 in upstream reach (10-25km) (d) day 18 in downstream reach

Figure 6.32 State-space plots of channel widths normalised by the average channel width for days 18 and 33.

Nevertheless, the space plots contain some crossing lines (Figures 6.32a and b). These lines were also found in plots by Sapozhnikov et al. (1998), and they were considered to indicate some stochastic behaviour of the river. Nonetheless, the plots still demonstrate the downstream influences for the spatial series of widths. The day 18 plot appears to contain more wide loops than that of day 33, which might result from the abundance of channels in different evolution stages. In the early stage, many

channels distributed in the flume, and as the river developed, some of them merged into each other to form a few major channels. Moreover, the plots of the upstream and downstream reaches also displayed some differences (Figures 6.32c and d). With the data of channel widths, a few long stretched loops were formed in the upstream reach, whereas in the midstream and downstream reaches, more and shorter loops developed as a result of the longer erosion-deposition length in the upstream reach.

The state-space approach can be extended to assess organisation in the river topography, with the total widths replaced by the sequential scour depths at channel confluences or the height of successive bars (Doeschl et al., 2006). Plots of scour depths for days 18 and 33 were constructed (Figure 6.33). Data are from maximum scour depth at confluences of sequential cross-sections and normalised to the average scour depth for the reach measured. As the maximum scour depth often occurred in sequential channel confluences in the modelled river, its value in each cross-section was chosen for state-space plotting. In contrast to the river width results, Figure 6.33 show well-looped plots. The smoothly stretched long loops indicate the deterministic downstream effect of scour depth in the modelled river. The scour data used for state plotting were compared with the river geometry in Figure 6.34a. Considering the main pool-bar units in the river, mostly one pool-bar unit includes one or two loops. Deep scour depths occurred in the scours of the bifurcation areas and confluences. If it was not connected with other neighbourhood channels, one loop formed. Otherwise, two or more loops might form. The length and width of the loop was mainly related to the length of bar major axis. These circles can demonstrate the periodical morphologic

changes in the river, with one or two loops representing one erosion-deposition cycle. Some typical loops (1 and 2 in Figure 6.34b) were chosen to illustrate the relationship of the state-space plots and channel geometry in Figure 6.34a. Take loop 2 as an example. The high value of the state plot occurred at the bend of a bar, which is located at the bifurcation area of two tributaries. The low value occurred in the middle of the two neighbourhood bifurcation areas and confluence in the pool-bar unit.

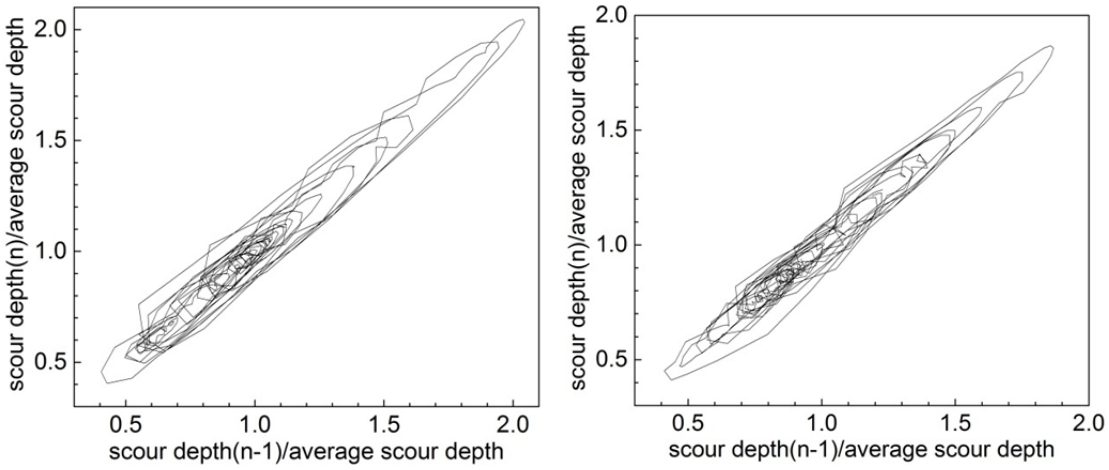

(a) day 18 (b) day 33

Figure 6.33 State-space plots of maximum scour depths normalised by the average maximum scour depth for days 18 and 33 in the reach of 10–50 km.

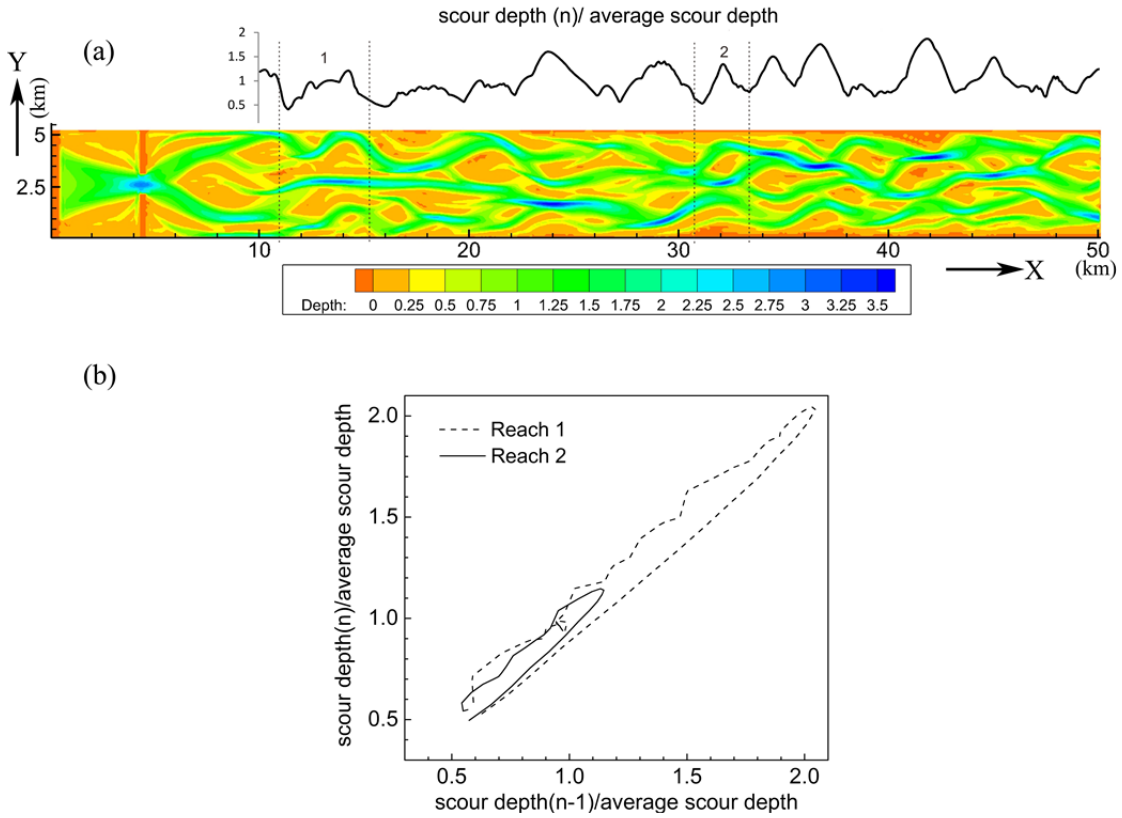

Figure 6.34 Periodical scour depths in the modelled river on day 33: (a) scour depths relating to channel geometry; and (b) typical loops in the reaches of 1 and 2.

6.8.2 Transect Topography

Some useful topography characteristics can be described directly by cross-section surveys, such as the transect topography and cumulative frequency of the link length and lateral slopes (Doeschl et al., 2006). They can be applied to assess the similarity between real rivers and modelled rivers. Several cross-sections of the river on day 33 were chosen to study the transect topography and two representative ones are shown in Figure 6.35. It can be seen that the deposition areas above the elevation median (the dotted line in Figure 6.35) are relatively wide and flat. In contrast, the areas mostly with erosion, which are below the elevation median, were relatively narrow and deep. The maximum scour depth of channels exceeds the

maximum deposition height of bars. Therefore, steep and narrow banks form in erosion areas, compared with the gentle and wide slips in deposition areas. However, the transects of the cellular modelled topographies do not share the same properties, with many cross-sections characterised by the coexistence of sharp peaks above and below the elevation median (Doeschl et al., 2006).

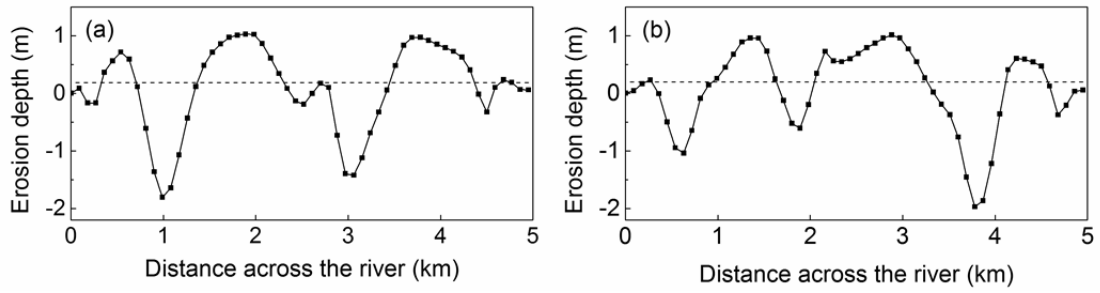

Figure 6.35 Deviations from the elevation median for cross-sections on day 33: (a) 30 km and (b) 35 km.

Note: Positive erosion depths are for deposition and negative values for erosion. The dotted line represents the deposition median.

The frequency distribution curves of cross-sectional slopes in the reach of 10–50 k m are shown in Figure 6.36, containing the data of more than 400 cross-sections. The deposition areas were mostly distributed on the curve with erosion depth above the median depth (dotted line). Yet the areas with erosion were all located on the curve with erosion depth below the median depth. The steep trends near zero slope compared with the gentle changes deviated from it illustrate the minority of comparatively steep areas. The curves corresponding to deposition areas with elevation higher than the median are significantly wider than those correlated with

erosion areas. Consequently, more of the deposition areas exhibit gentler elevation changes than erosion areas, which have also been illustrated in Figure 6.35.

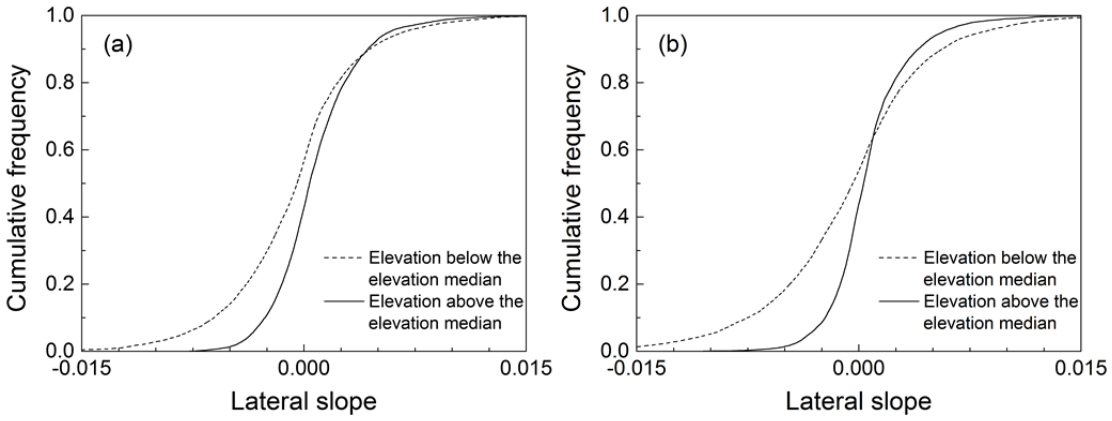

Figure 6.36 Cumulative distributions of lateral slopes for areas above the elevation median and for areas below the elevation median on days (a) 33 and (b) 66.

The gentle deposition areas and steep channels formed in certain hydraulic conditions. The modelled braided river developed mainly through deposition due to overloaded sediment concentration. The frequent channel shifting indicates that the river was in a very unstable status. In the areas with erosion, the flow was mainly faster and deeper than the areas with deposition. Except for the energy consumed by the sediments in transport, in channel areas, the flow energy was large enough for the sediments to erode the channel bed and take more sediments away. In contrast, in shallow areas with deposition, the flow energy was incapable of maintaining all the sediments in suspension, and consequently, deposition occurred. The energetic erosion activity in channels generated steeper sides, yet the opposite situation occurred in deposition areas.

6.8.3 Bar Scaling

Figure 6.37 shows the river planform geometry on day 33 with multiple intersecting channels and bars. Some key parameters of 18 bars, including major axis (B_x), minor axis (B_y), perimeter (B_p) and area (B_a), were collected and are shown in Table 6.2. Bars 6 to 18 were used in the correlation analysis, whereas the others (number 1 to 5) were excluded to avoid the influence of the upstream perturbation. Figure 6.38 illustrates the cross-plots of these parameters. Bar area and perimeter correlates strongly ($R^2 = 0.91$), with their regression relationship $B_p = 5.129B_a^{0.693}$. The high correlation between the area and parameter is a typical feature of objects that possess the same basic shape characteristics, particularly fractal or self-similar objects. The bar major axis correlates very strongly ($R^2 = 0.98$) with the perimeter, with a regression relationship of $B_p = 2.225B_x^{1.020}$. The bar major axis also correlates strongly ($R^2 = 0.91$) with bar area, with a regression relationship of $B_a = 0.342B_x^{1.346}$. Relatively, the bar minor axis does not correlate as well ($R^2 = 0.58$) with the perimeter yet relatively well ($R^2 = 0.8$) with the bar area, with a regression relationship of $B_a = 2.081B_y^{1.786}$. Except for the chart of the major axis-area, in all the other charts, bars 7 and 15 are the points farthest away from the best fitted line. Their different shapes from other bars can also be seen in Figure 6.37. They are longer with irregular edges compared with the other bars.

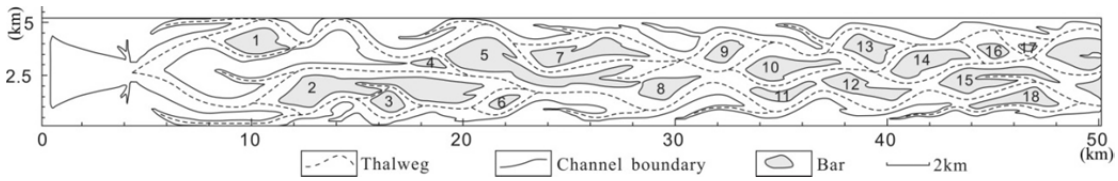

Figure 6.37 Bars in the modelled braided river on day 33.

Table 6.2 Characteristic parameters of the bars

No.	Major Axis(km)	Minor Axis(km)	Perimeter (km)	Area (km^2)	No.	Length (km)	Minor Axis(km)	Perimeter (km)	Area (km^2)
1	3.09	1.23	7.13	2.26	10	4.48	1.17	9.72	2.55
2	9.70	1.50	24.39	7.59	11	3.14	0.54	6.84	1.24
3	1.64	0.97	3.97	1.04	12	4.26	0.90	9.36	2.26
4	1.69	0.40	3.62	0.48	13	2.44	1.03	6.03	1.72
5	9.29	1.62	24.55	6.76	14	3.81	1.14	8.34	2.63
6	1.53	0.51	3.38	0.54	15	5.71	1.20	16.11	3.15
7	5.62	0.88	12.63	3.22	16	1.53	0.71	3.50	0.70
8	3.03	1.07	6.69	1.83	17	0.90	0.31	2.04	0.20
9	1.93	0.91	4.45	1.13	18	4.24	0.82	8.99	1.83

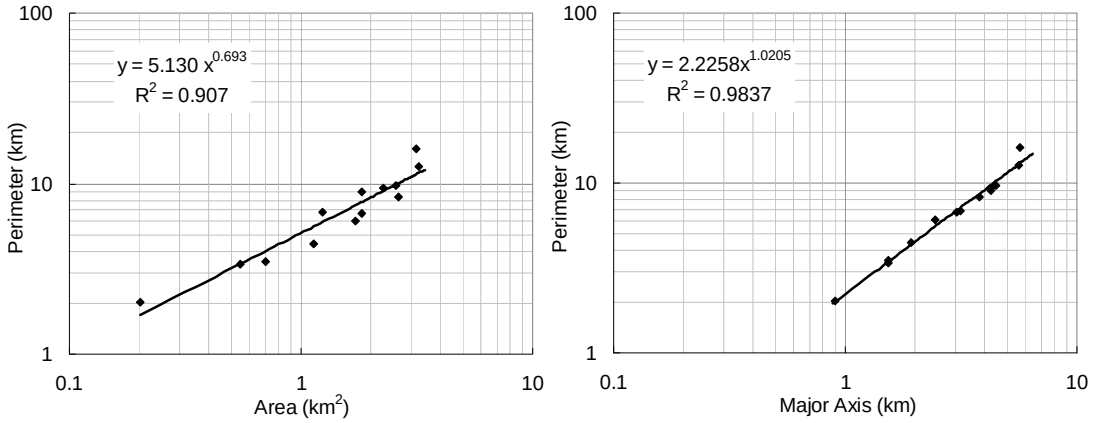

(a) (b)

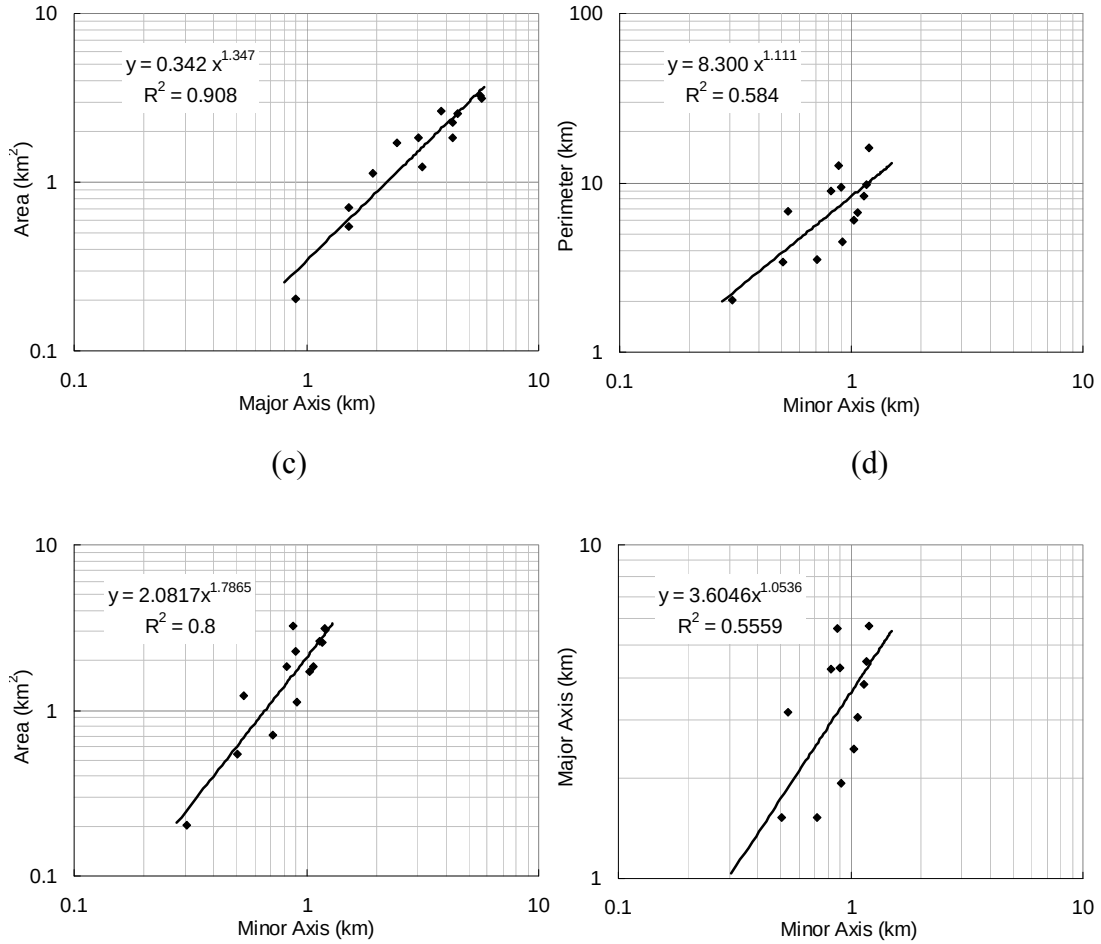

Figure 6.38 Correlation plots of parameters of 13 bars in modelled river.

The existence of scaling denotes that the sediment transport mechanisms tend to generate regular shapes and well-defined length scales. The regular braided pattern with channels and bars in our results exhibits scaling characteristics. Moreover, in a quantitative way, the high regression relationships of the area-major axis and perimeter-major axis and the relatively good regression relationships of area-minor axis and perimeter-minor axis also illustrate the existence of scaling in the modelled river. The better relationships of the major axis to area and perimeter than the minor axis may indicate that downstream growth plays a more important role than lateral

accretion in the development of bars. Rosatti (2002) analysed perimeter-area scaling and found a relationship of $P \sim A^{0.616}$ in a laboratory river. Similar to his result, a relationship of $P \sim A^{0.693}$ was found in the current modelled river. The bar major axis displays some correlation with the minor axis ($R^2 = 0.56$), yet the correlation factor is not as high as the result of Kelly (2006) ($R^2 = 0.96$). The higher coefficient in our result indicates the controlling effect of downstream accretion to bars is stronger than it is in the sample rivers of Kelly (2006). Although some limitations exist in the current analysis in that the sample size of bars is just 13, which is far from sufficient, but the high correlation factors still demonstrate the scaling characteristics. A further study on the scaling properties in the modelled river using another method will be discussed in the next section.

6.9 Model Sensitivity

To test the model sensitivity to different resolutions and the effects of Coriolis force and spur, cases with cell sizes of 45*45 m^2, 60*60 m^2, 90*90 m^2 with spurs and 90*90 m^2 without spurs have been developed (Figure 6.39). The river with a cell size of 60*60 m^2 generates more constrained channels than those of 90*90 m^2. However, as to the rivers with cell sizes from 60*60 m^2 to 45*45 m^2, it is hard to recognise the differences in their channel amounts and widths. They show similar channel pattern with each other. Compared with the river analysed in the previous part (Figure 6.3) with the consideration of the Coriolis force, the river which ignores it shows a more symmetrical pattern. The nonsymmetry might also partly result in the numerical error

caused by the numerical solution method. Without spurs, the model still produces braided pattern (Figures 6.39d and e), though it develops slower, with its channel pattern of day 33 similar to that of day 20 in the case with spurs.

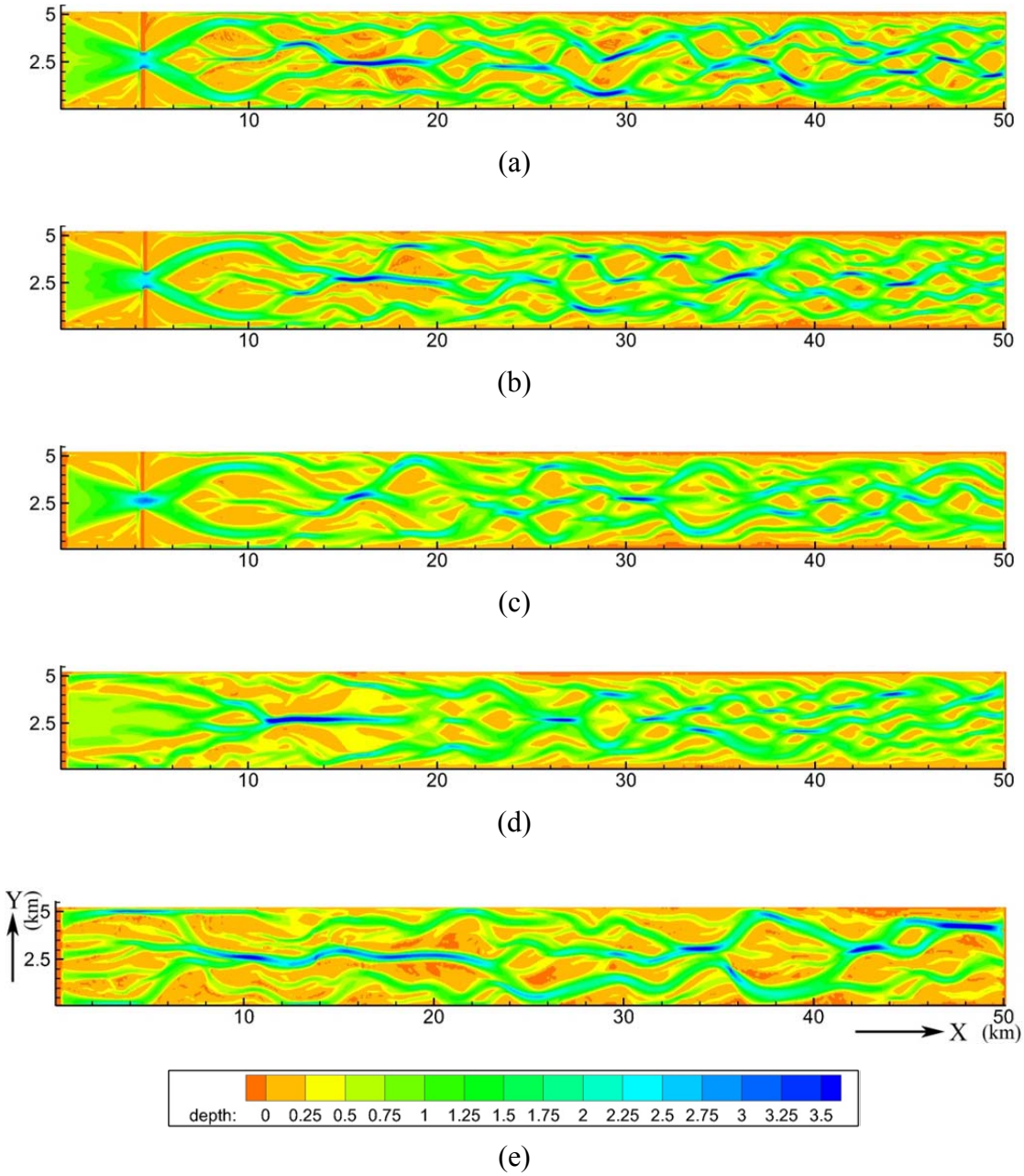

Figure 6.39 River planform for different resolutions without Coriolis force (water depth/m): (a)–(c) 45*45 m^2, 60*60 m^2, 90*90 m^2 with spurs on day 33, respectively; (d) and (e) 90*90 m^2 without spurs on days 33 and 66, respectively.

6.10 Comparisons among Predicted and Natural Rivers

Comparison between the two predicted rivers

Rivers with bed load and suspended load have been simulated respectively. They show differences yet share some common characteristics with each other. Both of the rivers generated their braiding from alternating pool-bar units, but fewer pairs existed in the river with bed load. The river with bed load presented a main channel for most simulation time except its late stage after discharge increased. Yet the river with suspended load did not show a main channel during most of its evolution process. For the river with bed load, bank erosion with secondary flow is essential for the generation of braiding. Without these two effects, no braiding occurs. However, for the river with suspended load, these two effects are not included in the model, yet typical braiding pattern has still been generated, in which overloaded sediments play an essential role.

The morphologic units in the two rivers present some differences. In the river with suspended load, the scour depths at confluences increased with the scour angle and decreased as the discharge concentrated in one of the anabranches; the flow around the bar showed similar flow field with natural rivers, and so was the sediment size distribution at the bar head and tail. Yet in the river with bed load, the bank of the bed load river was coarse than the channel, which has been observed in some experiments (Dietrich et al., 1989).

Braiding mechanisms of these two rivers share similarities and differences. First, the avulsion by annexation relating to the reoccupation of an abandoned channel was

found in the bed load river yet was not found in the suspended load river. Second, there was some difference in their evolution of choking avulsion. In the river with bed load, the tributary was quickly choked at the bifurcation area, yet most part of the channel was still there which was abandoned with no water flowing. On the contrary, in the river with bed load, the tributary in choking avulsion was totally flattened in the end of the avulsion. Third, in the river with bed load, the spray of flow could be recognised easily in the process of constriction avulsion, whereas in the river with suspended load it is hard to distinguish this boundary.

The rivers possess some statistical characteristics in their braided pattern. In the analysis of state-space plots, it is true for both the rivers that erosion depth is a better parameter than channel width in representing the state changes. Both of the modelled rivers present some spatial scaling characteristics, yet still show some differences in scaling activities.

Comparison with natural rivers

In the river evolution processes seen from the model, some phenomena similar to natural rivers deserve our attention: 1) The initiation of braided pattern occurred with the development of chute channels across alternating point bars, which is similar with the observation in a gravel river studied by Ashmore (1991a). 2) The orientation of the confluence is mainly controlled by the direction of the main channel, and the scour depth of the confluence increases with the angle of incidence θ, as found in previous studies (Ashmore, 1993; Mosley 1976). 3) The bar grows by lateral and downstream accretion simultaneously, just as the growth of many natural braided bars (Best et al.,

2003; Bridge and Lunt, 2006; Burge, 2006; Rice et al, 2009). 4) Both of the two channels around the bar have a net outward flow in the upstream segments of the bends and an inward flow in the downstream segments, similar to the previous study of Bridge (1993). 5) The internal sorting of sediments presents a tendency for coarse material to accumulate at the bar head and finer material to be concentrated near the centre.

Some phenomena in natural rivers were not observed in the present model, such as the central bar deposition, chute cutoff and typical bar dissection. It is hard for a central bar deposition to occur in the river with bed load, because mostly, the sediment transport rate was larger at the centre of the channel than the bank areas. An upstream flow cutting the point bar is necessary for the occurrence of chute cutoff, which is not easy to occur in the modelled river.

6.11 Discussion of Model Simulation Ability

The results from the present study show the potential for the physics-based model to simulate the morphodynamic processes and braiding characteristics in braided rivers. The sensitivity assessment illustrates that the braiding is independent of the upstream perturbance applied in the cellular model (Murray and Paola, 1994) and grid resolution as if the grid size has decreased to some value (Kelly, 2006). Typical braided pattern and morphologic elements are exhibited in the braiding evolution process of the modelled river.

Compared with cellular model, our physics-based model presents the hydraulic and morphodynamic processes better. In cellular model (Jerolmack and Paola, 2007), most morphologic changes are concerned with nearly one or two cells. It is hard for them to represent the hydrodynamic and morphodynamic conditions during in processes such as avulsion. Moreover, some white-noise elevation perturbations may be necessary for cellular model to produce a braiding (Murray and Paola, 1997). Nonetheless, our model can produce braiding without any perturbations. For cellular models, redeposition is essential for braiding generation. In the present model, deposition is the main cause of braiding in the river with suspended load. But for the river with bed load, bank erosion is more important for braiding generation.

The transect topography and frequency analyses have been applied to assess the modelling ability of cellular models by Doeschl et al. (2006). Compared with natural and laboratory rivers, the results produced by cellular models indicate different transect topography with the coexistence of sharp peaks above and below the elevation median. Nonetheless, in the present study, the bar areas usually developed wide and flat sides compared with the narrow and steep sides in the channel areas, with the maximum scour depth exceeding the maximum deposition height, which is similar to natural rivers. Moreover, the lateral bed slopes in cellular models indicated that they corresponding to areas above the median assume extreme values with a similar frequency as those corresponding to elevations below the median. Different from the cellular model, the present modelled river displayed wider distribution in deposition areas yet was narrower in erosion areas, which is more like real rivers. In

this case, the present river appears to represent real river morphology better than cellular models.

A typical braided river is characterised by the intertwining effect of a braid presented by the repeated division and joining of channels with bars between them (Bridge, 1993). This may result in the fact that the geometry of the flow at one point affects the geometry downstream. In the modelled rivers, the sequential plots of river widths and scour depths recorded this effect. The widths exhibited produced some typical plots yet did not represent the downstream effect very well, just as with many natural and laboratory rivers (Sapozhnikov et al., 1998). The cellular model displayed typical spatial patterns in plots of widths, illustrating the deterministic downstream influence of river width in cellular models (Murray and Paola, 1996). Despite the widths, the maximum scour depths in the present study recorded the periodical geometry well, with one major pool-bar unit in the flume forming one or two loops in the space plots. These results illustrate the better presentation of scour depths than river widths in reflecting downstream effects in our model.

Braided rivers are often characterised by a hierarchy of channels and bedforms, and their planform geometries are typically scale invariant (Sapozhnikov and Foufoula-Georgiou, 1996; Kelly, 2006). The high correlation factors reflect the close relationships of the parameters of the modelled bars, indicating that it is possible to predict the bar size if some parameter, such as the bar axis is known. Nonetheless, this analysis may suffer from the insufficient sample size. Furthermore, the river with bed load was assessed by spatial scaling and found to show typical scaling characteristics.

6.12 Summary

The model was applied to simulate an idealised braided river with suspended load, and produced important morphologic units and braiding processes similar to natural rivers. Typical morphologic units common in natural rivers and braiding mechanisms have been found in the fully developed river. The present simulation result shows that, channel avulsions are closely related to the hydraulic conditions in its morphologic unit. Choking avulsion, constriction avulsion and apex avulsion are intrigued respectively by continuous progradation in one tributary of a bifurcation, annexation of an active channel in neighbourhood, and incision and formation of a new channel. The evolution of channel nodes shows similar characteristics in natural rivers. For example, confluence angle varies with the discharge changes in its two tributaries; bar migrates by downstream translation and bend expansion, with fine sediments on bar and coarse sediments on bar head and in scour holes. Without initial perturbations, the model still produced typical braided pattern though a longer time was necessary.

A series of quantitative methods were applied to assess the extent to which the model reproduces the morphology in real rivers. Results indicated that the river sinuosity presents stage dependence, showing a more sinuous pattern with the river configuration evolution. The state-space plots of sequential maximum scour depths indicated a good representation for the downstream effect of erosion and deposition in the modelled river, yet those of channel widths did not show that good indication. The transect topography and slope frequency showed similar distribution with natural

rivers. Besides, the river exhibited scaling properties, with similar characteristics in bar parameters.

The above analyses illustrated that the present model can well represent the morphodynamics in a braided river. The essential elements for the model to achieve the braided river with suspended load include: 1) basic hydraulic and sediment transport principles controlling river pattern evolution and channel shifting; 2) consideration of graded sediments representing coarsening and fining effect with sheltering effect; 3) a multiple layer arrangement with vertical sorting process; and 4) deposition controlled morphodynamic process with high suspended load. The overloaded sediment promises the deposition activity as the dominant process in the river evolution, which is essential for braiding development in the modelled river.

Chapter 7 Conclusions

7.1 Conclusions

Considering the difficulties in measuring flow, sediment and bed processes in natural rivers, numerical models present an encouraging way to understand these complicated phenomena, in which physics-based models have shown their great potentials. However, in previous studies of physics-based models the braiding mechanisms and morphologic changes have been rarely discussed quantitatively. In the present study, efforts have been made to develop a physics-based morphodynamic model that can better represent the processes in natural braided rivers, and to quantitatively investigate the processes and braiding mechanisms in natural rivers.

The present model contains the basic hydraulic and morphodynamic principles and applies distinct solution methods for different flow patterns. The TVD-MacCormack scheme has been integrated into the model for solving the hydrodynamic equations of trans-critical flows. Separate transport theories of suspended load and bed load have been incorporated into the model, with their contributions combined in a bed deformation equation. Secondary flow and slope effect are integrated into the model by altering the sediment transport rate on slope

and the critical shear stress for the initiation of particle motion. A multiple layer technique with a vertical sorting process has been applied, including the bank erosion activity. Graded sediment fractions are adopted to represent the coarsening and fining processes with sheltering effect included. Consequently, the model has been tested and applied to predict braided rivers with suspended load and bed load transport separately. The main conclusions and findings from this research can be summarised as follows:

- Trans-critical flows often occur during the channel evolution processes in braided rivers. The TVD scheme adopted in this study works well for these processes.
- The newly developed model has been applied to simulate a laboratory river with bed load. A braided river has been produced, with braiding processes and morphologic changes resembling those in the laboratory river and natural rivers. Braided mechanisms including the avulsions by incision, by progradation and by annexation have been found to be the main braiding mechanisms in the predicted river. Their occurrences have close relationship with the temporal alternations of sinuous and straight channels especially the main channel. To consume the high energy the channel becomes more sinuous and then it adopts a new pathway by avulsion activities. The avulsion by incision can be triggered by the overflow of a curved bend, or by flow redirection promoted by the growth of some upstream tributary. The reoccupation of an abandoned channel can be initiated by the bent channel and the consequent higher shear stress. The temporal alternation of straight and sinuous channels is a most important characteristic in the evolution

process of the river.

- The modelled river with bed load responses to the abruptly increased discharge by eroding new channels and widening the river range. Active braiding intensity developed quickly to a stable state, whereas total braiding intensity increased to a stable state gradually. The trends of braiding intensity changes and existence of one main channel are also true for the laboratory river, yet in the late stage the braiding configurations of these two rivers are different. The sequential maximum scour depths represent the downstream spatial pattern well and the river geometry shows scaling characteristics similar to natural rivers such as the Sunwapta River.
- The model has been applied to simulate an idealised large river with suspended load transport. Choking avulsion, constriction avulsion and apex avulsion are intrigued respectively by continuous progradation in one tributary of a bifurcation, annexation of an active channel in neighbourhood, and incision and formation of a new channel. The initiation of braided pattern occurs with the development of chute channels across alternating bars generated in the initially straight channels.
- Similar phenomena in morphologic units to those observed in natural rivers have been found in the predicted river with suspended load. The orientation of the confluence is mainly controlled by the direction of the main channel and its scour depth increases with the angle of incidence θ where the upstream anabranches meet. A bar grows by lateral and downstream accretion simultaneously. Both of its two channels have a net outward flow in the upstream segments and an inward flow in the downstream segments, but show a variable distribution at different

flow increase and decrease stages. The internal sorting of sediments on a bar has a tendency for coarse material to accumulate at the bar head and fine material near the centre.

- Statistical properties of the river with suspended load have been investigated and found to possess similar geometric and morphologic patterns with those of natural rivers. The bar areas usually develop wide and flat sides compared with the narrow and steep sides in the channel areas. The frequency of slopes displays wider distribution in deposition areas yet was narrower in erosion areas, which is similar to natural rivers. The maximum scour depths other than the channel widths, record the periodical downstream geometry of braided rivers well. Scaling characteristic has been found in bars.
- The rivers with bed load and suspended load show some similarities and differences with each other. Both of them generate braided patterns with alternating pool-bar units, but different evolution processes occur after that. The river with bed load develops braiding with a main channel at an early stage, whereas the river with suspended load grows into one main channel at a late stage. For the former, bank erosion with secondary flow is important for braiding to occur. But for the latter, the dominant deposition process with overloaded sediments plays an essential role in the braiding generation. As to the avulsion activities, for the river with bed load, the channel choking process and water spray from the bent channel in choking avulsion are easy to differentiate, yet it is not true for the river with suspended load.

- The two rivers show similar interactions between flow, sediment and bed morphology in their evolution processes. The variations in flow velocity and shear stress cause local erosion and deposition activities, and cause consequent changes in sediment concentration and bed D_{50} distribution. Moreover, in the avulsion processes, high sediment concentration is not necessarily related to high flow velocity and shear stress. Instead, it often occurs in areas with intense erosion or deposition, usually on their boundaries. Sediment fining effect has been predicted well which is shown in the processes of avulsions.
- The model shows its ability in simulating the braiding mechanisms and processes in real braided rivers. It represents the braiding processes and real morphology better than the cellular models. The essential model elements required to achieve a braided river include: 1) basic hydraulic and sediment transport principles controlling river pattern evolution and channel shifting; 2) consideration of graded sediment fractions presenting coarsening and fining effect; 3) a multiple layer arrangement with vertical sorting effect; and 4) bank erosion and secondary flow or overloaded suspended load.
- Most existing models require perturbations for braiding, while the present model can produce braided pattern without any perturbation.

7.2 Recommendations for Future Study

Based on the present research, a number of recommendations for further study are proposed as follows:

- The model can be further used to predict natural rivers with bed load which often occur in mountain areas. Comparisons between rivers from nature, laboratory and numerical models can provide useful information for natural river studies and for the assessment of physical and numerical models.
- In the present study, the two rivers with bed load and suspended load are predicted respectively with one type of sediment transport mode, respectively. However, in nature sometimes both may exist in one river. The investigation of rivers including both of bed load and suspended load transport can provide a better understanding in river deformation processes.
- A lot of equations have been proposed to describe the complicated processes of sediment transport in natural rivers, yet most of them work well only under certain situations. Therefore, various equations can be tested to find the conditions suitable for them to be used in river simulation.
- Bank erodibility plays an important role in braiding evolution. The vegetation effect should be included in simulation work as in nature its condition can greatly alter bank erodibility. The compacting effect of sand should also be considered by some way.
- Sediment fining effect in bed and its consequent influence on sand deposition and erosion are different for bed load and suspended load. Therefore, it is meaningful to study them in a combination.

References

Ackers P, White WR. 1973. Sediment transport: new approach and analysis. *Journal of the Hydraulics Division*, ASCE, 99(11): 2041-2060.

Allen JRL. 1982. Sedimentary structures: their character and physical basis. *Developments in Sedimentology 30A*, Elsevier, Amsterdam; 593pp.

Ashida K, Michiue M. 1971. An investigation of river bed degradation downstream of a dam. In: *Proceedings of 14th Congress of the IAHR*, Paris, France; 247-255.

Ashmore PE. 1991a. How do gravel-bed rivers braid? *Canadian Journal of Earth Sciences*, 28(3): 326-341.

Ashmore PE. 1991b. Channel morphology and bed load pulses in braided, gravel-bed streams. *Geografiska Annaler. Series A. Physical Geography*: 37-52.

Ashmore PE. 1993. Anabranch confluence kinetics and sedimentation processes in gravel-braided streams. In: *Braided Rivers*, Best JL, Bristow CS (eds). Geological Society, Special Publications: London; 129-146.

Ashmore PE. 2001. Braiding phenomena: statics and kinetics. In: *Gravel Bed Rivers V*, Mosley MP (ed). New Zealand Hydrological Society: Wellington, New Zealand; 95-114.

Ashmore PE, Bertoldi W, Tobias Gardner J. 2011. Active width of gravel-bed braided rivers. *Earth Surface Processes and Landforms*, 36(11): 1510-1521.

Ashmore PE, Parker G. 1983. Confluence scour in coarse braided streams. *Water Resources Research*, 19(2): 392-402.

Ashmore PE, Sauks E. 2006. Prediction of discharge from water surface width in a braided river with implications for at-a-station hydraulic geometry. *Water Resources Research*, 42(3): W03406. DOI: 10.1029/2005wr003993.

Ashworth PJ. 1996. Mid-channel bar growth and its relationship to local flow strength and direction. *Earth Surface Processes and Landforms*, 21(2): 103-123.

Ashworth PJ, Best JL, Roden JE, Bristow CS, Klaassen GJ. 2000. Morphological evolution and dynamics of a large, sand braid-bar, Jamuna River, Bangladesh.

Sedimentology, 47(3): 533-555.

Ashworth PJ, Ferguson RI, Powell MD. 1992. Bedload transport and sorting in braided channels. In: *Dynamics of gravel-bed rivers*, Billi P, Hey R, Thorne C, Taconni P (eds). John Wiley and Sons: Chichester, UK; 497-513.

Bagnold RA. 1966. An approach to the sediment transport problem from general physics. *US Geological Survey Prof. Paper*, 422-I: 231-291.

Bartholdy J, Billi P. 2002. Morphodynamics of a pseudomeandering gravel bar reach. *Geomorphology*, 42(3): 293-310.

Bertoldi W, Gurnell A, Surian N, Tockner K, Zanoni L, Ziliani L, Zolezzi G. 2009. Understanding reference processes: linkages between river flows, sediment dynamics and vegetated landforms along the Tagliamento River, Italy. *River Research and Applications*, 25(5): 501-516.

Bertoldi W, Miori S, Salvaro M, Zanoni L, Tubino M. 2006. Morphological description of river bifurcations in gravel-bed braided networks. *River Flow 2006*, 1&2: 1311-1318.

Bertoldi W, Pasetto A, Zanoni L, Tubino M. 2005. Experimental observations in channel bifurcations evolving to an equilibrium state. In: *Proceedings of the 4th IAHR Symposium on River, Coastal and Estuarine Morphodynamics*, Parker G, Garcia M (eds). Taylor & Francis Group: Urbana-Champaign, Illinois, USA; 409-419.

Bertoldi W, Tubino M. 2007. River bifurcations: Experimental observations on equilibrium configurations. *Water Resources Research*, 43(10): W10437. DOI: 10.1029/2007wr005907.

Bertoldi W, Zanoni L, Tubino M. 2009. Planform dynamics of braided streams. *Earth Surface Processes and Landforms*, 34(4): 547-557.

Bertoldi W, Zanoni L, Tubino M. 2010. Assessment of morphological changes induced by flow and flood pulses in a gravel bed braided river: The Tagliamento River (Italy). *Geomorphology*, 114(3): 348-360.

Best JL. 1986. The morphology of river channel confluences. *Progress in Physical Geography*, 10(2): 157-174.

Best JL. 1987. Flow dynamics at river channel confluences: implications for sediment transport and bed morphology. In: *Recent developments in fluvial sedimentology*, Ethridge FG, Flores RM, Harvey MD (eds). Society of Economic Paleontologists and Mineralogists: Tulsa, Okla; 27-35.

Best JL. 1988. Sediment transport and bed morphology at river channel confluences. *Sedimentology*, 35(3): 481-498.

Best JL, Ashworth PJ. 1997. Scour in large braided rivers and the recognition of sequence stratigraphic boundaries. *Nature*, 387(6630): 275-277.

Best JL, Ashworth PJ, Bristow CS, Roden J. 2003. Three-dimensional sedimentary architecture of a large, mid-channel sand braid bar, Jamuna River, Bangladesh. *Journal of Sedimentary Research*, 73(4): 516-530.

Biron PM, Richer A, Kirkbride AD, Roy AG, Han S. 2002. Spatial patterns of water surface topography at a river confluence. *Earth Surface Processes and Landforms*, 27(9): 913-928.

Blanckaert K, Graf WH. 2001. Mean flow and turbulence in open-channel bend. *Journal of Hydraulic Engineering*, 127(10): 835-847.

Blom A. 2003. A vertical sorting model for rivers with non-uniform sediment and dunes. Universial Press: Veenendaal, Netherlands.

Brice JC. 1960. Index for description of channel braiding. *Geological Society of America Bulletin*, 71: 1833.

Brice JC. 1964. Channel patterns and terraces of the Loup Rivers in Nebraska. US Government Printing Office: Washington.

Brice JC. 1984. Planform properties of meandering rivers. In: *River Meandering, Proceedings of the Conference Rivers*, Elliott CM (ed). American Society of Civil Engineers: New York; 1-15.

Bridge JS. 1985. Paleochannel patterns inferred from alluvial deposits: a critical evaluation. *Journal of Sedimentary Research*, 55(4): 579.

Bridge JS. 1992. A revised model for water flow, sediment transport, bed topography and grain size sorting in natural river bends. *Water Resources Research*, 28(4): 999-1013.

Bridge JS. 1993. The interaction between channel geometry, water flow, sediment transport and deposition in braided rivers. In: *Braided Rivers*, Best JL, Bristow CS (eds). Geological Society, Special Publications: London; 13-71.

Bridge JS. 2003. Rivers and floodplains: forms, processes, and sedimentary record. Blackwell: Malden, Mass; 491pp.

Bridge JS, Lunt IA. 2006. Depositional models of braided rivers. In: *Braided Rivers: Process, Deposits, Ecology and Management*, Smith GHS, Best JL, Bristow CS, Petts GE (eds). Blackwell Publishing LTD, Special Publication: Malden, USA; 11-50.

Brierley GJ, Hickin EJ. 1991. Channel planform as a non-controlling factor in fluvial sedimentology: the case of the Squamish River floodplain, British Columbia. *Sedimentary Geology*, 75(1): 67-83.

Burge LM. 2006. Stability, morphology and surface grain size patterns of channel bifurcation in gravel–cobble bedded anabranching rivers. *Earth Surface Processes and Landforms*, 31(10): 1211-1226.

Cao Z. 1999. Equilibrium near-bed concentration of suspended sediment. *Journal of Hydraulic Engineering*, 125(12): 1270-1278.

Cao Z, Li Y, Yue Z. 2007. Multiple time scales of alluvial rivers carrying suspended sediment and their implications for mathematical modeling. *Advances in Water Resources*, 30(4): 715-729.

Cao Z, Pender G, Carling P. 2006. Shallow water hydrodynamic models for hyperconcentrated sediment-laden floods over erodible bed. *Advances in Water Resources*, 29(4): 546-557.

Carson M. 1986. Characteristics of high-energy" meandering" rivers: the Canterbury Plains, New Zealand. *Bulletin of the Geological Society of America*, 97(7): 886.

Chang HH. 1979. Minimum stream power and river channel patterns. *Journal of Hydrology*, 41(3-4): 303-327.

Chew LC, Ashmore PE. 2001. Channel adjustment and a test of rational regime theory in a proglacial braided stream. *Geomorphology*, 37(1): 43-63.

Clayton JA. 2010. Local sorting, bend curvature, and particle mobility in meandering

gravel bed rivers. *Water Resources Research*, 46(2): W02601.

Clayton JA, Pitlick J. 2007. Spatial and temporal variations in bed load transport intensity in a gravel bed river bend. *Water Resources Research*, 43(2): W02426. DOI: 10.1029/2008WR007669

Coulthard TJ, Hicks DM, Van De Wiel MJ. 2007. Cellular modelling of river catchments and reaches: Advantages, limitations and prospects. *Geomorphology*, 90(3): 192-207.

Coulthard TJ, Lewin J, Macklin MG. 2005. Modelling differential catchment response to environmental change. *Geomorphology*, 69(1): 222-241.

Coulthard TJ, Macklin MG. 2001. How sensitive are river systems to climate and land-use changes? A model-based evaluation. *Journal of Quaternary Science*, 16(4): 347-351.

Coulthard TJ, Van De Wiel MJ. 2012. Modelling river history and evolution. *Philosophical Transactions of the Royal Society A: Mathematical, Physical and Engineering Sciences*, 370(1966): 2123-2142.

Crosato A, Desta FB, Cornelisse J, Schuurman F, Uijttewaal WSJ. 2012. Experimental and numerical findings on the long-term evolution of migrating alternate bars in alluvial channels. *Water Resources Research*, 48: W06524. DOI: 10.1029/2011wr011320.

Crosato A, Mosselman E. 2009. Simple physics-based predictor for the number of river bars and the transition between meandering and braiding. *Water Resources Research*, 45(3): W03424. DOI: 10.1029/2008WR007242.

Crosato A, Saleh MS. 2011. Numerical study on the effects of floodplain vegetation on river planform style. *Earth Surface Processes and Landforms*, 36(6): 711-720.

Cui Y, Paola C, Parker G. 1996. Numerical simulation of aggradation and downstream fining. *Journal of Hydraulic Research*, 34(2): 185-204.

Davies TRH. 1987. Problems of bed load transport in braided gravel-bed rivers. In: *Sediment Transfer in Gravel-Bed Rivers*, Thorne CR, Bathurst JC, Hey RD (eds). John Wiley & Sons: New York; 793-811.

Dietrich WE, Kirchner JW, Ikeda H, Iseya F. 1989. Sediment supply and the

development of the coarse surface layer in gravel-bedded rivers. *Nature*, 340(6230): 215-217.

Doeschl AB, Ashmore PE. 2005. Assessing a numerical cellular braided-stream model with a physical model. *Earth Surface Processes and Landforms*, 30(5): 519-540.

Doeschl AB, Ashmore PE, Davison M. 2006. Methods for assessing exploratory computational models of braided rivers. In: *Braided Rivers: Process, Deposits, Ecology and Management*, Smith GHS, Best JL, Bristow CS, Petts GE (eds). Blackwell Publishing LTD, Special Publication: Malden, USA; 177-197.

Duc BM, Wenka T, Rodi W. 2004. Numerical modeling of bed deformation in laboratory channels. *Journal of Hydraulic Engineering*, 130(9): 894-904.

Egozi R, Ashmore PE. 2008. Defining and measuring braiding intensity. *Earth Surface Processes and Landforms*, 33(14): 2121-2138.

Egozi R, Ashmore PE. 2009. Experimental analysis of braided channel pattern response to increased discharge. *Journal of Geophysical Research: Earth Surface*, 114(F2): F02012. DOI: 10.1029/2008JF001099

Einstein HA. 1950. The bed-load function for sediment transportation in open channel flows. *Technical Bulletin 1026*, US Department of Agriculture: Washington; 1-71.

Engelund F. 1966. Hydraulic resistance of alluvial streams. *Journal of the Hydraulics Division*, 98: 315-326.

Engelund F. 1974. Flow and bed topography in channel bends. *Journal of the Hydraulics Division*, 100(11): 1631-1648.

Engelund F, Hansen E. 1967. A monograph on sediment transport in alluvial channels. Teknik Forlag, Copenhagen.

Engelund F, Skovgaard O. 1973. On the origin of meandering and braiding in alluvial streams. *Journal of Fluid Mechanics*, 57(2): 289-302.

Falconer RA. 1993. An introduction to nearly horizontal flows. Coastal Estuarial and Harbour Engineers, Reference Book, E and FN Spon Ltd., London.

Falconer RA, Chen Y. 1991. Improved representation of flooding and drying and wind stress effects in a two-dimensional tidal numerical model. *Proceedings of the Institution of Civil Engineers Part 2: Research and Theory*, 91: 659-678.

Falconer RA, Lin B, Kashefipour SM. 2001. Modelling water quality processes in riverine systems. In: *Computational Fluid Dynamics: Applications in Environmental Hydraulics*, Bates PD, Lane SN, Ferguson RI (eds). John Wiley & Sons, Ltd: London; 358-387.

Falconer RA, Lin B, Wu Y, Harris E. 2001. DIVAST Reference Manual. Environmental Water Management Research Centre, Cardiff University: Cardiff.

Fan X, Shi C, Zhou Y, Du J. 2012. Characteristics of flood regime in Ningxia-Inner Mongolia reaches of the upper Yellow River. *Resources Science*, 34(1): 65-73.

Federici B, Paola C. 2003. Dynamics of channel bifurcations in noncohesive sediments. *Water Resources Research*, 39(6): 1162.

Ferguson RI. 1987. Hydraulic and sedimentary controls of channel pattern. In: *River Channels: environment and process*, Richards K (ed). Blackwell: Oxford; 125-158.

Ferguson RI. 1993. Understanding braiding processes in gravel-bed rivers: progress and unsolved problems. In: *Braided Rivers*, Best JL, Bristow CS (eds). Geological Society, Special Publications: London; 73-87.

Ferguson RI, Ashmore PE, Ashworth PJ, Paola C, Prestegaard KL. 1992. Measurements in a Braided River chute and lobe: 1. Flow pattern, sediment transport, and channel change. *Water Resources Research*, 28(7): 1877-1886.

Fischer HB. 1979. Mixing in inland and coastal waters. Academic Press: San Diego, California; 483pp.

Foufoula-Georgiou E, Sapozhnikov V. 2001. Scale invariances in the morphology and evolution of braided rivers. *Mathematical Geology*, 33(3): 273-291.

Fredsoe J. 1978. Meandering and braiding of rivers. *Journal of Fluid Mechanics*, 84(4): 609-624.

Friend PF, Sinha R. 1993. Braiding and meandering parameters. In: *Braided Rivers*, Best JL, Bristow CS (eds). Geological Society, Special Publications: London; 105-111.

Frings RM. 2008. Downstream fining in large sand-bed rivers. *Earth-Science Reviews*, 87(1): 39-60.

Frings RM, Kleinhans MG. 2008. Complex variations in sediment transport at three

large river bifurcations during discharge waves in the river Rhine. *Sedimentology*, 55(5): 1145-1171.

Fujita Y. 1989. Bar and channel formation in braided streams. *Water Resources Monograph*, 12: 417-462.

Fukuoka S. 1989. Finite amplitude development of alternate bars. In: *River meandering*, Ikeda S, Parker G (eds). American Geophysical Union, Water Resources Monographs 12; 237-265.

Garcia M, Parker G. 1991. Entrainment of bed sediment into suspension. *Journal of Hydraulic Engineering*, 117(4): 414-435.

Hajek EA, Wolinsky MA. 2012. Simplified process modeling of river avulsion and alluvial architecture: Connecting models and field data. *Sedimentary Geology*, 257: 1-30. DOI: 10.1016/j.sedgeo.2011.09.005.

Ham DG, Church M. 2000. Bed-material transport estimated from channel morphodynamics: Chilliwack River, British Columbia. *Earth Surface Processes and Landforms*, 25(10): 1123-1142.

Harten A. 1983. High resolution schemes for hyperbolic conservation laws. *Journal of Computational Physics*, 49(3): 357-393.

Hasegawa K. 2000. Hydraulic characteristics of mountain streams and their practical application. *Lecture Notes of the 33rd Summer Seminar on Hydraulic Engineering, JSCE*.

Hickin EJ, Nanson GC. 1984. Lateral migration rates of river bends. *Journal of Hydraulic Engineering*, 110: 1557.

Hoey TB, Sutherland AJ. 1991. Channel morphology and bedload pulses in braided rivers: a laboratory study. *Earth Surface Processes and Landforms*, 16(5): 447-462.

Hong LB, Davies T. 1979. A study of stream braiding: summary. *Geological Society of America Bulletin*, 90: 1094.

Howard AD, Keetch ME, Vincent CL. 1970. Topological and geometrical properties of braided streams. *Water Resources Research*, 6(6): 1674-1688.

Hu HM, Wang KH. 1999. entrainment function of suspended sediment in open channels. *Journal of Sediment Research*, 14(3): 1-8.

Huang HQ, Chang HH, Nanson GC. 2004. Minimum energy as the general form of critical flow and maximum flow efficiency and for explaining variations in river channel pattern. *Water Resources Research*, 40(4): W04502. DOI: 10.1029/2003WR002539.

Ikeda S, Parker G, Sawai K. 1981. Bend theory of river meanders, part 1: Linear development. *Journal of Fluid Mechanics*, 112(1): 363-377.

Jang CL, Shimizu Y. 2005a. Numerical simulations of the behavior of alternate bars with different bank strengths. *Journal of Hydraulic Research*, 43(6): 596-612.

Jang CL, Shimizu Y. 2005b. Numerical simulation of relatively wide, shallow channels with erodible banks. *Journal of Hydraulic Engineering*, 131(7): 565-575.

Jerolmack DJ, Paola C. 2007. Complexity in a cellular model of river avulsion. *Geomorphology*, 91(3): 259-270.

Jones LS, Schumm SA. 1999. Causes of avulsion: an overview. *Fluvial Sedimentology VI 28*; 171-178.

Karim F. 1998. Bed material discharge prediction for nonuniform bed sediments. *Journal of Hydraulic Engineering*, 124(6): 597-604.

Kelly S. 2006. Scaling and hierarchy in braided rivers and their deposits: examples and implications for reservoir modelling. In: *Braided Rivers: Process, Deposits, Ecology and Management*, Smith GHS, Best JL, Bristow CS, Petts GE (eds). Blackwell Publishing LTD, Special Publication: Malden, USA; 75-106.

Kiss T, Sipos G. 2007. Braid-scale channel geometry changes in a sand-bedded river: significance of low stages. *Geomorphology*, 84(3): 209-221.

Klaassen GJ, Vermeer K. 1988. Confluence scour in large braided rivers with fine bed material. *International Conference on Fluvial Hydraulics*, Budapest.

Kleinhans MG. 2001. The key role of fluvial dunes in transport and deposition of sand-gravel mixtures, a preliminary note. *Sedimentary Geology*, 143(1): 7-13.

Kleinhans MG. 2005. Upstream sediment input effects on experimental dune trough scour in sediment mixtures. *Journal of Geophysical Research*, 110(F4): F04S06. DOI: 10.1029/2004jf000169.

Kleinhans MG. 2010. Sorting out river channel patterns. *Progress in Physical*

Geography, 34(3): 287-326.

Knighton DA. 1998. Fluvial forms and processes: a new perspective. Arnold, Hodder Headline, PLC: London; 383pp.

Knighton DA, Nanson GC. 1993. Anastomosis and the continuum of channel pattern. *Earth Surface Processes and Landforms*, 18(7): 613-625.

Korvin G. 1993. Fractal models in the earth sciences. *Science*, 259(5099): 1350-1351.

Krigström A. 1962. Geomorphological Studies of Sandur Plains and Their Braided Rivers in Iceland. *Geografiska Annaler*, 44(3): 328-346.

Lane SN, Bradbrook KF, Richards KS, Biron PM, Roy AG. 2000. Secondary circulation cells in river channel confluences: measurement artefacts or coherent flow structures? *Hydrological Processes*, 14(11): 2047-2071.

Leddy JO, Ashworth PJ, Best JL. 1993. Mechanisms of anabranch avulsion within gravel-bed braided rivers: observations from a scaled physical model. In: *Braided Rivers*, Best JL, Bristow CS (eds). Geological Society, Special Publications: London; 119-127.

Leopold LB, Wolman MG. 1957. River channel patterns: braided, meandering, and straight. United States Geological Survey Professional Paper, US Government Printing Office: Washington, DC, 282-B.

Liang D, Falconer RA, Lin B. 2006. Comparison between TVD-MacCormack and ADI-type solvers of the shallow water equations. *Advances in Water Resources*, 29(12): 1833-1845.

Liang D, Lin B, Falconer RA. 2007. Simulation of rapidly varying flow using an efficient TVD-MacCormack scheme. *International journal for numerical methods in fluids*, 53(5): 811-826.

Lien H, Hsieh T, Yang J, Yeh K. 1999. Bend-flow simulation using 2D depth-averaged model. *Journal of Hydraulic Engineering*, 125(10): 1097-1108.

Lin B, Falconer RA. 1997. Tidal flow and transport modeling using ULTIMATE QUICKEST scheme. *Journal of Hydraulic Engineering*, 123(4): 303-314.

Lotsari E, Wainwright D, Corner GD, Alho P, Käyhkö J. 2013. Surveyed and modelled one-year morphodynamics in the braided lower Tana River. *Hydrological*

Processes. DOI: 10.1002/hyp.9750.

Louaked M, Hanich L. 1998. TVD scheme for the shallow water equations. *Journal of Hydraulic Research*, 36(3): 363-378.

Luchi R, Zolezzi G, Tubino M. 2010. Modelling mid-channel bars in meandering channels. *Earth Surface Processes and Landforms*, 35(8): 902-917.

Marti C, Bezzola GR. 2006. Bed load transport in braided gravel-bed rivers. In: *Braided Rivers: Process, Deposits, Ecology and Management*, Smith GHS, Best JL, Bristow CS, Petts GE (eds). Blackwell Publishing LTD, Special Publication: Malden, USA; 199-215.

Maynord ST. 1991. Flow resistance of riprap. *Journal of Hydraulic Engineering*, 117(6): 687-696.

Meyer-Peter E, Müller R. 1948. Formulas for bed-load transport. In: *Proceedings of the 2nd Meeting of the International Association for Hydraulic Structures Research*, Stockholm, Sweden; 39-64.

Miall AD. 1977. A review of the braided-river depositional environment. *Earth-Science Reviews*, 13(1): 1-62.

Ming HT, Chu CR. 2000. Two-dimensional shallow water flows simulation using TVD-MacCormack scheme. *Journal of Hydraulic Research*, 38(2): 123-131.

Mingham CG, Causon DM. 1998. High-resolution finite-volume method for shallow water flows. *Journal of Hydraulic Engineering*, 124(6): 605-614.

Mingham CG, Causon DM, Ingram DM. 2001. A TVD MacCormack scheme for transcritical flow. *Proceedings of the ICE-Water and Maritime Engineering*, 148(3): 167-175.

Moreton DJ, Ashworth PJ, Best JL. 2002. The physical scale modelling of braided alluvial architecture and estimation of subsurface permeability. *Basin Research*, 14(3): 265-285.

Mosley MP. 1976. An experimental study of channel confluences. *The Journal of Geology*: 535-562.

Mosley MP. 1981. Semi-determinate hydraulic geometry of river channels, South Island, New Zealand. *Earth Surface Processes and Landforms*, 6(2): 127-137.

Mosley MP. 1982. Scour depths in branch channel confluences, Ohau river, Otago, New Zealand. *Proceedings of New Zealand Institute of Professional Engineers*, 9: 17-24.

Murray AB, Paola C. 1994. A cellular model of braided rivers. *Nature*, 371(6492): 54-57.

Murray AB, Paola C. 1996. A new quantitative test of geomorphic models, applied to a model of braided streams. *Water Resources Research*, 32(8): 2579-2587.

Murray AB, Paola C. 1997. Properties of a cellular braided-stream model. *Earth Surface Processes and Landforms*, 22(11): 1001-1025.

Murray AB, Paola C. 2003. Modelling the effect of vegetation on channel pattern in bedload rivers. *Earth Surface Processes and Landforms*, 28(2): 131-143.

Nevins THF. 1969. River training-the single-thread channel. *New Zealand Engineering*, 24(12): 367.

Nicholas AP. 2013. Modelling the continuum of river channel patterns. *Earth Surface Processes and Landforms*, 38: 1187-1196.

Nicholas AP, Quine TA. 2007. Crossing the divide: Representation of channels and processes in reduced-complexity river models at reach and landscape scales. *Geomorphology*, 90(3): 318-339.

Nicholas AP, Sandbach SD, Ashworth PJ, Amsler ML, Best JL, Hardy RJ, Lane SN, Orfeo O, Parsons DR, Reesink AJH, Smith GHS, Szupiany RN. 2012. Modelling hydrodynamics in the Rio Parana, Argentina: An evaluation and inter-comparison of reduced-complexity and physics based models applied to a large sand-bed river. *Geomorphology*, 169: 192-211. DOI: 10.1016/j.geomorph.2012.05.014.

Nicholas AP, Walling DE, Sweet RJ, Fang X. 2006. New strategies for upscaling high-resolution flow and overbank sedimentation models to quantify floodplain sediment storage at the catchment scale. *Journal of Hydrology*, 329(3-4): 577-594. DOI: 10.1016/j.jhydrol.2006.03.010.

Nykanen DK, Foufoula-Georgiou E, Sapozhnikov VB. 1998. Study of spatial scaling in braided river patterns using synthetic aperture radar imagery. *Water Resources Research*, 34(7): 1795-1807.

Paola C. 2001. Modelling stream braiding over a range of scales. In: *Gravel Bed Rivers V*, Mosley P (ed). New Zealand Hydrological Society: Wellington; 11-38.

Paola C, Parker G, Seal R, Sinha SK, Southard JB, Wilcock PR. 1992. Downstream fining by selective deposition in a laboratory flume. *Science*, 258(5089): 1757-1760.

Parker G. 1976. On the cause and characteristic scales of meandering and braiding in rivers. *Journal of Fluid Mechanics*, 76(03): 457-480.

Parker G. 1990. Surface-based bedload transport relation for gravel rivers. *Journal of Hydraulic Research*, 28(4): 417-436.

Parker G, Sawai K, Ikeda S. 1982. Bend theory of river meanders, part 2: Nonlinear deformation of Finite-amplitude bends. *Journal of Fluid Mechanics*, 115: 303-314.

Parker G, Wilcock PR, Paola C, Dietrich WE, Pitlick J. 2007. Quasi-universal relations for bankfull hydraulic geometry of single-thread gravel-bed rivers. *Journal of Geophysical Research: Earth Surface (2003 - 2012)*, 112(21): F04005.

Parsons DR, Best JL, Lane SN, Orfeo O, Hardy RJ, Kostaschuk R. 2007. Form roughness and the absence of secondary flow in a large confluence-diffluence, Rio Paraná, Argentina. *Earth Surface Processes and Landforms*, 32(1): 155-162.

Pittaluga MB, Repetto R, Tubino M. 2003. Channel bifurcation in braided rivers: Equilibrium configurations and stability. *Water Resources Research*, 39(3): 1046.

Preston RW. 1985. The representation of dispersion in two-dimensional shallow water flow. Central Electricity Research Laboratories, Report No. TPRD/U278333/N84, 13pp.

Rahuel JL, Holly FM, Chollet JP, Belleudy PJ, Yang G. 1989. Modeling of riverbed evolution for bedload sediment mixtures. *Journal of Hydraulic Engineering*, 115(11): 1521-1542.

Rhoads BL, Riley JD, Mayer DR. 2009. Response of bed morphology and bed material texture to hydrological conditions at an asymmetrical stream confluence. *Geomorphology*, 109(3): 161-173. DOI: 10.1016/j.geomorph.2009.02.029.

Rice SP, Church M, Wooldridge CL, Hickin EJ. 2009. Morphology and evolution of bars in a wandering gravel-bed river: lower Fraser river, British Columbia, Canada.

Sedimentology, 56(3): 709-736.

Richardson JF, Zaki WN. 1954. Sedimentation and fluidisation: Part I. *Transactions of the Institution of Chemical Engineers*, 32: 35-53.

Richardson WR, Thorne CR. 2001. Multiple thread flow and channel bifurcation in a braided river: Brahmaputra-Jamuna River, Bangladesh. *Geomorphology*, 38(3): 185-196.

Rogers B, Fujihara M, Borthwick AGL. 2001. Adaptive Q-tree Godunov-type scheme for shallow waterequations. *International journal for numerical methods in fluids*, 35(3): 247-280.

Rosatti G. 2002. Validation of the physical modeling approach for braided rivers. *Water Resources Research*, 38(12): 31-1. DOI: 10.1029/2001WR000433

Rundle AS. 1985a. The mechanism of braiding. *Zeitschrift für Geomorphlogie, Supplement Band*, 55: 15-37.

Rundle AS. 1985b. Braid morphology and the formation of multiple channels, the Rakaia, New Zealand. *Zeitschrift für Geomorphlogie, Supplement Band*, 55: 1-13.

Rust BR. 1978. A classification of alluvial channel systems. *Fluvial Sedimentology*, 5: 123-126.

Sapozhnikov VB, Foufoula-Georgiou E. 1995. Study of self-similar and self-affine objects using logarithmic correlation integral. *Journal of Physics A: Mathematical and General*, 28(3): 559.

Sapozhnikov VB, Foufoula-Georgiou E. 1996. Self-affinity in braided rivers. *Water Resources Research*, 32(5): 1429-1439.

Sapozhnikov VB, Foufoula-Georgiou E. 1997. Experimental evidence of dynamic scaling and indications of self-organized criticality in braided rivers. *Water Resources Research*, 33(8): 1983-1991.

Sapozhnikov VB, Murray AB, Paola C, Foufoula-Georgiou E. 1998. Validation of Braided-Stream Models: Spatial state-space plots, self-affine scaling, and island shapes. *Water Resources Research*, 34(9): 2353-2364.

Sarma JN. 2005. Fluvial process and morphology of the Brahmaputra River in Assam, India. *Geomorphology*, 70(3): 226-256.

Schumm SA. 1972. Fluvial paleochannels. *Recognition of Ancient Sedimentary Environments*, 16: 98-107.

Schumm SA. 1985. Patterns of alluvial rivers. *Annual Review of Earth and Planetary Sciences*, 13: 5-27.

Schuurman F, Kleinhans MG. 2011. Self-formed braid bars in a numerical model. In: *AGU Fall Meeting Abstracts*; 0672.

Seal R, Paola C, Parker G, Southard JB, Wilcock PR. 1997. Experiments on downstream fining of gravel: I. Narrow-channel runs. *Journal of Hydraulic Engineering*, 123(10): 874-884.

Slingerland R, Smith ND. 1998. Necessary conditions for a meandering-river avulsion. *Geology*, 26(5): 435-438. DOI: 10.1130/0091-7613(1998).

Slingerland R, Smith ND. 2004. River avulsions and their deposits. *Annual Review of Earth and Planetary Sciences*, 32: 257-285.

Smith ND. 1970. The braided stream depositional environment: comparison of the Platte River with some Silurian clastic rocks, north-central Appalachians. *Bulletin of the Geological Society of America*, 81(10): 2993-3013.

Smith ND. 1971. Transverse bars and braiding in the lower Platte River, Nebraska. *Geological Society of America Bulletin*, 82(12): 3407-3419.

Smith ND, Smith DG. 1984. William River: An outstanding example of channel widening and braiding caused by bed-load addition. *Geology*, 12(2): 78.

Szupiany RN, Amsler ML, Parsons DR, Best JL. 2009. Morphology, flow structure, and suspended bed sediment transport at two large braid-bar confluences. *Water Resources Research*, 45(5): W05415. DOI: 10.1029/2008WR007428

Takebayashi H, Okabe T. 2009. Numerical modelling of braided streams in unsteady flow. *Proceedings of the ICE-Water Management*, 162(3): 189-198.

Tal M, Paola C. 2010. Effects of vegetation on channel morphodynamics: results and insights from laboratory experiments. *Earth Surface Processes and Landforms*, 35(9): 1014-1028.

Thomas R, Nicholas AP, Quine T. 2007. Cellular modelling as a tool for interpreting historic braided river evolution. *Geomorphology*, 90(3): 302-317.

Tooth S, Nanson GC. 2004. Forms and processes of two highly contrasting rivers in arid central Australia, and the implications for channel-pattern discrimination and prediction. *Geological Society of America Bulletin*, 116(7-8): 802-816.

Tornqvist TE, Bridge JS. 2002. Spatial variation of overbank aggradation rate and its influence on avulsion frequency. *Sedimentology*, 49(5): 891-905. DOI: 10.1046/j.1365-3091.2002.00478.x.

Tubino M. 1991. Growth of alternate bars in unsteady flow. *Water Resources Research*, 27(1): 37-52. DOI: 10.1029/90wr01699.

van Rijn LC. 1984a. Sediment transport, part I: Bed load transport. *Journal of Hydraulic Engineering*, 110(10): 1431-1456.

van Rijn LC. 1984b. Sediment transport, part II: Suspended load transport. *Journal of Hydraulic Engineering*, 110(11): 1613-1641.

van Rijn LC. 1987. Mathematical modelling of morphological processes in the case of suspended sediment transport. Doctoral Thesis.Department of Fluids Mechanics, Delft University of Technology, Delft, The Netherlands.

van Rijn LC. 1990. Handbook sediment transport by currents and waves. Delft hydraulics: Delft,The Netherlands.

van Rijn LC. 1993. Principles of sediment transport in rivers, estuaries and coastal seas. Aqua publications: Amsterdam, The Netherlands; 614pp.

van Rijn LC. 2007. Unified view of sediment transport by currents and waves III: Graded beds. *Journal of Hydraulic Engineering*, 133(7): 761-775.

Varkaris FC. 2002. Variability in bedload sediment transport estimates, Sunwapta River, Alberta, Canada. MS thesis, University of Western Ontario, London, Ontario, Canada; 122 pp.

Walsh J, Hicks DM. 2002. Braided channels: Self-similar or self-affine? *Water Resources Research*, 38(6): 1082. DOI: 10.1029/2001WR000749.

Wang H, Zhou G, Shao X. 2010a. Numerical simulation of channel pattern changes, part I: Mathematical model. *International Journal of Sediment Research*, 25(4): 366-379.

Wang H, Zhou G, Shao X. 2010b. Numerical simulation of channel pattern changes,

part II: Application in a conceptual channel. *International Journal of Sediment Research*, 25(4): 380-390.

Wang J, Ni H, He Y. 2000. Finite-difference TVD scheme for computation of dam-break problems. *Journal of Hydraulic Engineering*, 126(4): 253-262.

Webb EK. 1994. Simulating the three-dimensional distribution of sediment units in braided-stream deposits. *Journal of Sedimentary Research*, 64(2): 219-231.

Webb EK. 1995. Simulation of braided channel topology and topography. *Water Resources Research*, 31(10): 2603-2611.

Whiting PJ, Dietrich WE. 1991. Convective accelerations and boundary shear stress over a channel bar. *Water Resources Research*, 27(5): 783-796.

Wilcock PR. 1993a. Critical shear stress of natural sediments. *Journal of Hydraulic Engineering*, 119(4): 491-505.

Wilcock PR, McArdell BW. 1993b. Surface-based fractional transport rates: Mobilization thresholds and partial transport of a sand-gravel sediment. *Water Resources Research*, 29(4): 1297-1312.

Wilcock PR, Southard JB. 1988. Experimental study of incipient motion in mixed-size sediment. *Water Resources Research*, 24(7): 1137-1151.

Williams RD, Brasington J, Hicks M, Rennie CD, Vericat D. 2013. Hydraulic validation of two-dimensional simulations of braided river flow with spatially continuous a Dcp data. *Water Resources Research*. DOI: 10.1002/wrcr.20391.

Wright S, Parker G. 2005. Modeling downstream fining in sand-bed rivers I: Formulation. *Journal of hydraulic research*, 43(6): 613.

Wu W. 2004. Depth-averaged two-dimensional numerical modeling of unsteady flow and nonuniform sediment transport in open channels. *Journal of Hydraulic Engineering*, 130(10): 1013-1024.

Wu W. 2007. Computational river dynamics. Taylor & Francis Group: London; 499pp.

Wu W, Wang SSY. 1999. Movable bed roughness in alluvial rivers. *Journal of Hydraulic Engineering*, 125(12): 1309-1312.

Wu W, Wang SSY, Jia Y. 2000. Nonuniform sediment transport in alluvial rivers.

Journal of Hydraulic Research, 38(6): 427-434.

Xu J, Lv G, Zhang S. 2000. Study of the regional boundaries and sediment production and transport in the coarse-sand areas of the midille Yellow River. Yellow River Water Conservancy Press: Zhengzhou; 17-21 (in Chinese).

Zhang R, Xie J. 1993. Sedimentation research in China: Systematic selections. Water and Power Press, Beijing, China.

Zhou J, Lin B. 1998. One-dimensional mathematical model for suspended sediment by lateral integration. *Journal of Hydraulic Engineering*, 124(7): 712-717.

Zhou J, Lin B. 2008. Modelling bed evolution processes in alluvial rivers. In: *Proceedings of the International Conference on Fluvial Hydraulics*, Altinakar M, Kokpinar MA, Aydin İ, Cokgor Ş, Kirkgoz S (eds). IZMIR: Turkey; 1305-1311.

Zhou J, Lin B, Lin B. 2003. Rational Basis for Suspended Sediment Modeling. *International Journal of Sediment Research*, 18(3): 177-195.

Zolezzi G, Bertoldi W, Tubino M. 2006. Morphological analysis and prediction of river bifurcations. In: *Braided Rivers: Process, Deposits, Ecology and Management*, Smith GHS, Best JL, Bristow CS, Petts GE (eds). Blackwell Publishing LTD, Special Publication: Malden, USA; 233-256.